The vertebrate retina: a functional review

Adrien Wohrer

INRIA

INSTITUT NATIONAL DE RECHERCHE EN INFORMATIQUE ET EN AUTOMATIQUE

The vertebrate retina: a functional review

Adrien Wohrer

N° 6532

May 2008

Thème BIO

ISSN 0249-6399

The vertebrate retina: a functional review

Adrien Wohrer*

Thème BIO — Systèmes biologiques
Projet Odyssée

Rapport de recherche n° 6532 — May 2008 — 186 pages

Abstract: In this report, we summarize the major properties of retinal filtering and organization, as understood by numerous experiments and models over the last decades. For this review, we take a *functional* approach, trying to answer this apparently simple question: What are the main characteristics of the retinal output in terms of signal processing, which should be retained in a functional model?

Key-words: Retina, function, filtering, contrast gain control, visual pathways, spikes, adaptation

* Adrien.Wohrer@sophia.inria.fr

La rétine des vertébrés: une étude fonctionnelle

Résumé : Dans ce rapport, nous résumons les principales propriétés de la rétine –son organisation et le traitement du signal qu'elle réalise– telles qu'elles sont comprises de nos jours, après plusieurs décennies d'expériences et de modélisation. Cette synthèse est axée autour de la question de la fonctionnalité de la rétine: Quelles sont ses caractéristiques en termes de traitement du signal, et lesquelles sont suffisamment importantes pour être reproduites dans un modèle à grande échelle?

Mots-clés : Rétine, fonction, filtrage, contrôle du gain au contraste, canaux, spikes, adaptation

Contents

INTRODUCTION

In this report, we summarize the major properties of retinal filtering and organization, as understood by numerous experiments and models over the last decades. For this review, we take a *functional* approach, trying to answer this apparently simple question: 'What are the main characteristics of the retinal output, which should be retained in a functional model?'.

In Chapter 1, we present an overview of retinal processing, including anatomy of the retina, and its place in the larger structure which is the visual system. In Chapter 2, we take a modeler's standpoint, and present various classical tools, derived from linear analysis, which have been used to account for signal processing in the retina. Once these preliminary facts and tools are settled, we enter in Chapter 3 the details of retinal function. This detailed chapter proceeds to the review of prominent features in the retina, from phototransduction to emitted spike trains, including the organization of the retina in parallel pathways, and various mechanisms of nonlinear adaptation.

This report has been written aiming at the whole 'visual neuroscience' community rather than only at retinal specialists – a type of approach which we could not find in the literature. Our hope is that the review will shed light on some intriguing features of retinal processing which are not universally known outside of the 'retina' community itself, even though they may convey advanced functionalities. Contrast gain control, numerous parallel pathways at the retinal output, or spiking synchrony, are some of these intriguing features. We also believe that this integrated presentation will prove useful to students wishing to discover the retina at a general level, yet more advanced than classical 'textbook' descriptions.

CHAPTER **1**

GENERAL ANATOMY AND PHYSIOLOGY OF THE RETINA

In this chapter, we present general properties of the retina. In Section 1, an overview of the eye and visual system is given, to situate the role of the retina in a wider processing structure. In Section 2, focus is given to the anatomical structure of the retina: Its different types of cells and their generic connectivity. Finally, Section 3 presents the general characteristics of the retinal output (center-surround organization, temporal band-pass behavior). The notions presented here provide landmarks for Chapters 2 and 3, where the retinal function is described in more detail.

Contents

1 ANATOMY OF THE VISUAL SYSTEM

The visual system is very developed in humans and primates (see Figure 1.1), and vision is by far the most processed sensory modality in terms of number of neurons involved: In the human brain, almost 30% of the cortical surface processes an information which is mostly related to vision [24]. Here, we provide an overview of the low-level visual system: First, the visual organ itself (the eye), and second the thalamo-cortical pathway that starts the processing of visual information in the brain. We hope that this overview can help non-specialist readers to situate retinal processing in the wider scheme of visual perception as a whole. Furthermore, the specific visual pathways and areas introduced here have a close relation to retinal processing, and we will sometimes mention them further in this work.

Our main sources for description of the visual system are the reference books *Principles of Neural Science* (2000, Kandel, Schwartz and Jessell, editors) [75], *Neuroscience* (2004, Purves *et al.*, editors), and *The Visual Neurosciences* (2004, Chalupa and Werner, editors) [24]. This last book offers an important and comprehensive documentation on most aspects of visual processing. Concerning anatomy of the eye, our main source is the website Webvision [83].

1.1 The eye

A human eye is about 2,5 cm in diameter. One is represented in Figure 1.2, along with its anatomical components. We rapidly present the main components and features of the mammalian eye.

Cornea and crystalline lens: An adapting converging lens. The eye contains two successive lenses, the cornea and the crystalline lens, which project incoming light on the back of the eye. The most powerful lens is the cornea (convergence of about 40 diopters), which accounts for roughly 70% of the eye's total convergence power[1]. The crystalline is a deformable lens controlled by zonule fiber muscles, that dynamically provides additional convergence so that the retinal image is always precise at the back of the eye, independently of the distance of the considered object. As we browse the visual space, our eyes constantly undergo this mechanism, known as *accomodation*. The converging power of the crystalline lens is of about 10 dioptres, but varies drastically with age (which can lead to presbytia in elderly individuals). Its accomodation range is of 2-3 dioptres, depending on age [119].

Retina: The neural captor. The retina is a thin (0.5 mm) sheet of neural tissue at the back of the eye, that transforms the incoming light into a neural message suitable for transmission to the brain. Amongst other cells, the retina contains *photoreceptors* that absorb a part of the light hitting the back of the eye, and convert the absorbed light signal into electrical activity, through a complex chemical

[1] This strong convergence is due to the large difference in refraction index between the air and the cornea. In fact, the convergence index of the cornea is closer to that of water, so that underwater the cornea is much less convergent, explaining the unfocused and distorted visual perception [119].

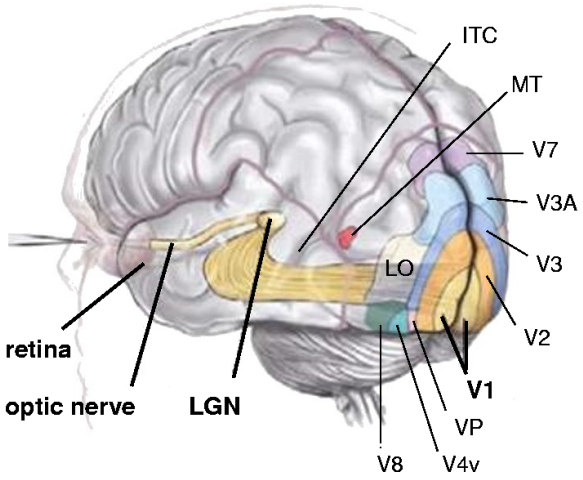

Figure 1.1: Visual pathway in the human brain. Visual signal from the retina travels along the optic nerve in the form of spike trains, to the Lateral Geniculate Nucleus (LGN) in the thalamus. Visual signal is then transmitted to the Primary Visual Cortex (V1), and is further processed in terms of shapes (V2,V3,V4...), color (V4,V8...) and movement (V2, MT, MST, IT...). Reproduced from Logothetis, Scientific American 99.

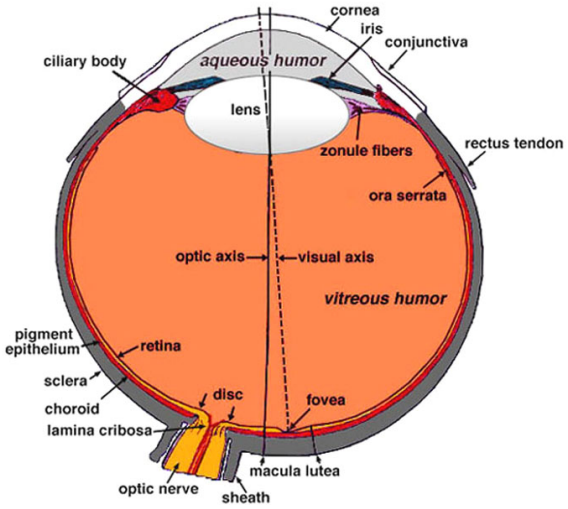

Figure 1.2: A human eye. The cornea and crystalline are lenses that allow the image at the back of the eye to be well-focused, especially at the *fovea* which is the central and most precise zone of the retina.

process known as *phototransduction*. In many mammal species, the retina has a central zone (called the *fovea* in primates and humans) where a high density of cells allows a high spatial resolution. The crystalline lens dynamically adapts its strength for the image to be most precise at this central zone.

The convergence power of the cornea and crystalline lens defines the projection ratio from the visual field to the retina. Typically, one degree of visual angle can correspond to 290 (human), 210 (macaque) or 170 (rabbit) μm on the retinal surface. As with any converging lens, the image projected on the retina is reversed: The left visual field is projected on the right side of the retina, the upper part of the visual field is projected on the lower part of the retina, and conversely. Naturally, this has no effect on our perception, because the visual perception is only defined by the neural connectivity, not the physical organization of the neurons.

Iris: An adapting diaphragm. The iris is the circular membrane whose colorful pigments define the color of our eyes. It plays the role of an optic diaphragm, with a variable aperture: the pupil. Through this variable aperture, the iris provides a first adaptation to the incoming levels of light in the eye. To account for the variation of pupil aperture, a psychophysical measure of illuminance at the back of the eye has been introduced: the photopic troland (tr). The retinal illuminance T in photopic trolands is defined through $T = Lp$, where L is the photopic luminance from the visual world, in cd/m^2, and p is the pupil aperture, in mm^2. Depending on their experimental protocols, neuroscientists use photopic trolands, or directly the input photopic luminance, which is much easier to measure [2].

Epithelium: An absorbing medium. Behind the retina is layer of cells called the epithelium. It contain visual pigments that absorb the light which has not been absorbed by photoreceptors. This prevents any diffuse light from being reflected at the back of the eye, which would make the retinal image less precise. The epithelium is always absorptive. However, in many nocturnal mammal species (such as cats and dogs), the epithelium is lined with a reflective layer called the *tapetum*, allowing the retina to absorb twice as much light because the light 'comes back'. This provides a better vision in weak illumination conditions, at the expense of a loss in retinal precision. In these animals, the pupils seem to glow at night, because the back of the eye reflects incoming light.

1.2 The lateral geniculate nucleus (LGN)

From the two retinas, the visual signal is transferred along the optic nerves to the lateral geniculate nucleus (LGN, see Figure 1.3), a specific nucleus in the thalamus (a part of the diencephalon). Information (from both eyes) concerning the left visual field is transferred to the right hemisphere LGN, and conversely. A key feature of retinal processing is that there is no backward projection

[2] In scotopic ('night-time') conditions, the psychophysical measure used is rather the *scotopic troland*, that includes a supplementary measure of the spectral composition of the incoming light, to account for the strong preference of our rod receptors to 'greenish' spectral light. See e.g. Lance Hahn's retina page at http://retina.anatomy.upenn.edu/~lance/modelmath/units_photometric.html

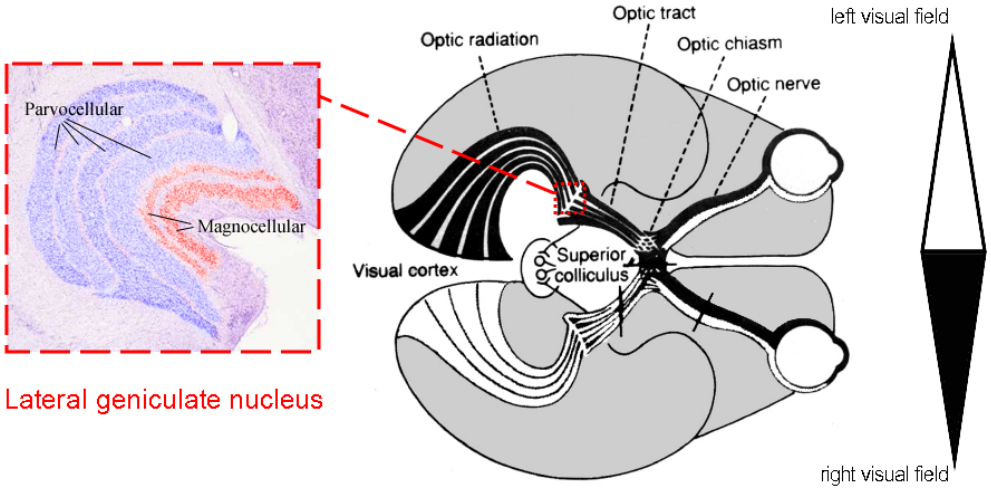

Figure 1.3: *The lateral geniculate nucleus (LGN) in the visual pathway.* The visual signal from the left visual field of both eyes (in white) is transmitted to the right hemisphere of the brain, while the visual signal from the right visual field (in black) is transmitted to the left hemisphere. The LGN is a thalamic nucleus that relays the visual signal before transmission to the cortex. It is a layered structure, and each layer *maps* the whole visual field, for a single eye. In the primate, some layers are associated to the Parvocellular pathway, and other layers to the Magnocellular pathway (see Chapter 3). The LGN is mostly a relay of the retinal signal, but there is strong evidence that it also has more complex and less well understood roles.

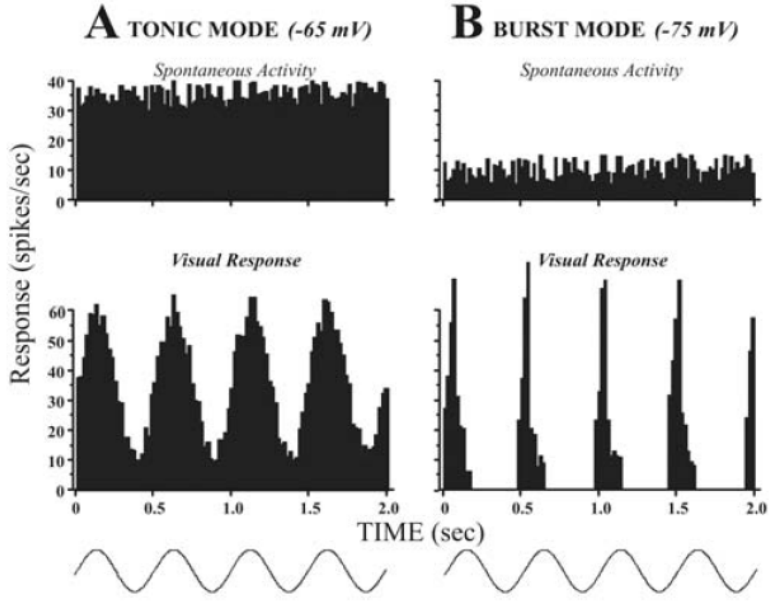

Figure 1.4: *Tonic and bursting activity in the LGN*. According to the value of their resting membrane potential (imposed by their synaptic entries), LGN relay cells can respond to a signal whether in a *tonic* fashion (large, regular activity) or in a *bursting* fashion (irregular activity with alternating bursts of spikes and silent periods). Cortical feedbacks are largely responsible for putting LGN cells in either spiking mode. From Sherman and Guillery [140].

from the LGN or other visual areas onto the retina[3]. As a result, unlike most areas of the brain, retinal processing can be studied as a closed problem involving solely the retina itself.

Traditionally, the LGN has been seen as a simple relay for the visual signal, to provide input to the visual cortex. This assumption was based on the fact that LGN cells respond to stimuli in a way very similar to the ganglion cells that form the output of the retina, with a strong *center-surround* opposition (Section 3.2). The center-surround opposition of LGN cells was found in many studies: For references, see e.g. the LGN chapter of Sherman and Guillery [140] in the reference book *The Visual Neurosciences* [24].

At some places of this manuscript, we will refer to specific works on the LGN that confirm its similarities with the retinal output organization. For example, we mention the works of Cai *et al.* [20] on LGN receptive fields (Chapter 2), or the works of Neuenschwander *et al.* [106] on spiking synchronies in the retina and LGN (Chapter 3).

However, it is now well established that by some aspects, the LGN is much more than a simple relay. Indeed, retinal inputs constitute only about 10% of the total inputs of the LGN. The remaining input comes as a *feedback* from different areas of the visual cortex and of the brainstem (midbrain), and as recurrent connections made with inhibitory interneurons in the LGN itself [140]. Such connectivity is not that of a relay, but rather of a *platform* for visual information, somehow integrating higher-level processing that occurs in different visual areas of the brain.

In particular, a specific functionality is present in the LGN and absent from the retinal output: An LGN relay cell can achieve two distinct spiking modes, the *tonic* and the *bursting* mode. This property is illustrated in Figure 1.4. The cell's tonic or bursting behavior depends mostly on the resting potential imposed on the cell by its synaptic inputs, and involves specific transient Calcium channels. It is believed that cortical feedbacks and brainstem inputs are largely responsible for the 'choice' of putting LGN cells in either of the two spiking modes. Possibly, the tonic mode could be more linked to attentional processes, while the bursting mode could allow the strong transmission of sudden unexpected visual cues. Sherman and Guillery 04 [140] are our reference for this whole paragraph.

To conclude, cells in the LGN display typical receptive fields very close to retinal receptive fields. Yet the LGN is clearly more than a simple relay and, as all areas of the brain, it displays complicated behaviors which are badly understood.

1.3 The primary visual cortex

From the LGN, the visual signal is mostly transmitted to the primary visual cortex, generally termed V1 (or area 17). The cortex (not only visual) is a two-dimensional, layered 'sheet' of neurons, which is strongly developed in primates and humans and responsible –amongst other things– for high-level perception and abstraction.

Both cerebral hemispheres display symmetric visual areas, each one in charge of one side of the visual field. V1, the entry of the visual cortex, is probably the most studied area of the visual

[3] In fact, some backward connections from LGN to the retina have already been reported anatomically, but rarely and with no known functionality.

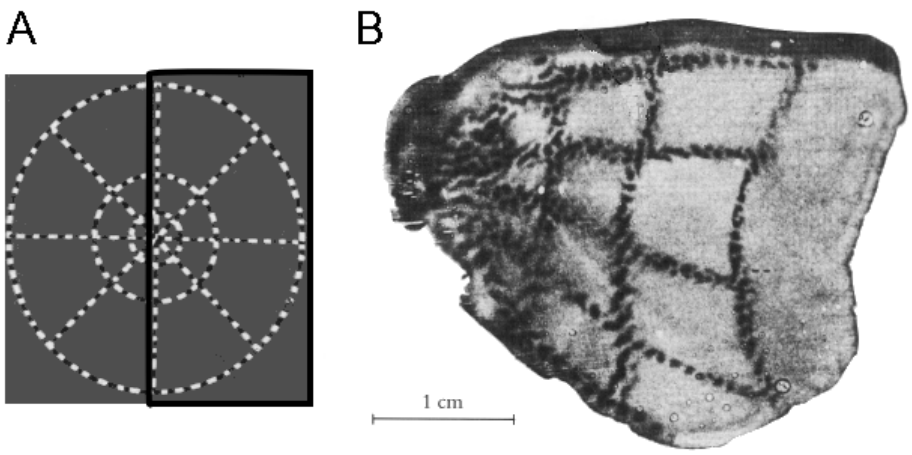

Figure 1.5: Retinotopic organization of the primary visual cortex (V1): The visual field is continuously mapped onto the visual cortex. *A*: A grid pattern made of concentric circles is presented to a macaque. The black box corresponds to the right visual field, that will be transferred to the left hemisphere of the brain. *B*: The grid pattern is reproduced at the level of the primary visual cortex (V1). The mapping from visual field to V1 is termed *retinotopic*, because it continuously preserves the topology of the retina. The central zone of the visual field is processed with great precision: It is processed by many neurons in V1, comparatively to the periphery. Mathematically, the mapping from visual field to V1 is well approximated by a log-polar scheme. From Tootell et al, 88 [149].

pathway. In humans and primates, V1 has been found to display a variety of neurons that form retinotopic maps of the visual field in a log-polar mapping, with many more neurons associated to the central region of the visual scene (see Figure 1.5). This predominance of the central region of the visual field reflects the architecture of the retina: in primates and humans, the center of the retina, termed the *fovea*, has a much greater spatial resolution than the periphery, with a greater density of retinal cells (see Section 2).

A striking feature of V1 is that several different types of visual informations are simultaneously mapped on the surface of the cortex. At each location of the visual field, the activity pattern at the corresponding location in V1 codes simultaneously for different features:

- The orientation of image contours at this location. If a contour is present at this location of the visual field, some cells in V1 will respond preferentially, but only if the contour is along their preferred orientation.
- Ocular dominance. Many V1 cells are only sensitive to input from one specific eye. Some cells are equally sensitive to both eyes.
- Color information. Specific cells in V1 code for red/green and blue/yellow color oppositions.

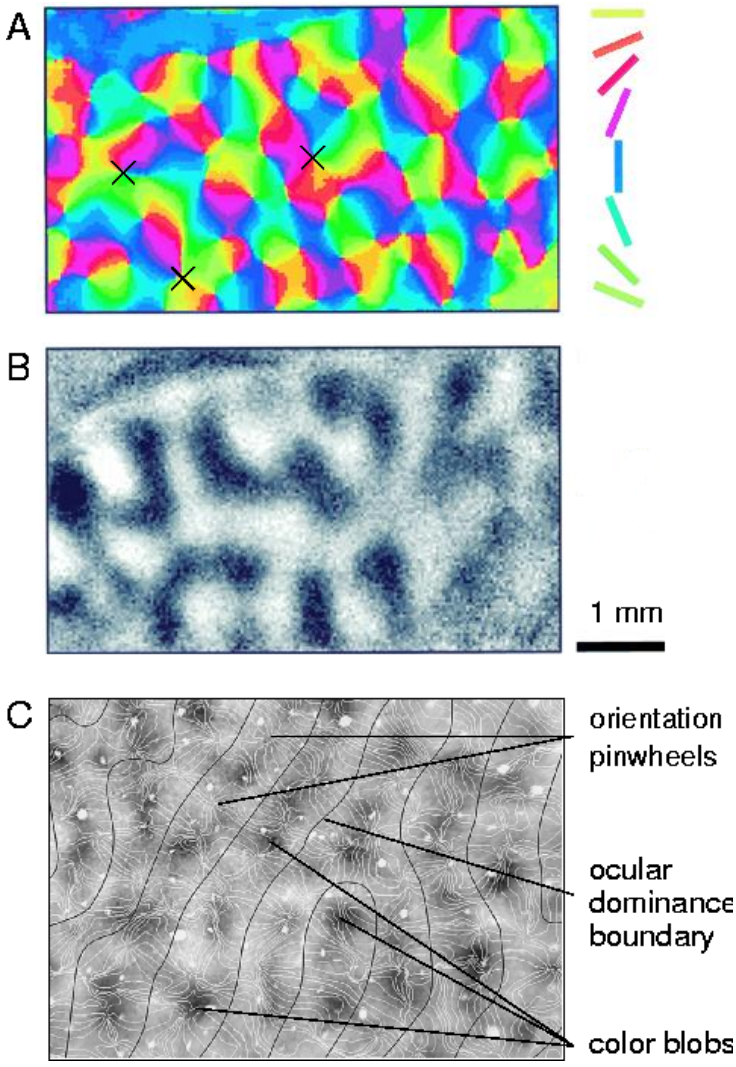

Figure 1.6: Simultaneous mapping of different visual features in the primary visual cortex. *A*: Orientation preferences in V1. Most V1 neurons respond preferentially to image edges in a particular orientation. Neurons are organized around 'orientation pinwheels', which are the singularities in the mapping of preferred orientations (examples marked with a cross). From [72]. *B*: Ocular dominance. Neurons in V1 respond preferentially to stimulation from one eye or the other. Scale for *A* and *B* represents 1 mm of visual cortex. From [72]. *C*: Color blobs, orientation preferences and ocular dominance. Aside from ocular dominance and orientation, V1 codes for color oppositions in special zones called cytochrome-oxydase (CO) *blobs* (in darker shade). Cells in the blobs are sensitive to color, and less sensitive to edges of high spatial frequency. Cells in interblobs (lighter shade) do not code for color, but respond to edges of high spatial frequency. The three simultaneous mappings (orientation, ocular dominance, color) have very correlated spatial structures. From [14].

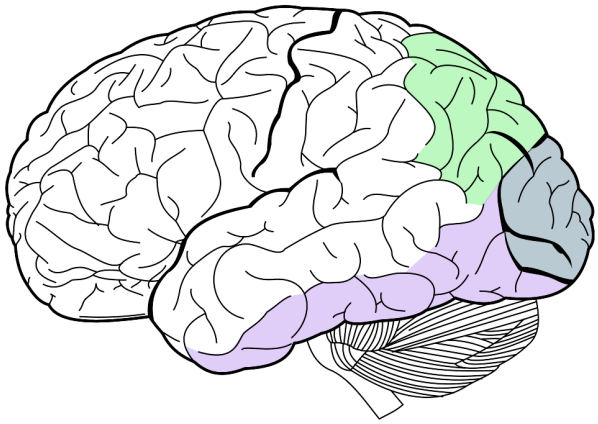

Figure 1.7: Ventral (purple) and dorsal (green) pathways schematically represented in the brain. Areas in the ventral - or 'What' - pathway are involved in precise form analysis and object recognition. Areas in the dorsal - or 'Where' - pathway are involved in general scene and motion analysis.

The spatial organization of these different maps on a single two-dimensional surface of cortex is achieved through a complex multi-dimensional organization of V1 neurons around typical structures called 'pinwheels' [75], as illustrated in Figure 1.6.

1.4 Ventral and Dorsal pathways of the visual system

From V1, the primary cortical input, several other cortical areas proceed to more advanced processing of the visual information. These cortical areas can be associated to two distinct pathways of visual processing, largely independent. The *ventral* pathway, which involves areas such as V2, V4, V8, etc. is mostly dedicated to precise analysis of shape, texture, color, object recognition, etc. It has been termed the 'Form', or 'What', pathway of the brain. By opposition, the *dorsal* pathway, involving areas such as V2, MT(V5) or MST, is dedicated to rough analysis of the visual scene as a whole, and of various movements in the visual field (objects, self-motion, etc.) It has been termed the 'Motion', or 'Where' pathway. These two distinct pathways are schematically represented in Figure 1.7.

The connections between various visual areas in the cortex are not obvious, and are less and less well understood as one gets to higher levels of processing. Many modulation feedbacks and thalamic relays strongly participate to the processing of visual information.

2 THE RETINA: A LAYERED NEURAL STRUCTURE

The retina is the neural entry of the visual system: It contains the first visual neurons, that convert the incoming light into an electrical signal sent to the brain. Here, we present a general anatomy of the retina. The main functions of the different types of retinal cells are evoked, providing landmarks for the detailed analysis that follows in Chapters 2 and 3.

2.1 Layered architecture of the retina

Visual cells in the retina are organized following a layered architecture, from light receptors responsible for the acquisition of incoming light, to ganglion cells that send the visual information to the brain in the form of *spike trains*. The successive layers of cells naturally define a functional architecture for the retina.

2.1.1 Five layers of cells

The retina contains five different types of visual neurons, that convey visual information thanks to their electrical activity. Figure 1.8(a) shows a section of a real mammalian retina and its anatomical interpretation. Cells of the same type are organized along layers, paving the whole retina. Layers are connected as described in Figure 1.8(b), and summarized in Figure 1.9. The five types of cells are:

- Light receptors
- Horizontal cells
- Bipolar cells
- Amacrine cells
- Ganglion cells

Their respective roles are briefly exposed in Section 2.2. We start by a general description of these cells and how they are organized in the retina.

Signal transmission in the retina

A first issue concerns the mode of electrical transmission used by neurons in the retina. In the brain, most neurons fire action potentials, or *spikes*, which are stereotyped electrical impulses well suited to relay the neural signal over long distances, along the neurons' axons (an axon is a typical elongated structure possessed by many cortical neurons to project their message far from their cellular body). Spikes form the basis of the neural code in the cortex.

By opposition, most retinal cells do note fire spikes. They are very localized cells, and most types do not possess any well-defined, elongated axon. Rather, retinal cells form organized mappings, with

only local connections between neighboring cells, which occur mostly through dendrites or small axonic processes. Instead of displaying spike trains, most retinal neurons respond through graded, 'continuous' electrical signals. Such graded transmission is well-suited for a structure like the retina, where the cells form very local connections.

As an exception, the output cells of the retina, called ganglion cells, have long axons which form the optic nerve to the brain. These cells fire spikes, in order to rapidly transmit the electrical information to the brain, along the long distance of the optic nerve.

An organization in layers

Retinal cells are organized in *layers*: Cells of the same type pave the whole visual field by forming a homogeneous and dense array of cells. As a strong expression of this layered architecture, neighboring cells of the same layer are linked one to another through **electrical synapses**, also called **gap junctions**, small ionic channels allowing the bidirectional circulation of ions between the cells' two cytoplasms. These junctions are present with different strengths in each of the five layers, and result in a local sharing of the information between cells of the same type. Functionally, this local sharing of information has many advantages, as detailed in Chapter 2, Section 6.

2.1.2 Synaptic connections between retinal layers

Neighboring cells from different layers are also linked one to another, this time through **chemical synapses**, i.e., mono-directional junctions involving neurotransmitter release from a pre-synaptic cell to a post-synaptic cell. Amongst neurons, some are *excitatory*, releasing neurotransmitters that tend to depolarize, or excite, their post-synaptic cells. Others are *inhibitory*, releasing neurotransmitters that tend to hyperpolarize, or inhibit, their post-synaptic cells. In the retina, both types of neurons are present.

Excitatory pathway. In the retina, light receptors, bipolar cells, and ganglion cells are excitatory neurons. They are represented in red in Figure 1.9, and their synaptic connections are depicted by red arrows. The synaptic pathway defined by the transmission *receptors→bipolar→ganglion* is thus a 'direct' excitatory pathway, that transmits the visual signal from the first cells of the processing (receptors) to the last (ganglion cells).

Inhibitory modulation. By opposition, the retina contains two types of inhibitory neurons: horizontal cells and amacrine cells. They are represented in blue in Figure 1.9, and their synaptic connections are depicted by blue arrows. As seen in Figure 1.9, inhibitory neurons are involved in 'indirect' signal transmission, in particular in feedback connections: horizontal cells onto light receptors, or amacrine cells onto bipolar cells.

Both horizontal and amacrine cells mediate modulation mechanisms, which serve to control and shape transmission through the 'direct' excitatory pathway. They have very important functional roles in the retina. They also have very *diverse* roles, especially amacrine cells which exist under various subtypes with different functionalities, not always well understood.

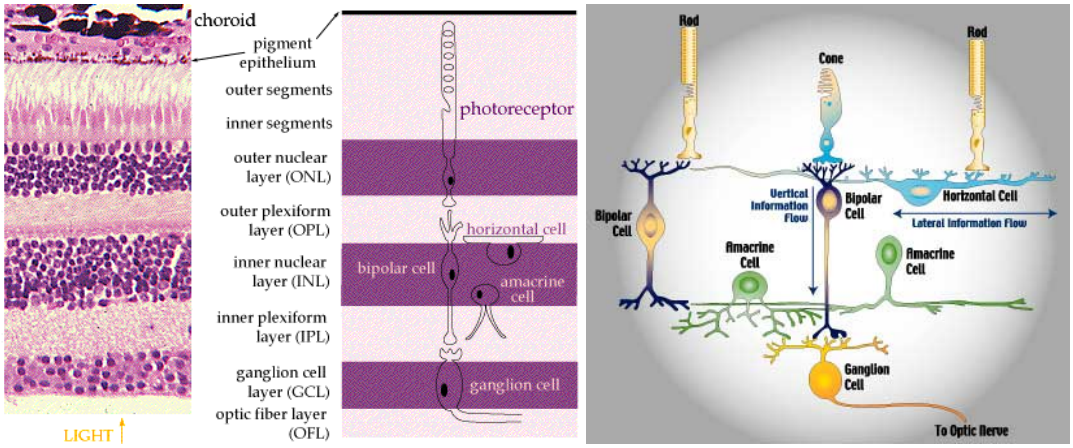

(a) Vertical section of a retina (b) Five retinal cell types

Figure 1.8: (a) Vertical section of a retina. There are five cell types, whose nuclei are located in three layers, and that make their synaptic connections in two plexiform layers. From [98]. (b) Schematic view of the five cell types and their connections. Found at [29].

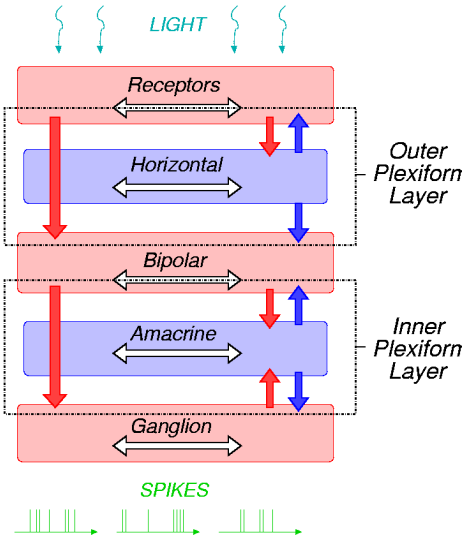

Figure 1.9: Schematic representation of retinal architecture. Excitatory cells are in red, inhibitory cells in blue. The direct excitatory pathway from light receptors to ganglion cells (thick arrows on the left) is modulated by the interstitial, inhibitory cells (small arrows on the right). Neighboring cells of the same type are generally linked through gap junctions (white horizontal arrows). Two distinct synaptic layers, the OPL and the IPL, define two successive filtering stages with similar excitatory-inhibitory patterns.

Two synaptic stages. All chemical synapses occur in two distinct layers, formed only of synaptic processes (Figure 1.8-a): the Outer Plexiform Layer (OPL) and the Inner Plexiform Layer (IPL)[4]. These two layers of synapses define *two (almost) independent processing stages*. The two layers are also represented functionally in Figure 1.9.

The OPL defines a first filtering structure through the interaction of light receptors, horizontal cells and bipolar cells. It is thought to mediate spatial oppositions that allow the retinal output to enhance image edges. The IPL defines a second filtering structure through the interaction of bipolar cells, amacrine cells and ganglion cells. It is thought to mediate additional spatio-temporal shaping of the visual signal.

2.1.3 Parallel pathways

Each type of retinal cell (receptor, horizontal, bipolar, amacrine and ganglion) exists under a variety of sub-types, with different morphological and physiological characteristics: Typical sub-types in a mammalian retina are represented in Figure 1.10. These sub-types are not connected to their neighboring cells randomly. Rather, distinct sub-types of cells connect into distinct pathways, and make the retinal output a combination of several parallel signals with different spatio-temporal properties. In terms of filtering, this means that the diagram in Figure 1.9 exists in several, parallel versions involving different sub-types of cells. Examples of different coexisting retinal pathways include ON or OFF cells, parvo- and magno- cells, color opponent cells... The main retinal pathways are detailed in Chapter 3, Section 3.

2.2 Functions of different retinal cells

We now provide a first, very general presentation of the different types of retinal cells, without mentioning the various sub-types and pathways. We just present the main roles of each type of cell.

Receptors

Receptors receive, sample and integrate the light arriving at the back of the eye. They are of two kinds: *cones* and *rods* (both represented on top of Figure 1.8-b).

- Cones are activated at high illumination levels (daytime, termed *photopic* light conditions). They are the most useful source of information for the 'form' pathway of the visual system (involved in precise shape analysis and object recognition, see Section 1.7). In primate and human retinas there are three types of cones, sensitive to different wavelengths (Red, Green and Blue): cones encode color. Figure 1.11 shows a paving by cones in a primate retina.
- On the contrary, rods exist in a single version: They only see 'in black and white'. Rods are very sensitive to light, and their response saturates at high illumination (daytime). They are much more numerous than cones. The rod signal is most useful at night (*scotopic* light conditions), and for the 'motion' pathway of the visual system (Section 1.7). Phylogenetically, rods seem to have appeared later in the evolution.

[4] Their name refers to the network (*plexus*) organization formed by the numerous synapses.

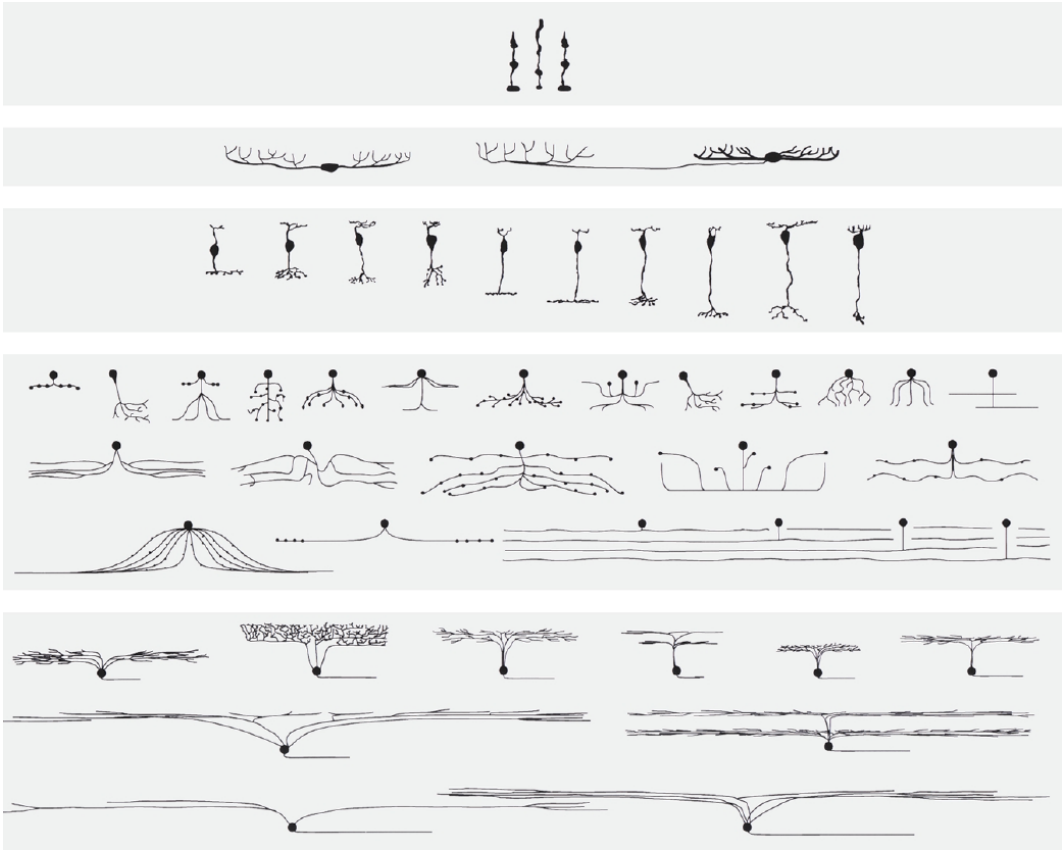

Figure 1.10: *Major types of cells in a typical mammalian retina.* From top to bottom: *Photoreceptors* are rods and two types of cones (three in some primates including humans). *Horizontal cells* exist in two major morphological subtypes termed *A* and *B*. *Bipolar cells*, present under 11 subtypes in primate retinas, have a typical elongated structure. *Amacrine cells* are the most various type of cell: 29 subtypes have been reported [92] that fall into two broad categories: small-field and wide-field cells. *Ganglion cells*, the output spiking cells of the retina, exist in 10 to 15 morphological subtypes in mammals. Images from the rabbit retina, except bipolar cells (rat retina). From Masland 01 [92].

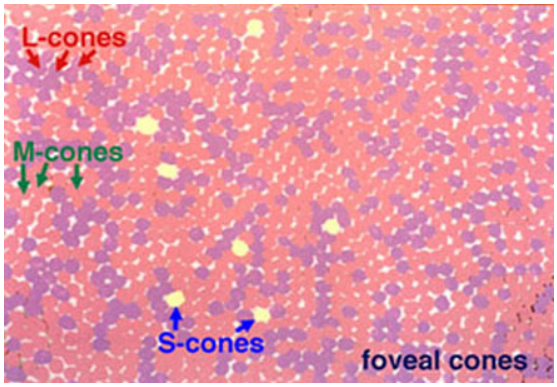

Figure 1.11: Paving of a primate fovea by cones. Notice how sparse short wavelength ('Blue') cones are. From [83], reproduced from *Lall and Cone, 1996*.

The integration of light by receptors is known as *phototransduction*. The output signal of the receptors is then transmitted to horizontal cells and bipolar cells, in the OPL.

Horizontal cells

Horizontal cells relay the signal from the receptors (through chemical synapses in the OPL), and are also highly coupled to their neighboring horizontal cells (through electrical synapses). This intra-layer coupling makes a horizontal cell sensitive to the *average* illumination in its neighborhood. Thanks to this measure of average luminance, horizontal cells modulate the transmission from light receptors to bipolar cells, in order to improve the invariance to luminance in the retinal output. Horizontal cells make feedback connections to receptors, and also feed-forward connections to bipolar cells.

Bipolar cells

In the OPL, bipolar cells are connected with both receptors and horizontal cells. But the sign of these two types of connexions are always different: If a bipolar cell is depolarized by the signal of receptors, it is hyperpolarized by the signal of horizontal cells, and vice-versa. Hence, a bipolar cell is always sensitive to a difference between the signal from receptors and its averaged version by the horizontal cells.

Such excitatory/inhibitory interaction is called a *synaptic triad*. The synaptic triad makes bipolar cells spatial and temporal *band-pass* filters: they behave like edge detectors. According to the respective signs of the connexions from receptors and horizontal cells, there will be ON-center cells and OFF-center cells (Chapter 3, Section 2).

Bipolar cells are also the input to the second filtering stage of the retina, the IPL. They possess an elongated structure with two dendritic trees (Figure 1.8-b), that gave them their name of 'bipolar'.

Amacrine cells

Synaptic transmissions in the IPL are relatively similar to those in the OPL, but less well understood. Indeed, amacrine cells, that play the same interstitial role as horizontal cells in the OPL, are a very *diverse* class of cells. They exist in various subtypes, many of which are still poorly understood. However, some specific subtypes (AII, starburst) are now well known.

Generally speaking, amacrine cells can be classified in two broad categories: Small-field and wide-field amacrine cells. Small-field amacrine cells are more involved into a temporal shaping of the retinal responses. Wide-field amacrine cells, some of which emit action potentials, are supposed to be involved in long-range synchronizations between the spike trains of neighboring ganglion cells.

Ganglion cells

Ganglion cells receive signal from bipolar and amacrine cells. They are the output of the retina, and they all fire *spikes* to the brain. They are the only retinal cells to possess a well-defined axon. The axons from ganglion cells form the optic nerve, and make their axonal terminations at the level of the LGN (Section 1.2).

2.3 Central vs. peripheral vision

When one wants to have a precise look at an object, one needs to move the eyes on it, so as to have the considered object projected at the very center of the retina. This is because in several species, the retina exhibits a particular radial structure, with a central region that displays a much higher density of cells and, subsequently, a much better image resolution than the periphery. This central region is known as the *area centralis* in cats and dogs[5]. In primates and humans, the central region is even more specialized and precise: It is called the *fovea*. In humans, it covers about 6 degrees of visual field, the size of a fist at arm length. Humans even possess a more precise zone in the very center of the retina (diameter of 1.5 degrees, one or two fingers at arm length) called the *foveola*, at the core of our ability to execute very precise visual tasks such as reading.

Radial densities of photoreceptors

Figure 1.12 shows the densities of both types of receptors in a human retina, as a function of eccentricity r (distance from the center of retina). The fovea is packed with cones, which are the most spatially and temporally precise type of light receptors. Then, the density of cones follows a typical power law, proportional to r^{-1}. This translates into our decreasing ability to precisely see objects far from the center of our retina.

On the contrary, rods are virtually absent from the fovea. The density of rods reaches its peak at around 20 degrees of eccentricity. Then it decreases slowly, but no power law exists as obviously

[5] Many mammalian retinas display an alternative structure known as the *visual streak*: A quite narrow horizontal zone that spans the whole width of the retina, and roughly corresponds to the projected location of the horizon on the retina. The density of cells and subsequent resolution is greater in this horizontal strip. For example, rabbits, horses and some species of dogs possess a visual streak. Cats, and some other species of dogs, possess *both* a visual streak and an even more precise *area centralis*.

as for cones. Rods are much more numerous than cones, especially in peripheral regions. The great number of rods allows the retina to detect subtle illumination changes through *population coding*, even in the daytime when they are mostly saturated. It makes rod signal a good basis for movement detection. The counterpart of rods' population coding is the loss of spatial acuity. For this reason, the fovea doesn't contain rods: It is dedicated to precise, daytime, shape analysis based on cone signals.

The organization of rods and cones in our retina is well-adapted to the way we use the fovea and periphery of our eyes. Thanks to the high sensitivity of rods, the retinal periphery is useful for coarse detections of movement or salient image features. In a second time, the detected feature can be analyzed more precisely by cones in the fovea, after an appropriate eye movement.

Radial structure of the whole retinal scheme

The density decrease with eccentricity r is not only observed for receptors, but also for all subsequent retinal cell types, including ganglion cells. At the same time, the sizes of the cells' dendritic trees (the arborescence of synapses connecting a cell to its pre-synaptic cells) increase with r. An example is given for ganglion cells the primate retina, in Figure 1.13.

The increase of dendritic trees with r is very coherent from the point of view of signal sampling: If receptors are seen as the discrete sampling of a continuous illumination signal, then a decrease in the density of receptors means a decrease of the sampling frequency. To avoid aliasing[6], the subsequent retinal cells must integrate the receptor signal from a larger region, which the cells insure by increasing the size of their receptive fields. Perceptually, the image becomes less precise far from the fovea.

Figure 1.13 illustrates the global scaling of dendritic trees with eccentricity r. The two types of ganglion cells measured here, Midget and Parasol, are discussed in Chapter 3. For the current discussion, it is sufficient to know that Midget cells take their input mostly from cones, whereas Parasol cells take a mixed input from cones and rods. The authors [32] estimate the average Midget dendritic trees to approximately scale with r, while Parasol cells' dendritic trees rather scale with $r^{0.65}$. These power laws are interesting to compare with the receptor densities illustrated in Figure 1.12, and in particular with cone density that grossly scales with r^{-1}. Midget cells receive their inputs mostly from cones, and their dendritic trees follow a law inversely proportional to cone density: this suggests that the whole cone pathway might scale with r. Conversely, Parasol cells receive a mixed input of rods and cones, and rod density decreases much slower than cone density. As a result, the Parasol receptive field size increases more slowly with eccentricity, with a power law approximated by $r^{0.65}$.

[6] In fact, aliasing removal starts as early as in the receptors' inner segments, which are electrically coupled one to another –see, e.g., Chapter 3, Section 2.3.

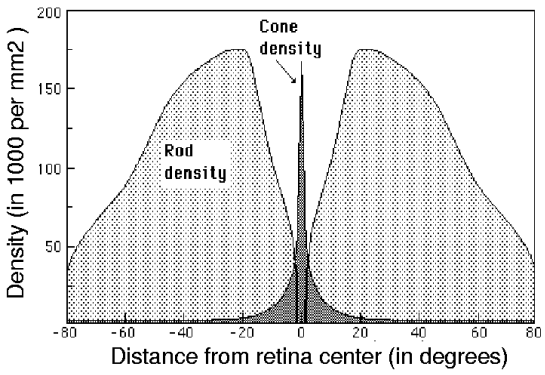

Figure 1.12: Density of receptors found in human retina. Reproduced from Osterberg 35 [111].

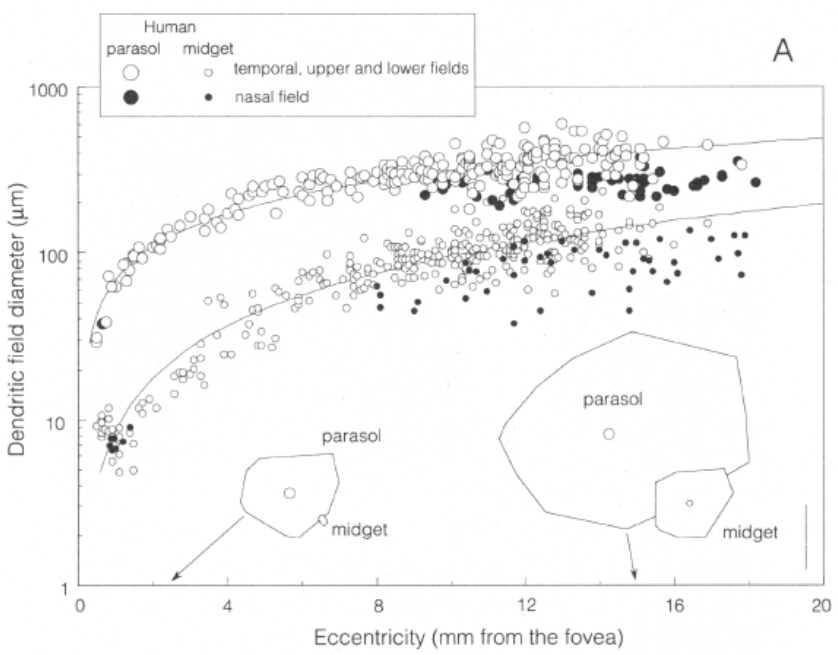

Figure 1.13: Measurements of ganglion dendritic tree sizes with respect to eccentricity, in the primate. The two sets of curves correspond to two distinct sub-types of ganglion cells, respectively Midget and Parasol cells. From Dacey-Petersen 92 [32].

3 GENERAL CHARACTERISTICS OF THE RETINAL OUTPUT

In this last Section, we present the main characteristics of retinal filtering: First, retinal cells are divided in ON and OFF pathways. Second, retinal cells display a preference for stimuli with a strong spatial structure (edges), thanks to a *center-surround* organization of their receptive fields. Finally, retinal cells can be distinguished according to their temporal behavior: Some cells, termed *transient*, respond by short peaks of activity and remain silent otherwise, while other cells, termed *sustained*, have a longer lasting activity in response to stimuli.

When light hits the back of the eye, it is absorbed by specific photopigments in the outer segments of the first retinal neurons, the light receptors. The subsequent mechanism, phototransduction, involves a complex cascade of catalyzed reactions, which end up in the creation of a light-induced electrical current, or *photocurrent*, through the membranes of light receptors.

After phototransduction has given rise to the photocurrent, connectivity of the subsequent layers of cells serves to shape and transform the visual signal, defining what we could term the retinal code. Finally, ganglion cells, which form the last layer of the retina, send the signal to the brain in the form of spike trains.

Historically, this spiking output has been the first and privileged subject of study for experimentalists. Naturally, a first reason is that the retina's functional importance lies precisely in the output of ganglion cells, as received and processed by the brain. A second, practical reason is that measurements were much easier than elsewhere in the retina: Ganglion cells are much larger than other retinal cells, whose small sizes make experimental measures difficult, in particular in mammalian and primate retinas. Also, ganglion cells fire spikes that are easily captured by extra-cellular recordings, whereas other retinal cells can only be studied by intra-cellular techniques.

In this section, we only focus on the properties of the retina's output, as measured from the emitted spike trains of ganglion cells. Physiological properties of the intermediate signals are discussed more thoroughly in Chapter 3.

3.1 Responses to light steps (ON and OFF cells)

The first distinction that can be made between retinal cells is their behavior in response to a sudden steps of light in their receptive field. Some cells respond strongly to light increments, while others respond strongly to light decrements. The first are termed 'ON', and the second 'OFF' cells. This property is illustrated in Figure 1.14, that presents schematized responses of ON and OFF cells.

ON-OFF symmetry. A first observation from Figure 1.14 is that qualitatively, ON and OFF cells seem to respond symmetrically: Their behaviors seem identical, except the response of an ON cell to a light increment is that of an OFF cell to light decrement, and reciprocally. In fact, the relative symmetry between ON and OFF cells also holds for more complex stimuli: As a first approximation, *an OFF cell responds to an image as an ON cell would respond to the image with inversed luminosity* (as a photograph negative).

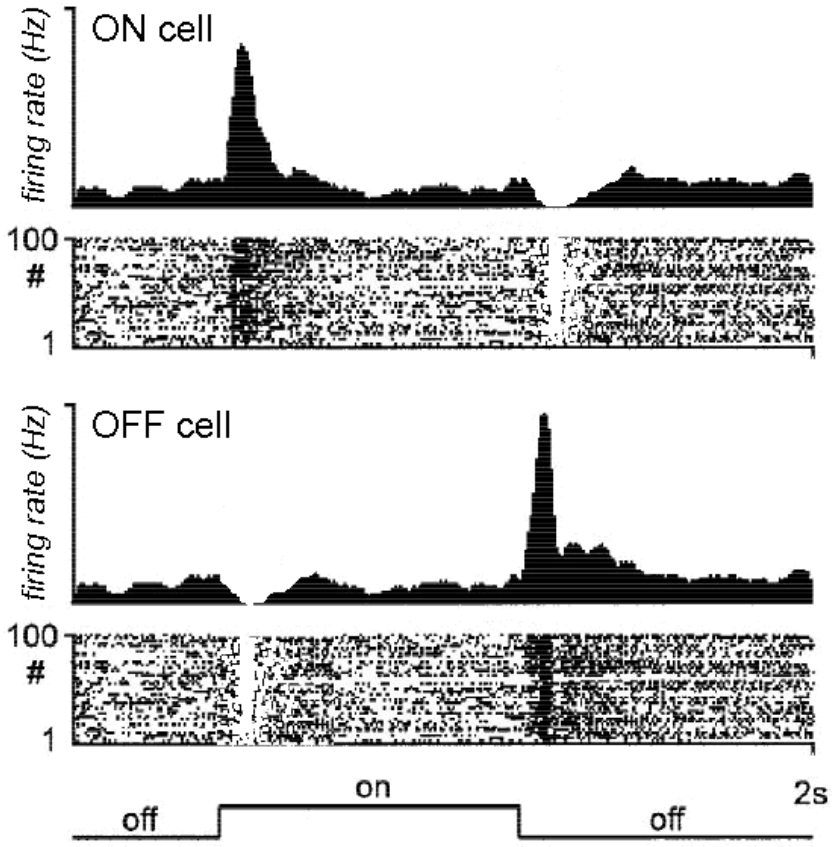

Figure 1.14: *Schematic behavior of ON and OFF cells.* In response to a uniform flash of light (of approximately 1 second, schematically represented in lower trace), ON cells (upper panel) respond at light onset while OFF cells (lower panel) respond at light offset. For each cell, the spike trains resulting from different trials can be considered separately as a raster plot, or summed in a histogram to consider the *average mean firing rate* in response to the stimulus. Figure is modified from real data: Two artificial ON and OFF raster plots are derived from the firing of a single perigeniculate ON-OFF cell in the cat thalamus, from [56].

ON-OFF asymmetries. At a more detailed level, several asymmetries exist between ON and OFF pathways. Examples of these asymmetries can be found in Chapter 3, Section 3.2.2.

Spontaneous firing activity. In the absence of visual stimulation (for example, in the dark), an important proportion of retinal cells already have a spiking activity, which is generally termed 'spontaneous'. By opposition, other cells are totally silent in the absence of a strong visual stimulation. Spontaneous activity can be observed in Figure 1.14, where the considered cells fire spikes throughout the whole stimulation, even when there is no specific stimulus to trigger them. A cell's spontaneous activity during an experiment can depend on the cell's intrinsic properties, but also on the general state of the network in the given experiment. It is thus a complex and ill-defined phenomenon.

Trial-to-trial variability and average firing rate. Finally, Figure 1.14 is the occasion for us to remind the concept of *average firing rate* for a spiking neuron: When the same experimental protocol is repeated several times on a neuron, the emitted spike trains show some variability between the trials, due to internal noise etc. The average firing rate is obtained by counting the emitted spikes over several repetitions of the same experiment, to obtain an 'average instantaneous activity' for the neuron in response to the stimulus. The average firing rate provides a more intuitive, and likely reliable, measure of the neuron's response. However, important information lying in the precise times of the spikes might be lost in the process. The problematic of spike coding is presented in Chapter 3, Section 4.

3.2 Center-Surround architecture (concentric cells)

Receptive field

As a necessary foreword, let us remind the notion of a cell's receptive field: The *classical receptive field* of a retinal cell is the area of the visual field where a light stimulation has an influence on the firing of the cell, when the rest of the visual field is not stimulated (gray field). Generally, in the litterature, this is the notion referred to when using the term 'receptive field'.

By opposition, the *non-classical* receptive field describes the visual region that has potential influence on the firing of the cell, although a light stimulation in this region does not modify the firing if the rest of the scene is a gray field. It is a secondary influence, requiring stimulation on the classical receptive field (see e.g. the LED cell in Chapter 3, Section 3.2.6).

In the retina, the (classical) receptive field of most ganglion cells displays a characteristical *center-surround* architecture.

Center-surround opposition

The center-surround architecture is probably the most well-known fact about retinal filtering. It was first observed in the mammalian retina by Kuffler in the 50's [84]. When a small spot of light is presented in front of a ganglion cell's receptive field, it evokes different reactions according to the precise location of the spot:

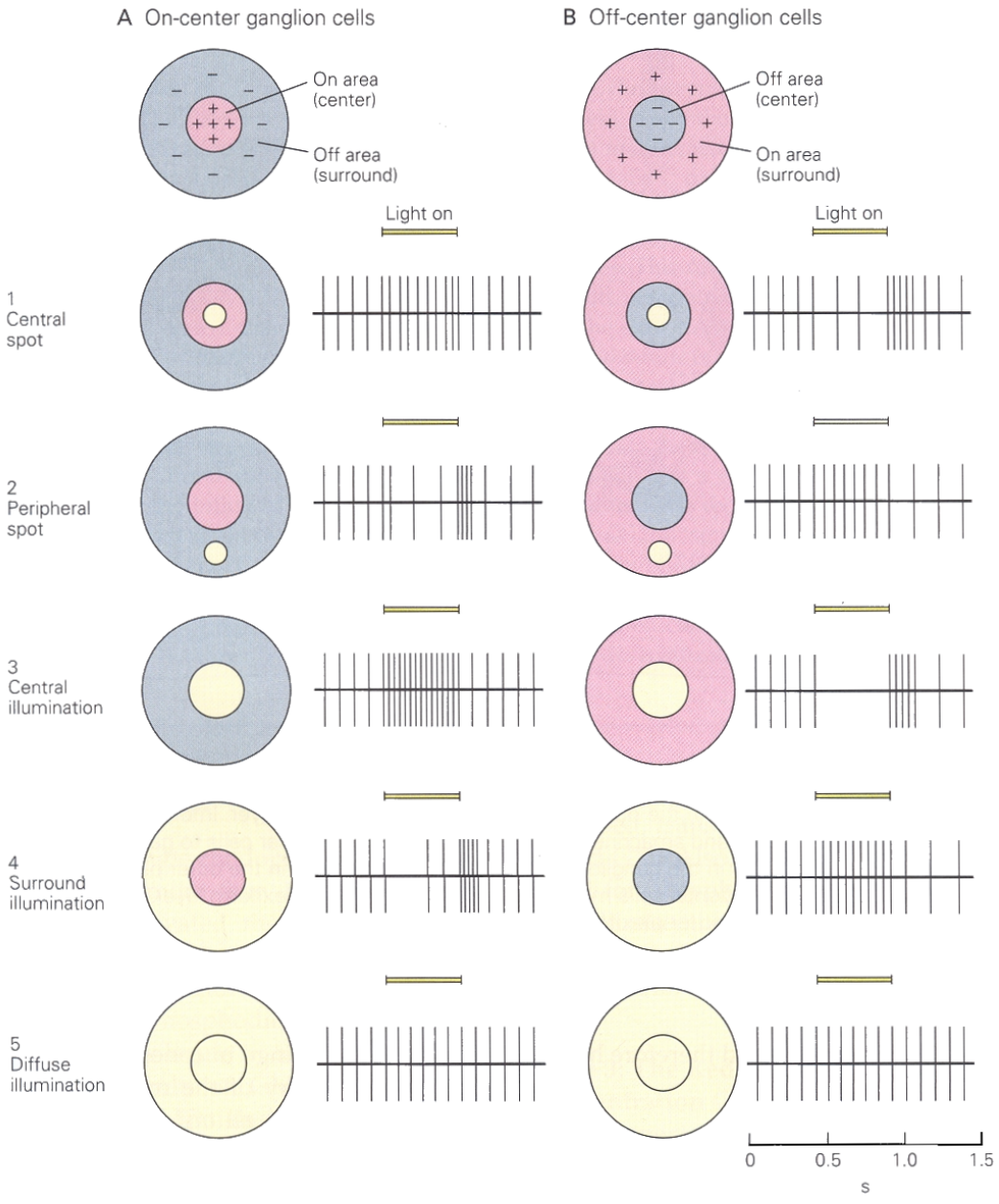

Figure 1.15: Response of ON and OFF retinal cells, with a center-surround architecture. Figure from [75], after the works of Kuffler [84].

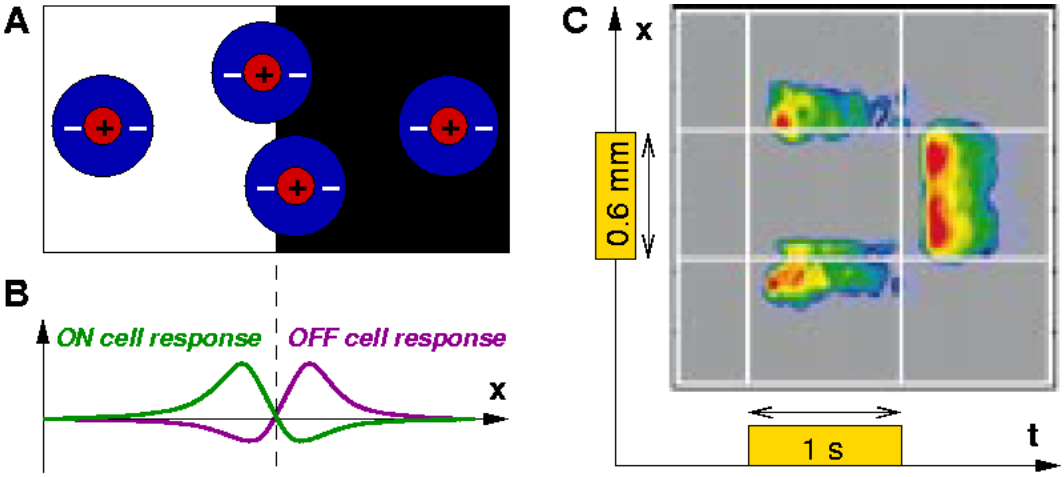

Figure 1.16: Edge detection via the center-surround architecture. *A:* Different locations of a center-surround receptive field, near an image edge. *B:* corresponding spatial profile of activity for ON and OFF cells, along a one-dimensional line perpendicular to the edge. *C: Edge detection in OFF-center ganglion cells of the rabbit.* The average firing rate of a one-dimensional line of cells (vertical axis), in response to a square spot of light, is represented at each time t (horizontal axis). From Roska-Werblin 01 [129], activity pattern inferred from the responses of a single cell (see text).

- If the spot is at the *center* of the receptive field, it elicits a positive response of the ganglion cell - that is, an increased firing of spikes.
- If the spot is at the *surround* of the receptive field, then it inhibits the ganglion cell: If the cell has a significant spontaneous firing rate, then this firing rate decreases when the spot is in the surround. If the cell has no spontaneous firing rate, the spot still has an inhibitory effect, making the cell harder to excite by a second simultaneous stimulus.

Both ON and OFF cells display a similar opposition. This is represented in Figure 1.15. Note that we have just enounced the center-suround behavior for an ON ganglion cell, stimulated by a spot of light brighter than the ambient illumination. For an OFF cell to have the same reaction, the spot should be *darker* than the ambient illumination. On the contrary, when an OFF cell is stimulated with a spot of bright light, it displays an opposite behavior: Stimulation in the center inhibits the cell, while stimulation in the surround excites it.

Edge detection

The center-surround architecture is well-known because of its important functional consequences: As a result, retinal ganglion cells act as detectors of *strong spatial contrast*, such as object edges.

Indeed, the *surround* signal provides an average of the illumination in the neighborhood of the cell, to which the more precise *center* can be compared, thus increasing retinal sensitivity to small details.

For example, when an edge is present in the image, the strongest responses are for cells located near the edge, such that:

- The *center* receptive field lies on a single side of the edge, providing strong excitation to the cell.
- The *surround* receptive field lies *accross* the edge, providing little inhibition on the cell.

This property is schematized in Figure 1.16 *A* and *B*. As an illustration of edge detection in real retinas, Figure 1.16 *C* presents a reconstructed recording for an array of rabbit OFF-center ganglion cells, in response to an appearing square spot of light. The simultaneous activity of a one-dimensional array of ganglion cells was recorded over time [7]. The square spot of light was on for a second. The size of the square was 600 μm on the retina, which corresponds roughly to the size of two fingers at arm length. Two simultaneous properties of OFF ganglion cells can be simultaneously observed in this recording.

First, during the presence of the square on the retina, these ganglion cells indeed have a strong response near to the square's edges. More precisely, strong responding cells are on the *dark* side of the square's edges, since they are OFF cells (see Figure 1.16 *B*).

Second, all cells have a strong activity at offset of the square (after one second), including cells which are not near the edges of the square. Indeed, all cells observe a sudden temporal light decrement at that instant, and respond to it because they are OFF cells.

This experiment is a good illustration of the *dual* coding, spatial and temporal, that simultaneously occurs in most ganglion cells.

Concentric vs. non-concentric receptive fields

Cells with a receptive field displaying a center-surround architecture are often termed *concentric*. In most mammalian retinas, concentric receptive fields form an important proportion of the retina's output cells (although the exact proportion is not well established, and varies according to the species considered).

However, non-concentric cells are also present in the retina, probably in a 'comparable' proportion. Such cells are generally less well understood. In most of them, a center-surround architecture still underlies their behavior, although modified or masked by subsequent interactions: See Chapter 3, Section 3.

A complex phenomenon

As we present in Chapter 2, a simple model of linear filtering, based on Difference-of-Gaussians (DOG) filters, accounts for several aspects of the center-surround opposition in retinal receptive fields. However, many questions remain unsolved concerning the center-surround architecture:

[7] In fact, the authors [129] used a smart experimental protocol where a *single* ganglion cell provided the whole reconstructed array: It was the square stimulus that was moved between successive trials, to obtain the response of the cell at each position relative to the square.

- The biological origin of the phenomenon is still controversial. The opposition is known to arise, at least in part, through synaptic interactions in the OPL. However, for many types of ganglion cells, interactions in the IPL have been found to largely contribute to the phenomenon (Chapter 3, Sections 2.3 and 3).

- Center-surround opposition is not a static feature in our retinas. For example, the relative size and influence of the *surround* varies according to the ambient level of light, through the influence of a particular class of dopaminergic amacrine cells. This particular adaptation effect is supposed to improve the signal-to-noise ratio (SNR) in dark conditions where the photocurrent is particularly noisy (Chapter 3, Section 5).

- The center-surround architecture is often associated to edge detection. But at a more detailed glance, the perceptual correlate of center-suround oppositions is not evident. According to the sizes and relative weights of *center* and *surround* receptive fields, the activity pattern of the cells can vary drastically (see Figure 2.2).

3.3 Temporal behavior (transient and sustained cells)

In Figure 1.14, it can be observed that the considered cells, ON or OFF, do not respond throughout the whole presence of their preferred stimulus, but only at *onset*. In other words, the depicted cells seem to be preferentially sensible to *temporal change*. This is in fact a very intrinsic behavior, shared by virtually all sensory neurons. This behavior is strongly related to the notion of information transmission, and can be explained intuitively: *If a stimulus is kept constant, then information transmission about this stimulus is redundant because it has already been transmitted in the past. As a result, after an initial phase of coding, the neuron needs not keep on coding for a constant stimulus*.

However, in the retina, strong differences exist between ganglion cells, concerning the shape and time scales of their temporal behavior. Figure 1.17 illustrates these differences, between *sustained* -or *tonic*- cells, and *transient* -or *phasic*- cells. The tonic-phasic opposition is a general concept in physiology that can be described in simple words: *"A tonic process is one that continues for some time or indefinitely after being initiated, while a phasic process is one that shuts down quickly"* [50]. Figure 1.14 displays two 'extremes' for transient and sustained cells: The transient cells (left column) respond for one or two hundreds of milliseconds only, while the sustained cells (right column) respond for a whole second.

Multiple origins of temporal transients

When considered in detail, the temporal response of retinal cells is an extremely complex phenomenon. Between the two extremes depicted in Figure 1.14, there is a huge variety of possible temporal behaviors, according to the type of cell, the stimulus it undergoes, and the species considered.

The explanation for this complexity is simple: Each biological relay of signal transmission (cellular integration, synaptic transmission, membranar ionic channels, control mechanisms...) has its typical temporal behavior, and internal time scale. The temporal behavior of retinal processing as a

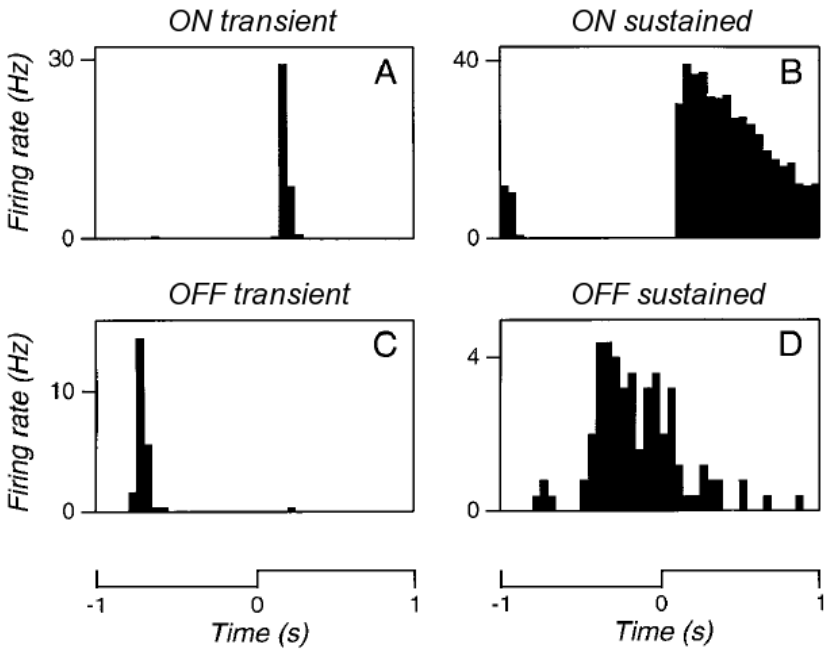

Figure 1.17: *Transient and sustained cells in the retina.* In response to a continuous stimulation, some retinal cells have a sustained response (right-hand side), while others have only a short response at stimulus onset (left-hand side). Sustained cells are termed *tonic*, and transient cells are termed *phasic*. Mouse retina, from [107].

whole, results from the addition of all these successive processing stages, and is thus a very complex and *distributed* phenomenon.

For example, the fast shutting down (a few hundreds of milliseconds) of the *transient* cells in Figure 1.14 results largely from a network architecture: These cells receive a delayed inhibition from other cells, that helps to cut their response. By opposition, the slow decrease in the response of the *sustained* cells in Figure 1.14 is largely due to slow cellular adaptation: A general 'calming down' of all neurons in the pathway due to the stationarity of their responses. We refer to the next chapters for more details.

As a result of the distributed nature of the retina's temporal behavior, a large-scale model must introduce some drastic simplifications regarding temporal processing. Some functional principles must be found, that yield both conceptual simplicity and a relative similarity with the real retinal output. In particular, we believe that temporal behaviors in the retina could be better understood if they were related to information-theory calculations and interpretations.

CONCLUSION

In this chapter, we have presented an overview of retinal filtering and its role in the larger scheme of our visual system. The two following chapters study in more details the retinal properties introduced here. Chapter 2 takes the modeler's point of view by introducing linear filtering, an unavoidable tool to model retinal function. By opposition, Chapter 3 takes the experimentalist's point of view, going further into the architecture and physiology of real retinas. Both chapters must be seen as serving a common purpose: Find a model that can encompass the *functionality* enbedded in the retina's complex physiology.

CHAPTER **2**

LINEAR APPROXIMATIONS AND MODELING

In this chapter, we present the linear tools which are widely used to account for retinal filtering. Linear filtering is a necessary tool for a retinal model. First, it is a conceptually simple and mathematically well-defined framework for which a powerful theory is available, e.g., thanks to Fourier analysis. At the same time, linear models have a lot of experimental successes, yielding many correct predictions of real data. As a result, linear filtering is a strong component of virtually all retinal models, including those which possess additional nonlinear properties.

Contents

1 INTRODUCTION: LINEAR RECEPTIVE FIELDS

Consider a retinal cell centered in (x_0, y_0) on the retina, with a receptive field RF having (x_0, y_0) as its spatial origin. A linear approximation of its activity consists in finding the spatio-temporal kernel $K(x, y, t)$ for which the following equation is best verified:

$$A(t) = \int_{u=0}^{+\infty} \int_{(x,y)\in \mathrm{RF}} I(x_0 - x, y_0 - y, t - u)\, K(x, y, u)\, dx\, dy\, du, \tag{2.1}$$

where $I(x, y, t)$ is the luminance profile of the image, and $A(t)$ is a measure of activity appropriate to the type of cell (its membrane potential if it is a non-spiking cell, or its firing rate if it is a spiking cell). This is a formal way to write that $A(t)$ depends linearly on all past values for the input image I located in the cell's receptive field RF. By extent, K is often described as the *linear receptive field* of the cell.

Convolution

In fact, the operation performed in (2.1) corresponds to the well-defined mathematical concept of *convolution*. Accordingly, (2.1) can be rewritten:

$$A(t) = \big(I * K\big)(x_0, y_0, t), \tag{2.2}$$

where symbol $*$ denotes spatio-temporal convolution. Fourier analysis is particularly suitable for the study of that kind of filter, because convolution corresponds to multiplication in the Fourier space.

Separating time and space

Often, one desires to study separately the spatial and temporal properties of filtering for the cell. For example, one can craft a input sequence whose spatial structure at each time t is entirely defined by a single number $I(t)$ (for example, a uniform flickering screen, or a static image whose illumination is modulated in time). In this case, the temporal behavior of the cell can be studied linearly by:

$$A(t) = \int_{u=0}^{+\infty} I(t - u)\, K_{\mathrm{temp}}(u)\, du.$$

Conversely, one can only be interested in some measure of the cell's activity, in response to a static image $I(x, y)$. This can be linearly modeled by:

$$A = \int_{(x,y)\in \mathrm{RF}} I(x_0 - x, y_0 - y)\, K_{\mathrm{spat}}(x, y)\, dx\, dy.$$

However, in this case, the exact nature of activity A is more ambiguous, and depends on the nature of the experiment. It can be an equilibrium activity for the cell (after waiting for sufficiently long – but remember that in most cases, cellular activity to a static stimulus declines over time). Rather, it

can be a peak of activity, soon after image onset. Also, it can be some integrated measure of activity over time.

In fact, linear kernels for retinal cells are generally *non-separable* in time and space: The best-fitting linear kernel $K(x, y, t)$ cannot be written as a product $K_{\rm spat}(x, y)K_{\rm temp}(t)$. As a result, all reductions to either temporal or spatial properties only necessarily imply a loss of information: Measuring separately filters of the form $K_{\rm spat}(x, y)$ or $K_{\rm temp}(t)$ through specific experiments, does not allow to reconstruct the best spatio-temporal filter.

To conclude, many magnitudes measured in different experiments can be approximated by linear models. Such magnitudes include: Average firing rate, peak of activity for a cell, synaptic inputs to a cell, etc. According to the experiment, the accent can be put on the whole spatio-temporal pattern of the stimulus, or on simpler expressions of the stimulus that are temporal only or spatial only. In the second case, information is lost about the 'real' spatio-temporal kernel, because retinal receptive field is generally not separable.

Whatever the experiment, the best-fitting linear kernel will always be an approximation that depends on the particular experimental conditions. A different experiment, especially at different illumination levels, will provide a different best-fitting linear kernel, although probably related to the first one. This is because many nonlinear adaptation factors influence retinal processing (Chapter 3,Section 5).

In Sections 2 and 3, we present separately spatial and temporal linear approximations for the retina. In Section 4 and 5, we present more general tools of linear modeling.

2 CENTER-SURROUND ORGANIZATION AND THE DIFFERENCE OF GAUSSIANS

The DOG model

In the 60's, Rodieck [126] and Enroth-Cugell and Robson [48] showed that the spatial center-surround opposition is well approximated by a filter consisting of a Difference of Gaussians:

$$K_{\rm spat}(x, y) = w_C G_{\sigma_C}(x, y) - w_S G_{\sigma_S}(x, y), \tag{2.3}$$

where w_C and w_S are the respective weights of the *center* and *surround* components of the receptive field, and $G_\sigma(x, y)$ is a normalized, two-dimensional Gaussian function of standard deviation σ:

$$G_\sigma(x, y) = \frac{\exp\big(-(x^2 + y^2)/(2\sigma^2)\big)}{2\pi\sigma^2}. \tag{2.4}$$

By 'normalized', we mean that the spatial integral of G_σ is 1: When applied as a filter, it has a linear gain of 1, so that the linear gains are only fixed by w_C and w_S. The DOG approximation of retinal receptive fields is illustrated in Figure 2.1 *A*.

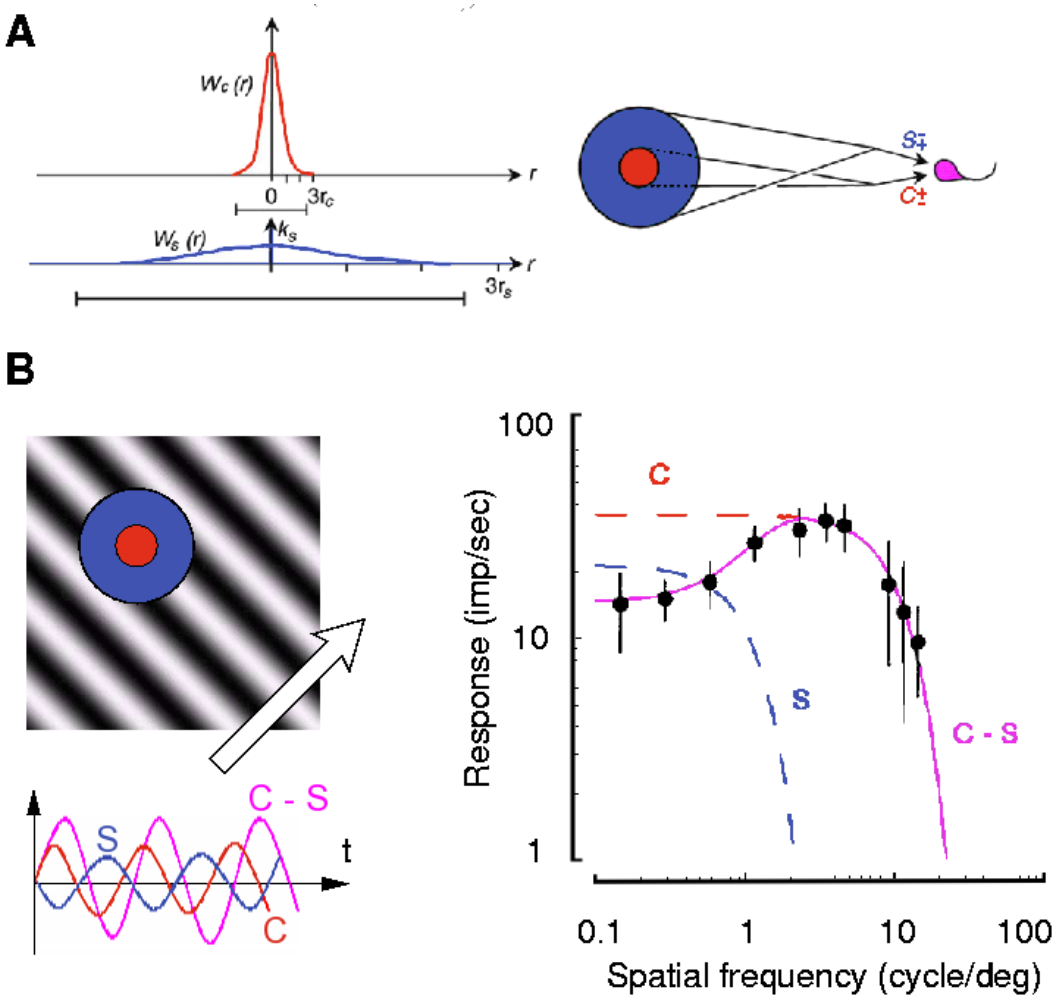

Figure 2.1: *A:* The Difference-of-Gaussians (DOG) approximation for center-surround receptive fields. Reproduced from [83], and the original works of Enroth-Cugell and Robson 66 [48] *B:* Response of a primate ganglion cell to drifting gratings of different spatial frequencies is by a DOG model. The measured output is the amplitude of the cell's center, surround, and total response. Drift frequency of 4 Hz. From Croner-Kaplan 95 [30].

Figure 2.1 *B* shows an application of the DOG model to predict the response of a primate ganglion cell to gratings of different spatial frequencies [30], measured as the amplitude of variation in the cell's firing rate. This type of study is closely related to Fourier analysis: The output log-log curves in Figure 2.1 *B* represent the amplitude of the Fourier transform of the cell's best fitting linear kernel $K_{\mathrm{spat}}(x, y)$. In this particular experiment, the fit is very good.

Not all retinal cells are well fit by a DOG model. Some cells have a very linear spatial behavior (X cells in cat, Parvo cells in primate...). They generally coincide with the spatially precise cells, that provide input to the *Form* pathway of the brain. Other cells display a strong spatial nonlinearity (Y cells in cat, M cells in primate...). They generally coincide with the temporally precise cells, that provide input to the *Motion* pathway of the brain (see Chapter 3, Section 3).

Remark: Note that in the experiment of Figure 2.1 *B*, this particular measure of 'spatial' response also relies on temporal properties, since the grating *drifts* in front of the cell with a temporal frequency of 4 Hz. It allows to directly calculate the 'spatial amplitude' of the cell's response with a single trial, since the output amplitude of response directly accounts, through temporal integration, for all possible spatial phases of the grating in front of the cell.

By opposition, one could get another measure of a spatial linear kernel, from the responses of the cell to purely static images. This would be more complicated, because: (i) In response to a static image, the cell's response is transient at image onset, then declines; so the measure of activity is less reliable (e.g, amplitude of the transient peak). (ii) One would have to do several trials with different spatial locations of the grating in front of the cell, to reconstruct a 'two-dimensional map' of the cell's responses to the grating, and measure amplitudes of variations among this map.

Whatever the experimental protocol chosen to do this, some temporal information (phases for the cell's responses) interferes with the 'purely spatial' information sought by the experiment, because the cell's real receptive field is not separable (see Section 4). As a result, the 'spatial' linear filters measured through both experiments would surely display slight, but relevant, differences. ■

Parameter fitting in the DOG model

The DOG model in (2.3) is driven by four parameters. Here, we review the functional importance of each of these parameters, and compare it with its experimental estimations. Our goal is to illustrate how hard it is to link a cellular model with functional and perceptual consequences, even using a simple retinal model such as the DOG (linear, and with a spatial behavior only). From the point of view of functional image transmission by whole layer of cells, the parameters of the DOG model have the following interpretation:

- **Spatial resolution** σ_C. This is a measure for the 'fundamental' blur applied to the light image hitting the retina. From a signal processing point of view, it defines the spatial frequency cut-off of retinal filtering. The width of the *center* signal has several biological origins, starting with the sampling frequency of light receptors. Furthermore, a local sharing of information between neighboring light receptors (Chapter 3, Section 2.3), helping to prevent aliasing and reduce phototransduction intrinsic noise, also contributes to the width of σ_C.

  A fundamental difference between the retinas of different species lies in their spatial resolution, as measured from the extent of their *center* signal. For example, in the mammalian

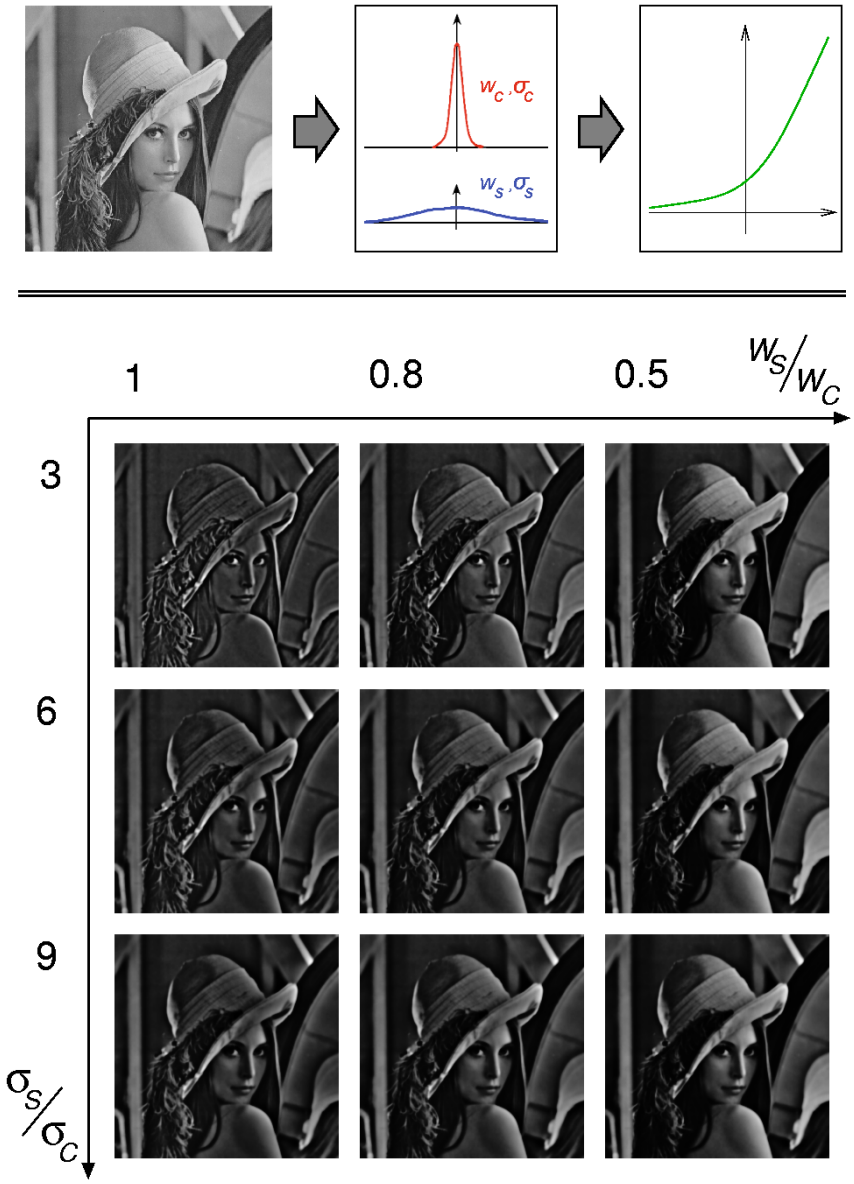

Figure 2.2: Perceptual impact of parameters in the DOG model. *Up:* Input image is convoluted with a DOG filter of parameters $w_C = 1$, $\sigma_C = 2$ pix, and with various values for σ_S and w_S. To provide a 'biological' output for ON cells, the resulting images are normalized between -1 and 1, and passed in a smooth static rectification, as inspired by LN models (see Section 5). *Down:* Results, for various sets of biologically-plausible *surround* parameters. When large-scale filtering is inferred from a DOG model, the perceptual output can vary a lot depending on the parameters chosen. In particular, edge detection can be obvious (upper left image) or not (lower right images).

retinas, cells with the smallest receptive fields have different scales according to the species considered: σ_C can be as small as 0.03 deg in the primate[30], but is rather around 0.3 deg in the cat[48], reflecting that the cat vision is several times less precise than our central foveal vision.

- **Linear gain** w_C. This gives the orders of magnitudes for retinal amplification, from input luminance (various possible units) to a spiking activity (generally in impulses/sec). In fact, this 'linear gain' is all but a constant: It is highly controlled, in a nonlinear fashion, by statistics of the input image such as luminance or contrast. All these nonlinear mechanisms are generally termed *gain controls*, and are an expression of retinal *adaptation* (Chapter 3, Section 5).

- **Relative *surround* extent:** $\frac{\sigma_S}{\sigma_C}$. Expressed relatively to the 'fundamental' precision of the retina as measured by σ_C, the extent of the best-fitting Gaussian for the *surround* is highly variable across retinal ganglion cells, even across cells supposedly of the same sub-type. For example, Enroth-Cugell and Robson 66 [48] measured relative extents of the *surround* that ranged roughly from 3 to 10.

  Biologically, this fact probably has a moderate importance: after all the DOG model is just an approximation. Combined with a natural cell-to-cell variety, a three-fold variation in the ratios is not so surprising. However, when pasted into a functional model, the extent of the *surround* has strong perceptual consequences: see Figure 2.2. In particular, it raises the question to what extent the *surround* signal allows edge detection, or simply increased invariance to luminance.

- **Relative *surround* weight:** $\frac{w_S}{w_C}$. Similarly, the best-fitting weights for *center* and *surround* are biologically measured to display a strong cell-to-cell variability. For example, in Figure 2.1 *B*, the weights w_C and w_S can be measured in response to a 'uniform screen' stimulus, i.e, for low spatial frequencies (left of the diagram). One thus reads $w_C \simeq 12.5$ and $w_S \simeq 11$, so that they are in a ratio of approximately 0.9.

  Amongst cat X cells, Enroth-Cugell and Robson 66 [48] measure relative weights ranging from 0.8 to 0.95. An even stronger variability can be observed in other species/pathways (Chapter 3, Section 3). Again, this raises questions about these cells really being edge detectors, as illustrated in Figure 2.2.

Whatever these perceptual issues, the DOG model remains a strong and important influence throughout all retinal models. Also, it presents an excitation-inhibition structure that has a direct equivalent at the level of temporal filtering, and temporal linear models.

3 LINEAR MODELS FOR TEMPORAL TRANSIENTS

Exponential and Gamma functions

The linear modeling of temporal delays and transients in the retina is very close to the spatial DOG modeling, except that the base filter is not the Gaussian, but the Exponential and/or Gamma filters:

$$E_\tau(t) = \frac{1}{\tau}\exp(-t/\tau), \tag{2.5}$$

$$E_{n,\tau}(t) = \frac{(nt)^n}{(n-1)!\tau^{n+1}}\exp(-nt/\tau), \tag{2.6}$$

if $t > 0$, and zero otherwise. We refer to filter (2.5) as the Exponential filter, and to filter (2.6) as the Gamma of order n. These filters are normalized to have a temporal integral of one. Unlike Gaussian filters, these filters are null for $t < 0$, which means that they are *causal* filters: This insures that, in the linear model, the present state for the cell is linearly calculated only from the past values of the input stimulus.

These filters also have the nice property to all result from self-convolutions of an Exponential filter. One has:

$$\underbrace{E_\tau \overset{t}{*} E_\tau \overset{t}{*} \cdots \overset{t}{*} E_\tau}_{n+1}(t) = \frac{t^n}{\tau^{n+1}n!}\exp\left(-\frac{t}{\tau}\right) = E_{n,n\tau}(t). \tag{2.7}$$

where sign $\overset{t}{*}$ denotes temporal convolution. The Gamma filter can thus also be termed an '*Exponential Cascade*' filter: It is obtained as a succession of low-pass Exponential filters with similar time scales. Conversely, the Exponential filter is the Gamma filter of order 0. In fact, any succession of Exponential filtering stages – even with inhomogeneous time constants – is reasonably approximated by a single filter $E_{n,\tau}$. The more homogeneous the different time constants in the cascade, the better the fit by filter $E_{n,\tau}$. We refer to Appendix 5.3.2 for more details.

This composition property is interesting, since it allows to encompass in a single linear filter the distributed low-pass stages that occur along the retinal pathway (synapses, cellular integrations, etc). An illustration of the filters and of the composition property is shown in Figure 2.3.

In formula (2.6), rather than defining $E_{n,\tau}$ as the n-fold auto-convolution of the Exponential filter, we preferred to divide the time-scale by n. As a result, all filters E_τ and $E_{n,\tau}$ have the same first-order approximation for their Fourier transform: At first order, each of these filters induces a temporal delay of magnitude τ to the signal. The parameter n is just a secondary influence, allowing more liberty in fitting the filter's shape to experimental data. In the Fourier domain, higher values for n induce a steeper frequency cut-off after frequency $1/\tau$.

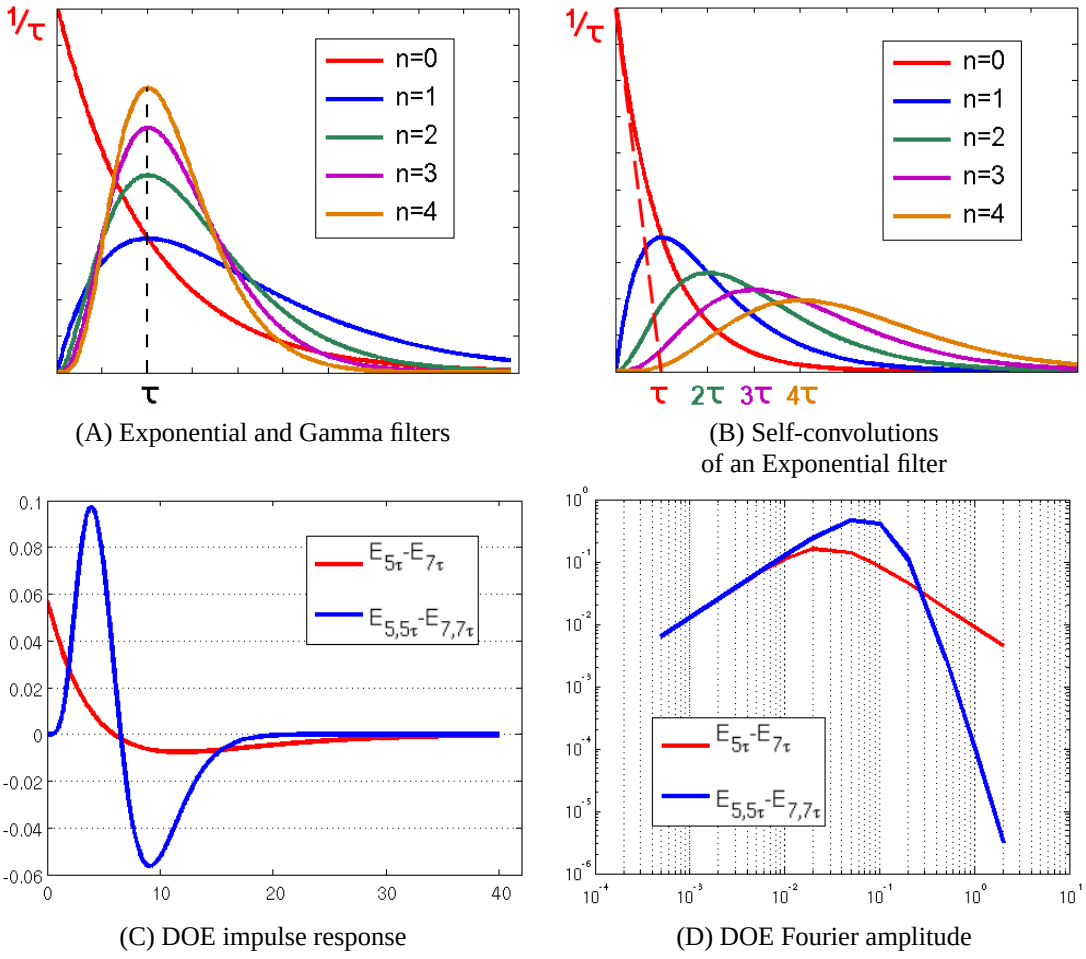

(A) Exponential and Gamma filters

(B) Self-convolutions of an Exponential filter

(C) DOE impulse response

(D) DOE Fourier amplitude

Figure 2.3: Exponential, Gamma and Differences of Exponentials (DOE) filters. *A:* The first five Gamma filters ($n = 0$ being the Exponential filter). They all peak at time τ and induce a temporal delay of order τ when applied on a signal. The bigger the exponent n, the more 'concentrated' the filter is around time τ. In the Fourier domain, higher values for n induce a steeper frequency cut-off after frequency $1/\tau$ (curves not shown). *B:* Filters $E_{n,n\tau}$ defined the successive auto-convolutions of the Exponential filter E_τ. *C:* Two different DOE filters with similar time scales and first-order behavior in the frequency range. The Cascade DOE is closer to experimentally measured shapes. Parameter τ=1. *D:* Corresponding amplitudes for the Fourier transform. The Cascade DOE displays a stronger frequency cut-off.

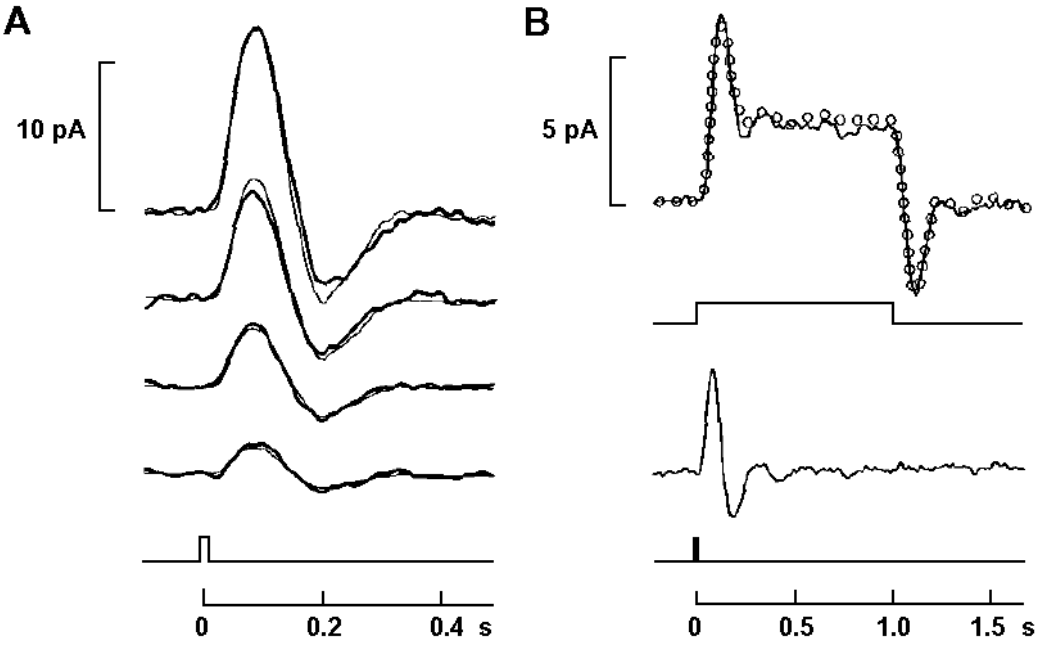

Figure 2.4: *Linear filtering in primate cones.* At small illuminations, the temporal response of cone light receptors is well modeled by a linear filter. Note the resemblance with a Difference-of-Exponentials (DOE) filter. *A:* The impulse response of a single macaque cone is tested, by applying short pulses of light (approximation for a Dirac input). *B:* The response of a cone to a step of light is well modeled by linear convolution with its impulse response. From Schnapf et al 90 [133].

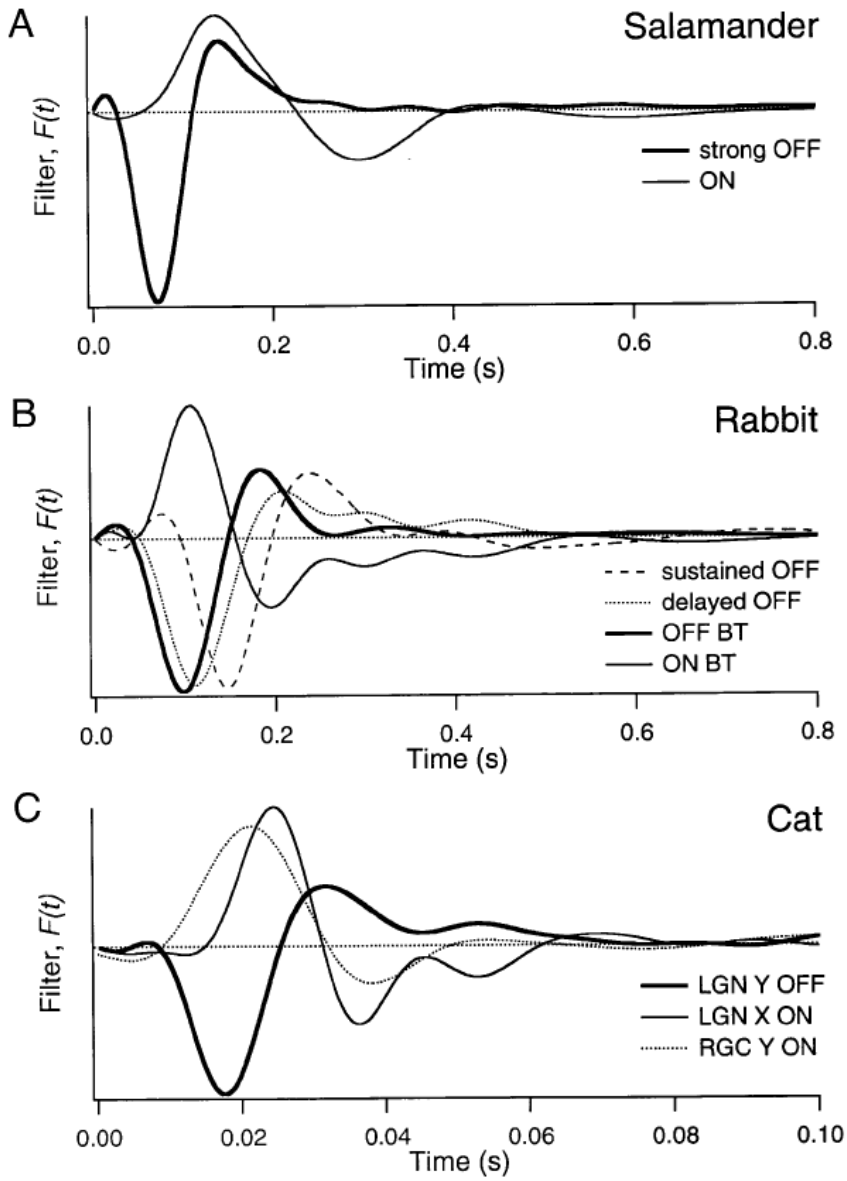

Figure 2.5: Best-fitting linear temporal filters, for different ganglion cells (and LGN cells) stimulated by a random flickering screen. For most cells, the best-fitting filter is biphasic, reflecting the *transient* behavior of retinal ganglion cells (see text). Approximation by a DOE is generally a suitable approximation. However, real cell impulse responses can sometimes display slow oscillations, reflecting the internal complexity of a distributed temporal processing. Also, these linear filters reflect the cells' behavior *for this specific experiment*, with spatially uniform stimuli. From Keat *et al.* 01 [77].

A transient filter: The Difference of Exponentials (DOE)

Just as the center-surround opposition can be modeled as a difference of two low-pass Gaussian filters, linear transients in the retina can be modeled as the difference of two low-pass Exponential (or Gamma) filters:

$$K_{\text{temp}}(x,y) = w_1 E_{n_1,\tau_1}(t) - w_2 E_{n_2,\tau_2}(t), \tag{2.8}$$

where τ_2 is bigger that τ_1.

This is a band-pass temporal filter, which displays a strong functional resemblance with the DOG model:

- Filter E_{n_1,τ_1} reflects the low-pass properties of the considered filtering stage, due to successive delays in the internal transmission of the signal. It defines the frequency cut-off of the filtering stage: Temporal variations faster than $1/\tau_1$ Hz are attenuated in the transmission.
- Filter E_{n_2,τ_2} represents the delayed inhibition that makes the response *transient*: In response to an input step function, filter (2.8) displays a peak of activity, and then a decrease of activity as the inhibition, of time scale τ_2, 'catches up' with the direct signal of time scale τ_1. This behavior is illustrated in Figure 2.4 *B*.
- The ratio $\frac{w_2}{w_1}$ defines the *strength* of the transient. For a ratio of 1, the filter is totally transient: Its response to an input step displays a peak of activity, and then returns to zero. For a ratio smaller than 1, a residual activity remains after the peak of activity: see Figure 2.4 *B*.

However, a major difference exists with the DOG model: Temporal filtering in the retina is distributed along many filtering steps, from phototransduction to spike emission. As a result, the DOE model applies to many different stages of retinal filtering, with different precision, and different time scales:

- First, consider Figure 2.4: The photoresponse of cones to input light is well-modeled by a linear DOE filter with a typical time scale of 100ms (the impulse response resembles $E_{5,100} - E_{7,140}$: compare with Figure 2.3 *C*, taking $\tau = 20$ ms).
- Then, consider Figure 2.5: Best-fitting temporal kernels are calculated for ganglion cells of various species, in response to a uniform flickering screen. In Figure *C*, a cat ganglion cell (RGC Y ON, same temporal behavior as a primate cell) is well modeled with a DOE of typical time scale 20 ms.

So, the best-fitting DOE filter for a ganglion cell is about five times faster than the best-fitting DOE filter for the cones, which are upper in the pathway. This counter-intuitive result is due to successive high-pass transients in retinal processing, that enhance fast frequencies in the retinal output.

This example illustrates how DOE filters are a much more 'relative' modeling than DOG filters, and strongly depends on which filtering structure is being modeled, and at what precision. As a result, the fitting to experimental data is generally looser than for the DOG model: For example, see how ganglion cell impulse responses (Figure 2.5) can display attenuated oscillations, not accounted for by a DOE filter.

Also unlike the Gaussian filters, a supplementary liberty is given for the two low-pass Exponential filters used: The choice of their exponents n_1 and n_2. This liberty is convenient to provide better fit to data (see Figure 2.3 *D*), but the resulting choices for n_1 and n_2 are often arbitrary, and not necessarily useful from a functional point of view.

A simplified transient filter

The high number of parameters (5) in the generalized DOE filter somewhat 'drowns' the main functional role of the DOE filter, which is to provide high-pass ('transient') behavior. A simpler DOE filter can be introduced to model transients in the simplest functional way:

$$T_{w,\tau}(t) = \delta_0(t) - wE_\tau(t), \tag{2.9}$$

This filter is a simple extrapolation on the DOE filter (2.8), except that the fast exponential is 'removed' by taking its limit when $\tau_1 \to 0$, becoming a Dirac $\delta_0(t)$, and that the slow exponential takes its simplest form with exponent $n = 0$. When filter (2.9) is applied to an input $X(t)$, its output simply corresponds to

$$Y(t) = T_{w,\tau} \overset{t}{*} X\,(t) = X(t) - w\,E_\tau \overset{t}{*} X\,(t).$$

The two parameters are sufficient to model the 'high-pass' functionality of a DOE filter:

- τ fixes the time delay between the initial signal and its 'removed average'.
- w fixes the relative weights of original signal and 'removed average' in the output.

Temporal convolution and ODEs

Remark that temporally, convolution by E_τ in (2.5) or $T_{w,\tau}$ in (2.9) amounts to passing the signal through specific linear ordinary differential equations (ODE). Let us remind these results:

$$Y(t) = E_\tau \overset{t}{*} X\,(t) \qquad \Longleftrightarrow \qquad \tau\frac{dY}{dt} = X(t) - Y(t) \tag{2.10}$$

$$Y(t) = T_{w,\tau} \overset{t}{*} X\,(t) \qquad \Longleftrightarrow \qquad \tau\frac{dY}{dt} = \tau\frac{dX}{dt} + (1-w)X(t) - Y(t), \tag{2.11}$$

these relations being true once that the initial condition of the ODE is forgotten. Convolution by $E_{n,\tau}(t)$ is equivalent to an n-th order ODE, obtained by cascading (2.10) n times.

4 GENERALIZED SPATIO-TEMPORAL RECEPTIVE FIELDS

After the first DOG models, several specific works have revealed other subtleties in the spatio-temporal structure of retinal filtering. Amongst these new properties, most concern nonlinear behaviors, which we address more specifically in Chapter 3. Also, some new properties were found, that can be well modeled linearly as enhancements of the DOG model. We review them here.

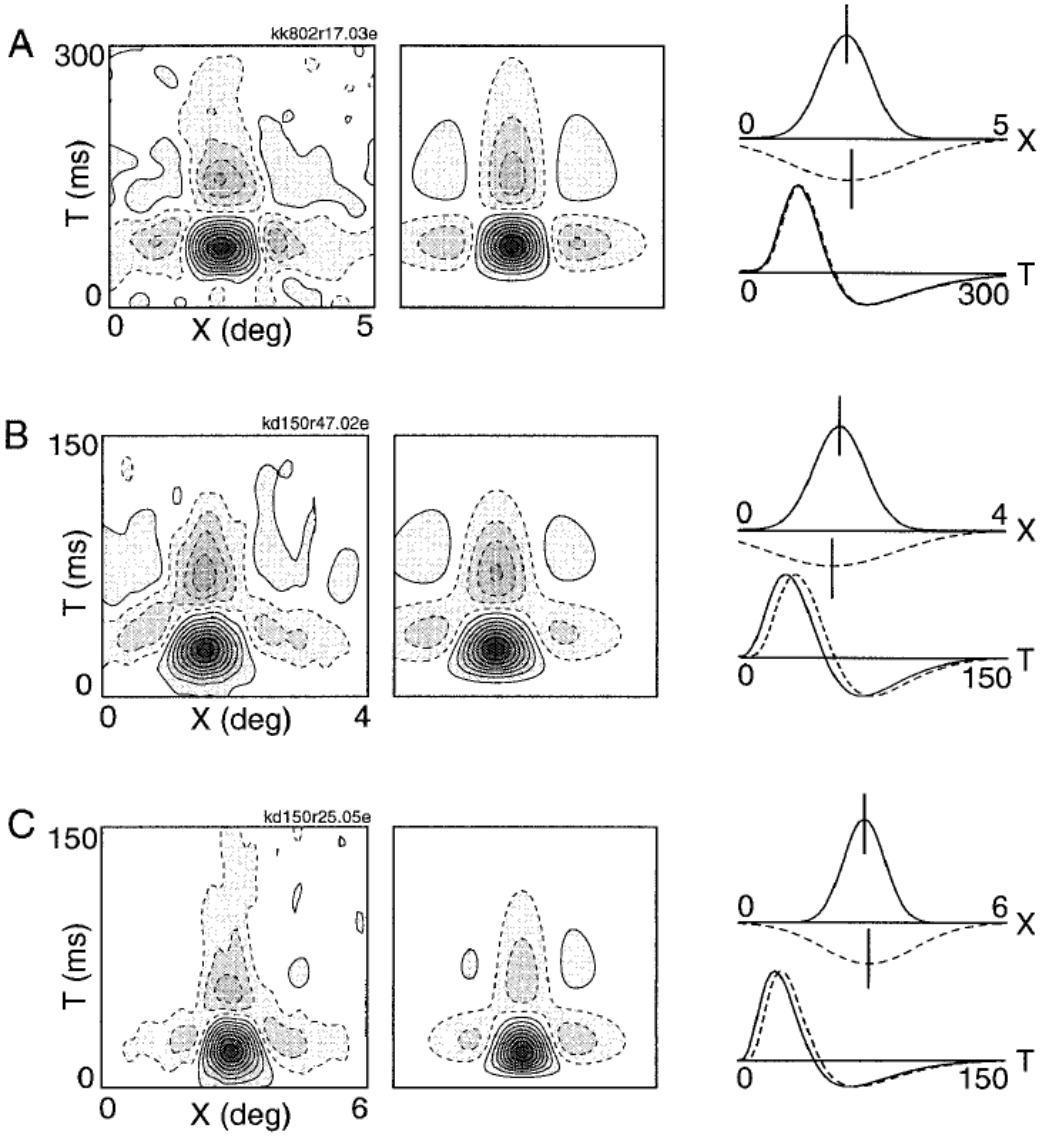

Figure 2.6: *Non-separable receptive fields and generalized DOG models in the cat LGN. Left column:* Spatio-temporal receptive fields (with a single spatial dimension) revealed through reverse correlation analysis. *Middle column:* Fit by a generalized DOG model. The $X - T$ profile is rather separable for cell A, but not for cells B and C. *Right column:* Parameters of the generalized DOG models. The *surround* signal (dotted lines) is associated to a different DOE filter than the *center* signal (continuous line). Best-fitting DOE filter for the *surround* reveals a supplementary time delay. Note also that the *center* and *surround* Gaussians are allowed to have different offsets. From Cai *et al.* 97 [20].

Delayed surround

As mentioned already, the best-fitting linear kernel for a cell is generally not separable in time and space. One of the first observations of the phenomenon was by Enroth-Cugell *et al.* 83 [49]: They found that measures of spatial sensitivity using drifting grating (as in Figure 2.1 *B*) were different according to the temporal frequency used for the grating – which would not be the case for a separable filter.

Furthermore, the authors found that the non-separability is well accounted for by a linear model where the spatial *surround* signal is transmitted with a supplementary delay, of a few milliseconds. This is illustrated in Figure 2.6, which displays non-separable kernels, from cat LGN cells [20]. Although very small ($3 - 7$ ms in cat [49, 20] and primate [10]), this delay likely has important perceptual consequences (Meister and Gollisch 08 [60]; see also our model simulations in Wohrer 08 [163], Chapter 4).

In the case of cat LGN cells, Cai *et al.* 97 [20] suggest that the total receptive field structure is well encompassed by a modified Difference-of-Gaussians, where both Gaussians are associated to a different DOE temporal profile:

$$K(x, y, t) = w_C G_{\sigma_C}(x, y)\mathrm{DOE}_C(t) - w_S G_{\sigma_S}(x, y)\mathrm{DOE}_S(t), \tag{2.12}$$

where both filters DOE_C and DOE_S are DOE filters as in 2.8, with slightly longer time scales for the *surround*. This is the type of linear model that we kept in our model (Wohrer 08 [163], Chapter 4).

Modified Gaussians

Other detailed studies have revealed that ganglion cells' *center* and *surround* can display geometrical asymmetries. First, the *center* and *surround* filters may display a small relative offset in their respective spatial positions. This fact can be introduced in a linear DOG model by adding a spatial offset to the *surround*. Second, the receptive fields are generally not perfectly spheric: The *center* and *surround* receptive fields can have slightly ellipsoidal profiles (see e.g. DeVries-Baylor 97 [45] in the rabbit retina). In our model, we did not include such asymmetries, whose functional interest is not clear.

5 REVERSE CORRELATION AND LN ANALYSIS

Reverse correlation

We now give a few words on *reverse correlation* methods, which are widely used nowadays to study linear receptive fields in low-level visual areas (see e.g. Ringach and Shapley 04 [124] for review).

Consider a ganglion cell centered in (x_0, y_0) and driven linearly by its input, through formula (2.1). Reverse correlation studies the statistical dependence of the cell's activity at time t, on all past values of image I in the cell's receptive field. For a spatio-temporal offset (a, b, s), the reverse correlation $C(a, b, s)$ is formally defined as:

$$C(a,b,s) = \frac{1}{T}\int_{t=-\infty}^{+\infty} I(x_0 - a, y_0 - b, t - s)\, A(t)\, dt, \tag{2.13}$$

where $[-\infty, +\infty]$ is the formal notation for the real recording period $[0, T]$, where T is supposed 'long enough'.

The reverse correlation $C(a, b, s)$ is very interesting in neuroscience because it is a quantity experimentally measurable, which allows to find back kernel $K(x, y, t)$ under a variety of models and experimental conditions. It can be calculated spatio-temporally (Figure 2.6 was obtained with this procedure), or simply temporally, forgetting the two first coordinates.

To prove the interest of function C, rewrite (2.13) with the linear expression (2.2) for $A(t)$:

$$C(a,b,s) = \frac{1}{T}\int_{t=-\infty}^{+\infty} I(x_0 - a, y_0 - b, t - s)\, \big(I * K\big)(x_0, y_0, t)\, dt. \tag{2.14}$$

This expression is problematic because it involves only a specific spatial location (x_0, y_0) on the retina, which prevents from doing well-suited spatial averages and subsequent Fourier analysis. So, to continue the reverse-correlation analysis from (2.14), the input stimulus must necessarily have some form of translational spatial invariance, so that 'all spatial locations are statistically equivalent' over a long run of stimulus. Mathematically, this writes

$$\forall (x_1, y_1, x_2, y_2, \delta),\ \int_{t=-\infty}^{+\infty} I(x_1, y_1, t) I(x_2, y_2, t + \delta) = F(x_1 - x_2, y_1 - y_2, \delta), \tag{2.15}$$

dependent only on the spatial *offset* (translational invariance). Relation (2.15) is verified for three particular experimental conditions:

- If the input image is spatially uniform at each time t. In this case, one focuses only on the temporal properties of the cell, through some filter $K_{\mathrm{temp}}(t)$.

- The stimulus is created as a pseudo-random sequence with translational invariance. This is the case, for example of white-noise stimulus, which is often used. Also, random bar apparitions can be used to test the summation properties along a single spatial direction (e.g., by Cai et al 97, Figure 2.6).

- The stimulus is a natural scene movie sequence, long enough for property (2.15) to be approximately true.

If (2.15) is verified, one can check that (2.14) becomes independent of the choice of (x_0, y_0), so that one can 'artificially' express $C(a, b, s)$ as an average over the whole spatial domain:

$$\begin{aligned} C(a,b,s) &= \frac{1}{TM} \iiint_{x,y,t} I(x-a, y-b, t-s) \big(I * K\big)(x,y,t)\, dx\, dy\, dt \\ &= \frac{1}{TM} I^- * I * K\ (a,b,s), \end{aligned}$$

where M is the spatial area of summation, and $I^-(x,y,t) = I(-x,-y,-t)$. Then, switching to the Fourier domain:

$$\widetilde{C}(\xi_x, \xi_y, \xi_t) = \frac{1}{TM} \widetilde{I}(-\xi_x, -\xi_y, -\xi_t) \widetilde{I}(\xi_x, \xi_y, \xi_t) \widetilde{K}(\xi_x, \xi_y, \xi_t),$$

so that one has an exact access to filter K, through the formula

$$\widetilde{K}(\xi_x, \xi_y, \xi_t) = TM \frac{\widetilde{C}(\xi_x, \xi_y, \xi_t)}{|\widetilde{I}(\xi_x, \xi_y, \xi_t)|^2}, \tag{2.16}$$

an equation which can be understood, whether as a spatio-temporal relation, whether only through its temporal part in the case of a spatially uniform stimulus.

White noise

The only condition to find K back from C with (2.16), is to know precisely $|\widetilde{I}(\xi_x, \xi_y, \xi_t)|^2$, called the *power spectrum* of the input stimulus (it is the Fourier transform of the auto-correlation of I). A good experimental way to get rid of this problem is to have I as close as possible to *white noise*, which verifies $|\widetilde{I}(\xi_x, \xi_y, \xi_t)|^2 = \sigma^2$ for all frequencies.

Remark: In experiments, white noise is just an abstraction, that can be be built experimentally only up to a certain cutting frequency ξ_0 (possibly a vector), which determines the spatial and temporal precision of the measure for K. Problematically, to elicit a fixed response of the cell, the power σ^2 of the white noise should be kept constant; But in order to keep a constant σ^2, the amplitude of the white-noise should tend to $+\infty$ when ξ_0 tends to zero. This is unrealizable, so ξ_0 cannot be made too small: The precision obtained by reverse correlation with a white noise is limited in practice. ■

LN models

Aside from experimental limitations, formula (2.16) can be tested on any cell, in response to any stimulation, and thus provide a linear filter K for the cell. However, one might argue that given the many nonlinearities in retinal processing, the obtained filter K may not be very relevant for a real cell. How can one measure the information lost when approximating the cell by a linear model?

The simplest answer is to compare the real response of the cell $A(t)$, with the linear prediction $I * K(t)$. Even for cells termed *linear*, there is of course a discrepancy between the two signals. *LN*

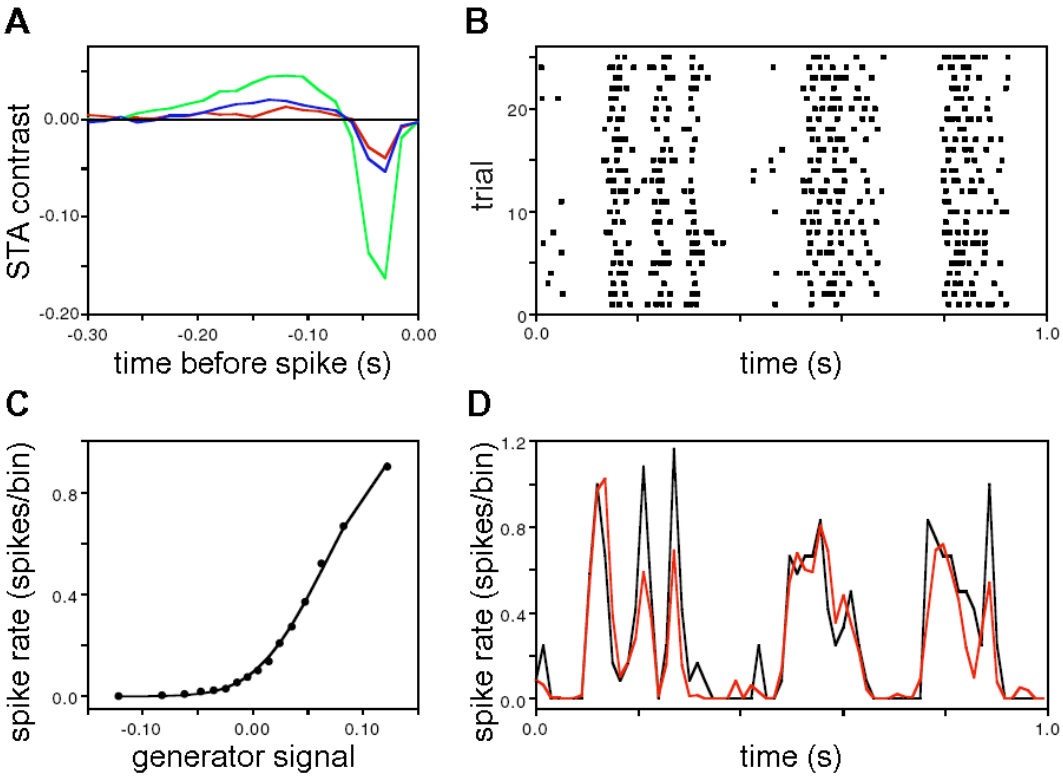

Figure 2.7: *The LN model applied to a macaque OFF cell.* An LN analysis is derived from the spiking response of a ganglion cell to white noise stimulus (in color). *A:* The reverse correlation, here, is a Spike-Triggered Average (STA). The chromatic structure of the input allows to separate the cellular responses to Red, Green and Blue components. *B:* The best-fitting static nonlinearity N is then calculated (see text). *D:* Comparison of the real cell's firing rate (black, reconstructed from the various trials in *C*), and of the output of the LN model. From Chichilnisky 01 [25].

models try to compensate for part of that of that discrepancy by adding a supplementary stage to the model. *LN* models have become an increasingly popular model for low-level visual processing over the last decade: They have even been termed the *standard* model for retinal processing by Carandini *et al* [23].

The initials LN stand for *Linear – Nonlinear*. In this 'enhanced' linear model, cellular filtering is supposed to consist of a linear filter, followed by a static nonlinearity accounting for part of the inherent nonlinearities in retinal processing. With the same notations as before, the activity of the cell becomes

$$A(t) = N\big(I * K(x_0, y_0, t)\big), \tag{2.17}$$

where N is a static nonlinear function. Note that there is an undetermined parameter in this model: Multiplying K by λ and dividing the input scale of N by λ yields the exact same behavior.

Introducing this nonlinearity is a natural, and often mandatory, idea. First, all ganglion cells are limited in the negative range of signal transmission, because their output firing rate cannot be negative. Typically, a cell with a low spontaneous firing rate cannot code linearly when it is inhibited. A simple rectification $N(r) = [r]_+$ (positive part) will naturally provide a better fit to the cell's real response! But rectification is also a *distributed* phenomenon, which does not only concern spike generation. In fact, any stage of transmission relying on a physical magnitude that cannot get negative (synaptic transmission, conductance opening...) is likely to display a signal rectification.

Experimentally, the best-fitting couple (K, N) for the cell is found from its real response $A(t)$, as a two-step procedure:

- First, a reverse correlation analysis yields the best-fitting linear kernel K (formula 2.16).
- Second, the linear reconstruction $r(t) = I * K(t)$ is calculated, and a two-dimensional map is constructed with the ensemble of points $(r(t), A(t))$ at all simulation times. Through various methods, the best fitting static curve $A(t) = N(r(t))$ is then derived from the map.

A mathematical result (sometimes known as Bussgang's Theorem [19]) insures that if a cellular model really behaves as equation (2.17), then the preceding two-step procedure, with white-noise input stimulus $I(x, y, t)$, finds the exact K and N back. Note that this result is not trivial, because the nonlinearity N prevents from doing the linear analysis that led to (2.16).

Remark: Naturally, real cells do not follow an exact LN model either. There is still a discrepancy between the LN model's prediction and output spikes. Even with our simulator (though close in conception to an LN model, see Wohrer 08 [163] Chapter 4), when an LN analysis was applied to the output spikes, we sometimes found a strong dispersion of the maps $(r(t), A(t))$ around the theoretical line $A = N(r)$. ■

The LN model can also be enhanced to a spiking model, where $A(t)$ in (2.17) serves to generate the spikes with an inhomogeneous Poisson process (LNP model, see Section 4). In this case, the reverse correlation can be done directly from the spike train, considered as a discrete series of Dirac pulses: The reverse correlation is then called a *Spike Triggered Average* (STA).

Because Poisson spike trains are statistically 'transparent' (see Chapter 3, Section 4.2.1), the two-step reconstruction from the STA also provides back the exact K and N of an LNP model [25].

6 LINEAR MODELS FOR ELECTRICAL COUPLING

We now present linear models which have been proposed to account for electrical coupling between neighboring cells of a same layer through *gap junctions*. Gap junctions are ionic channels between two cells' cytoplasms, which allow the circulation of ions - generally in both directions. Whatever unsolved questions remain concerning the arousal of center-surround opposition in the retina, there seems to be a consensus that gap junctions between neighboring cells of the same type are responsible for a good part of the spatial extent of *center* and *surround* signals.

Electrical coupling in horizontal cells

Gap junction coupling is particularly strong and well assessed in horizontal cells, which provided some of the first intracellular recordings of retinal neurons (Svaetichin 53 [146]). Morphologically, this has been revealed by experiments such as that of Figure 2.8 *A*: Dye injected in one horizontal cell's cytoplasm spreads to all neighboring horizontal cells through the gap junctions.

The effect of horizontal cell coupling is also well understood: Photoreceptors transmit the visual information to horizontal cells through excitatory synapses. Then, electrical coupling between horizontal cells results in a local *averaging* of this visual information, so that horizontal cells are sensitive to the sum of visual inputs over a wide spatial range. This is verified in the rabbit retina, in Figure 2.8 *B*: Horizontal cell responses grow linearly with the size of a stimulating light spot, over a 'long' distance (relatively to the response of photoreceptors).

From the standpoint of image processing, horizontal cells thus 'see' an image much more blurred than photoreceptors. From a physiological standpoint, gap junctions create wide receptive fields in horizontal cells, which probably contribute significantly to the creation of the *surround* signal (Chapter 3, Sections 2 and 3).

Linear models for electrical coupling

Coupling through gap junctions is well modeled in a linear framework, as proposed by Naka-Rushton 67 [101] for horizontal cells (see also Lamb 76 [85]). In these models, a layer of cells with membrane potentials V, modeled as leaky membranes, integrate a current I, with static conductances G linking neighboring cells. According to the framework, the model can involve a discrete array of cells (here, a one-dimensional array):

$$c\frac{\mathrm{d}V_i}{\mathrm{d}t}(t) = I_i(t) - g^L V_i(t) + G(V_{i+1}(t) + V_{i-1}(t) - 2V_i(t)), \tag{2.18}$$

or rather a continuous framework involving Partial Derivative Equations (PDEs):

$$c\frac{\mathrm{d}V}{\mathrm{d}t}(x,y,t) = I(x,y,t) - g^L V(x,y,t) + \mathcal{G}\,\Delta V(x,y,t), \tag{2.19}$$

where $\Delta V = \partial_x^2 V + \partial_y^2 V$ is the Laplacian of potential V, and the leak conductance g^L is associated to a rest potential E^L taken as 0.

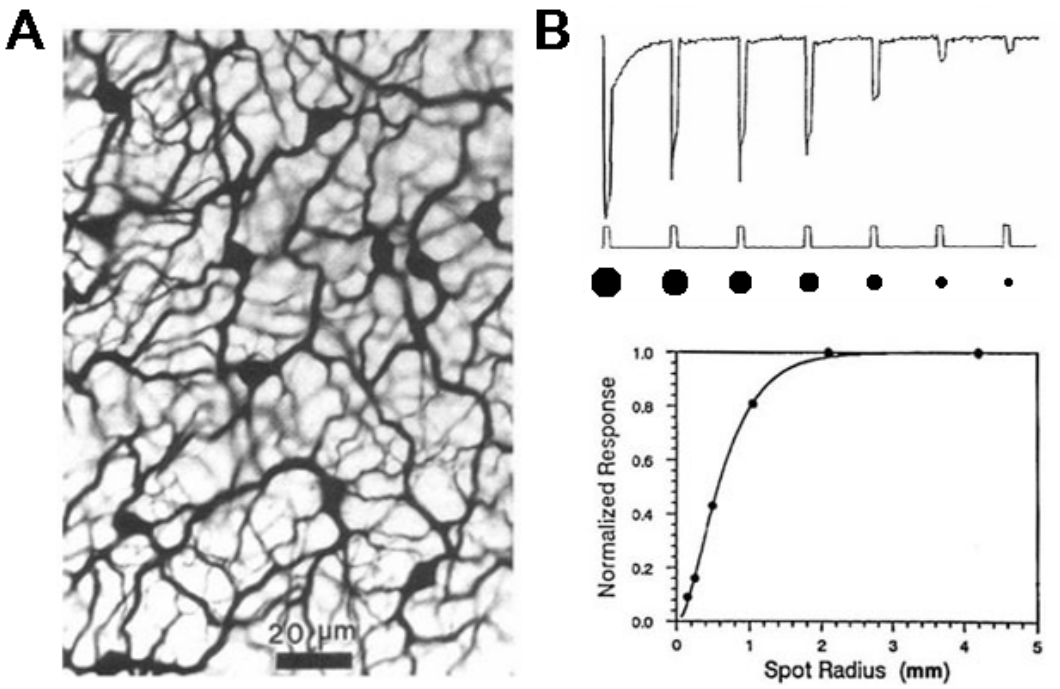

Figure 2.8: Spatial coupling in horizontal cells. *A:* Gap junctions between neighboring horizontal cells are revealed: Dye injected in one cell's cytoplasm propagates to the neighboring cells through gap junctions. Rabbit cells, from [97] *B:* The responses of a horizontal cell to spots of increasing size reveal spatial summation over a wide distance, due to gap junctions. Note that horizontal cells are always hyperpolarized by increased light ('OFF' behavior, see Chapter 3, Section 1). Turtle cells, from [113].

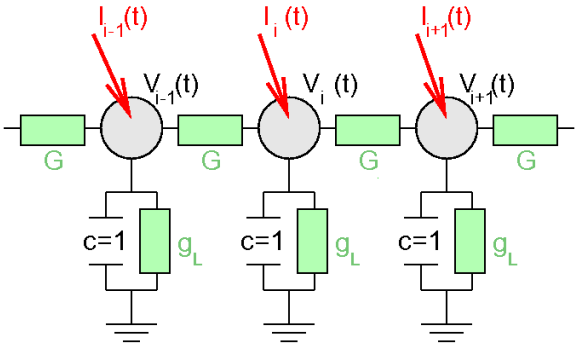

Figure 2.9: An electrical model for coupling through gap junctions. Cells with potentials V_i are modeled as linear capacitors linked to their nearest neighbors by static conductances G (gap junctions), and integrating an input synaptic current I_i.

Formulation (2.18) is written for a one-dimensional array of cells with membrane potentials $V_i(t)$, integrating their input current as a current $I_i(t)$ (see Figure 2.9). The gap junctions are modeled as static conductances G, and are supposed to only occur between closest neighbor cells. This formulation is well suited for hardware implementations of coupling, as proposed by Mahowald and Mead 91 [88] to produce one of the first 'retina-inspired' chips. This discrete model has a simple equivalent for two-dimensional arrays, and has been tested with connections more complex than just closest neighbors: See, e.g., the works of Herault [65, 68] and Beaudot 94 [9]. The properties of the resulting filter are best expressed in the Fourier domain.

By opposition, formulation (2.19) can be seen as the continuous limit of (2.18) (or its two-dimensional version) when the step between the discrete units tends to zero and the neurons can be seen as a continuum: Suppose that cells are separated by a spatial step s, and that the (serial) conductances G behave as $G = \mathcal{G}/s$, while the (parallel) conductance g^L, capacity c and input currents scale with s. Then, leading s to zero in (2.18) yields (2.19).

For our model (Wohrer 08 [163] Chapter 4) which uses a formalism of continuous maps, we find formulation (2.19) better suited. We often refer to (2.19) as a 'leaky heat equation' (without the leak term $-g^L V$, it would be a simple heat equation). It bears the analytical solution:

$$V(x,y,t) = H \overset{x,y,t}{*} I \ \ (x,y,t), \tag{2.20}$$

where H, impulse response of the filter, is given by:

$$H(x,y,t) = \frac{1}{c} G_{\sigma\sqrt{t/\tau}}(x,y) \exp(-t/\tau). \tag{2.21}$$

In (2.21), G_σ is the normalized Gaussian kernel of standard deviation σ and integral 1, as in (2.4), and σ and τ are the typical spatial and temporal extent of the impulse response:

$$\sigma = \sqrt{2\mathcal{G}/g} \tag{2.22}$$

$$\tau = c/g. \tag{2.23}$$

Similarities and discrepancies w.r.t. Gaussian filtering

Filtering by (2.20)-(2.21) has a close relation to the Gaussian kernels introduced in Section 2 to model *center-surround* interactions. When a signal is convoluted by filter H in (2.21), it is low-passed as with a Gaussian kernel. However, filter H is not separable in time and space: The spatial blur through $G_{\sigma\sqrt{t/\tau}}$ spreads in time. Such spread of the signal has indeed been observed in the responses of some ganglion cells to static squares by Jacobs-Werblin 98 [73], probably imputable to gap junction diffusion of the signal.

However, the 'spreading' gap junction filter (2.21) is not widely used in the field of retinal models. Often, a layer of electrically coupled cells is rather associated to a simple separable filter:

$$H_{\text{sep}}(x, y, t) = \frac{1}{c} G_\sigma(x, y) \exp(-t/\tau), \tag{2.24}$$

with σ and τ still defined in (2.22)-(2.23). There are several conceptual advantages in this simplification:

- Filter H_{sep} in (2.24) can also account for static pooling of a pre-synaptic signal as caused by the spread of a cell's dendritic tree.

- If filters of the form H_{sep} are successively applied to the signal at successive stages of the retinal pathway, the resulting filter keeps a simple expression: Since filters like H_{sep} are separable in time and space, their successive convolutions remain separable in time and space, and their spatial component remains a Gaussian, as the convolution of Gaussians. By opposition, convolutions of filters of the form H in (2.21) have no simple expression, except in the Fourier domain.

- At the same time, filter H_{sep} in (2.24) remains close to filter H in (2.21): In the Fourier domain, they have the same asymptotical expression for small spatio-temporal frequencies (see equations (2.25)-(2.26)).

It is not clear to our mind, whether the original 'spreading' filter in (2.21), probably closer to biological reality, has specific functional interests which are lost in the simplification to (2.24). This is indeed possible, because filter (2.24) displays a much stronger frequency cut-off at high spatial

frequencies. To verify this, express the respective Fourier transforms of the two filters:

$$\widetilde{H}(\xi_x, \xi_y, \xi_t) = \frac{1}{c\left(1 + \frac{\sigma^2}{2}(\xi_x^2 + \xi_y^2) - \mathbf{i}\tau\xi_t\right)} \tag{2.25}$$

$$\widetilde{H}_{\text{sep}}(\xi_x, \xi_y, \xi_t) = \frac{1}{c\,(1 - \mathbf{i}\xi_t\tau)} \exp\left(-\frac{\sigma^2}{2}(\xi_x^2 + \xi_y^2)\right), \tag{2.26}$$

so that the spatial frequency cut-off is exponential for H_{sep}, versus a simple power law for the 'real' H. Furthermore, the typical spatial cut-off frequency of H_{sep} is constant: $\sqrt{2/\sigma}$, whereas in the case of H, it depends on the temporal frequency ξ_t^0 of the stimulus: $\tau\xi_t^0\sqrt{2/\sigma}$.

This is an interesting feature because it means that, for similar typical parameters σ and τ (which can be experimentally measured), the filtering through gap junctions might allow higher spatio-temporal cut-offs than what is generally believed. As a result, the simulator *Virtual Retina* allows to chose any of the two filtering schemes H and H_{sep} at the level of the Outer Plexiform Layer. In experiments involving frequency kernels, we did find improved results when the 'spreading' filter H was used.

7 CONDUCTANCE EQUATION AND OTHER NONLINEAR FILTERING: THE LINEAR ODE FRAMEWORK

To conclude this chapter, we give a few words on the *conductance* driving equation for a neuron:

$$\frac{dV}{dt} = \sum_i I_i(t) + \sum_j g_j(t)(E_j - V(t)), \tag{2.27}$$

where currents in the neuron's membrane can be modeled either as currents $I_i(t)$, or more precisely as conductances $g_j(t)$ associated to Nernst potentials E_j.

If only currents are present in (2.27), then it subtends a *linear filtering* relation between the neuron's input currents and the subsequent potential $V(t)$. By opposition, time-varying conductances induce a nonlinear filtering relation between the neuron's inputs and $V(t)$.

However, even if it induces nonlinear *filtering*, (2.27) is still a *linear ODE* w.r.t. V (if V_1 and V_2 are solutions, so is $V_1 + V_2$), and it can be solved. Let us introduce the general solution of a 1d linear ODE.

Linear ODE. Consider the variable $X(t)$ driven by a stable linear ODE:

$$\frac{dX}{dt} = A(t) - B(t)X(t), \tag{2.28}$$

where $B(t)$ is supposed to be always positive and to accept a strictly positive lower bound $B_0 > 0$ (This condition insures stability of the ODE; In a cell membrane model, the inert leaks play the role of B_0).

Once initial conditions are forgotten (with time constant no longer than B_0^{-1}), the solution to (2.28) writes

$$X(t) = \int_{u=0}^{=+\infty} A(t-u) \exp\big(-\int_{s=t-u}^{t} B(s)ds\big)du, \tag{2.29}$$

$$= \int_{u=0}^{=+\infty} \frac{A(t-u)}{B(t-u)} \left(B(t-u) \exp\big(-\int_{s=t-u}^{t} B(s)ds\big)\right) du. \tag{2.30}$$

The second line (2.30) is a simple rewriting of (2.29) which puts forth the dual functional implications of ODE (2.28):

1. $V(t)$ is driven by the *driving potential* $A(t)/B(t)$.
2. Kernel $\left(B(t-u) \exp\big(-\int_{s=t-u}^{t} B(s)ds\big)\right)$ is a normalized kernel (integral of one), which *averages* the driving potential, with a typical time extent proportional to $B^{-1}(t)$. It can thus be seen as a low-pass filter, but with varying time constant ($V(t)$ sticks closer to the driving potential when $B(t)$ is large).

The linear ODE in neuroscience. In the case of conductance equation (2.27):

1. The driving potential is $\dfrac{A(t)}{B(t)} = \dfrac{\sum_i I_i(t) + \sum_j g_j(t)E_j}{\sum_j g_j(t)}$,
2. The instantaneous time constant is $B(t)^{-1} = \big(\sum_j g_j(t)\big)^{-1}$.

Through Point 1, conductances have a divisive effect on the values taken by $V(t)$. Through Point 2, conductances make the response of $V(t)$ faster. This effect is more and more explicitly taken into account by modelers, as it provides interesting normalization behaviors.

But linear ODEs have other fields of applications in neuroscience and biology in general. For example, catalyzed reactions –as occurring during phototransduction in the retina– can also be modeled following a linear ODE (Chapter 3, Section 1.1.2), and with the same double effect of divisive behavior and time constant modulation. Linear ODEs also occur in precise models of synaptic transmission (Dayan and Abbott [38]), and more generally in all biological stages that imply chemical equilibriums between different chemical species.

The linear ODE in our work. In our model (*Wohrer 08* [163], Chapter 4), we use an explicit conductance equation to account for contrast gain control. We mathematically study the behavior of the resulting feedback loop (*Wohrer 08* [163], Chapter 5), and we implement a general computer object that can account for any equations of the form (2.28) at the level of retinal maps (the CondCellMap object, *Wohrer 08* [163], Chapter 6, Section 3.3.4).

This means that our model and software *Virtual Retina* can easily be extended to incorporate any specific nonlinear filtering effects relying on linear ODEs.

CHAPTER **3**

SPECIALIZED FUNCTIONALITIES IN THE VERTEBRATE RETINA

In this chapter, we go deeper into the retina's internal architecture and physiology. After a rapid presentation of light receptors and phototransduction (Section 1), we present the physiology of bipolar cells (Section 2), which are a functional turntable in the retina, being at the interface of the two plexiform layers (OPL and IPL). In particular, we report how the 'traditional' characteristics of retinal filtering (center-surround organization, temporal band-pass) are already present at the level of bipolar cells. We then report the diversity of ganglion cells at the output of the retina (Section 3), which proceed to different spatio-temporal transformations of the signal from bipolar cells. This diversity suggests the existence of parallel channels of information at the output of the retina, with different roles in cortical processing. In Section 4, we question the nature of spike emission, and its possible specific roles in retinal coding. Finally, we mention the different processes of adaptation that constantly help to shape and adapt the retinal output in a nonlinear fashion (Section 5).

Contents

1 PHOTORECEPTORS AND HORIZONTAL CELLS

Photoreceptors are in charge of converting the incoming light into variations of their membrane potential and thus, into synaptic activity. The process by which this happens, known as *phototransduction*, occurs in the receptors' *outer segments* (Figure 3.1). It is a complex cascade of molecular reactions which involves several intermediate catalyzers, and many feedback loops.

In turn, the *inner segments* of the receptors act as a 'traditional' layer of retinal cells, spatio-temporally integrating the current provoked by phototransduction. The inner segments are in strong interplay with horizontal cells, which provide modulatory feedback.

The whole architecture forms a very complex mechanism. This complexity serves a difficult goal: Allow the retina to function under the wide variety of illuminations in our environment. From dark night to bright sunlight, the light hitting the back of the retina can vary in ratios of order 10^{10}, requiring powerful and distributed control mechanisms.

However, modeling light adaptation in its complexities is not mandatory in the scope of our simulator (Wohrer 08 [163], Chapter 4), which aims at working on normalized computer images. For this reason, phototransduction and light adaptation are presented here only succinctly. Yet, it seemed impossible not to say a few words about this strong initial stage of visual processing.

1.1 Phototransduction

1.1.1 Molecular basis of phototransduction

Phototransduction is the conversion from an input light, consisting of photons, into an electrical current. More precisely, a cation current (85 % Na^+ , 15 % Ca^{2+}) constantly circulates between the receptor's outer and inner segments (Figure 3.1). In the inner segments, the current flow is created by ionic pumps: The famous (2 K^+/3 Na^+) exchanger (not shown) produces the Na^+ outflow, while the (4 Na^+/Ca^{2+},K^+) exchanger (Figure 3.2 A, top right) produces the Ca^{2+} outflow[1].

In the outer segment by opposition, ionic channels (Figure 3.2 A, bottom right) insure the inflow of Na^+ and Ca^{2+}. These ionic channels are the ultimate target of phototransduction: Incoming light results in a closing of these channels, and thus in a *reduction* of the circulating current, which allows the receptor to code for its light stimulus.

Figure 3.2 presents the main steps of phototransduction. Panel A, reproduced from Burns and Lamb [18], presents the main chemical species involved in the process. Panel B takes a more functional approach, oriented around four 'crucial' steps, and associated chemical species. Let us present the principles of phototransduction through successive description of these four steps.

1. Light absorption. Rhodopsin (R) is the photosensitive molecule. Numerous rhodopsin molecules are inserted in the membranes of the stacked sacs (in cones) or disks (in rods) which form the receptor's outer segment. Absorption of an incoming photon produces a change in the rhodopsin's 3D structure, transforming it into its activated form R^*.

[1] At the expense of an Na^+ inflow, so it seems...

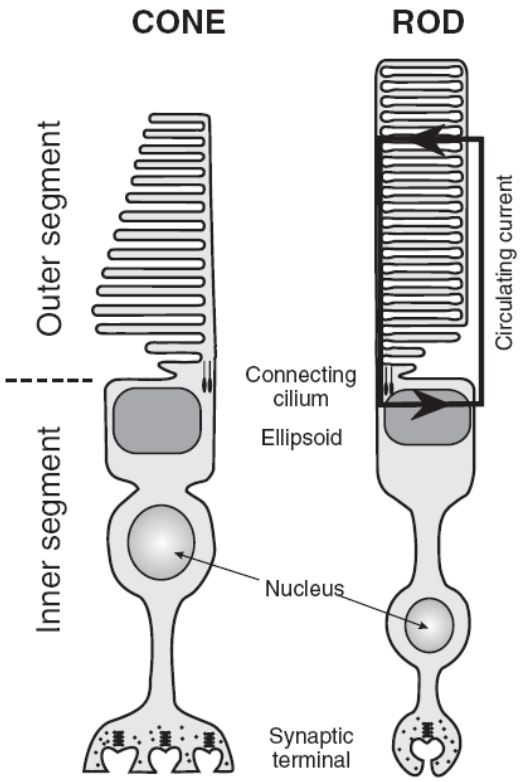

Figure 3.1: *Anatomy of cone and rod receptors.* Both types of receptors possess two distinct segments. The *inner segment* is in charge of conventional cellular metabolism. The *outer segment* is in charge of phototransduction. It contains *rhodopsin* molecules that can capture incoming photons, thus initiating a molecular cascade which leads to a *reduction* of the ionic current flowing through the outer segment. From Burns and Lamb [18].

2. Disc membrane cascade. Each activated rhodopsin R^* repeatedly contacts transducin molecules G (a G-protein) and thus catalyzes their transition to an active form G^*. In turn, two activated G^* can bind to an effector protein PDE also inserted in the disk membrane, transforming it into its activated form PDE^{**}. The whole reaction occurs on the 2D surface of the disk (or sac): The freely moving intermediate molecule, the G-protein, rarely dissociates from the membrane's surface.

The catalyzed reaction allows very high gains of response (detection of down to single quanta of lights in dark adapted rods). But because of this high gain, the cascaded reaction is also under control of various inactivation mechanisms. The most important inactivation is naturally that of R^*, at the root of the cascade. This shutting off is a complex mechanism which occurs through different mechanisms and different time scales, not all understood (see Burns and Lamb [18] for reference).

3. Channel opening and photocurrent. Activated PDE^{**} acts as a catalyzer on the destruction of cyclic guanosine monophosphate cGMP (noted cG in Figure 3.2), a soluble molecule. In turn, the variations of concentration [cGMP](t) are directly linked to the photocurrent, because the target ionic channels open only when bound to cGMP (Figure 3.2 A, bottom right).

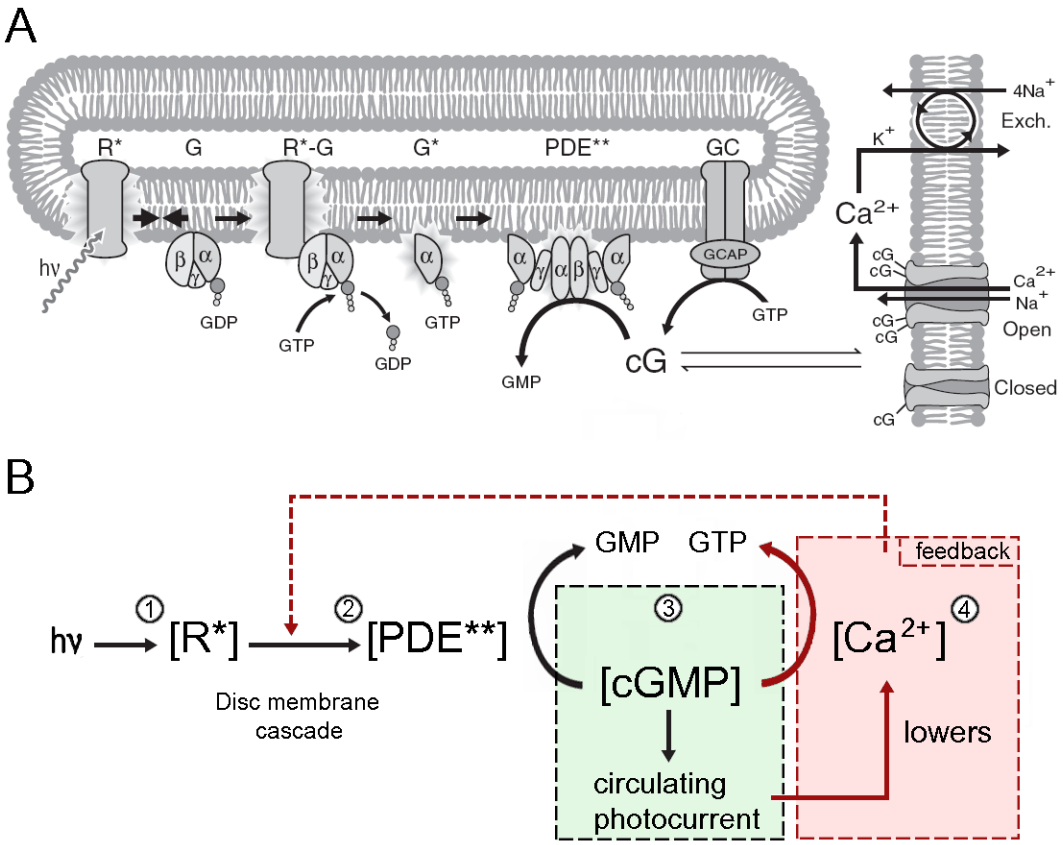

Figure 3.2: *The phototransduction cascade. A:* Most important chemical reactions involved in the phototransduction cascade, from Burns and Lamb [18] (see text). *B:* Functional approach based on the evolution of four key chemical species (see text). Feedbacks modulated by intracellular calcium play an important role both in rapid recovery to a pulse, and in adaptation to light. The arrow involving Ca^{2+} and cGMP is not a catalyzed reaction but an integrated functional dependence (see text and Panel *A*).

Remark: Note that guanosine is a crucial transmitter involved at other locations of the process in its di- (GDP) and tri- (GTP) phosphate forms. ■

4. Calcium and adaptation to light. Calcium is the number one mediator of adaptation to light during phototransduction (Torre *et al.* 86 [150], Polans *et al.* 96 [114], and Burns and Lamb [18] for supplementary reference). When the photocurrent is reduced by light absorption, following the previous explanations, the influx of Ca^{2+} decreases because of the closure of the ionic channels. Because Ca^{2+} is continually expelled by the exchanger (Figure 3.2, top right), the intracellular concentration $[Ca^{2+}]$ rapidly decreases, so that $[Ca^{2+}]$ becomes a *marker of the receptor's recent level of response*.

Exploiting this property, a number of feedback gain controls are based on Ca^{2+}. A major effect of Ca^{2+} is to inhibit GCAP molecules (Figure 3.2, Panel A). By opposition, at low $[Ca^{2+}]$ concentration, the inhibition on the GCAP disappears and they start to regenerate cGMP, thus counterbalancing the effects of light. This effect allows:

1. To speed up the recovery from a light pulse (thus reducing the low-pass properties of the cascade).
2. To prevent channel saturation by divisively controlling the levels of [cGMP], thus providing adaptation to the level of light.

In Figure 3.2 Panel B, we show the functional equivalent of this property: Calcium contributes to the deactivation of cGMP. Besides, calcium also has strong modulatory effects on the disk membrane cascade, including its inactivation mechanisms (Pugh *et al.* 99 [118]).

1.1.2 Modeling phototransduction

The number of reactions involved, including feedbacks, makes the detailed modeling of phototransduction a difficult task. However, nice quantitative reproductions are now obtained, at least to reproduce responses to simple stimuli such as pulses of different intensities.

Catalyzer equations. The key type of mathematical calculation involved appears to be catalyzer equations. As an example, consider this simple case of catalyzed reaction:

$$X_1 \xrightarrow{Z_1} Y,$$
$$Y \xrightarrow{Z_2} X_2$$

where a single molecule of each species is involved in the reactions. We focus here on the dynamics of $Y(t)$, a measure (possibly normalized) of the concentration of species Y. We consider two reactions: A creative and a destructive one, which is the strict minimum to define a dynamic concentration equilibrium for Y. Both reactions in this example are *catalyzed*, respectively by chemical species Z_1 and Z_2. The evolution of $Y(t)$ is then well modeled by

$$\frac{dY}{dt} = \alpha X_1(t) Z_1(t) - \beta Z_2(t) Y(t), \tag{3.1}$$

where α and β are constants. More complex chemical equilibriums can be modeled, but the concept is similar: Catalyzers serve as multiplicative factors for the destruction of reactives (sign -) and the creation of products (sign +).

Remark: Linear ODE framework
Interestingly, equation (3.1) (or any other simple catalyzed reaction) is formally similar to the *conductance* driving equation in a neuron: It is a linear ODE (Chapter 2, Section 7), with specific effects on the time constant and gain with which the reaction product Y evolves.

Because linear ODEs are generically implemented in software *Virtual Retina*, it can easily be extended to incorporate the dynamics specific of phototransduction. ■

Responses to pulses of light. A direct cascade of catalyzer equations can successfully reproduce the *rising phase* (so, before the apparition of inactivation reactions) of receptors' response to pulses of light (Pugh and Lamb 93, [117]).

In addition, inactivation reactions have also been modeled, as well as Calcium adaptation to levels of illumination. We give the single example of the recent model of Van Hateren and Lamb 06 [156], which reproduces correctly the responses of cones to pulses of different intensities (Figure 3.3). Here are the main components of the model:

1. Inactivations in the disk membrane cascade are simply modeled as linear exponential decays, meaning that [PDE**] is obtained as a linearly low-passed version of the input luminance.

2. Concentration of [cGMP] is driven by a catalyzer equation involving [PDE**] and the feedback Calcium current. The model relies on variable $\beta(t)$ which sets simultaneously the gain and time constant for the evolution of [cGMP], as arises from the general formula of a linear ODE such as (3.1) (see Chapter 2, Section 7).

3. Activation steps which require the simultaneous binding of multiple reactives are modeled with the introduction of a Hill exponent.

4. The feedback arising from variations in $[Ca^{2+}]$ is obtained as a low-passed version of the circulating current, followed by a static function with a Hill exponent, modeling the binding of calcium to GCAP molecules.

Analysis, and links with linear modeling. Analyzing in details the shape of the various pulse responses (Figure 3.3 *A*) and how they relate to different elements of the model, is beyond our scope here. Let us simply note that the model behaves quite linearly at low intensities, with a typical monophasic shape.

This linear behavior at low intensities is in agreement with the previous findings of Schnapf *et al.* 90 [133] (Figure 2.4). However, note that in these previous recordings, the impulse response was biphasic. A possible explanation for this discrepancy with Figure 3.3 is the level of extracellular calcium between the in-vivo conditions of Figure 3.3 and the in-vitro conditions of Figure 2.4. The Van Hateren *et al.* model of Figure 3.3 does start to become bi-phasic when the Calcium feedback time constant is set at longer values [156].

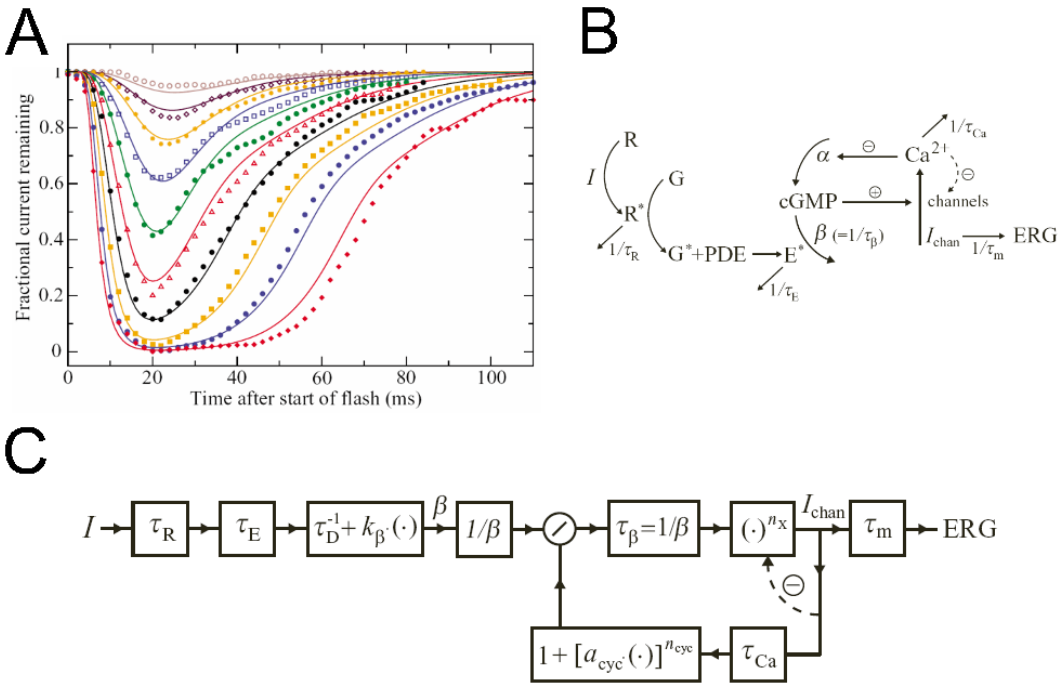

Figure 3.3: *A model for cone responses to pulses of increasing intensities. A:* Responses of a real cone from the squirrel retina, and fit by the model. *B:* Link of the model with phototransduction cascade, and *C:* Functional architecture of the model. Boxes marked τ_X symbolize low-pass exponential filters ($E_\tau(t)$ in our notations). Boxes marked $a + b(.)^n$ implement the transform $x \to a + bx^n$, where n is a Hill coefficient, often introduced to account for activation steps that require the simultaneous binding of several molecules. Finally, signal $\beta(t)$ models the nonlinear catalyzer effect of PDE**, like variable Z_2 in our equation (3.1). From Van Hateren and Lamb 06 [156].

At higher intensities, nonlinear behaviors occur:

- Intrinsic saturation due to the limited number of channels.
- Shorter time constant for the rising time, as resulting from the catalysis by [PDE**] ('linear ODE' framework, see above description of the model).
- An increased plateau before the decay, at high illuminations. We have not investigated how model equations account for this phenomenon, very typical of phototransduction responses.

1.1.3 Functional implications

To conclude, we mention the functional implications of the phototransduction process for subsequent retinal processing.

Rods and cones. The rod and cone pathways function with very similar principles, but the rods' phototransduction cascade is many orders of magnitude more sensitive than the cones', for reasons which are not totally understood (different concentrations of the chemical species involved, organization of the outer segments in dissociated disks rather than sacs, rapidity of the inactivation mechanisms, etc. [18]). In this chapter and in the sequel, we rather focus on the cone pathway, at the base of our precise daytime vision. The rod pathway, more useful at night and for movement detection, is mentioned specifically in Section 3.2.4.

Light receptors and horizontal cells have 'OFF' polarity. Due to the nature of phototransduction, incoming light reduces an incoming cation current, and thus lowers (hyperpolarizes) the cell's membrane potential, which corresponds to an 'OFF' behavior. This is true for rods as well as cones. Coherently with their single type of polarity, all light receptors express a single type of neurotransmitter: glutamate, which is an *excitatory* neurotransmitter.

In turn, horizontal cells post-synaptic to receptors are depolarized by glutamate (the natural response to this excitatory transmitter), and thus inherit from receptors' OFF polarity.

Adaptation to light. The main effect of phototransduction is the adaptation to various levels of luminance, mostly thanks to the modulatory effects of Calcium (and also pigment bleaching –pure inactivation of rhodopsin– at very high light levels).

To a first approximation, this adaptation can simply be modeled by the divisive effect of Calcium on [cGMP], as in the Van Hateren *et al.* model, without taking into account the supplementary effects of Calcium on the disk membrane cascade (in the model, a simple linear conversion from incoming light to [PDE**]). In this case, the divisive effect of Calcium on the steady-state level of [cGMP] allows to find back the parallel shift of photoreceptor response curves with increasing background light (Section 5.1).

1.2 Further processing in light receptors and horizontal cells

After phototransduction, light receptors' inner segments behave as 'traditional' retinal cells. They are linked to their neighbors by gap junctions, and have a complex interaction with horizontal cells and bipolar cells.

Gap junctions between receptors.

Light receptors are coupled through gap junctions, although not as strongly as horizontal cells (see e.g. Raviola-Gilula 73 [120] who demonstrate the results in primate, rabbit and turtle retinas). These gap junctions are partly responsible for the spread of the retinal *center* signal. Likely, they play a fundamental role in the retina's robustness to noise, by homogenizing the phototransduction noise between neighboring receptors, prior to any subsequent treatment.

Horizontal cells.

Light receptors make feed-forward connections to horizontal cells, and receive feedback from these. Modalities of the feedback are not totally understood, neither its global functional effects (supplementary adaptation to the local luminance and/or beginning of the *surround* opposition signal). This issue is discussed in the next section, where we present bipolar cells and the arousal of the center-surround organization.

2 BIPOLAR CELLS: THE RETINAL TURNTABLE

This section is devoted to bipolar cells, the intermediate excitatory cells which make synaptic connections both in the OPL and IPL (see Figures 1.8 and 1.9 in Chapter 1). The 'take-home message' of this section is that bipolar cells already display the typical spatio-temporal sensitivity evoked in the two preceding sections: They exist in ON and OFF versions (Section 2.1), have a center-surround architecture of their receptive field (Section 2.3), and exist in transient and sustained versions (Section 2.4). Furthermore, bipolar cells exist in several different subtypes, which mark the beginning of differentiation of the retinal output into various parallel pathways (Section 2.2).

One might ask then, what is the precise role of the many amacrine and ganglion cells which interact with bipolar cells in the IPL. Are all these diverse cells only dedicated to generating a spiking output from the signal of bipolar cells?

Nowadays, the current opinion [92, 129] is that the bipolar signal is a 'basis' signal, for which the typical spatio-temporal band-pass operations have already been performed, and that is combined by cells in the IPL in various ways – often nonlinearly – to produce parallel flows of information at the retinal output, with different properties. The combination of the bipolar signal into various retinal pathways, at the level of the IPL, is developed in Section 3.

2.1 ON and OFF pathways arise at the level of bipolar cells

Unlike photoreceptors and horizontal cells that exist in a single polarity (OFF), bipolar cells exist under ON and OFF versions, marking the initiation of the 'ON' and 'OFF' cellular pathways. At each cone synaptic terminal, the receptor's signal is transmitted to both an ON and an OFF bipolar cell, through different synaptic interactions :

- OFF bipolar cells make 'basal' junctions with their presynaptic cones (Figure 3.4). There, OFF bipolar cells express ionotropic receptors to glutamate, which tend to depolarize ('excite') the cell when glutamate is released by the cone. As a result, these synapses preserve the polarity of the cones' response, making the bipolar cells 'OFF' type.
- ON bipolar cells make 'invaginating' junctions with their presynaptic cones (Figure 3.4). Unlike OFF bipolar cells, ON bipolar cells must invert the polarity of their response to light, and be inhibited by the cones' released glutamate, although this is a typically excitatory neurotransmitter. To achieve this, ON bipolar cells express a specific *metabotropic* receptor to glutamate, termed mGluR6, which in turn activates a G-protein, causing the cell to hyperpolarize in response to glutamate [102].

2.2 Subtypes of bipolar cells

Unlike photoreceptors and horizontal cells which exist in relatively few subtypes in mammalian retinas (3-4 subtypes of receptors, including color sensitivity, and 2-3 types of horizontal cells), bipolar cells exist in around 10 different subtypes.

Primate retina. In the primate retina, Boycott and Wässle 91 [16] have established the morphological classification of 11 subtypes of bipolar cells (Figure 3.6). Here are the main subtypes identified:

- A single ON cell is dedicated to integration of the rod signal (see Section 3.2.4).
- A single ON cell is dedicated to integration of the signal from 'Blue' (S-type) cone receptors (see Section 3.2.3).
- One ON and one OFF type, known as '*Midget*' bipolar cells, are the most numerous, and spatially precise. Each midget cell connects only a small number of cones: In the fovea, cones and midget bipolar cells are even in a one-to-one connection (Masland 01 [92]). In turn, midget bipolar cells connect 'midget' ganglion cells (Section 3), also in a one-to-one connection at the level of the fovea.
- The remaining cells, known as '*Diffuse*' bipolar cells, connect more cones, so that they have less spatial precision. 'Diffuse' is a rather generic term which applies to all 'non-midget' bipolar cells of the primate. Several different types of diffuse bipolar cells make contact with the wide α ganglion cells which form the basis for the 'Movement' pathway in the brain (Section 3.2.2). But diffuse cells also provide input to other, less well known ganglion cells. Globally, little is known about the specificities and roles of each different type of diffuse cell.

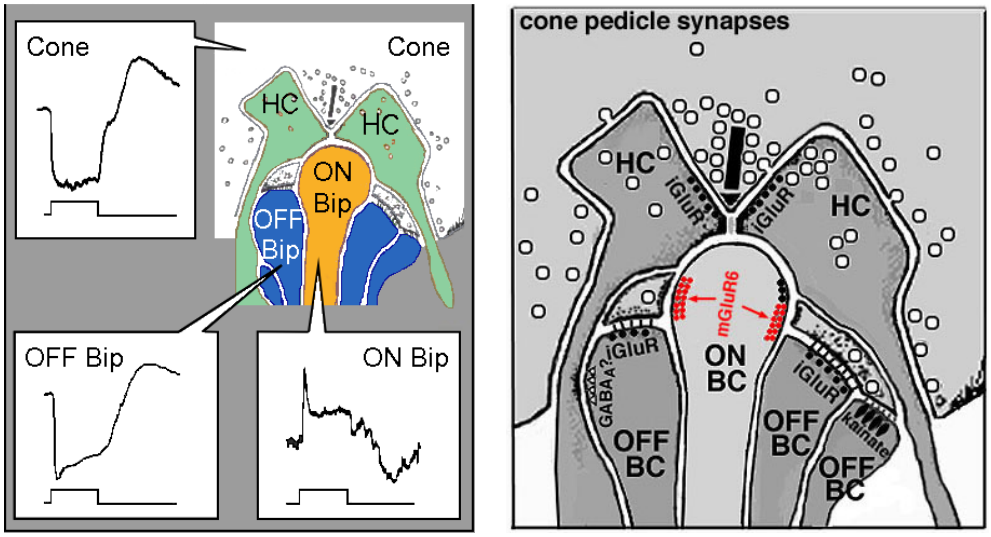

(A) The OPL synaptic triad (B) Known synaptic receptors

Figure 3.4: *Signal transmission from a cone to ON and OFF bipolar cells occurs at the cone's pedicle synapses. A:* In response to a step of light, cones are hyperpolarized and diminish their release of glutamate. OFF bipolar cells make basal junctions with the cones, while ON bipolar cells make invaginating junctions, and display and inversion of polarity w.r.t. cones. *B:* Known synaptic receptors expressed at the level of the cone pedicles. Horizontal cells and some OFF bipolar cells express the ionotropic receptor iGluR to glutamate, preserving the polarity of signal transmission. ON bipolar cells express the metabotropic receptor mGluR6 that allows a hyperpolarization by glutamate (polarity inversion). From [83].

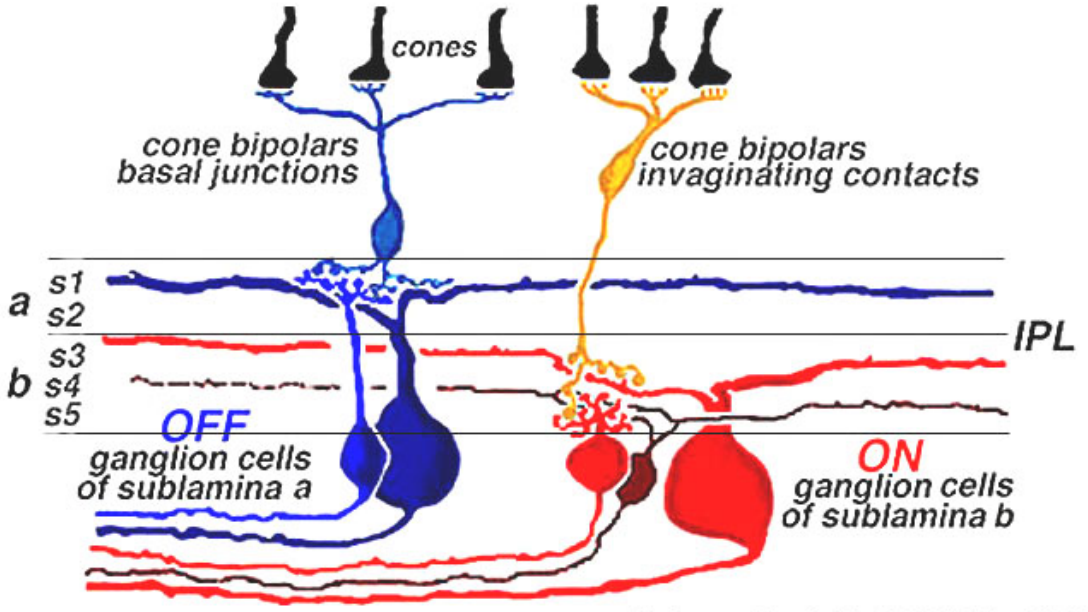

Figure 3.5: Synapses in the IPL occur in two distinct laminae involving respectively the ON and the OFF pathways (with different bipolar, amacrine and ganglion cells). The laminae are further divided into five strata, denoted s_1 to s_5 (see Section 3). From Nelson *et al.* 78 [103], found at [83].

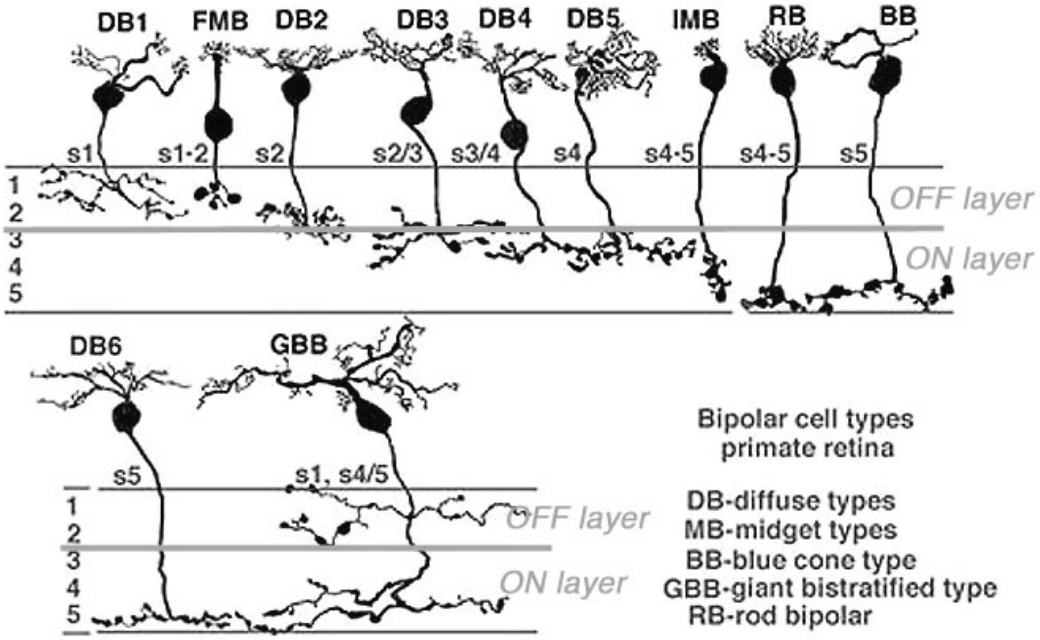

Figure 3.6: Morphological classification of bipolar cells in the primate retina. From Boycott-Wässle 91 [16], found at [83].

Other mammalian retinas. In other mammals also, there are around 10 different subtypes of mammalian cells (see e.g. Boycott and Wässle 74 [15] or McGuire *et al.* 84 [95] in the cat retina). The classification previously given for primate retinas holds, with one difference: Other mammals do not possess such specialized and precise cells as primate 'midget' cells. However, distinct subtypes still display different sizes of dendritic trees, implying different levels of spatial precision and different functions [95].

Bipolar cell axons in the IPL. The IPL is a thick (as compared to the OPL) and very ordered synaptic structure. Several parallel pathways of information emerge there, each involving different bipolar, amacrine and ganglion cells, and the corresponding synapses of the different pathways are segregated vertically (see Section 3). As a result, various sub-types of bipolar cells have their axonic arborization at different depths in the IPL.

First, ON and OFF pathways are anatomically segregated: The IPL is divided in two *laminae*, termed a and b, and each of these laminae is specifically concerned with all the synaptic interactions of only one polarity: a is the OFF lamina, and b the ON lamina (see Figure 3.5). Second, the two laminae are further divided into five specific synaptic *strata*, termed $s1$ to $s5$, and different sub-types of bipolar cells have their axon terminals in different strata (Figure 3.6).

2.3 Center-surround architecture of bipolar cells

It is now well established that bipolar cells already display the center-surround spatial opposition so typical of retinal processing. In this section, we first present the characteristics of bipolar cells' center-surround filter: Most bipolar cells display the center-surround sensitivity, but the size of their receptive field depends on the subtype considered. Then, we question the nature of bipolar cells' center-surround opposition: Does it arise from synaptic interactions in the OPL (as caused by horizontal cells), or in the IPL (as caused by amacrine cells)? Also, does it rely on synaptic feedbacks, or on feedforward transmission from horizontal cells? To these last questions, only partial answers exist.

2.3.1 Center-surround receptive field in bipolar cells.

Bipolar cells have long been suspected to display center-surround organization of their receptive fields. The result was proved a long-time ago for the salamander retina (Werblin and Dowling 69 [162]) where the cells are fairly large (see also Hare and Owen 90 [61, 62]). By opposition, mammalian and especially primate bipolar cells have been subject to much more interrogations, because intracellular recordings were much harder in these cells with a very small soma: As a result, some 'old' recordings reported little or no *surround* component in the receptive fields of mammalian bipolar cells (Nelson and Kolb 83 [104]).

Though, recent studies tend to prove that a center-surround opposition is also present in mammalian bipolar cells (see Dacey *et al.* 00 [31] for the primate retina, and supplementary reference). In the primate, both diffuse and midget cells display a center-surround opposition, but with much larger receptive fields in the case of diffuse cells, in particular concerning the *center* signal (Figure 3.7).

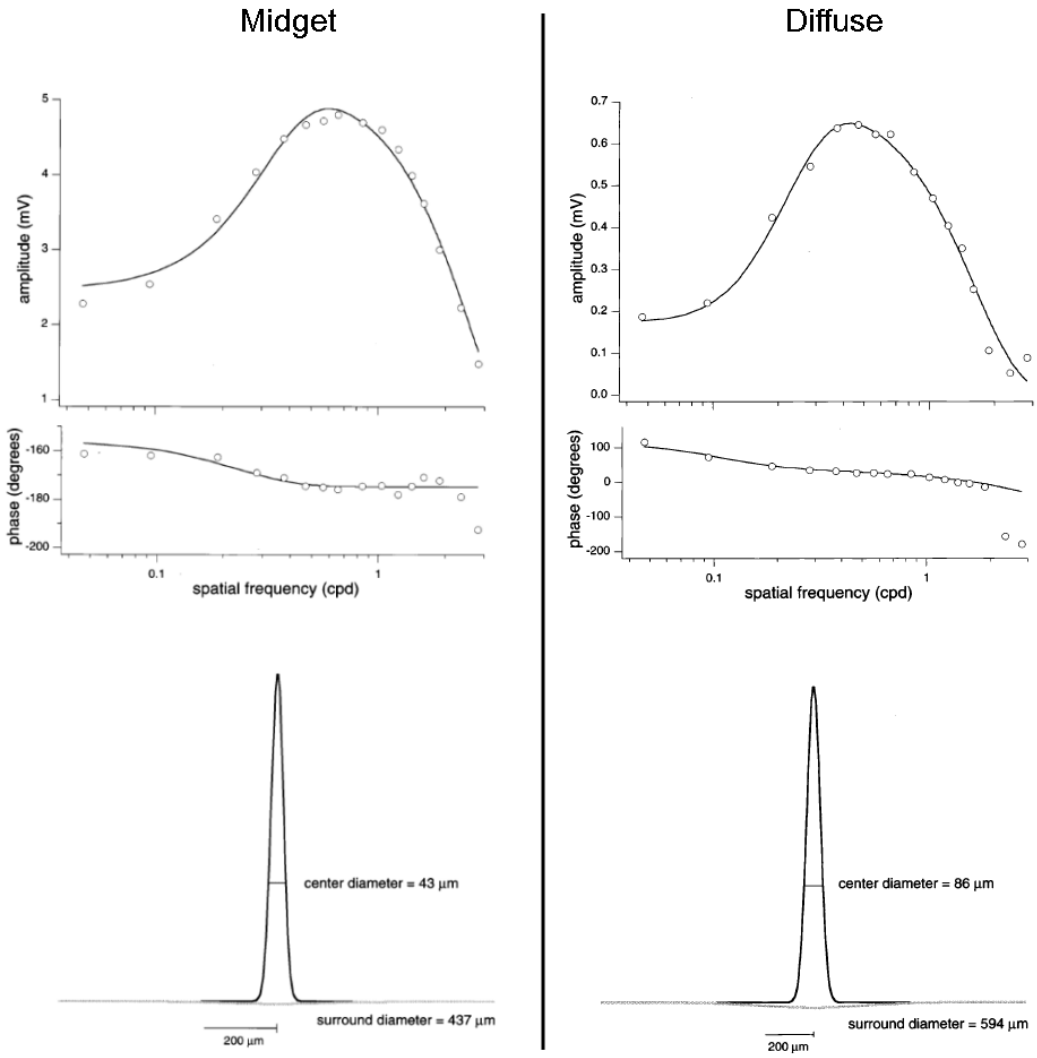

Figure 3.7: *Center-Surround structure in primate bipolar cells.* Sensitivity to drifting gratings and DOG approximation for one 'midget' and one 'diffuse' bipolar cell in the primate retina. Note that the cells are from the retinal periphery: In central retina, all scales would be much smaller. From Dacey *et al.* 00 [31].

Relative weight of center and surround. The authors in [31] measured the relative weights of *center* and *surround* signals: These relative weights were close to 1 in average, but with a certain variability, especially for diffuse bipolar cells (some relative weights were close to 3). By this aspect too, midget bipolar cells appear to form a homogeneous class well suited for precise vision, while diffuse bipolar cells appear more heterogeneous, and possibly mediating other visual features. In the salamander retina also, some variability is seen in the relative weight between *center* and *surround*: Hare and Owen 90 [61] find it around 0.6 for ON cells and 0.9 for OFF cells.

Relative sizes of center and surround. An even more striking feature is the relative sizes of *center* and *surround* signals: The authors in [31] found that, for midget bipolar cells, *center* and *surround* sizes are in an average ratio of 10. This result compares relatively well to the average ratios of 7-8 found between *center* and *surround* for primate midget *ganglion* cells by Croner and Kaplan 95 [30]. This intriguing number raises important issues concerning the edge detection capabilities of our retinas: We have seen in Section 2 how a linear model with such a ratio between *center* and *surround* is likely *not* to be able to detect edges.

2.3.2 Controversial origin of the center-surround mechanism

Although center-surround opposition is probably one of the best known properties of retinal filtering, its biological origins are still somewhat controversial. The basis principle is relatively well-settled: Some inhibitory interneurons – horizontal cells and/or amacrine cells – compute a local average of the excitatory cells' signal, and transmit it back to excitatory cells through inhibitory synapses, thus creating the *surround* signal.

It is also well settled that the spatial extent of the *center* and *surround* signals is due in good part to gap junctions between neighboring cells – although naturally, the morphological spread of dendritic trees (and even axons, for some amacrine cells) also plays a role in the spatial extent of receptive fields. Actually, gap junctions between neighboring cells of the same type have been observed for all types of retinal cells (see e.g. Kolb 79 [82] in the IPL).

But a distinct question is the nature and location of synaptic interactions that mediate the *opposition* between *center* and *surround*. The existence of two successive layers of inhibitory cells in the retina raises strong questions concerning their respective roles in spatial (and temporal) oppositions, especially since the traditional center-surround opposition could be theoretically explained by a single layer of inhibitory cells.

Bipolar cells are at the core of these intriguing questions, since they receive synaptic inputs from both horizontal and amacrine cells.

2.3.3 Center-surround opposition in the OPL

The 'mainstream', or 'historical', view is that the center-surround mechanism arises mostly due to the synaptic opposition between receptors and horizontal cells, in the synaptic triad onto bipolar cells.

Feedback to receptors. Feedback synapses from horizontal cells onto receptors are traditionally cited as the primary origin of center-surround opposition. For example, a strong feedback has been shown from horizontal cells to cones in non-mammalian retinas such as salamander or turtle[2]. However, the precise medium for this feedback is not known: GABA synaptic inhibition is the traditional assumption, yet it lacks experimental evidence [161]. Other models have been proposed that do not involve feedback synapses, but rather electrical gradients at the synaptic terminal of cones (work of Kamermans and colleagues [74]).

Also, the 'main' functional role of the feedback is not clearly assessed. Rather than creating a linear surround, the main role could be to provide nonlinear *divisive invariance* to cones, based on the local level of light in the neighborhood as measured by horizontal cells. A 'linear ODE' formalism (e.g., conductance feedback) could account for this phenomenon, pretty much like the contrast gain control loop used in our model (Wohrer 08 [163], Chapter 4, Section 4). See for example the model of Van Hateren of cone/horizontal coupling [155]. In this case, the linear center-surround observed in cones may be only a secondary effect, due to the synaptic conductances' hyperpolarizing Nernst potential.

Feedforward to bipolar cells. Furthermore, a *feedforward* transmission from horizontal cells to bipolar cells has also been observed, both in mammalian and non-mammalian species, that very likely adds its effects to the feedback mechanism onto receptors. Interestingly, the best candidate for synaptic transmission between horizontal and bipolar cells is also GABA, traditionally an inhibitory transmitter, which is supposed to provide simultaneously inhibition to OFF bipolar cells and excitation to ON bipolar cells: It is believed that ON and OFF bipolar cells express different chloride transporters, to achieve different equilibrium potentials for ion Cl^- that is associated to the GABA receptors (works of Vardi and colleagues)[3].

Whatever the medium (feedforward or feedback), there is undeniably a *surround* influence of horizontal cells at the level of bipolar cells. It should be noted that, when solely a *linear* feedback is implemented between cones and horizontal cells, it produces a relative weight of *center* and *surround* signals strictly smaller than 1. So, relative weights of *center-surround* equal or bigger than 1 (as observed in many bipolar cells by Dacey *et al.* [31]) necessarily imply feed-forward transmission and/or nonlinear feedback enhancements of the *surround* signal.

Remark: Linear feedback from horizontal cells

Let us prove that a linear feedback cannot achieve a relative *center-surround* weight of 1: Let $V_R(x, y, t)$ and $V_H(x, y, t)$ be the respective potentials of receptor and horizontal layers. The excitatory current on receptors provoked by phototransduction is noted $I^{exc}(x, y, t)$. Then, the feedback couples linearly $V_R(x, y, t)$ and $V_H(x, y, t)$, through two equations similar to (2.19):

[2]Many references can be found at website Webvision [83], more precisely at the page of horizontal cells: http://webvision.med.utah.edu/HC.html#Feedback

[3]We refer to the 'horizontal cell' page of website Webvision [83] for further details and references: http://webvision.med.utah.edu/HC.html#Functional%20Roles

$$\frac{dV_R}{dt}(x,y,t) = \mathcal{G}_R \Delta V_R(x,y,t) - g_R V_R(x,y,t) + I^{exc}(x,y,t) - (aV_H(x,y,t) + b) \tag{3.2}$$

$$\frac{dV_H}{dt}(x,y,t) = \mathcal{G}_H \Delta V_H(x,y,t) - g_H V_H(x,y,t) + (cV_R(x,y,t) + d), \tag{3.3}$$

where $cV_R(x,y,t) + d$ represents the (linear) excitatory current from receptors to horizontal cells, while $aV_H(x,y,t) + b$ represents the (linear) feedback current from horizontal cells to receptors, which is always inhibitory. $\mathcal{G}_R$ and $\mathcal{G}_H$ model gap junctions between receptors and horizontal cells respectively.

Through subtraction of the static solution of this system, we can always suppose $b = 0$ and $d = 0$. Then, $V_H(x,y,t)$ and $V_R(x,y,t)$ bear Fourier transforms, for which the coupled system can be solved, yielding:

$$\widetilde{V}_H(\xi_x,\xi_y,\xi_t) = \widetilde{H}_H(\xi_x,\xi_y,\xi_t)\widetilde{I}^{exc}(\xi_x,\xi_y,\xi_t),$$

with

$$\widetilde{H}_H(\xi_x,\xi_y\xi_t) = \frac{c}{ac + \big(g_R + \mathcal{G}_R(\xi_x^2+\xi_y^2) - \mathbf{j}\xi_t\big)\big(g_H + \mathcal{G}_H(\xi_x^2+\xi_y^2) - \mathbf{j}\xi_t\big)}. \tag{3.4}$$

This is also the asymptotical expression found by J. Hérault in the case of a discrete array of cells (forthcoming book Hérault 08 [67], see also Hérault 01 [66]).

Equation (3.4) involves the total gain of the feedback loop, ac. By studying the partial derivatives of $\widetilde{H}_H(\xi_x,\xi_y,\xi_t)$ w.r.t. ξ_x, ξ_y and ξ_t, one finds that $\widetilde{H}_H$ is always a spatial low-pass, but that it can become temporally band-pass if the gain of the feedback loop gets too high, possibly implying undesired oscillations.

More importantly, when the horizontal signal is transmitted back to cones through (3.2), it creates a *surround* component in the cone response whose Fourier transform is $a\widetilde{H}_H(\xi_x,\xi_y,\xi_t)$, so that the relative weight of *surround* w.r.t. *center*, measured at the DC output of cones (null frequencies in the Fourier transform), is $w = ac/(ac + g_R g_H)$, a number always strictly smaller than one. Furthermore, in real retinas, the gain of the feedback loop ac cannot get too high, in order to avoid strong temporal oscillations (see Hérault 08 [67]).

Hence, in the case of a linear model, a supplementary feedforward transmission from horizontal cells to bipolar cells is mandatory to obtain a relative gain of 1 or more. ■

2.3.4 Center-surround opposition in the IPL

In parallel to the 'textbook' version of center-surround interactions arising between light receptors and horizontal cells, different considerations speak in favor of a contribution of amacrine cells to the observed *surround* of ganglion cells, and also possibly of bipolar cells through feedback interactions.

The various roles of amacrine cells in shaping ganglion cells' responses are rather discussed in Section 3 when presenting the different retinal output pathways. Here, we take a different, more generic approach: What is known concerning the compared contributions of OPL and IPL processes to the overall center-surround organization in ganglion cells?

Amacrine surround in bipolar cells. In our readings, we have not come across the unambiguous proof of an amacrine *surround* component in bipolar cells. However, anatomical considerations (and, likely, articles unknown of us) speak in favor of such a fact: Several identified types of amacrine cells are linked by gap junctions to their neighbors (bipolar and/or amacrine and/or ganglion, according to the type of amacrine cell considered), possibly implying a consequent extent of their receptive

fields[4]. Simultaneously, several amacrine cells make feedback connections to bipolar cells, through gap junctions or chemical synapses[5]. Should one type of amacrine cells display both features simultaneously (spatial extent and feedback to bipolar cells), it would naturally provide their target bipolar cells with an extended *surround*.

Horizontal cells have too big receptive fields. Various physiological measurements directly on ganglion cells add direct or indirect evidence to the roles of some amacrine cells in spatial oppositions. In the rabbit retina, typical receptive fields for horizontal cells have been measured between 2 and 3 mm (Dacheux and Raviola 82 [36]), whereas brisk sustained (X) ganglion cells (Section 3.2.1) *surround* receptive fields, in response to drifting gratings, are often measured at less than 1 mm (DeVries and Baylor 97 [45]). It is thus possible that the 'overall' *surround* of these cells rather arises from inhibition by neighboring amacrine cells [6].

Still in the rabbit, the most spatially precise retinal cells, the local edge detectors (LEDs, Section 3.2.6) can have inhibitory *surround* receptive fields markedly smaller than 1 mm, and in this case the effect has been demonstrated to arise from amacrine cells.

Experimental comparisons of OPL and IPL contributions. Experimentalists have recently started to question the respective impacts of OPL and IPL with more quantitative tools, at the ganglion cell output. In the primate retina, Mc Mahon *et al.* 04 [96] found that GABA-ergic amacrine cells (generally wide-field) have a minority influence on parasol cells' classical *surround*. In rabbit cells however, Flores-Herr *et al.* 01 [54] measured an influence (moderate) of amacrine cells on the *surround* of most ganglion cells.

Nature of the amacrine surround. In conclusion, the spatial effects of amacrine cells are far from being well understood, and two strong questions remain. First, is the amacrine-related *surround* a specificity of particular sub-types of ganglion cells? Second, to what extent do amacrine *surround* oppositions correspond to the 'traditional' *surround* observed in receptive fields and reverse correlation analysis, or to secondary 'silencing' effects modulating the already spatially band-pass signal of bipolar cells?

Partial answers can be found in the presentation of the different types of ganglion cells, in Section 3.2.

2.4 Temporal shaping in bipolar cells

To finish this presentation of bipolar cells, we mention their temporal behavior: All bipolar cells have a rather *transient* response to light stimulation, which arises simultaneously from different origins, and can have different time scales according to the sub-type of bipolar cells considered.

[4] From website Webvision [83], more precisely at the page of amacrine cells: http://webvision.med.utah.edu/amacrines1.html

[5] idem as footnote 4

[6] It is not possible to totally exclude other explanations for this discrepancy, without the need for amacrine cells: By differences of experimental protocols, or by an 'attenuation' of weak signals from horizontal cells' remote *surround* due to successive synaptic rectifications from horizontal cells to ganglion cells.

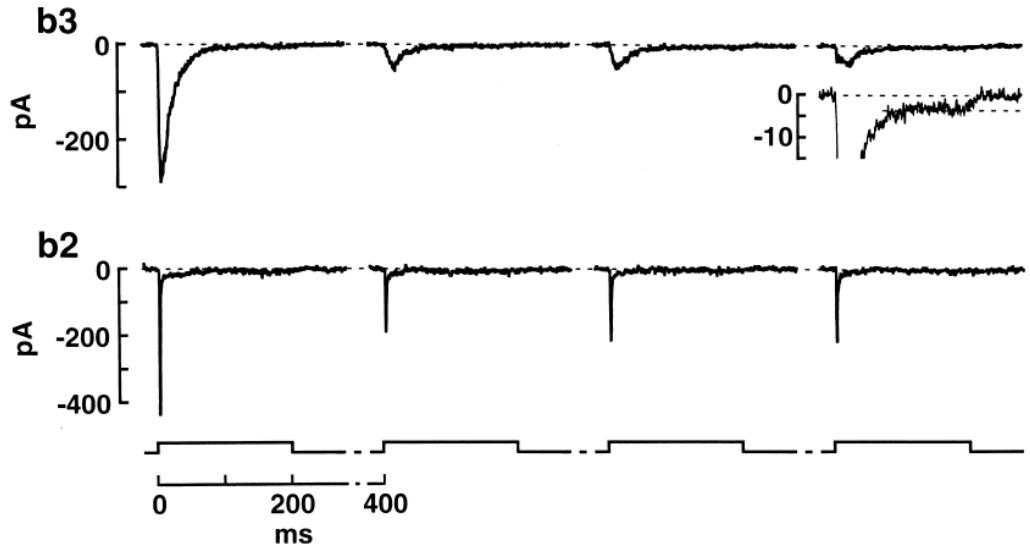

Figure 3.8: *Temporal band-pass properties of various bipolar cells.* Synaptic input currents of two types of bipolar cells (from ground squirrel retina). According to the type of synaptic receptor to glutamate they express, different bipolar cells filter the input cone signal with different time constants. For b2 bipolar cells (morphologically close to a primate DB3 diffuse bipolar cell [44]), a fast transient response arises from the fast alternation of desensitization and recovery in their AMPA receptors to glutamate. For b3 cells, kainate receptors to glutamate are *permanently* desensitized because of a longer recovery time constant, so their response reflects only the slow transient of the cone's response. From DeVries 00 [44].

Slow phototransduction transients

Phototransduction in cones may already display a partially transient response, with a time scale of approximatively 100 ms, as we have shown in Figure 2.4, from the experiments of Schnapf *et al.* 90 [133] on single cones. However, more recent results (Van Hateren and Lamb 06 [156], Section 1.1) tend to show that the photoresponse in humans (in vivo!) is actually monophasic and much faster (time constant around 10 ms): The authors suggest that the slow biphasic shape previously observed [133] was due to the *in vitro* conditions.

Horizontal cell opposition

Whether resulting from feedback or feedforward opposition, the *surround* signal provided by horizontal cells to bipolar cells can induce temporal transients because it is delayed in time, due to the supplementary membrane integration in horizontal cells. The strength of the horizontal cell opposition is probably dependent on the spatial structure of the image: the opposition should be rather strong in the uniform zones of the image, where the horizontal signal is as strong as the cone signal. Near image edges, where the cone signal is stronger than the horizontal signal, the temporal influence of horizontal cells is probably weaker.

Band-pass filtering by synaptic receptors

More importantly, it has been recently shown that the synaptic transmission from cone to bipolar can also induce intrinsic transients on the visual signal. DeVries and Schwartz 99 [46, 44] showed that the synaptic transmission from cones to OFF bipolar cells is very affected by rapid *desensitization* of the synaptic receptors to glutamate in the membrane of the bipolar cells: In a few tens of milliseconds, the *effective* synaptic transmission is reduced in a factor of 10, by a complex desensitization of most of the synaptic receptors.

The effect is represented in Figure 3.8: When a presynaptic cone undergoes a series of voltage steps (alternatively stopping and starting the glutamate release by the cone synapse), the synaptic current induced in the bipolar cells is a series of transient waves, whose amplitude is high during the first glutamate release of the experiment (left of the Figure), but consequently smaller during the next synaptic releases, because the synapse is *desensitized*. These 'reduced' responses are in fact the 'normal' responses of the synapse, because glutamate is continuously released by the cone in normal visual conditions.

Furthermore, as demonstrated by DeVries 00 [44], different bipolar cells express different synaptic receptors to glutamate, with different time constants for *recovery* from desensitization. Some cells, that have fast-recovering AMPA receptors, have a synaptic transmission that continuously undergoes alternate desensitization and recovery in response to the cone's glutamate release, and thus provide a very *high-pass* temporal filtering of the cone signal (b2 cells in Figure 3.8). Other cells, that have slow-recovering kainate receptors, are continuously desensitized during 'normal' visual stimulation, and thus provide a more low-pass filtering of the cones signal (b3 cells in Figure 3.8).

As argued by the author, very likely, the 'fast' AMPA cells are rather 'diffuse' bipolar cells specialized in temporal sensitivity, while the 'slow' kainate cells rather correspond to the primate

'midget' bipolar cells, less sensitive temporally but with a stronger spatial resolution. However, it should be remarked that even the 'slow' b3 cells display a *transient* synaptic current, although with a slower time scale: According to the author, this transient shape directly reflects the cone's synaptic release.

Band-pass filtering by amacrine cells

The preceding experiment concerned only cone synaptic inputs to bipolar cells (the bipolar cells' axons had been removed). A supplementary source of temporal transient has been found in bipolar cells, through the reciprocal inhibition of some amacrine cells in the IPL. Amacrine cells are known to be involved in the temporal shaping of ganglion cells' responses (Nirenberg *et al.* 97), and part of their temporal cutting effects are done by feedback connections to bipolar cells. These results were demonstrated for example by Euler and Masland 00 [52] in the rat retina.

Conclusion: A strong need for further exploration

In conclusion, the combined effects of synapses in the OPL and IPL provide bipolar cells with the spatio-temporal band-pass structure typical of retinal processing: ON and OFF cells, center-surround oppositions and temporal transients.

Also, separation of the visual signal into distinct pathways starts at the level of bipolar cells: The distinction is mostly between midget-like and diffuse-like bipolar cells ('midget' and 'diffuse' being a terminology reserved to the primate retina). Midget-like bipolar cells are the most precise spatially, and display temporal responses which are relatively sustained (or rather, transient with a longer time scale). By opposition, diffuse-like bipolar cells are less precise spatially, but display a series a temporal transients (including a very fast desensitization and recovery at their synaptic receptors) that helps to shape and enhance fast temporal variations in their input.

Bipolar cells, with their role of 'turntable' between OPL and IPL, are a fundamental key to understand the complex nature of further filtering in the IPL, and the functional 'task repartition' between OPL and IPL. Bipolar cells are still in a strong need of further exploration, and particularly the response characteristics of their different subtypes. Unfortunately, experimental exploration is made difficult by their small somata and 'hidden' locations in the Inner Nuclear Layer.

3 PARALLEL PATHWAYS OF THE RETINAL OUTPUT

3.1 Introduction: Ganglion cells and the Inner Plexiform Layer

3.1.1 Historical landmarks and bibliography

Concentric X and Y cells

Kuffler 53 [84] was the first to measure the center-surround, or concentric, receptive field architecture shared by many ganglion cells. Hubel and Wiesel 60 [71] also measured the concentric architecture, in their seminal series of papers on the receptive fields of low-level visual processing.

A few years later, Enroth-Cugell and Robson 66 [48] revealed the distinction between two distinct types of ganglion cells in the cat retina, which they named X and Y cells, that had markedly different physiological properties (detailed in the sequel). Since then, many subsequent pieces of work have reinforced knowledge on these two types of cells in different ways: Equivalents for X and Y cells have been found in other species, models have been proposed for the particular nonlinearity in the responses of Y cells, and the distinction between the two cell types has been further investigated in the light of other specific retinal effects such contrast adaptation, connectivity, temporal behavior, synchronies, etc.

Sluggish and non-concentric cells

In parallel, other work has revealed several types of ganglion cells which could not be labeled 'X-like' or 'Y-like'. In the 60s, Barlow, Levick and colleagues started a systematic study of ganglion cell types encountered in the rabbit retina, which revealed interesting new types of ganglion cells: Direction-selective (DS) cells (Barlow-Levick 65 [6]), local edge detectors (LED) and suppressed-by-contrast cells (Levick 67 [87]). Further studies have then revealed similar cells in the cat retina (Cleland and Levick 74 [27, 28], Stone and Fukuda 74 [145], Rowe and Stone 76 [130]). These cells were long thought marginal because rarely encountered. Only recently, it became increasingly clear that they all possess important and distinct functional roles.

For the occasion, Cleland and Levick also introduced the concept of *brisk* and *sluggish* cells, accounting for the fact that some ganglion cells ('brisk') have strong, fast and rather transient responses to light stimuli, while others ('sluggish') have slow responses, of smaller amplitude and which can develop over several seconds [27]. In this alternative classification, the X and Y cells of Enroth-Cugell and Robson were the *brisk* cells (X cells as 'brisk sustained' and Y cells as 'brisk transient'): Likely, it is the 'brisk' nature of their response (very reactive) that has made them the privileged targets of first physiological measures in the retina. Originally, Cleland and Levick reserved the 'brisk'-'sluggish' terminology to *concentric cells* only (with a clear center-surround architecture), but the terminology seems to have switched to a more general signification of 'sluggish', since some non-concentric cells (LED, suppressed-by-contrast) also have rather sluggish responses. Stone and Fukuda 74 [145] introduced the terminology of 'W cells' to designate all these sluggish, non-X and non-Y cells of the cat retina.

The primate retina

As opposed to other mammal species, primate retinas possess a much greater number of ganglion cells, due to the existence of a specialized pathway formed by the tiny and numerous 'midget' cells (see Section 3.2.1). As a result of the overwhelming statistical predominance of midget cells, non-concentric cells have been much less encountered and studied in the primate retina. However, non-concentric cells have occasionally been found (see e.g. De Monasterio-Gouras 75 [39]), and there is now an increasing certitude that all the typical mammalian concentric and non-concentric cells also exist in the primate retina, in numbers similar to other mammalians (Masland 01 [92]).

Morphology of ganglion cells

In parallel to the study of ganglion cells' various physiological properties, their *morphology* has been subject to a detailed analysis, especially in cat and rabbit retinas. Morphological studies, through various staining techniques, have long been favored as a relevant medium to classify the various types of ganglion cells, for two striking reasons:

1. The morphology of retinal cells is very stable across mammalian species. Although the sizes and relative proportions of ganglion cells vary from one species to another, there is an overall correspondence of morphological types across species.

2. There is a striking correspondence between morphology and physiological behavior: Both criteria (morphology and physiology) lead to the same classification of ganglion cells (see Masland 01b [93] for review).

Both facts tend to prove that the various morphological types of ganglion cells serve very precise, and distinct, functional roles.

Boycott and Wässle 74 [15] led the first 'modern' morphological study of the cat retina, distinguishing four morphological types that they referred to as α, β, γ and δ cells. It soon appeared that α cells correspond to the physiological Y cells, β cells to the physiological X cells, and that these two morphological-physiological associations hold across most mammalian species.

More recently, new techniques have provided accurate and systematic description of ganglion cells in the rabbit (Amthor *et al.* 89 [2], Rockhill *et al.* 02 [125]) and cat (works of Berson's lab, as cited in O'Brien *et al.* 02 [109]). In the primate retina, morphological descriptions also exist (Rodieck and Watanabe 93 [127], works of Dacey and colleagues as cited in Dacey 99 [33]). Although less systematic than in cat or rabbit, both these works are particularly interesting because they back-propagated a cellular staining from different visual areas onto the retina, thus giving insights on the cerebral projections -and hence of the function- of the different ganglion cells. However, their results remained partial and purely morphological.

Intracellular recordings

For electrophysiological measurements, intracellular recordings of ganglion cells are more and more favored. Where extracellular recordings allow only to measure a cell's emitted spikes, intracellular recordings also provide good approximations of *the excitatory and inhibitory synaptic inputs to the*

neuron (thanks to voltage clamps at different potentials). These techniques allow to gain insight on the connectivity of the measured cells, and they have recently provided interesting new results (some detailed in the sequel).

Interesting examples of such recordings in the rabbit retina are the work of Roska, Werblin and colleagues [129, 128], the work of Taylor, Vaney and colleagues (on DS cells [148] and on LED cells [158]), the work of Fried, Münch and Werblin on DS cells [55].

3.1.2 Architecture of the Inner Plexiform Layer

We now report more specifically what morphological studies have revealed concerning the spatial organization of the various subtypes of ganglion cells and amacrine cells in the IPL. First, the synaptic processes of cells from different morphological types are strongly segregated into different strata of the IPL. Second, all retinal cells of a same morphological type provide a continuous *paving* of the visual space. These two observations confirm the functional unity formed by cells of the same morphological type, and hence the notion of *parallel visual pathways* forming the retinal output.

Synaptic strata in the IPL define different pathways

We have already presented in Section 2 how the IPL is divided in two laminae involving respectively OFF and ON pathways (Figures 3.5 and 3.6). These laminae are further divided into five strata, termed s1 to s5, and different types of bipolar, amacrine and ganglion cells make their synaptic connections in different strata of the IPL (see Figure 3.6 for bipolar cells).

The dendrites of different subtypes of ganglion cells are represented in Figure 3.9. The first obvious vertical segregation is between the ON and OFF pathways, in the two sublaminae a and b. But there is also a clear vertical segregation between the different physiological pathways of ganglion cells[7].

However, although their synapses are spatially segregated, the various ganglion cell pathways are not independent. It has recently been demonstrated that many vertical flows of information between different pathways are present, likely mediated by amacrine cells: See Section 3.1.3.

Different pathways tile homogeneously the visual space

In addition to this 'vertical' architecture, the IPL should be well organized 'horizontally': If the various types of morphological cells really correspond to different functional pathways, then cells of the same type should be present at all locations of the retina, with receptive fields that provide a tiling, without holes, of the whole visual space. And indeed, this property of regular tiling has been proved for most morphological types of ganglion cells, and likely holds for all morphological types. Figure 3.11 shows the tiling of α (Y) and β (X) cells in the cat retina.

Note that this tiling property implies an inverse dependency between the size of a morphological cell type's dendritic tree, and the number of such cells present in the retina. This inverse dependency

[7] The central strata (close to the boundary between ON and OFF sublaminae) are sometimes said to involve more transient pathways than the exterior strata (close to INL or ONL), which involve more sustained pathways (Awatramani and Slaughter 00, Roska *et al.* 06 [128]). We personally did not find this division very obvious in our readings.

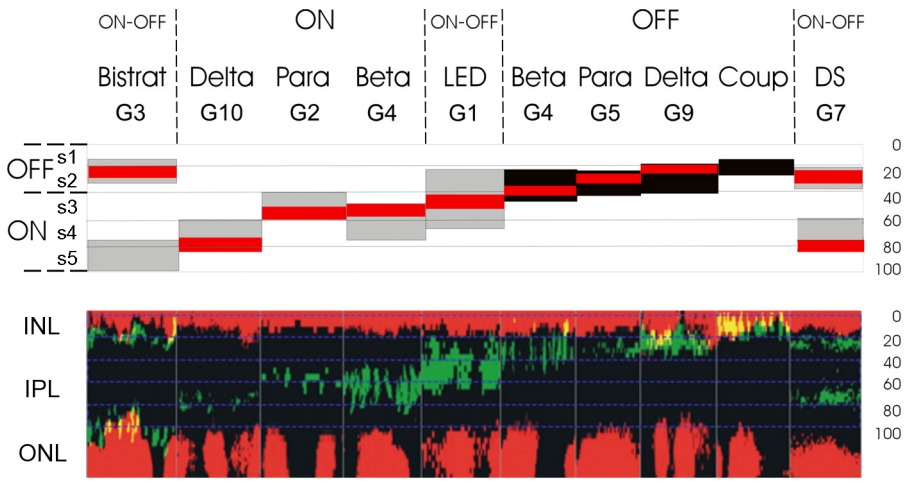

Figure 3.9: *Different pathways use different synaptic strata in the IPL. Up:* Correlation between ganglion types (morphological and physiological) and the locus of dendrites in the IPL. ON cells have their dendrites in sublamina b of the IPL, OFF cells in sublamina a. Three types represented here are ON-OFF cells having dendrites in both layers: Bistratified cells, local edge detectors (LEDs) and direction selective (DS) cells. From Roska *et al.* 06 [128]. The 'Gx' notations are the morphological classification of Rockhill *et al.* 02 [125]. *Down:* Corresponding microscopic images from the IPL (one different image per cell type), with the dendrites stained in green. All cellular bodies are in red (up: bipolar and amacrine cells in the INL, down: ganglion cells in the ONL). From Roska *et al.* 06 [128].

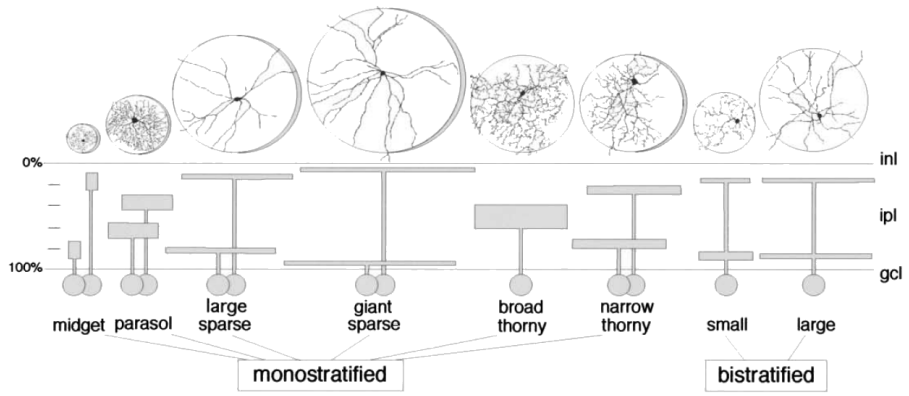

Figure 3.10: *Morphological types of primate ganglion cells that project to the LGN.* In addition to 'traditional' LGN-projecting cells (midget cells projecting to the P layers, parasol cells to M layers ans small bistratified cells to the K layers), other subtypes of ganglion cell seem to provide input to the LGN, and possibly to our conscious perception. From Dacey *et al.* 03 [35].

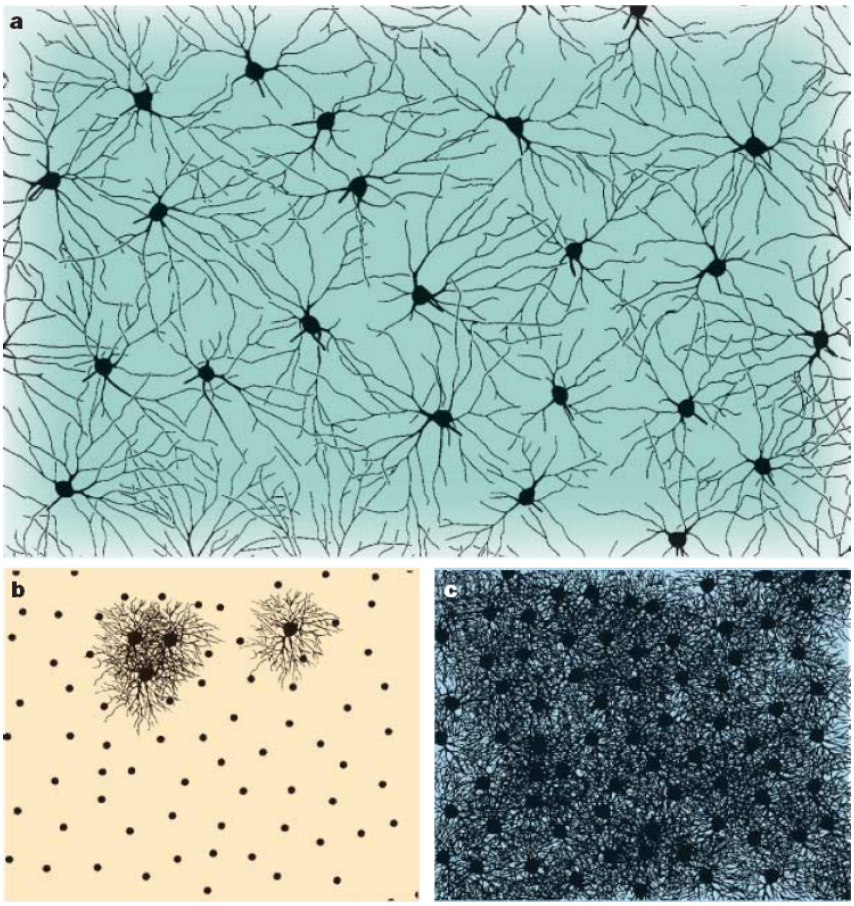

Figure 3.11: *Tiling of the visual space by α and β cells. a:* ON α ganglion cells in a 1.2 x 1.8 mm patch of cat retina. *b:* ON β ganglion cells in the cat retina, with roughly the same scale. The dots indicate the cell's locations. *c:* Computer reconstruction of all dendritic trees from the data in b. From Wässle 04 [161].

is well verified by most known types of cells (De Vries and Baylor 97 [45], Wässle 04 [161]).

To conclude, the spatial organization of synapses in the IPL allows various pathways of cells to simultaneously tile the visual space, thanks to a vertical segregation of their dendrites in the different strata of the IPL. These various pathways form parallel flows of information at the output of the retina, most likely with different and specific functions.

3.1.3 Amacrine cells

Amacrine cells are the most diverse class in the retina: Around thirty different subtypes have been reviewed morphologically (Masland 01 [93]). They are also, by far, the less well-understood type of cell. Although they are putatively associated to many different tasks of signal shaping in the IPL, there are only few examples for which the role of a particular subtype of amacrine cell has been rigorously proved, in association with a precise description (morphological of physiological) of the subtype in question.

Throughout the following presentation of ganglion cells (Section 3.2), amacrine cells will be mentioned several times as playing an important role. Here, we give general landmarks on the nature of amacrine cells, and a summary of their presumed functionalities, with pointers to the corresponding sections in the sequel.

Narrow-field and wide-field amacrine cells. The major distinction in the amacrine cell population can be done between *narrow-field* and *wide-field* amacrine cells. The two types possess fundamentally different roles. Narrow-field amacrine cells are involved in local calculations, providing a constant shaping of the bipolar and ganglion signals (for example, through delayed inhibitions). Wide-field amacrine cells, by opposition, are involved in transmitting remote inhibitions to ganglion cells, and likely contribute to create the wide, nonlinear inhibitions generically referred to as the *non-classical surround* of ganglion cells (Troy and Shou 02 [152]). As an additional particularity, many wide-field amacrine cells fire spikes, and can thus be involved in complex synchronization effects.

GABA and glycine. An alternative criterion to distinguish amacrine cells is according to the type of neurotransmitter they release. Amacrine cells use two main[8] neurotransmitters: GABA and glycine. Interestingly, the resulting classification of amacrine cells has strong overlaps with the wide/narrow field classification: All wide-field cells are GABA-ergic, and most narrow-field cells are glycinergic, although some narrow-field GABA-ergic cells also exist.

This provides a good experimental means to assess the different roles of narrow- and wide- field amacrine cells, through the use of chemical antagonists: Picrotoxin blocks all GABA-ergic amacrine transmissions, while strychnine blocks all glycinergic amacrine transmissions (see, e.g., Caldwell *et al.* 78 [22] for a more detailed description of the effects of these antagonists).

[8] Rarer neurotransmitters (acetylcholine in DS cells) and neuromodulators (dopamine) are also released by some amacrine cells.

Presumed roles of amacrine cells. Here are the different presumed roles of narrow-field and wide-field amacrine cells, as presented in the sequel:

- Temporal shaping (transient) of ganglion cells responses, especially Y cells (Section 3.2.2). Narrow-field amacrine cells likely play the strongest role in this shaping.
- Contribution to the spatial *surround* of the most 'precise' ganglion cells. Narrow-field amacrine cells are responsible for the strong and narrow inhibitory *surround* of LED cells (Section 3.2.6). Likely, similar inhibitions also occur in X cells (Section 3.2.1).
- Suspected 'vertical' transmission of information between the ON and OFF pathways, otherwise segregated. A 'push-pull' transmission of 'negative' signals to ON ganglion cells by OFF amacrine cells, and reciprocally, has been hypothesized (Figure 3.29), probably relying on narrow-field amacrine cells.
- Inhibition related to global movements of the background is likely provided by wide-field spiking amacrine cells to 'object motion sensitive' ganglion cells, such as ON Y cells (Section 3.2.2).
- Stimulus-dependent spike synchronies (Section 4.3) very likely rely on wide-field amacrine cells.

Inhibition as the dominant shaping factor of the IPL. To conclude on the general importance of amacrine cell inhibition, we review this intriguing observation (Brivanlou *et al.* 98 [17], salamander retina): When *all* synaptic transmission (excitatory and inhibitory) was blocked in the IPL (so that ganglion cells were, so to speak, 'left on their own'), the net number of emitted spikes *augmented*. This observation can be explained by intrinsic depolarizing conductances in ganglion cells' membranes.

Even if these results are possibly linked to the given experimental setup, they suggest that ganglion cells undergo a constant and strong inhibition from amacrine cells during normal visual stimulation (see also Figure 3.29). So likely, amacrine inhibition has a fundamental role in shaping ganglion cell responses, comparable or even superior to direct excitation from bipolar cells.

3.2 Physiology of the different visual pathways

In this central section, we present the physiological properties of the various types of ganglion cells forming the retinal output. We try as much as possible to link these properties to specific functional roles of the associated visual pathway in further cerebral processing. However, for most types of cells, the precise functional roles are still hypothetical, based on inferences from their physiological type of response.

We start by presenting the classical 'brisk' retinal cells, respectively 'brisk sustained' (X) (Section 3.2.1) and 'brisk transient' (Y) (Section 3.2.2) cells.

The two following sections review how the initial diversity of photoreceptors (various color cones and rods) is relayed at the retinal output. Cells involved in the coding of color are specifically

mentioned in Section 3.2.3, and the integration of the rod signal to the retinal output, by various pathways, is mentioned in Section 3.2.4.

Section 3.2.5 is dedicated to a short presentation of direction-selective (DS) cells in the retina, whose working principles and function in visual processing remain somewhat mysterious after 40 years of intensive studies.

The remaining sections are devoted to the description of 'sluggish' ganglion cells, which have been subject to much less investigation until recent years. These ganglion cells were once termed 'rare' because they were less numerous than β cell, and less remarkable than α cells. It now appears likely that some of them are more numerous than α cells, and have important but badly established roles in visual processing. Without entering too much details, we specifically present one such type of sluggish cell, the local edge detector (LED), in Section 3.2.6. Section 3.2.7 then evokes other observed types of sluggish cells, and hints for their roles in visual processing.

Throughout this presentation, we try to provide references to relevant bibliography which can serve as an 'entrance door' to these different types of cells. Before we move on, let us review here some especially important references of our work: A general review of most types of retinal cells can be found in Troy and Shou 02 [152], and compared to the very interesting and visual work of Roska *et al.* 06 [128] presenting response patterns for most types of rabbit ganglion cells.

A good introduction to DS cells is provided by the recent works of Fried *et al.* 02 [55], and the review of Taylor and Vaney 03 [148].

Finally, most types of sluggish cells are very well presented in the classic work of Levick 67 [87]. Caldwell *et al.* 78 [22] provide interesting insights on the roles of amacrine cells in shaping the complex and slow responses of these cells. More recently, the dynamics and sensitivity of sluggish cells have been studied by Xu *et al.* 05 [165]. Hendry and Reid 00 [63] have reviewed the projections of sluggish cells to the koniocellular layers of the LGN, implying possible perceptual roles - yet unknown.

3.2.1 Brisk sustained (X) cells

These cells, originally termed 'X cells' by Enroth-Cugell and Robson 66 [48] in the cat retina, are the 'archetypal' ganglion cells. Their mode of response, illustrated for a static grating in Figure 3.12 *A*, correspond to what could be termed the 'generalist' vision of retinal processing:

- They have fast and strong ('brisk') responses to changes in contrast of the input image.
- Their response to a change in contrast is rather sustained, consisting of a strong initial transient that slowly declines over several hundreds of milliseconds.
- Their response is fairly linear with the spatial profile of the input image, and their linear receptive field is well modeled by a DOG, reflecting a strong center-surround organization. This is illustrated by the 'null position' test of Figure 3.12 *A*, or by responses to a drifting grating, as in Figure 2.1 which displays the response of a primate 'midget' cell.
- They have small receptive fields, resulting in a sensitivity to image details at fine scales (sensitivity to high spatial frequencies).

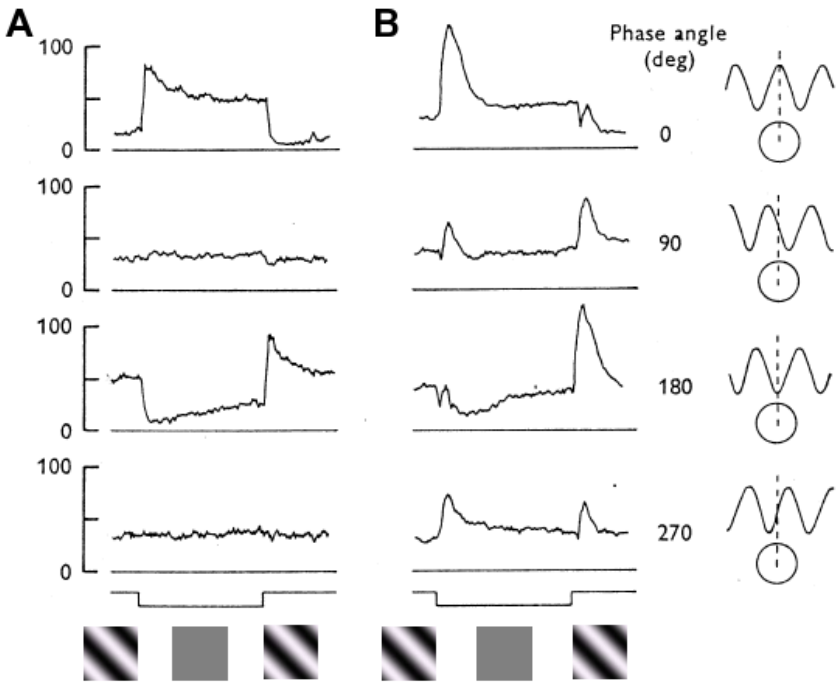

Figure 3.12: *Response of X and Y cells to a flashed grating.* Trial-averaged firing rates of a cat OFF-center X cell (*A*) and OFF-center Y cell (*B*), in response to the disappearance and reappearance of a static grating with different spatial offsets (right). If the cell proceeds to linear summation of its input, there is an offset of the grating for which the cell has a null response, when the positive and negative parts of its signal counterbalance each other. The 'null position' exists in X cells but not in Y cells, revealing a nonlinearity. Also, Y cells are more transient than X cells. Total time 2s. From Enroth-Cugell and Robson 66 [48]

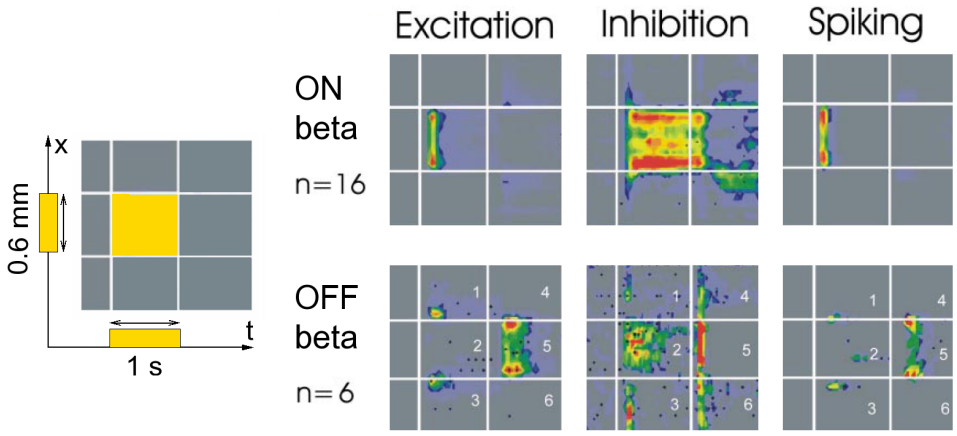

Figure 3.13: *Rabbit β (X) cells respond to a static square. Left:* Stimulus is the apparition of a static square of light for one second, here represented along time and one spatial dimension. *Right:* Reconstructions of the response of ON and OFF rabbit β (X) cells to the stimulus, with the same space-time representation. Excitatory and inhibitory input conductances to the cells are represented, and the resulting spiking activity for the cells. Both ON and OFF β cells have rather transient responses (although they are known as *sustained* cells), and respond preferentially to the square's edges, as predicted from a DOG model. Each reconstruction is obtained from a single cell in response to different offsets of the square stimulus. Then, reconstructions are averaged over the indicated number n of cells of the same type. From Roska *et al.* 06 [128].

- They exist in ON and OFF versions, allowing the separate detection of light and dark contrasts.

Morphologically, brisk sustained cells correspond to the β type, which is observed in all mammalian retinas. The β type is characterized by its small dendritic tree, in good adequation with the small receptive fields observed physiologically. As expected from the tiling principle presented above, β cells are therefore numerous, providing a dense tiling of the retinal space (see Figure 3.11). They account for around 50 % of ganglion cells in the cat retina (Wässle 04 [161]).

Functionally, the brisk sustained (X) cells are well suited for providing the 'precise' vision pathway of the animal. Their small receptive fields and rather long-lasting responses make them a suitable source of information to transmit precise, static image contours. As an argument for this 'precise' role, β cells are particularly small and numerous in the *area centralis* of cats and in the *fovea* of primates ('midget' cells). In the primate retina, midget cells are connected to the Parvocellular pathway of the LGN, and they constitute the primary source of information for the 'Form' pathway of visual processing.

In dichromat mammals (most mammals, with only two different types of cones), brisk sustained (X) cells are achromatic: They only see 'in black and white'. Indeed, in dichromat mammals, a strong majority of cones are of the 'L'-type (long wavelength), and thus provide a monochromatic input to β cells. See Section 3.2.3 about color pathways for more details.

It should be noted that β cells are not the only candidate for precise vision in mammalian retinas. The much less understood local edge detectors (LEDs, see Section 3.2.7) play a role very similar, with small dendritic trees and responses to fine contrast. In the rabbit, β cells seem to be *less* precise than LEDs. In cat and primate, β cells seem to be the most precise cells.

Finally, β cells are generally renowned as 'simple' retinal cells, with a simple center-surround architecture quite similar to that presumed in their presynaptic bipolar cells. Figure 3.13, in the rabbit retina, illustrates how even β cell can possibly receive a strong inhibition from amacrine cells, whose role is not clear yet (possibly, a 'tightening' of the cells' spatial sensitivity, as mentioned in Sections 2.3 and 3.1.3). Also note that, in spite of their 'brisk sustained' denomination, the β cells represented in Figure 3.13 have a markedly transient response to that type of stimulus.

Midget cells in the primate retina

A few words should be said specifically about primates' 'midget' cells. These cells have been termed the 'P' cells, because they project to the Parvocellular ('small cells') layers of primates' LGN. In the common opinion, these cells correspond to a specialization of other mammals' β cells, but driven to a spatial precision unequaled in other species. In the fovea, the midget pathway has even reached its upper-limit precision, where a single cone contacts a single 'midget' bipolar cell, which in turn contacts a single midget ganglion cell. As a result, the very numerous midget cells constitute more than 70-80 % of the roughly 1,000,000 ganglion cells in a primate retina (compared to the 200,000 ganglion cells of a cat retina)(Masland 01 [92], Wässle 04 [161]).

It is still controversial whether midget cells are an evolution of other mammals' β cells, or a 'new' type of cells (Masland 01 [92], Wässle 04 [161]). Morphologically, midget cells are relatively close to the β archetype. However, midget cells display some physiological specificities. For example, unlike cat X cells, midget cells are very little subject to contrast gain control (as measured by

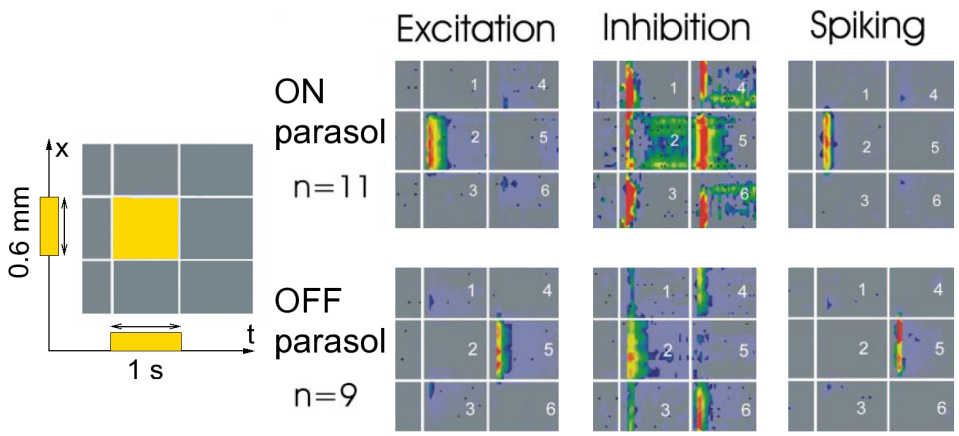

Figure 3.14: *Rabbit 'parasol' (Y) cells respond to a static square.* Same experimental protocol as in Figure 3.13. Both ON and OFF 'parasol' cells (a name usually reserved to primate retina) have transient responses, with no significant preference for edges, due to the relatively big size of their receptive fields, as compared to the size of the square stimulus. Notice the long-range inhibitory connections, likely mediated by wide-field amacrine cells, and the quantitatively stronger inhibitory patterns in ON cells (see text). From Roska *et al.* 06 [128].

Bernadete and Kaplan 99 [10], see Section 5.2). Also, unlike other mammals' X cells, midget cells are sensitive to a special color opposition, as we explain in Section 3.2.3 (color pathways).

3.2.2 Brisk transient (Y) cells

These cells were originally introduced as 'Y cells' by Enroth-Cugell and Robson 66 [48] in the cat retina, to designate cells that did not fit into the 'linear DOG framework' of X cells. Indeed, Y cells display a typical nonlinearity, whose most famous expression is the absence of a 'null position' in their response to a static grating (see Figure 3.12 *B*). More generally speaking, the physiological characteristics of Y cells are the following:

- They have fast and strong ('brisk') responses to changes in contrast of the input image, with a higher sensitivity to contrast than X cells.
- Their response to a change in contrast is strikingly transient: Y cells fire strongly to a change of illumination in their stimulus, but their response totally shuts down in a few hundreds of milliseconds if their input remains constant.
- Y cells generally have a lower spontaneous firing rate than X cells: Many Y cells are virtually silent in the absence of an image change in their receptive field (This is not the case, however, of the Y cell depicted in Figure 3.12 *B*).

- They have wide receptive fields, resulting in a bad spatial resolution (sensitivity to low spatial frequencies only).
- They exist in ON and OFF versions, allowing the separate detection of light and dark contrasts.
- Their response displays a strong spatial nonlinearity, as detailed in the sequel. However, Y cells are still 'concentric cells', in the sense that they possess an excitatory *center* and an inhibitory *surround*.

Morphologically, brisk transient cells correspond to the α type, observed in all mammalian retinas. Quite opposite to the β type, the α type has a big cell body and a wide dendritic tree, in adequation with its wide receptive field. Following the tiling principle, α cells are very sparse cells, but their dendritic trees still tile the whole visual space (see Figure 3.11). α cells are thought to account for only 3 - 8 % of ganglion cells in the retina (with some variation between species) (Masland 01 [92], Webvision [83]). However, these cells were rapidly remarked because of their brisk responses (early experimentalists localized cells thanks to the sound produced by their spike trains through an amplifier), and of their large cell bodies that were often found by the electrodes.

Brisk transient cells are movement detectors

Physiologically, the brisk transient (Y) cells are well suited to be the animal's primary 'movement detection' pathway. Indeed, they are very transient cells who only respond to sudden illumination changes – most often produced by movement, in the animal's everyday life. Furthermore, these cells have been measured to have the highest gain of response to contrast (see Croner and Kaplan 95 [30] in the primate): They can detect strongly small variations in intensity over their receptive fields. Likely, this high sensitivity results from their wide dendritic trees, implying that they have many more synaptic inputs than X cells (for example, Chichilnisky and Kalmar 03 [26] found a correlation in the primate retina between receptive field size and full-field sensitivity). Conversely, the wide receptive fields lead to a decrease in the spatial precision of the cells: This is why one often speaks of the *trade-off* between spatial accuracy and sensitivity to contrast.

In the primate retina, brisk transient cells are termed 'Parasol' cells because of their large dendritic trees, or 'M' cells because they connect to the 'Magnocellular' ('big cell') layers of the LGN. From there, they are the privileged input for the 'Motion' pathway of visual processing.

The Y cell spatial nonlinearity

Enroth-Cugell and Robson 66 [48] observed that Y cells could not be well modeled by a linear kernel. A classical expression of the nonlinearity is the absence of a 'null position' for the cell when a static grating is presented in front of it (Figure 3.12 *B*): If the cell responded linearly, there would be a spatial offset for the grating for which the positive and negative contributions to the cell's response cancel each other out, resulting in a null response of the cell (as is the case with X cells). Instead, at what should be its 'null position' (90 $\deg$ and 270 $\deg$ experiments in Figure 3.12 *B*), a Y cell still responds, both at onset and offset of the grating.

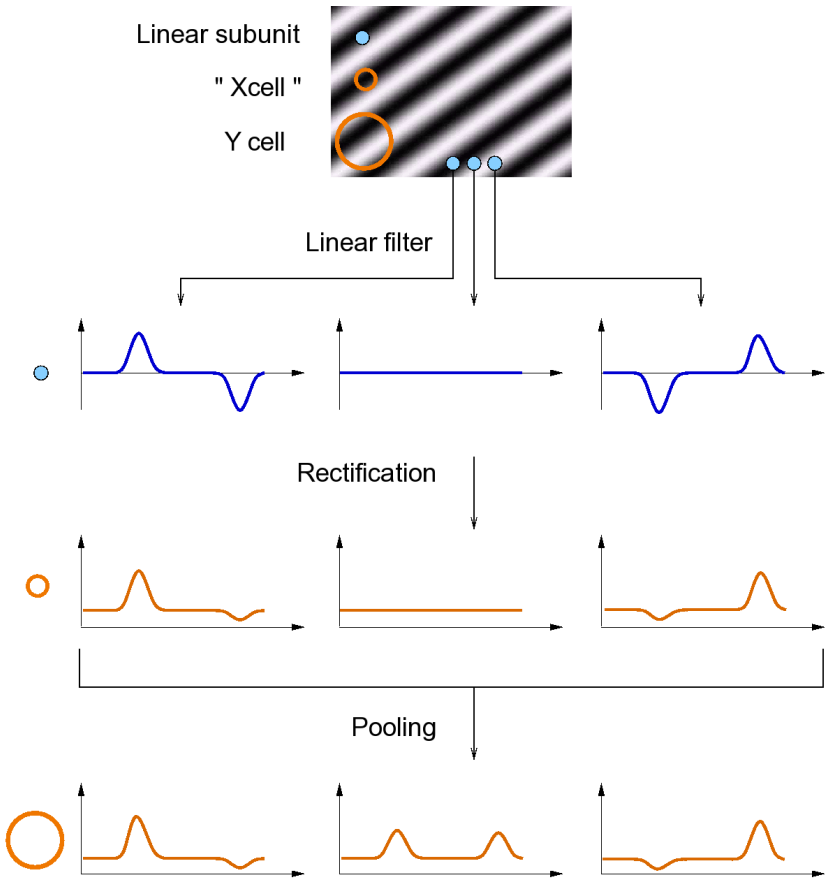

Figure 3.15: *A subunit model for Y cells' spatial nonlinearity.* In this model, 'subunits' with small receptive fields compute a linear filtering over the input sequence. The nonlinearity of Y cells in response to a static grating apparition (Figure 3.12 *B*) can be explained if their response is obtained by spatially summing the rectified versions of subunit responses over a broad spatial neighborhood. By comparison, the responses of X cells are well modeled only by a rectification of the subunits' response, without the final pooling. However, note that Y cells do not pool their responses from X cells, but directly from input bipolar cells and amacrine cells, which are the likely biological correspondence of the 'subunits'. This model, schematically inspired from Enroth-Cugell and Freeman 87 [47], may be an oversimplified representation of real Y cells, which also have a purely linear component in their response (Hochstein and Shapley 76 [69]).

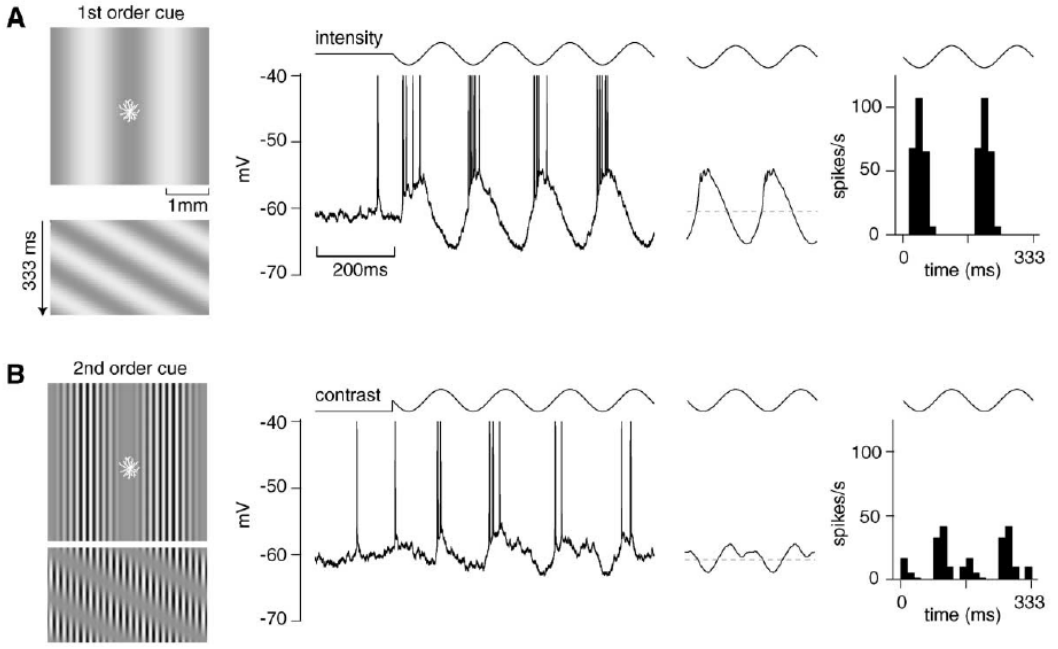

Figure 3.16: *Y cells respond to first- and second- order motion cues. A:* First order motion (drifting grating) in front of a Y cell (represented by its dendritic tree). *B:* Second-order motion, consisting of a contrast modulation (with same spatial scale as the previous first-order motion) drifting over a finer and static spatial structure. Thanks to their rectification and pooling, Y cells respond to both movements. There would be no response in *B* if Y cells had the same size of receptive fields, but responded linearly. From Demb *et al.* 01b [42]

Equivalently, the Y cell nonlinearity results in a *frequency doubling* when the cell is presented with a drifting grating of small spatial frequency, whereas a linear filter always responds to a drifting grating with a frequency equal to the drift frequency (see e.g. the experiments of Hochstein and Shapley 76 [69]).

Hochstein and Shapley 76 [69] found that both experiments (no 'null position' for a static grating and frequency doubling for a drifting grating) could be accounted for by a same model, in which (part of) the Y cell's response is spatially pooled from a rectified set of smaller, linear receptive fields, which they termed 'subunits'. Their idea was later extended into a functional model by Enroth-Cugell and Freeman 87 [47], amongst others. The underlying idea of this model is depicted in Figure 3.15.

The natural biological candidates for the 'subunits' are bipolar cells: We have seen how bipolar cells already have the *center-surround* architecture, with small receptive fields, and are well modeled by linear filters. And indeed, it has been proved by Demb *et al.* 01 [40] that the spread of the dendritic tree of Y-type cells is large enough to account for the functional pooling in the subunit model. However, many amacrine cells also interact with Y-type cells, and likely contribute to the nature of Hochstein and Shapley's functional 'subunits'.

Remark: Other explanations have been proposed to account for the nonlinearity of Y cells. For example, Hennig *et al.* [64] find that part of the nonlinearity might be due to the spatial integration by Y cells of a temporal nonlinearity due to phototransduction. Although they propose a different model, their explanation is also based on a wide spatial pooling at the level of Y cells. ■

Y cells detect second-order motion

Whatever its biological origin, it is not clear if the spatial nonlinearity of Y cells has a specific functional role or not. The argument has been given that the rectification-pooling architecture of Y cells provides them with an ability to detect second-order motion: Movements based on the contrast information rather than on the luminance information (see Demb *et al.* 01b [42] and their associated references). This is illustrated in Figure 3.16: Because they pool and rectify the signal from subunits with smaller receptive fields, Y cells can respond to 'contrast movements' created by the contrast modulation of a fine, underlying grating whose stripes remain static.

However, this presumed functionality raises some questions. First, it is not clear what kind of natural stimulus indeed creates this sort of second-order movement. Second, the detection of second-order contrast is made possible only by the finer spatial resolution of the subunits: The subsequent spatial pooling by Y cells is not the key feature of detection, it only leads to a loss in spatial precision!

We rather believe that the rectification-pooling scheme must be seen as an 'economical' feature: It allows a small number of output cells with wide receptive fields (remember that α cells account for only 5 % of retinal cells) to transmit a movement information without losing the fine *spatial sensitivity* of the subunits. The *precise location* of the stimuli are lost in the pooling operation, but this information is probably not mandatory to the 'movement' pathway initiated by Y cells.

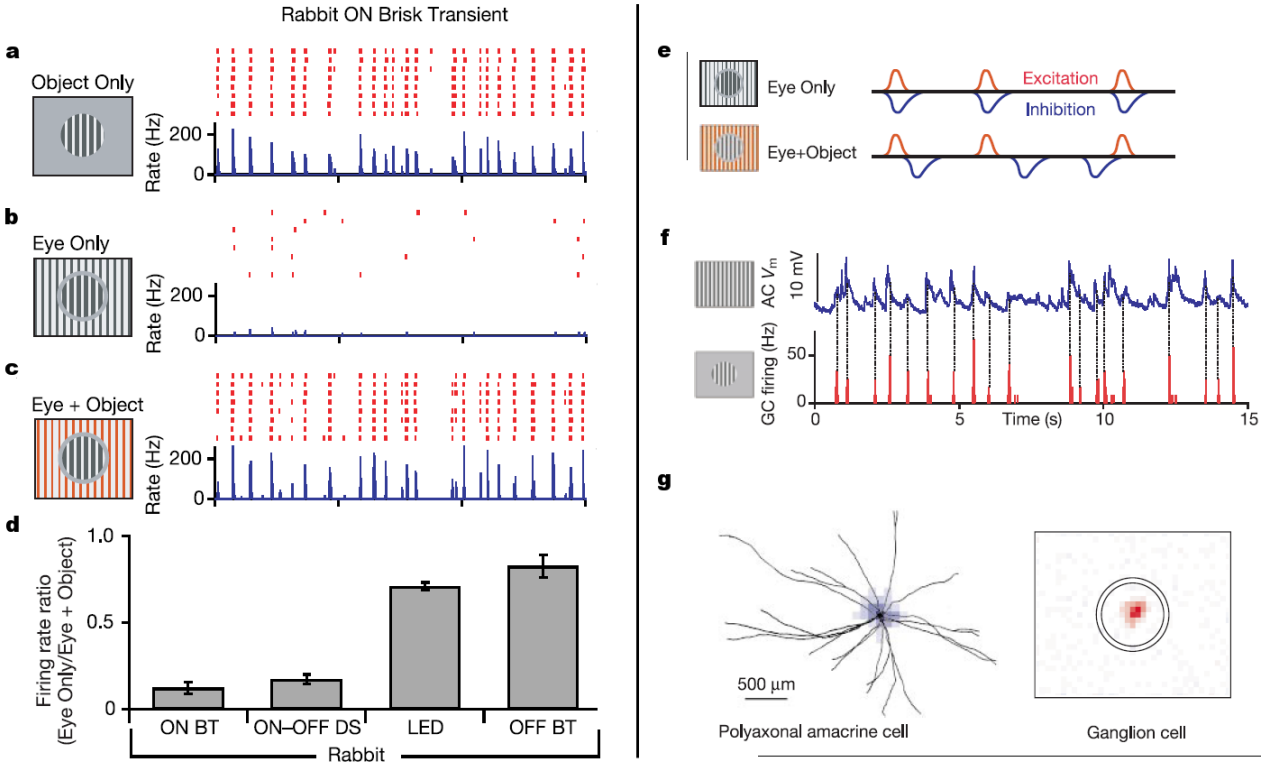

Figure 3.17: *Inhibition of movement detection by coherent background motion. a:* A small patch of grating moves in front of a rabbit ON α cell, with a trajectory typical of small fixation eye movements, eliciting a strong response. *b:* When the grating is made full-field, the response is abolished. *c:* If the background grating undergoes a different motion than the center, the response is not suppressed. However, if the background undergoes a movement *exactly opposite* to the center's, the response remains suppressed (not shown). *d:* Strength of the effect in various rabbit cells. Note the asymmetry between ON and OFF α (BT) cells. *e,f,g:* Presumed explanation of the phenomenon, by synchronous inhibition of amacrine cells from the *surround*, when *center* and *surround* movements are synchronized. From Ölveczky *et al.* 03 [110].

The surround of Y cells

Although they display a singular nonlinearity, Y cells still possess a marked inhibitory surround (Enroth-Cugell and Robson 66 [48]). This raises questions, especially when one keeps in mind the rectification-pooling model: When the *surround* of a Y cell is stimulated by a small spot of light, it probably inhibits the presynaptic bipolar cells -the presumed subunits- for which the spot is in the *surround* (since bipolar cells already display a center-surround sensitivity, see Section 2). However, this inhibition signal should be greatly lost in the rectification from bipolar cells to the Y cells, and intuitively the observed *surround* of Y cells should be greatly reduced through the rectification-pooling operation. Likely, the observed *surround* of Y cells also reflects an interaction with different types of amacrine cells.

And indeed, recent results of Ölveczky *et al.* 03 [110] suggest the presence of a strong amacrine-related *surround* in some brisk transient cells, allowing them to detect object motion from global eye movements. Their results are illustrated in Figure 3.17. When the center of a rabbit brisk transient (Y) ON cell is stimulated by random movements of a grating, it fires vigorously and reproducibly. However, when the stimulus becomes full-field, the response of the ganglion cell is totally suppressed. Furthermore, this suppression occurs only if the background's motion is synchronized with the central motion. The authors suggest that this mechanism is mediated by wide-field 'polyaxonal' amacrine cells outside the ganglion cell's receptive field (so, in the background), whose synchronous response serves to shut down the ganglion cells' response when movement is similar in its receptive field and in the background.

As a result, the brisk transient ON cell, coupled with polyaxonal amacrine cells, might implement the equivalent of a center-surround mechanism, but on a very broad spatial scale, and applied on an already transformed version of the image: The rectified, spatio-temporal band-pass image from bipolar cells. The resulting ganglion cells would detect (very coarsely) the edges of moving objects, but not global background motion, which is 'uniform' from the point of view of bipolar cells' rectified spatio-temporal band-pass signal.

Asymmetries between On and Off pathways

The selectivity to object motion was observed by Ölveczky *et al.* 03 [110] only in a subset of ganglion cells (see Figure 3.17 *d*).

Interestingly, as for 'Y-type' cells are concerned, On brisk transient (Y) cells were affected, but not Off brisk transient (Y) cells, suggesting that On and Off 'Y' cells might play a different perceptual role. Previous studies had already found evidence for a strong asymmetry between On and Off 'Y' type cells: In the primate retina, Chichilnisky and Kalmar 03 [26] find that On parasol cells are faster than Off cells, have markedly larger receptive fields (20 % on average), display more contrast gain control (see Section 5.2) and have a more linear input-output response, as measured through LN analysis (see Figure 3.18).

This asymmetry may seem surprising at first, but consider the following argument: If On and Off 'Y' cells both functioned along a simple 'rectification-pooling' scheme, then their signals would be very redundant. Indeed, most image edges are dark on one side and bright on the other, so their

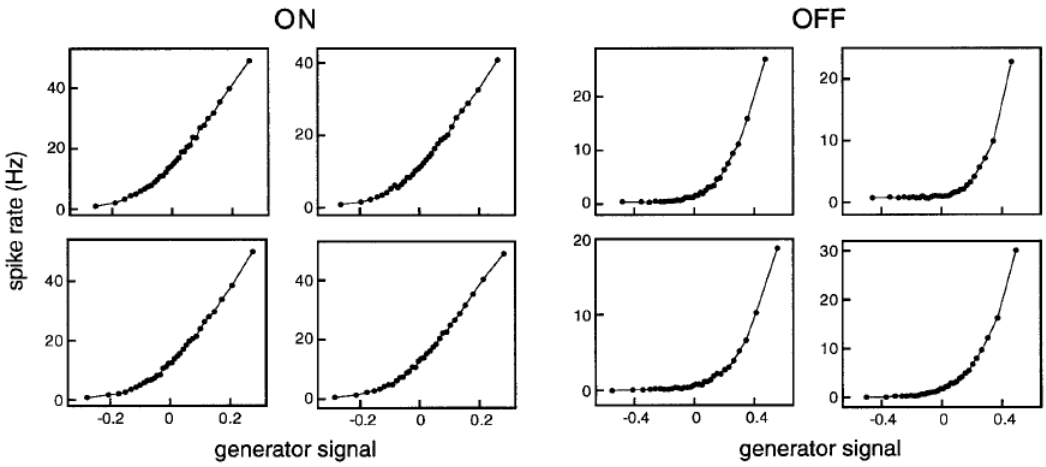

Figure 3.18: *Asymmetries between ON and OFF cells.* OFF cells are more rectifying than ON cells, as observed from an LN analysis of their receptive fields. From Chichilnisky-Kalmar 03 [26].

motion should activate both On and Off 'Y' pathways. But after a relatively large spatial pooling, the On and Off 'Y' signals would then end up very similar, raising questions about the usefulness of having both pathways. Instead, if the On pathway segregates background from motion, both On and Off 'Y' cells gain different functional roles.

3.2.3 Color-coding ganglion cells

Color processing in the retina is a wide problem, subject to complex phenomena –especially of adaptation– that we do not discuss in detail here. We only mention the existence of two very distinct pathways for color information in mammalian retinas: The first pathway is that of 'blue/yellow' oppositions, which is shared by all mammals and relies on a specific circuit that involves sparse 'color cones' ('S', or blue) whose information is relayed by the similarly sparse 'blue On' bipolar and ganglion cells. The second pathway, specific to some trichromat primates including humans, is that of 'red/green' oppositions which are transmitted by midget cells. This presentation focuses on the primate retina, based on the reviews of Martin 98 [91] and Dacey 99 [33].

Blue-yellow color-coded cells

Most mammals are dichromats, having only two types of cones: The numerically dominant 'L' cone, sensitive to low spectral frequencies, and a much sparser 'S', or 'blue', cone sensitive to higher spectral frequencies. Then, similarly sparse bipolar and ganglion cells calculate color opponents based on the 'S' signal. These cells only exist with an 'On' polarity and account for the totality of color perception in most mammals, resulting in a 'blue-yellow' dichromatic vision.

In the primate retina, the 'blue-yellow' opponent cell is called the 'small bistratified' cell (since its discovery by Dacey and Lee 94 [34])[9]. Thanks to its bistratified dendritic tree, it opposes a 'blue-on' signal, from 'blue-on' bipolar cells, to an Off signal from a diffuse non-chromatic bipolar cell (see Figure 3.19 *B*, in the case of a primate retina). As expected from its active role in conscious vision, this cell projects to the LGN (see Section 1.2), mainly to one of the koniocellular layers (Hendry and Reid 00 [63]), and also probably to the parvocellular layers (Rodieck and Watanabe 93 [127]).

In cat and rabbit, the color-coded cell has often been observed in early studies, but only in small samples because of its sparseness, and not all records agree on its properties. The main opinion seems to be that this cell is rather 'brisk' (Cleland and Levick 74b [28]), possibly with the spatial and temporal characteristics of X cells (Caldwell and Daw 78 [21] in the rabbit). We have not come across the specific structure of this cell in our documentation, but it must likely be bistratified, like its equivalent in the primate retina.

Red-Green oppositions in primate midget cells

In parallel to the increased precision of their midget cells, some primates (humans and Old World primates) have developed a trichromatic vision, thanks to the division of the predominant type of cone into two distinct types, the 'L' (low wavelength, or 'red') and the 'M' (middle wavelength, or 'green') type. The resulting scheme of cones in trichromats consists of two dominant types of cones ('red' and 'green') randomly distributed, and a third type of cone ('S' or 'blue', the original color cone of dichromat mammals) distributed along a sparser, but more regular, sampling. This is illustrated in Figure 1.11 of Chapter 1.

Midget cells are the relays of this new color information specific to trichromats. The most usual interpretation of their color sensitivity is the 'random wiring' hypothesis (Martin 98 [91]): Because midget cells are directly connected to a single cone (at least in the fovea), they gain *de facto* a color sensitivity, with a *center* signal respectively sensitive to 'L' or 'M' wavelength according to the cone they connect (Figure 3.19 *A*). By opposition, the *surround* of midget cells arises in good part of horizontal cells, which contact 'L' and 'M' (and sometimes 'S') cones indifferently. As a result, half of the midget cells code for the color opposition R-(R+M) while the others code for the opposition M-(R+M). In this 'random wiring' hypothesis, trichromacy probably appeared in the evolution *after* the spatial specialization of midget cells into a one-to-one connection from cones. Yet, this wiring hypothesis raises issues concerning our color perception in the peripheral retina, where midget cells starts to contact many cones (Wässle 04 [161]).

Interestingly, this color opposition remains a *secondary* source of information for midget cells: The wavelength sensitivities of 'L' and 'M' cones remain very close one from another, so that a strong luminosity contrast will always be favored by midget cells, whatever the colors in opposition. This double carrying of information (edges and color) through a single signal is called *multiplexing*. It is intriguing, how the brain manages to exploit both sources of information simultaneously. Since information from a single midget cell is ambiguous, and dominated by the edge information, it is likely that red-green oppositions carried by midget cells are integrated over a wider spatial range,

[9] A 'large bistratifed' cell, with similar 'blue on' opposition, has recently been discovered, see Figure 3.10.

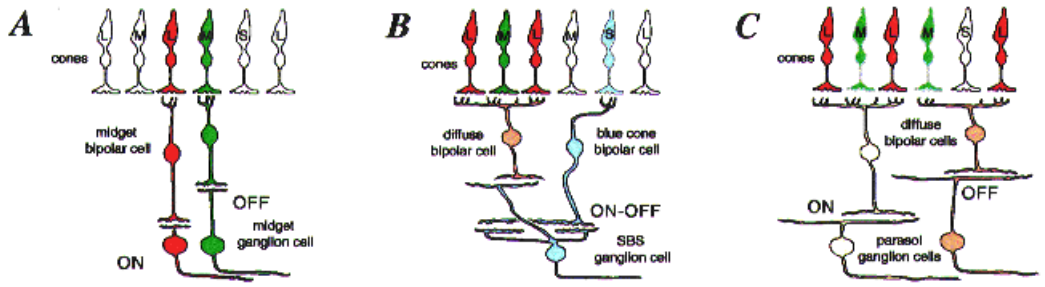

Figure 3.19: *Color pathways in the primate retina. A:* Midget cells connect randomly a 'L' or a 'M' cone, and thus fall into two distinct categories of color sensitivity. *B:* The bistratified blue-yellow opponent cell, typical of all mammalian retinas. *C:* Parasol ganglion cells have no specific color sensitivity. From Martin 98 [91].

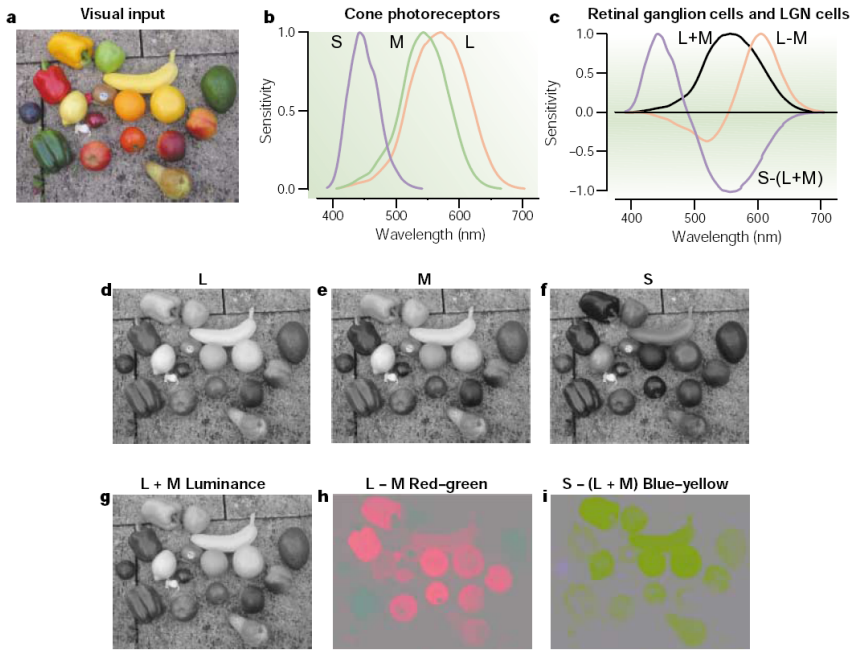

Figure 3.20: *Perceptual luminance and color opposition signals of the primate retina a:* Original color image. *b:* Spectral sensitivities of the three types of cone. *c:* Spectral sensitivities of the signals L+M (luminance), L-M (red-green signal) and S-(L+M) (blue-yellow signal). *d,e,f:* Response components of the three cone sensitivities S,M and L. *g:* Resulting L+M luminance image. *h,i:* Resulting color signals, if the luminance and other color channel are set at zero. Notice how we fail to find spatial precision in these iso-luminant color images. From Gegenfurtner 03 [59].

for the brain to grasp the 'color-related bias' in the output of a population of neighboring cells (see e.g. the color demosaicing model of Alleysson *et al.* 05 [1]).

After this necessary spatial integration to 'demultiplex' the midget signal, the red-green *chromatic* signal ends up with a relatively poor spatial resolution, comparable to the blue-yellow signal mediated by the sparse blue-yellow color-coded cells (Mullen 85 [99])[10].

Color pathways and perception

To conclude, both our color vision pathways (sparse 'blue-yellow' cells and multiplexed 'red-green' midget cells) have a spatial acuity much lower than the achromatic image carried by midget cells (see the respective dendritic tree sizes in Figure 3.10). So, the fact that our color percepts are always linked to observed objects, even at very fine spatial resolution, probably results from an efficient multi-modal sensory integration in our brain, and remains an exciting and intriguing phenomenon.

Figure 3.20 presents the respective spectral sensitivities of our three types of cones, and how they can be decomposed in a luminance image, and two iso-luminant red/green and blue/yellow images. Very little shape information subsists in the isoluminant color images (especially in the blue-yellow image[11]), reflecting the poor spatial resolution of our color pathways. We refer the interested reader to the review of Gegenfurtner 03 [59] on color pathways in the cortex.

3.2.4 The rod pathway

Rods are by far the most numerous light receptors in mammalian retinas, especially in nocturnal species (see the density diagram of Figure 1.12 in Chapter 1). A detailed study of their light response is not in the scope of this work. We will only remark the following characteristics of phototransduction in rods:

- An increased sensitivity allowing very efficient detection of light in dark-adapted (scotopic) illumination conditions: Reliable detection of flashes of ~ 20 incident photons over the whole retina, and better-than-chance response to single photons [136, 134].
- In scotopic illumination, a monophasic and long-lasting (typically between 0.5 and 1 sec, Baylor *et al.* 84 [7]) impulse response to dim flashes of light.
- In scotopic illumination, a saturating and nonlinearly delayed response to stronger pulses of light (Baylor *et al.* 84 [7]).
- A general and progressive saturation at higher illumination levels, starting at around 100 scotopic trolands (typically, the luminance of a very cloudy sky[12]).

[10] By 'spatial resolution', we mean the spatial cut-off frequency of the chromatic sensitivity curves. However, a difference remains between the red-green and blue-yellow systems in terms of absolute sensitivity, which is markedly higher for the red-green system (Mullen 85 [99], Mullen and Kingdom 02 [100]).

[11] and yet more especially if you have printed this thesis in black and white!

[12] See e.g. Lance Hahn's retina page at http://retina.anatomy.upenn.edu/l̃ance/modelmath/units_photometric.html.

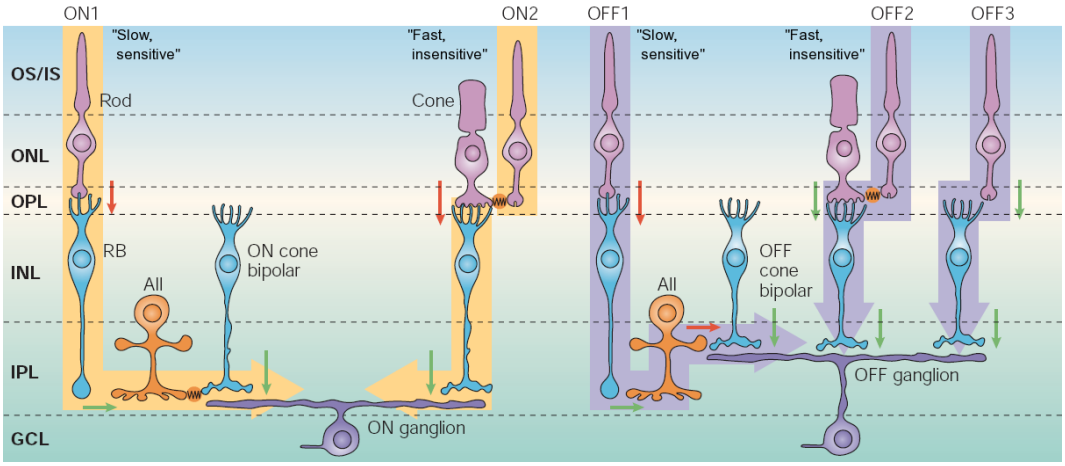

Figure 3.21: *Rod pathways in the mammalian retina.* The rod signal is grafted on the cone-dominated retinal output by two main pathways with sensibly different spatio-temporal characteristics (see text). A third 'OFF3' pathway of transmission, with 'fast, insensitive' characteristics, has also been observed in rodent retinas (see Sharpe and Stockman 99 [139]). From Wässle 04 [161], adapted from Demb and Pugh 02 [41].

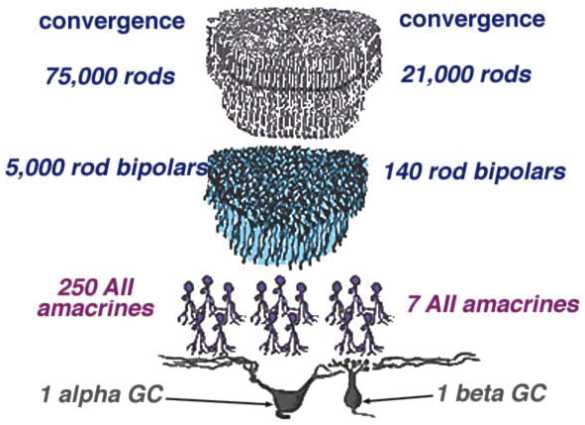

Figure 3.22: *Convergence of the 'slow sensitive' rod pathway.* The strongly convergent scheme of rods onto ganglion cells confers the 'slow sensitive' pathway with a strong sensitivity to light (better-than-chance detection of individual photons in dark-adapted conditions), at the expense of a loss in spatial and temporal precision. From Webvision [83].

There is phylogenetic evidence that rods have appeared later than cones in the course of evolution. In coherence with this fact, there is no specific ganglion cell associated to rods. Instead, the rod signal is transferred back to the traditional, cone-dominated pathways, by two distinct mechanisms represented in Figure 3.21. Interestingly, these two pathways have different spatio-temporal characteristics, that allow to use the rod information in two different functional ways.

1. A 'slow, sensitive' pathway of transmission transits through the specific 'rod bipolar' cells (see Figure 3.6), which in turn synapse onto dedicated amacrine cells, termed 'AII'. From AII amacrine cells, the signal is transferred back onto both ON and OFF cone pathways, respectively thanks to gap junctions with On bipolar cells ('ON1' pathway of Figure 3.21) and inhibitory synapses to Off bipolar cells ('OFF1' pathway of Figure 3.21).

   This pathway, rod-specific up to AII cells, displays a very strong convergence ratio from rods to ganglion cells (see Figure 3.22). Furthermore, rod bipolar cells integrate the rod signal with a high gain and slow response kinetics (Dacheux and Raviola 86 [37]). In the end, this results in a pathway that displays: (i) a high sensitivity and rapid saturation as background illumination increases, (ii) slow response kinetics, and (iii) poor spatial resolution.

2. By opposition, a 'fast, insensitive' pathway transits directly from rods to cones, through gap junctions between the receptors' inner segments ('ON2' and 'OFF2' pathways of Figure 3.21). And indeed, a delayed 'rod contribution' of small amplitude can be observed in the responses of individual cones (Schneeweis and Schnapf 95 [134]). Gap junction coupling is the only source of spatial convergence for this rod pathway. Afterward, this pathway benefits of the specific properties of cone bipolar cells, including precise spatial treatment and high-pass temporal transmissions.

   In the end, this pathway is thus characterized by: (i) a poor sensitivity to light increments, that prevents from saturation until strong photopic illuminations, (ii) fast response kinetics, and (iii) relatively good spatial resolution.

As a result, the two dominant rod pathways are well suited for an optimal exploitation of the rod signal over a broad range of intensities: The 'slow, sensitive' pathway allows to cover dark scoptopic ranges, while the 'fast, insensitive' pathway covers a higher illumination range (up to dark daylight), likely providing an important component of our 'precise' vision in mesoscopic conditions (nightfall, moonlight, etc.).

An interesting evidence for the two rod pathways can be found in Sharpe and Stockman 99 [139], through psychophysical experiments on human subjects: Destructive temporal interferences between the 'fast' and the delayed 'slow' rod pathways result in a 'blind' zone in the perception of light flickers at 15 Hz, at contrasts well above the absolute psychophysical detection threshold.

3.2.5 Direction-Selective (DS) cells

On and On-Off DS cells

Direction-Selective cells have been observed more than forty years ago in the rabbit retina by Barlow and colleagues [5, 6], but their specific circuitry is not fully understood yet. Two main types of DS

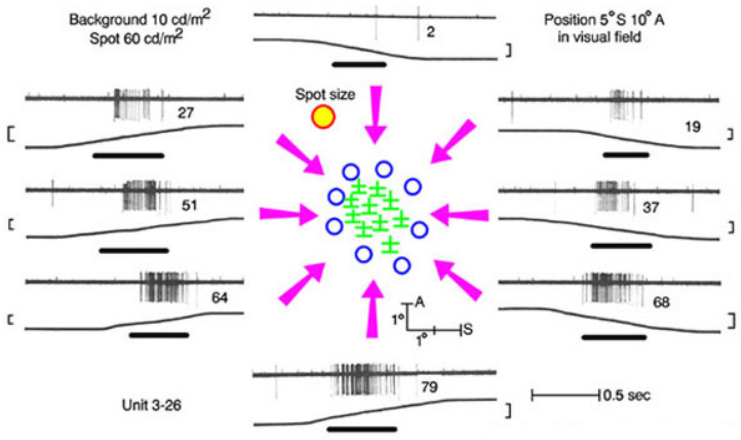

Figure 3.23: *On-Off direction selective (DS) cells in the rabbit retina.* DS cells respond to the movements of contrasted targets in their preferred direction (here, upwards), but not in their 'null' direction (here, downwards). From Barlow *et al.* 64 [5].

cells have been found, the On DS cell and the On-Off DS cell. The On DS cell is a monostratified cell (with dendrites only in sublamina b of the IPL) that projects to the accessory motor system, where it drives optokinetic eye movements, that allow the eyes to compensate for head movements during fixation (Oyster *et al.* 72 [112], Masland 01b [93]).

The second type, the On-Off bistratified cell (with two dendritic trees, in both sublaminae a and b of the IPL), has been subject to much more studies concerning its architecture and the arousal of movement selectivity. It is a very important type of cell, which constitutes around 10 % [148] of ganglion cells in the rabbit retina (other studies have met it even more often [21, 45]). An example of tiling by On-Off DS cells is provided in Figure 3.24 *a*.

Physiology and function of the On-Off DS cell

When a small contrasting shape (light or dark) passes in front of them, On-Off DS cells display an opposition between a 'preferred' direction of movement, and the opposite (180 deg) 'null' direction, for which the cells remain totally silent (Figure 3.23). The typical range of speeds thus detectable is 1 to 10 $\mathrm{deg\ s^{-1}}$ [87, 112]. In the rabbit, four parallel tilings by DS cells have been observed, corresponding to the main four cardinal directions for motion sensitivity [148]: See Figure 3.24 *e*.

To our knowledge, it is not known with certainty to which regions of the brain On-Off DS cells project, and what their main function in visual processing is. However, by comparing the respective sensitivity curves to motion speed of On-Off DS cells and of the optokinetic reflex, Oyster *et al.* 72 [112] have suggested that On-Off DS cells may have the same functional role as On DS cells: Driving optokinetic eye movements. In their optic, On DS cells could provide the control signal for

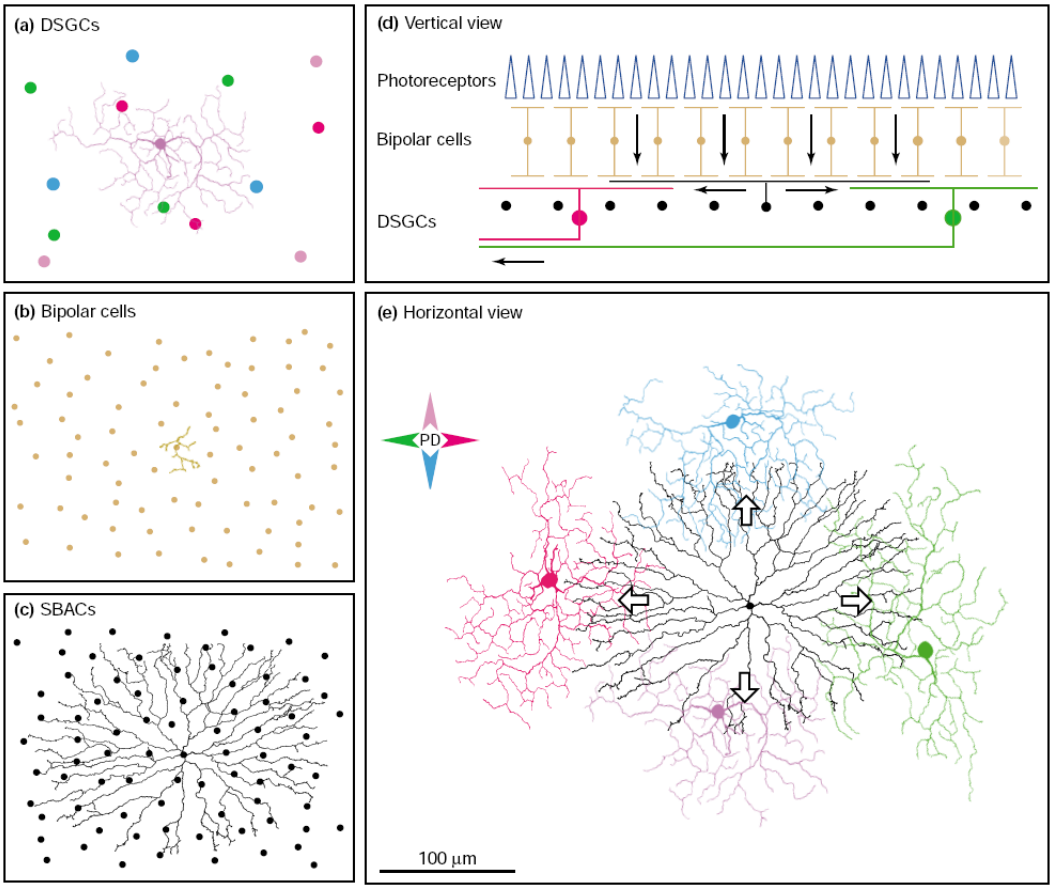

Figure 3.24: *On-Off direction selective (DS) cells, and their interaction with starburst amacrine cells. a:* Tiling of the visual space by On-Off DS cells. Four parallel populations of cells respond preferentially to each of the four cardinal directions (color code as in *e*). *b,c:* Tiling of the visual space respectively by bipolar cells and starburst amacrine cells. *d:* Vertical schema of the interaction. Notice the centrifugal sensitivity of starburst amacrine cells. *e:* A single starburst amacrine cell has dendrites which are largely independent, and each respond preferentially to centripetal motion from the amacrine cell's center (thick arrows), for a reason yet to be discovered. Asymmetric connections then transmit this directional sensitivity to DS cells (see text). From Taylor and Vaney 03 [148].

slow movements (0.01 to 5 $\mathrm{deg\ s^{-1}}$), and On-Off cells for faster movements (1 to 10 $\mathrm{deg\ s^{-1}}$), thus requiring a denser tiling of the retina.

By opposition, direction-selective cells have never been observed in the LGN to our knowledge. So, it is likely that DS cells do not constitute a source of input for cortical calculations, but rather directly for motor control areas.

Starburst amacrine cells and their role in direction selectivity

It is now understood that the directional selectivity of On-Off DS cells strongly relies on the properties of particular glycinergic amacrine cells: The *starburst* amacrine cells, which densely tile the visual space (equivalently to bipolar cells, see Figure 3.24 *b-c*). As a proof of the important role of starburst amacrine cells, direction selectivity ceases when they are blocked by picrotoxin (Caldwell *et al.* 78 [22]).

Starburst amacrine cells have very dense and circular dendritic trees. Very intriguingly, their dendrites at different locations behave independently one from another, and are strongly excited by *centrifugal* movement, from center of the amacrine cell to its periphery (Euler *et al.* 02 [51], and for review Taylor and Vaney 03 [148]). It is not known what mechanism –electrotonic or resulting from a network interaction– creates this centrifugal sensitivity of starburst cells' dendrites.

In turn, On-Off DS cells receive inhibition from starburst amacrine cells with a strong directional bias: Most of the 'starburst to DS' inhibitory synapses are located only on the 'null' side of the DS cell (Fried, Münch and Werblin 02 [55], and for review Taylor and Vaney 03 [148]). As a result, movement in the DS cell's null direction will first reach the presynaptic starburst, that will inhibit the DS cell before a response can be elicited by the stimulus. By opposition, movement in the DS cell's preferred direction first excites the cell and produces its firing, while the starburst amacrine cell *does not* provide inhibition since the input movement is centripetal for the starburst's dendrites at contact with the DS cell. More controversially, this mechanism is also suspected to be enhanced by an excitatory acetylcholine release from the starburst cells on the *preferred* side of the DS cell [148]. Indeed, it has been proved that the excitatory input to the cell is also direction selective [55].

Figure 3.24 *e* represents how a single starburst amacrine cell can make inhibitory connections and provide directional sensitivity simultaneously to four DS cells with different preferred directions, according to the mechanism explained above.

DS cells are an intriguing feature of the retina that still puzzles neuroscientists after forty years of studies. Their synaptic inputs are not fully understood yet (for example, they also display an inhibitory *surround*, Troy and Shou 02 [152]). Knowing to which regions of the brain they project is an important functional issue.

3.2.6 Local edge detectors (LEDs)

We now come to the best-described 'sluggish' retinal cell, the local edge detector (LED). LEDs were first observed by Levick in the rabbit retina, and his work (Levick 67 [87]) is likely the first reference to be checked. Later studies found LEDs in the cat retina as well (Cleland and Levick 74b [28]). These cells are now thought to constitute a functionally very important pathway: They account for

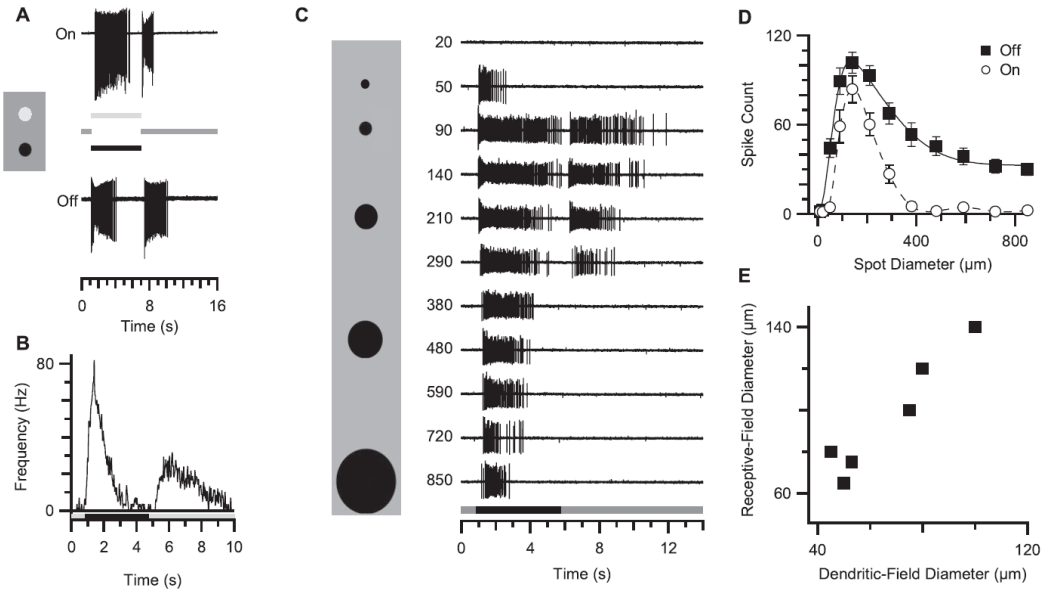

Figure 3.25: *Local edge detector (LED) in the rabbit retina. A:* LEDs display On and Off responses, both at onset and offset of small contrasting spots (light or dark). *B:* Corresponding spike-triggered average, for the dark spot stimulus. *C:* Both the On and Off components of the cells' response rapidly fail to detect stimuli of increasing sizes: A strong inhibitory surround provides LEDs with a strong spatial band-pass property. *D:* Tuning of the 'On' and 'Off' components of the LED's response depicted in *C*. *E:* Correlation between the cells' dendritic tree and receptive fields sizes. From Van Wyk *et al.* 06 [158].

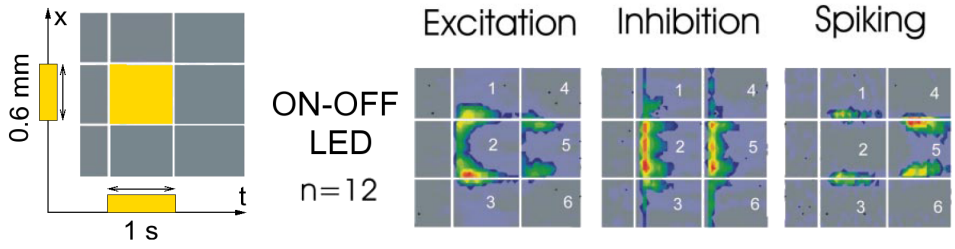

Figure 3.26: *Rabbit LEDs respond to a static square.* Same experimental protocol as in Figure 3.13. A broadly band-pass and sluggish excitatory input is shaped by a strong amacrine inhibition, resulting in an increased sensitivity to image edges at the spiking output of the cell. From Roska *et al.* 06 [128].

15 % of ganglion cells in the rabbit retina, which makes them one of the most present types (Van Wyk *et al.* 06 [158]), and their receptive fields are of a size comparable to the brisk transient (X) cells: Around 1 or 2 degrees of visual angle in cat [28] and rabbit [87] (or equivalently, 170 to 350 μm of retinal surface, in the rabbit).

Sluggish, On-Off detector of localized contrast

Levick 67 [87] termed the cells 'local edge detectors' because they respond only to contrasts of small objects, whether brighter (On behavior) or darker (Off behavior) than the surround. The 'On-Off' behavior, typical to these cells, is likely due to their thick dendritic tree which spans both the On and Off laminae of the IPL (see Figure 3.9). However, when a reverse correlation analysis is performed, LEDs appear as Off-sensitive cells (Van Wyk *et al* 06 [158]), revealing an asymmetry in the strengths of On and Off inputs.

Temporally, LEDs could be termed 'sluggish sustained' cells (but do not confuse with the concentric sluggish sustained type, Section 3.2.7). Quite incredibly, their response develops over several seconds after a contrasting stimulus: In Figures 3.25 *A* or 3.26, even the offset of a pattern elicits a response over several seconds, even though the light stimulus has just 'switched back' to a uniform screen! The lengthy responses of LEDs is reflected in their excitatory inputs (most likely from bipolar cells), and yet enhanced by their high membrane resistance (M. Van Wyk, personal communication).

Strong inhibitory surround

A specificity of LEDs is their reduced responses whenever the immediate surround of the cell is also stimulated. This translates in the rapid apparition of inhibition in the LED response (On and Off) to spots of light with increasing diameter (Levick 67 [87], Cleland and Levick 74b [28], Van Wyk *et al.* 06 [158]), as depicted in Figure 3.25.

The underlying mechanism for this strong inhibitory surround is not well understood yet, but it clearly involves the specific contribution of glycinergic (small-field) amacrine cells: Caldwell *et al.* 78 [22] observed that when glycine amacrine cells were inhibited with strychnine, the LEDs' specific sensitivity to small spots disappeared. The important effect of amacrine inhibition in shaping the LED response is also obvious in Figure 3.26: It results in a spiking pattern much more concentrated on edges than the cells' presynaptic excitatory signal is.

In particular, there is still debate over the spatio-temporal preference of the LEDs' inhibitory surround. Levick 67 [87] suggested that the inhibitory surround was stronger when it contained itself edges (implying that LEDs perform a center-surround operation on a presynaptic signal where edges are already enhanced). Indeed, the response to a dark spot is inhibited when an annulus structure creates edges in the *surround* (Figure 3.27 *C*). But by opposition, in response to a square pattern (Figure 3.26), the inhibitory inputs to the LED do not appear to display any preference for the squares' edges. Finally, another recent experiment (Figure 3.27 *A* and *B*) has provided some partial insights on the nature of the LED surround. However, to understand unambiguously all these experiments and the general organization of LEDs' receptive field, a better knowledge of their presynaptic bipolar cells'

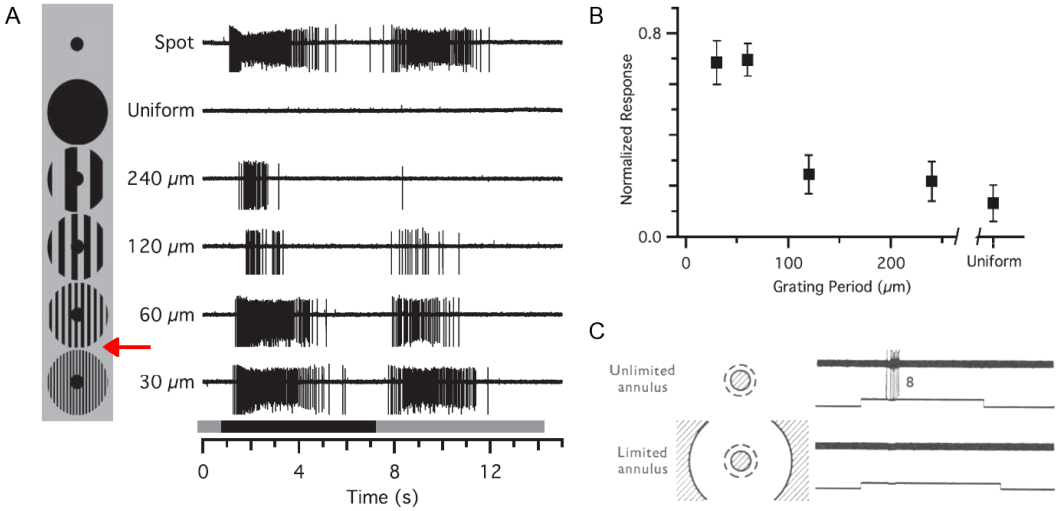

Figure 3.27: *Properties of the LED surround. A:* Between the extreme responses to small (100 μm) and large spots (850 μm) (first two lines), the strength of the LED's surround inhibition depends on the spatial frequencies it contains. The reduced inhibitory effect as the spatial frequency augments reveals the intrinsically *low-pass* properties of the surround, reflecting the spatial sensitivity of the presynaptic bipolar cells. Coherently, the last spatial frequency where surround inhibition is visible ('60 μm' line, red arrow) also corresponds to the psychophysical detection threshold of gratings in rabbits. This experiment does not allow any conclusion on possible band-pass preferences of the surround. *B:* Quantified data from *A*. *C:* An experiment suggesting a band-pass sensitivity in LEDs' surround: The response of a central spot (85 μm) is reduced when an annular structure (500 μm) introduces edges in the cell's surround. But all results in this figure cannot provide any definitive conclusion until the tuning properties of presynaptic bipolar cells are better known. From Van Wyk *et al.* 06 [158] (*A*,*B*), and Levick 67 [87] (*C*).

spatial tuning is still required.

Remark: The LED's inhibitory surround mentioned here is generally considered a part of the *non-classical* receptive field of this cell, because direct stimulation in the surround elicits no response from the cell. But to our minds, this fact is simply due to the low spontaneous activity of LEDs, implying that pure inhibition cannot have any visible influence on their spiking output. ■

Excitation and inhibition patterns typical of 'sluggish' cells

There are interesting and significant discrepancies between the respective behaviors of the excitatory and inhibitory synaptic inputs received by a LED: The excitatory input is sluggish, developing over several seconds, while the inhibitory input displays both a sluggish and a brisk component, particularly strong at stimulus onset (Van Wyk *et al.* 06 [158], not shown). Likely, LEDs receive different simultaneous sources of inhibition. This can also be seen in the patterns of excitation and inhibition in Figure 3.26.

The strong inhibition, with a fast initial transient, is largely responsible for the 'sluggish' nature of LEDs, because it totally shuts down their response during the few first hundreds of milliseconds following stimulus onset. Very likely, similar strong inhibitory transients exist in other 'sluggish' cells with complex responses (Xu *et al.* 05 [165]), and might be a common feature of these cells.

Furthermore, the experiments of Van Wyk *et al.* 06 [158] (their Figures 8 *E* and 12) provide strong hints of an interplay between the LED's excitation and inhibition, one possible explanation being that the rapid inhibition also acts directly on the presynaptic excitatory inputs to the LED.

Comparison with brisk sustained (X) cells

In the rabbit retina, it has now been demonstrated (Roska *al.* 06 [128], Zeck *et al.* 05 [166]) that LEDs are more spatially precise cells than brisk transient (X) cells. This can be seen by comparing the response of the β (X) cells and of the LEDs in response to a static square (respective 'Spiking' responses in Figures 3.13 and 3.26): The response of the LED is very localized on the edges of the square, whereas the responses of the β cell displays a consequent width.

By opposition, LEDs in cat and primate retina have been less studied, but they are supposed to be less precise than β cells. For example, Figure 3.10 (from Dacey *et al.* 03 [35]) displays a plausible candidate for the LED in the primate retina: Their 'broad thorny' cell, with the typical 'thick' dendritic tree overcrossing the On and Off sublaminae. If this cell is indeed a LED, then its typical dendritic tree is far bigger than those of midget cells. In fact, it is even larger than the dendritic trees of parasol cells. However, note that the cells in Figure 3.10 are cells projecting to the LGN, so that our 'presumed LED', the 'broad thorny' cell, likely plays a role in cortical processing and thus in 'conscious' visual perception.

3.2.7 Other 'sluggish' ganglion cells

To conclude, we mention here the remaining types of ganglion cells that have been observed. Most of these remaining cells have small somata and slow, 'sluggish' responses, which have contributed

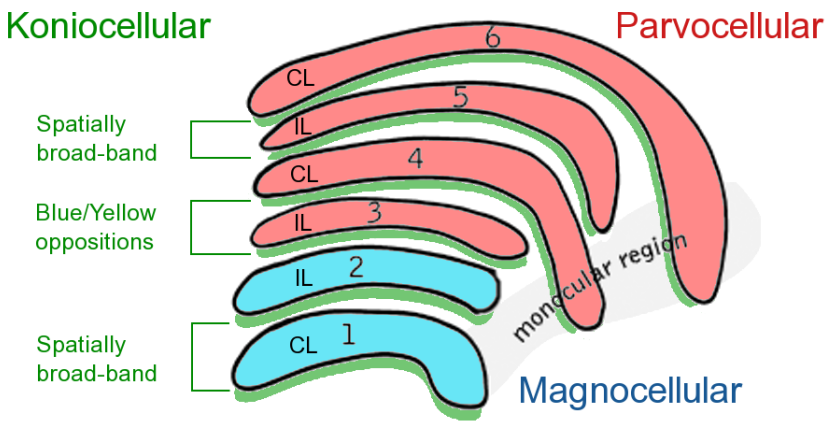

Figure 3.28: *Koniocellular layers in the macaque LGN.* Schematic view of a macaque LGN: The layers go in functional pairs, respectively associated to the ipsilateral (IL) and contralateral (CL) eye. Magnocellular (M) cells map the visual field once (one layer per eye) and Parvocellular (P) cells map the visual field twice (two layers per eye). Ventral to each of the P and M layers is a layer of koniocellular (K) cells. The medial K cells relay the blue/yellow oppositions from retinal small bistratified cells, making the resulting medial P/K complex the primary source of color information to the CO blobs of V1. The dorsal and ventral K layers arise from distinct retinal cells, most likely sluggish cells. These K cells are supposedly sensitive to broad spatial frequencies, but their physiology and functional role is still badly known (Hendry and Reid 00 [63]).

to their 'discrete' place in the field of retinal physiological studies. However, all these cells now appear to constitute distinct, functional pathways, with cellular densities that can be comparable to those of α cells.

The origin of these cells' sluggish response remains quite enigmatic. It seems attributable to the combined effects of (i) slow presynaptic bipolar cells, (ii) strong inhibitory shaping by amacrine cells (Xu *et al.* 05 [165]), possibly including a fast initial transient inhibition, and (iii) a high membrane resistance that implies a very long time constant for the cells. All these points have been mentioned previously through the detailed presentation of the local edge detector (LED, Section 3.2.6).

Importantly, it should be noted that although sluggish cells are less reactive and fire less spikes than 'brisk' cells, they display the same absolute sensitivity to contrast (Xu *et al.* 05 [165]), so they are also able of carrying an important quantity of information. They appear to saturate faster than brisk cells at high levels of contrast.

Possible cortical roles (LGN koniocellular layers)

The nature and importance of sluggish cells have recently been re-estimated, as it now appears that many of them likely provide input to the LGN, and from there to cortical processes. Indeed, in

addition to the best-known Parvocellular and Magnocellular layers, the LGN displays interstitial layers of cells with very small somata: The *Koniocellular* (K, 'sand-like') layers. In the macaque LGN, there is one layer of koniocellular cells ventral to each of the four Parvo and two Magno layers (see Figure 3.28). Likely, each of the six resulting Konio layers displays a full map of the visual receptive field, and is associated to a precise functional treatment (see Hendry and Reid 00 [63] for an interesting review).

It is now well established that the medial K layers relay the blue/yellow color oppositions arising from retinal bistratified cells. By opposition, much less is known concerning the physiology of the ventral and dorsal K layers. A few studies have revealed their sensitivity to broader spatial stimuli than Parvo and Magno layers (Hendry and Reid 00 [63]). It is likely that some retinal sluggish cells constitute the main source of input to these K layers, with a possible associated role in cortical processing (especially because specific neural projections exist from the K layers to V1 and V2 [63]).

Unfortunately, in the retina, documentation on sluggish cells remains rare and often ambiguous: To date, the unification between morphological and physiological classifications has not been realized (see Troy and Shou 02 [152]), while the functions of these cells remain globally unknown. We now rapidly present what we have identified as the most important types of sluggish cells in mammalian retinas. Interested readers are referred to the review of Troy and Shou 02 [152] for further details and references on these cell types.

Sluggish concentric cells. The term of 'sluggish' cells was originally introduced by Cleland and Levick 74a [27], to designate cells with a marked center-surround architecture and responses of small amplitude. Just like concentric brisk cells, they were reported to enter four possible categories, being either 'On' of 'Off' and 'sustained' or 'transient'. Although these cells have been termed 'sluggish' because of their low response rates, they appear to have a fairly good temporal precision, discriminating signals up to 15 Hz (Troy and Shou 02 [152]). We now present both types, sustained and transient.

Sluggish-sustained concentric (Q) cells. Sluggish-sustained cells have a relatively linear *center-surround* behavior, as 'brisk sustained' (X) cells, but with a low spatial precision, an order of magnitude smaller than X cells. Their wide dendritic trees and receptive fields are rather comparable to those of Y cells. Their spiking activity is sustained and regular (Cleland and Levick 74a [27]). In the cat, they probably correspond to the linear 'Q' cells of Enroth-Cugell *et al* 83 [49], and to the respective δ (On sluggish-sustained) and ε (Off sluggish-sustained) morphological types (Troy and Shou 02 [152]).

Their functional role or cerebral projections are not known with certitude, but the On sluggish-sustained cells have been observed to project to the LGN in the cat (Pu *et al.* 84 [115]). This remark is interesting because the dual functionality of the Q and X cells, with qualitatively the same linear behavior but different scales of filtering, is reminiscent of multi-scale techniques used in image processing. Q cells could thus help to cortical interpretation of uniform zones, in addition to the precise 'edge-dominated' signal of X cells. In particular, it would be interesting to know whether 'Q-like' cells contribute input to the K cells of the LGN in primates.

Sluggish-transient concentric cells. These are the other type of sluggish concentric cells first classified by Cleland and Levick [27]. They also exist in On and Off version, and have low and irregular firing patterns that show a transient wave of activity at stimulus onsets. They are an intriguing class of cell, because while little is known about their functionality, they seem to be a very frequent type of cells with small dendritic trees (between β and α), that would account for around 10 $\%$ of cells in the cat retina [152].

We now present other types of non-concentric cells, which we have also termed 'sluggish' in allusion to their small and relatively slow response rates.

Suppressed-by-contrast (SbC) cells. Found in rabbit (Levick 67 [87]), cat (Cleland and Levick 74b [28], Troy *et al.* 89 [151]) and primate (De Monasterio and Gouras 75 [39]) retinas, these cells seem to have the exact opposite behavior of LEDs: They have a sustained firing in the presence of uniform light, which decreases whenever a contrasting stimulus (light or dark) appears in their receptive field. Temporally, the responses are sluggish and can be rather sustained or transient according to the type of cell studied (it has been argued that 'SbC' cells may in fact consist of two or more cell types with different physiologies: See [28, 152]). Spatially, there is a striking similarity between the SbC receptive fields and those of Y cells: They have the same typical sizes, and the same tuning to drifting gratings at different frequencies, including the doubled harmonic response typical of Y cells' spatial nonlinearity. It is not known to what extent this similarity is significant of a common input.

We ignore the functional roles of these cells and the nature of their cerebral projections. We note that such 'uniformity detectors' (an alternative name for this class of cells) could have a useful function in computational models of diffusion processes in the visual cortex, as markers of zones where visual diffusion can be important.

Orientation selective cells. In the rabbit, orientation selective cells with particularly elongated receptive fields have often been reported (Levick 67 [87], Caldwell *et al* 78 [22]). Again, amacrine cells play a large role in this selectivity, which disappears when GABA-ergic (so, likely, wide-field) amacrine cells are inhibited by picrotoxin. Both their excitatory and inhibitory receptive fields were reported to be oriented along parallel bars [22].

We have not come across the cerebral projections of these cells. Their biological role remains mysterious, since directional selectivity is rather a strong attribute of cortical V1 and V2 areas, where it arises through specific connectivity patterns.

Photosensitive ganglion cells. To conclude this presentation of the diversity of retinal ganglion cells, a rare (1-3 %) ganglion cell has recently been found which expresses melanopsin, a particular photopigment. As a result, this cell possesses an intrinsic photosensitivity, independently of its retinal connectivity. It is supposed to play a strong role in the regulation of circadian rythms and pupillary reflexes (Wässle 04 [161]).

Conclusion: Diversity of ganglion cell responses

To conclude this presentation, we reproduce in Figure 3.29 the very interesting inventory of ganglion cell responses by Roska *et al.* 06 [128], to their 'static square' stimulus. Amongst their sample population of 'classic' (β, parasol) and more 'original' ganglion cells, a striking feature is the fact that excitation and inhibition are often anticorrelated.

The spatial anticorrelation of inhibitory and excitatory inputs is best seen in the 'Region of Interaction' column of Figure 3.29. At most spatial locations (corresponding to successive trials on the same cell, with different offsets for the input stimulus), the cell receives an input where either excitation or inhibition is largely dominant.

In the authors' interpretation, this observation reflects the fact that some short-range amacrine cells transmit inhibitory information vertically between the 'On' and 'Off' pathway, in a 'push-pull' manner: For example, an 'On' β cell could receive its inhibitory inputs from an amacrine cell relaying the signal of 'Off' bipolar cells. This mechanism would allow to enhance the dynamic range of the ganglion cell in both 'On' and 'Off' directions, and thus counteract the compression of the 'Off' signal due to rectification in the direct synaptic transmission from 'On' bipolar cells to the ganglion cell.

However, we remark that the anticorrelated pattern of excitation and inhibition could also be explained by amacrine cells providing an inhibition simultaneously to ganglion cells and to their presynaptic bipolar cells.

4 PROPERTIES OF RETINAL SPIKE TRAINS

4.1 The issue of spike coding in the retina

Spike emission by ganglion cells is a particular subject in the general scope of retinal studies. Historically, although spikes were discovered very early as being the manifestation of retinal output activity, their individual role for coding was long overlooked, in favor of some more continuous information integrated from the spike trains (whether temporally, or over successive trials). There have been two main reasons for neglecting individual spikes: First, the role of spikes in retinal coding is not obvious, as they could logically be seen only as a means of physical transmission. Second, the precise study of spike trains requires relatively complex theoretical frameworks, as compared to analogic signals.

4.1.1 Spikes as a simple means of physical transmission

The first reason to neglect individual spikes is an Occam's razor argument: Retinal spikes have an obvious physical role that has nothing to do with coding efficiency. The axons of ganglion cells,

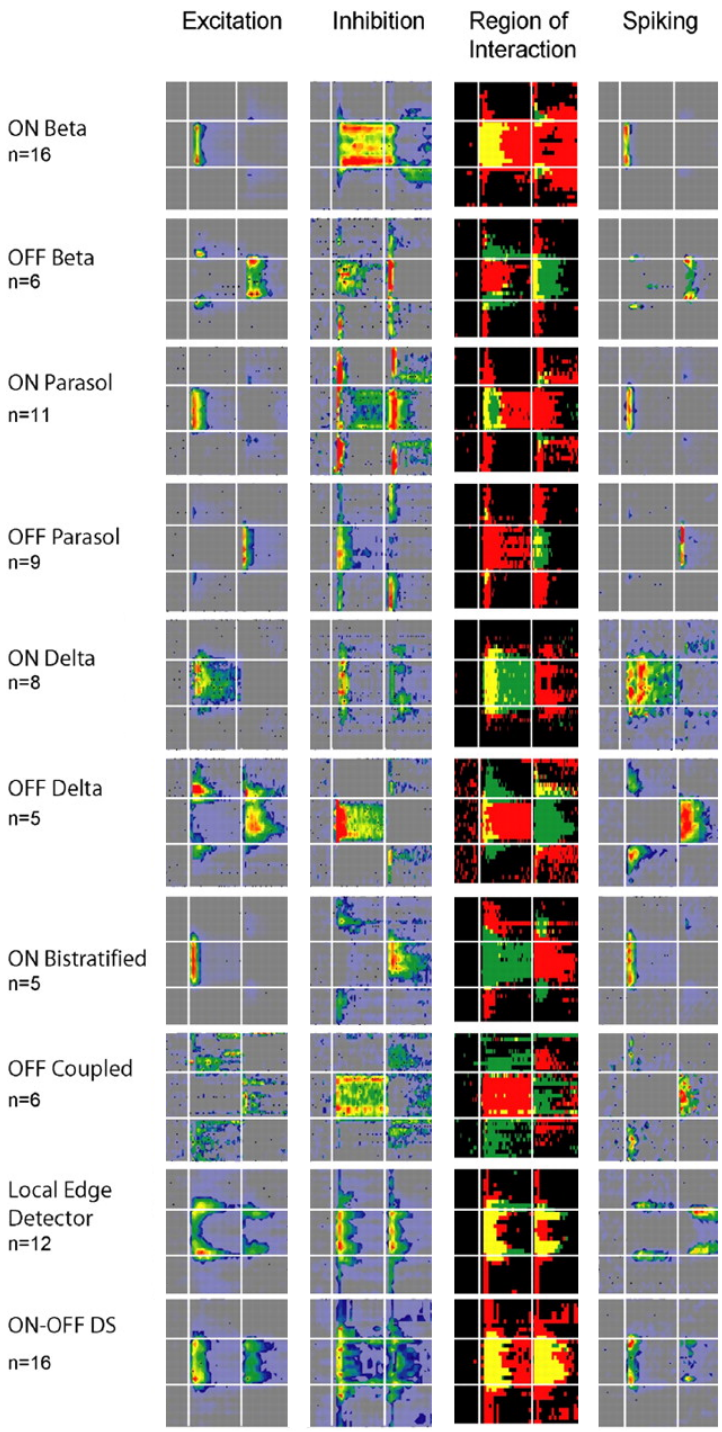

Figure 3.29: *Different ganglion cells respond to a static square stimulus.* Same stimulus and representation as in Figure 3.13. In most cells, the output spiking pattern strongly resembles the input excitatory pattern, because the excitatory and inhibitory inputs show little overlap (as indicated by yellow regions in the 'Region of Interaction' column). This suggests a 'push-pull' organization of excitation and inhibition (see text). From Roska *et al.* 06 [128].

thanks to their myelinated sheath and Ranvier nodes, allow the transmission of spikes over long distances, whereas a continuous graded signal would be transmitted slowly and with strong attenuation. With this obvious physical role of spikes, their existence needs not be explained by a role in *coding* as well. A basic working assumption can then be, that spikes are only sources of noise in the retinal code, imposed by the need for transmission over long distances.

Following this assumption, the nature of retinal coding is best studied through some averaging over the spikes, to wipe-out the noise added by the spike generation: This justifies the study of trial-averaged firing rates as the most informative output. The argument that 'spikes are only coding noise' has strong theoretical links with the modeling of spikes as Poisson processes (see Section 4.2.1).

4.1.2 Spike emissions lack a unified theoretical framework

A second and more prosaic reason to neglect individual spikes is that the question of spike coding is theoretically difficult: Defining a correct framework is not obvious, and deriving mathematical results from this framework is accordingly hard.

The fundamental problem is that spike emission involves very rapid and nonlinear variations of the underlying physical magnitudes (membrane potentials, synaptic release, etc.). To account for this intrinsic complication, two options are available, which result into fundamentally different mathematical frameworks.

If one really wishes to stick to the physical nature of the spike, it can be modeled as a fast oscillation resulting from specific, very nonlinear dynamic systems (models of Hodgkin and Huxley, FitzHugh and Nagumo, Mainen and Sejnowski, etc.), or as the explosion in finite time of a nonlinear system (models of Gerstner, Izhikevich, etc.). However, these equations rapidly become hard to interpret, and the functionality attached to the spikes hard to study.

Rather, one can consider the spikes as discrete stereotyped events, each associated to a precise instant in time, and claim that the retinal code is totally contained in this discrete set of events. This is a strong and fundamentally *interpretative* claim, which does not reflect a physical reality, but an intrinsically human segmentation procedure [13].

Maybe because spikes are such a subjective interpretation of the physical reality, their mathematical analysis is difficult, as classical tools (L^2 distance, Fourier analysis, ODEs) are not available anymore. Naturally, strong theoretical frameworks for spikes also exist. From the point of view of an *emitting* cell, a spike train emission is well accounted for by the formalism of *point processes*. From the point of view of a *receiving* cell, a spike is often modeled as a Dirac function[14]. However,

[13] It could be replied that any physical observation and measure is fundamentally human and interpretative, and eventually depends on our mental representation of the perceived world. Here, we mean that 'visually' segmenting a signal into discrete spikes is a much stronger interpretative leap, than simply associating physical quantities (charge, intensity, etc.) to phenomena. In other words, there is no simple and rigorous mathematical definition of a spike, and yet least of a spike train, or spike burst. Instead, spikes can only be defined through specific threshold criteria on the underlying continuous signal, derived from our perceptual analysis. This is quite anecdotic, but an epistomologist might remark that there is some paradox in claiming that the cerebral code is associated to spikes, when spikes themselves do not have a precise physical definition, but rather result from our own human interpretation capabilities.

[14] By Dirac, we mean 'the distribution that, when applied to any signal, returns the value of this signal at one particular instant in time', a definition which applies to both continuous and discrete time scales.

the junction of these two formalisms (emission and reception) in network models generally leads to complex frameworks where mathematical analysis is difficult. As an example, note that such a simple notion as that of a *distance* between two spike trains, so intuitive in the continuous case, becomes a challenging problem (see Victor 05 [160] for review).

4.1.3 A theoretical framework for spike coding in the retina

In its most general expression, the question of spike coding in the retina amounts to finding the relation –necessarily statistical, because of the intrinsic trial-to-trial variability of the cells– between a visual stimulus and a cell's spiking output. Given the particular functional spaces for the input (a three dimensional vectorial space) and for the output (discrete trains of temporal Dirac functions), this is a mathematical problem for which very few tools are available.

As a result, the theoretical framework must again be considerably reduced. In the retina, all models are based on the same theoretical simplification by a two-step procedure:

1. First, some continuous activity $\mathbf{A}(t)$ (possibly multi-dimensional) is calculated for each ganglion cell, which reflects all continuous filtering prior to spike generation.

2. Second, each ganglion cell generates a discrete train of spikes from its activity $\mathbf{A}(t)$, plus possibly from previous spikes of other spiking cells, following some specific *spiking procedure*.

This two-step model architecture is the simplest extension of 'continuous' models, for which only the first step is present. In the retina, this two-step model is rather well justified, since cells prior to ganglion cells do not fire spikes. Roughly speaking, the activity $\mathbf{A}(t)$ may be associated to the synaptic inputs of the ganglion cell. It may be multi-dimensional if one wants to model both excitation and inhibition on a ganglion cell. Note however that, even in the retina, this is a reduced model of the biological reality (for example, the spikes from ganglion cells could have an influence on bipolar cells, through amacrine cell feedback).

The most classical example of such a two-step spike coding is the LNP model (Chapter 2, Section 5). Because it is conceptually simple, this sort of model is also used to model the spiking activity of other low-level visual areas (LGN, V1...), but in that case the model is less justified biologically, since many successive spiking layers are modeled through a single spiking step.

In the retina, most work has been done on two main aspects of the spike emission. The first aspect (Section 4.2) is the characterization of the spiking procedure for a single cell, and how it can be modeled by specific point processes. The second aspect (Section 4.3) is the study of correlation between the spike trains from neighboring cells, in the dark and under visual stimulation, and how they could mediate advanced coding schemes.

4.2 Spike-emission process for a single cell

Here we review models that have been proposed to understand the spike emission of a single ganglion cell in response to a visual stimulus, and the experiments on which these models rely. For the models presented here, the underlying framework is the two-step spiking procedure presented in

the preceding paragraph, with the added supposition that *ganglion cells do not exchange spiking information*: The spiking of a single ganglion cell is totally determined by its input $\mathbf{A}(t)$. We will now refer to such models as 'single-cell models'.

In Section 4.2.1, we rapidly present the Poisson model and its implications in terms of spike coding. A classical extension, the 'simple modulated renewal process' (SMRP) is presented in Section 4.2.2, that allows to take more biological constraints into account. We then switch to real retinal measurements (Section 4.2.3) and compare them to Poisson and SMRP models. This allows us to understand which alternative and more efficient model of spike generation can be proposed, in Section 4.2.4.

4.2.1 The Poisson process

The non-homogeneous Poisson process is the simplest way to generate a discrete and random set of events (the spikes) from an underlying continuous variable. Mathematically, it can be defined in several equivalent ways, and it has several properties, which it is not our goal to explore here. For this report, we choose a presentation which allows direct extension to SMRPs (next paragraph).

Let $\lambda(t)$ be a strictly positive function of time, defining the *instantaneous rate* of the Poisson process. Let $U(t)$ be the transformed time scale

$$U(t) = \int_{s=0}^{t} \lambda(s) ds. \tag{3.5}$$

A Poisson process of instantaneous rate $\lambda(t)$ is a random distribution of discrete and growing event times $\{T_n\}$, such that for any spike time T_n, the probability of occurrence of the next spike in the Poisson process is defined by:

$$P(T_{n+1} \in [T_n, t]) = \int_{U(T_n)}^{U(t)} \exp(-\tau) d\tau. \tag{3.6}$$

One can check that the process defined by (3.6) fires on average $U(b) - U(a)$ spikes in any interval $[a, b]$, so that $U(t)$ can be called the *average spike count measure*: On average, one spike is emitted every $\Delta U = 1$. Coherently, the temporal derivative of the spike count $U(t)$ is the instantaneous firing rate $\lambda(t)$ (equation (3.5)). The bigger values $\lambda(t)$ takes, the faster $U(t)$ grows, so the more spikes are emitted.

It should be noted (although we do not prove it here) that a Poisson process verifies the Markov property (conditional independence of past and future), which is a strong theoretical advantage.

A 'transparent' process

In the optic of transforming a continuous firing rate into a discrete and random set of spike trains, the Poisson process is the most 'transparent' possible, in terms of the statistical links between the spike train and the underlying firing rate. This link can be resumed as follows:

1. Maximum entropy process: Of all renewal processes which share the same trial-averaged firing rate $\bar{\lambda}(t)$, the Poisson process of instantaneous firing rate $\bar{\lambda}(t)$ is the one which has the maximum Shannon entropy. So, if no other information is known about a spike train than its trial-averaged firing rate, it should be modeled as Poisson to minimize artificial, model-related correlations.

2. Reciprocally, if a spike emission procedure is based on a Poisson model, the underlying continuous processing $\lambda(t)$ can be reconstructed from the averaged firing rate $\bar{\lambda}(t)$ (over an infinity of trials): $\bar{\lambda}(t) = \lambda(t)$.

   This property is particularly interesting for the LNP model (Chapter 2, Section 5): When a spike-triggered average (STA) is performed on the output, the spikes are 'transparent', so the STA amounts to performing a 'classical' reverse correlation analysis which allows to find back the best-fitting linear kernel and nonlinearity (Chapter 2, Section 5).

To sum up, being 'transparent' confers a strong theoretical advantage to Poisson processes, but also a lack of interest as far as spike coding in concerned: No information is embedded in the precise spike emissions of a Poisson process.

Rather, the only effect of a Poisson process in the transmission of a signal, is the addition of a specific stochastic *noise*: If the successive emitted spikes are considered as Diracs localized at successive times T_n, then the Poisson emission transforms the continuous signal $\lambda(t)$ into signal $O(t) = \sum_{n=0}^{+\infty} \delta(t - T_n)$. On a trial-average, $O(t)$ and $\lambda(t)$ have the same integral in each interval (e.g., the average number of spikes in this interval), but in the case of $O(t)$ the power is randomly re-concentrated on a discrete set of points.

4.2.2 Gamma, and other simple modulated renewal processes (SMRP)

Real neurons show deviation from the exponential inter-spike interval (ISI) distribution of Poisson models, as defined by (3.6). In particular, in a particular realization of a Poisson emission, two successive spikes can be very close one from another: If a short interval of time dt is considered, (3.6) implies that $P(T_{n+1} \in [T_n, T_n + dt]) = \lambda(T_n)dt + o(dt)$. Taking $\lambda(T_n)$=100 Hz and $\Delta t = 1$ ms, the probability of a second spike being separated by less than 1 ms is around 0.1. This behavior is in contradiction with the *refractory* behavior of real neurons, which ensures that two successive spikes can never get closer than a few milliseconds (typically 5 ms, but with consequent variation between neurons).

The Poisson model can thus be extended to the more general class of 'simple modulated renewal processes' (SMRPs, using the terminology of Reich *et al.* 98 [121]), to impose a more biological ISI distribution. In SMRP models, the underlying continuous variable $\lambda(t)$ still defines the instantaneous firing rate, so the model is still based on the average spike count measure $U(t)$ in (3.5). However, one now has the choice of the probability distribution for the interspike intervals (ISI):

$$P(T_{n+1} \in [T_n, t]) = \int_{U(T_n)}^{U(t)} f(\tau) d\tau, \tag{3.7}$$

where f defines the *probability density function* (*pdf*) of the ISI, with the properties that $\int_0^\infty f(\tau) = 1$ (probability distribution) and

$$\mathbb{E}(T_{n+1} - T_n) = \int_0^\infty \tau f(\tau) d\tau = 1,$$

to respect the definition of $U(t)$ as an average *spike count*. This liberty allows a better fit to experimentally measured ISI distributions.

A particular parametric class of functions allows a direct extension of Poisson models: They are Gamma processes, based on 'Gamma' *pdf*s:

$$E_{\alpha,\tau}(t) = \frac{(\alpha t)^\alpha}{\Gamma(\alpha)\tau^{\alpha+1}} \exp(-\alpha t/\tau), \tag{3.8}$$

where α is the parameter of the function (necessarily positive with the definition chosen here), and Γ is the Gamma function (the traditional interpolation of the integer factorial, which has improperly given its name to these 'Gamma' functions).

We have already met such functions when modeling linear temporal kernels in the retina (equation (2.6) and Figure 2.3, for *integer* parameter $\alpha = n$). For $\alpha \to 0$, they tend to a decaying exponential, and thus a Poisson process. By opposition, the bigger α gets, the more regular and deterministic the spike emission, as resulting from the more peaked shape of the *pdf* [15].

In particular, Gamma processes account better for the cells' refractory period, since for the Gamma process of parameter α, one now has $P(T_{n+1} \in [T_n, T_n + dt]) = \lambda(T_n) dt^{\alpha+1} + o(dt^{\alpha+1})$, which greatly minimizes the probability of successive spikes being too close.

However, the increased biological plausibility allowed by generalized SMRP processes has a theoretical price: The Markov property does not hold anymore for such processes, since it resulted exclusively from the exponential expression of the *pdf* in the case of Poisson processes. Also, the link between the instantaneous firing rate $\lambda(t)$ and the trial-averaged firing rate $\bar{\lambda}(t)$ which can be measured becomes slightly more complicated, but as a correct approximation, one still has $\bar{\lambda}(t) = \lambda(t)$ as in the Poisson process [16].

4.2.3 The statistics of retinal spike trains

Along with proposed models for retinal spiking, comes the need for theoretical and mathematical tools to confront the models to experiments. For example, how can one quantify to what extent a

[15] For $\alpha = n$ integer, the Gamma process can also be generated from a Poisson process with an n-fold bigger instantaneous firing rate, but where only one spike every n is kept. Each resulting ISI is thus the average of n Poisson ISIs, providing another intuitive interpretation of the increased regularity.

[16] After reconsidering this problem in the spike-count time scale $U(t)$, one can get persuaded that the only possible discrepancy between $\lambda(t)$ and measure $\bar{\lambda}(t)$ comes from the initial condition of the SMRP process, if it is imposed that the process starts at time $t = 0$ as if a spike had just been emitted. If the first time in the SMRP process is initialized with a correct random probability, or if one considers the system only long after onset (ergodic conditions), then $\bar{\lambda}(t) = \lambda(t)$ becomes true with exactitude.

real ganglion cell follows or deviates from a Poisson behavior? This question is in strong relation to the remarks we made previously about the theoretical difficulty of studying spike trains: A spike train as itself is not very informative visually, and many of its characteristics are stochastic. As a result, more than in any other domain of the retina, a strong theoretical framework is necessary even at the experimental level, to produce meaningful results from the raw data.

Here, we present the classic tools which have been used to quantify the response and stochastic variability of ganglion cells, and what properties of retinal spiking have thus been revealed. As an illustration of the difficulty of theoretically grasping spike trains, any one of these tools only provides a partial view of the spiking phenomenon as a whole.

Trial-averaged firing rate

This is obviously the first statistical indicator which can be derived from sets of spike trains. It grasps the whole information available in a Poisson process, and almost all the information available in a SMRP (see Section 4.2.2), but significant information can be lost for other spiking procedures.

Inter-spike interval (ISI) histogram

This measure is obtained by constructing a histogram of all interspike times $T_{n+1} - T_n$ emitted during the process. In the case of a *homogeneous* spiking procedure (if the statistical properties of the process are stationary over time), the ISI histogram gives access to the *pdf* of the renewal process $dP(T_{n+1} = T_n + \tau)$.

Unfortunately, a real retinal spike emission is generally not homogeneous, since it depends strongly on the temporal evolution of the visual input. As a result, ISI histograms have a very limited signification, except in the case of cells receiving a temporally constant input. It is possible to compensate for (part of) this input-related variability by plotting the ISI histogram in the spike-count reduced time scale as in equation (3.5) (see next paragraph).

Interval maps

Reich *et al.* 98 [121] proposed a two-dimensional representation of spike trains allowing to represent simultaneously trial-averaged firing rates, ISI histograms, and supplementary statistical information, in a single representation that they called the *interval map*. This map is constituted of a plot of all couples $(T_n, T_{n+1} - T_n)$, over successive trials. Interestingly, the projection of this map on the abscissa is the average firing rate, and the projection on the ordinates is the ISI histogram. Such 'interval maps', in response to a drifting grating, are represented in Figure 3.30, left column.

A striking feature is that, even after averaging over all stimulus cycles, strong peaks remain in the average firing rate. A natural explanation of these peaks is that the precise spike times are relatively deterministic over the cycles, at odds with Poisson or other simple modulated renewal processes (SMRP, see Section 4.2.2). And indeed, a spiking procedure based on a noisy integrate-and-fire model (see Section 4.2.4) allows to reproduce this statistical 'phase locking' between the spikes and the stimulus cycles.

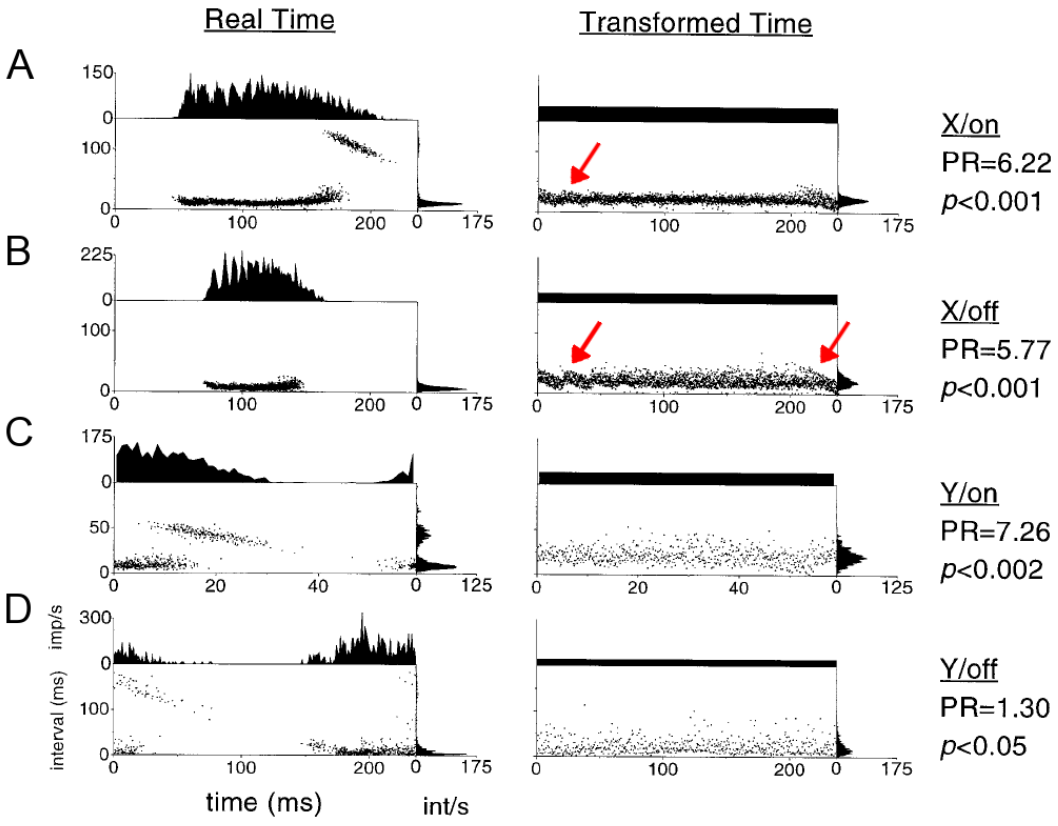

Figure 3.30: *Interval maps of cat ganglion cells over one cycle of drifting grating. Left column:* Plots of the couples $(T_n, T_{n+1} - T_n)$ for different ganglion cells, averaged over the repeated cycles of a drifting sinusoidal grating at 4.2 Hz (except *C:* 16.9 Hz). Average firing rate (top) and ISI histograms (right) can be derived from the interval map by simple projection. Longer intervals at the end of the cycle correspond to the time to wait before first spike of the next cycle (too big to be represented in *B*). *Right column:* Same data in a spike count time scale, using the empirical average firing rate. These cells differ strongly from Poisson or SMRP behavior, as marked by the bumps in the rescaled maps (see text). From Reich *et al.* 98 [121].

Remark: Note however that such an experiment cannot prove *a priori* that these oscillations come only from a statistical phase locking of the spiking response to the stimulus: Theoretically, they could also arise from 'real' oscillations in the IPL, followed by a simple Poisson spike emission. The results of the following paragraph prove that, independently of the shape of the average firing rate, the spike statistics *are not* Poisson.

Still, 'continuous' oscillations in the IPL might be *coupled* to the spiking procedure, and account for part of the oscillations seen in Figure 3.30 (see the results of Sakai and Naka, Figure 3.36). Such oscillations cannot be accounted for by the two-step procedure of Section 4.1.3. In the end, the interpretation of Figure 3.30 remains very dependent on the underlying 'frame of modeling', a sort of problem often encountered when dealing with precise spike models. ■

More precise properties of the cells' spiking procedure appears when the interval map is replotted in the empirical spike count time scale given by

$$\bar{U}(t) = \int_{s=0}^{t} \bar{\lambda}(s) ds, \tag{3.9}$$

where $\bar{\lambda}(s)$ is the empirical average firing rate measured over the trials. Replotted interval maps are presented in Figure 3.30, right column. They allow to estimate the relation of the cell's spiking procedure to a SMRP, independently of its average firing rate. Indeed, in a SMRP, the rescaled interval map is by definition translationally invariant, and its associated *pdf* can be found by measuring the 'rescaled' ISI histogram, after projection along the abscissa axis.

As a result, the rescaled interval map provides both:

1. A measure for the 'best-fitting *pdf*' if the cell was to be modeled as a SMRP.

2. The discrepancy between the cell's actual emission and a SMRP model, visible in deviations of the interval map from translational invariance.

And indeed, the interval maps of real cells often display significant bumps (arrows in Figure 3.30), with a typical diagonal orientation. This diagonal orientation indicates an anti-correlation between the time of the current spike and the next spike time, and it has a typical slope of -1. Such bumps appear when the 'next spike following the bump' (quite an approximate definition!) is more deterministic than what would be predicted by Poisson. For example, if the next spike $T_{n+1} = t_0$ was totally deterministic, then the cluster would be a single diagonal line, consisting of all points $(T_n, t_0 - T_n)$.

The authors [121] then propose an empirical measure called the *power ratio* (PR), based on the Fourier transform of the rescaled interval map, to measure the strengths of such clusters, and hence deviations from SMRP behavior. Typically, the PR of Poisson or Gamma SMRPs is smaller than 1, whereas most cells have a PR significantly higher: See Figure 3.30, on the right.

The authors show that a noisy leaky integrate-and-fire spiking model (nLIF, Section 4.2.4) has a high PR in response to sinusoidal stimulation, and the same characteristic 'diagonal bumps' in the rescaled interval map.

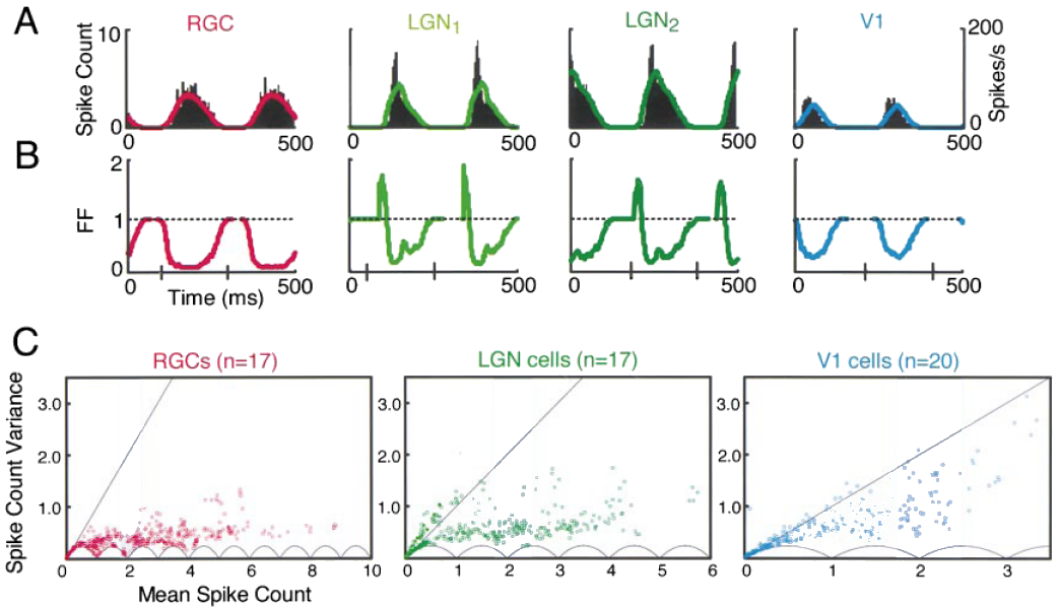

Figure 3.31: *Fano factors in the cat visual system, responding to a drifting grating. A:* Mean spike count (firing rate) of different cat visual cells, using binning windows of 50 ms. *B:* Corresponding Fano factors (FF) calculated from the same 50 ms intervals. The clear anti-correlation between spiking activity and Fano factor reveals that spikes are relatively 'more regular' at high firing rates. The high FF of LGN cells is attributable to spike bursts (Chapter 1, Section 1.2). *C:* Mean spike count versus variance, for all 50 ms intervals and all measured cells from each area. The scalloped curve at the bottom is a theoretical lower bound for the spike count, due to the fact that it can only take integer values. From Kara *et al.* 00 [76].

Fano factor, and other spike count measures

Alternatively, many authors have been using the *Fano factor* (FF) to measure the variability of spike trains. The Fano factor is defined on any time interval W from the statistics of $N(W)$, stochastic number of spikes falling into interval W during a trial:

$$FF(W) = \frac{\mathrm{Var}\big(N(W)\big)}{\mathbb{E}\big(N(W)\big)}. \tag{3.10}$$

Interestingly, a non-homogeneous Poisson process always verifies $FF(W) = 1$, independently of W and of the instantaneous firing rate $\lambda(t)$. Unfortunately, for other processes, the FF has no simple expression. For a SMRP, calculations derived from the central limit theorem insure that asymptotically

$$FF(W) \to \frac{\sigma^2}{\mu^2} \text{ when } L(W)\mu^{-1} \to +\infty, \tag{3.11}$$

where $L(W)$ is the time length of interval W, and μ and σ^2 are the respective mean and variance of the pdf of the ISI for the process. This is true only when the average number of spikes $L(W)\mu^{-1}$ tends to infinity. It thus appears that the Fano Factor is linked to the *coefficient of variation* σ/μ, another traditional statistic on interspike intervals. Hence, for a Gamma process of order α, one has:

$$CV = 1/\sqrt{\alpha}, \text{ and } FF(W) \to 1/\alpha \text{ when } L(W)\mu^{-1} \to +\infty.$$

In real ganglion cell spike trains, the Fano factor is not constant: There is a striking anti-correlation between the value of the FF on short intervals (typically, 50 ms) and the average firing rate in these intervals (Figure 3.31). This means intuitively that spike trains get more deterministic – even relatively to their firing rate- - at high firing rates. To account for this fact, some models such as Gazères *et al.* 98 [58] have introduced enhanced LNP models, where the choice of the spiking process depends on the strength of the instantaneous firing rate $\lambda(t)$: It is Poisson for small values of $\lambda(t)$, and switches to a higher-order Gamma process, with lower FF, when $\lambda(t)$ crosses a threshold.

However, in the case of a real cell, the Fano factor is not at all the intrinsic characteristic which it is for a theoretical Poisson spiking procedure[17]. Due to its definition, the FF depends not only on the state of a cell at a given time t_0, but also strongly on the length of the measuring interval W around t_0. As a result, we believe that FF-related studies should rather be taken as benchmarks to test the plausibility of a spiking procedure, than as an interpretative tool to directly derive parametrized models, as in Gazères *et al.* 98 [58].

Furthermore, as we present in the next paragraph, the particular nature of retinal coding might be such that spike counts, and thus Fano factors, are not the most relevant statistic to estimate the reliability of the retinal code.

Firing events: A strong coding principle?

Another line of work has investigated how the nature of the input stimulus could dramatically change the statistics of the spiking output. In the recent years, it has become clear that grating stimuli -so

[17] And for SMRPs to a lesser extent, with the asymptotic limit (3.11).

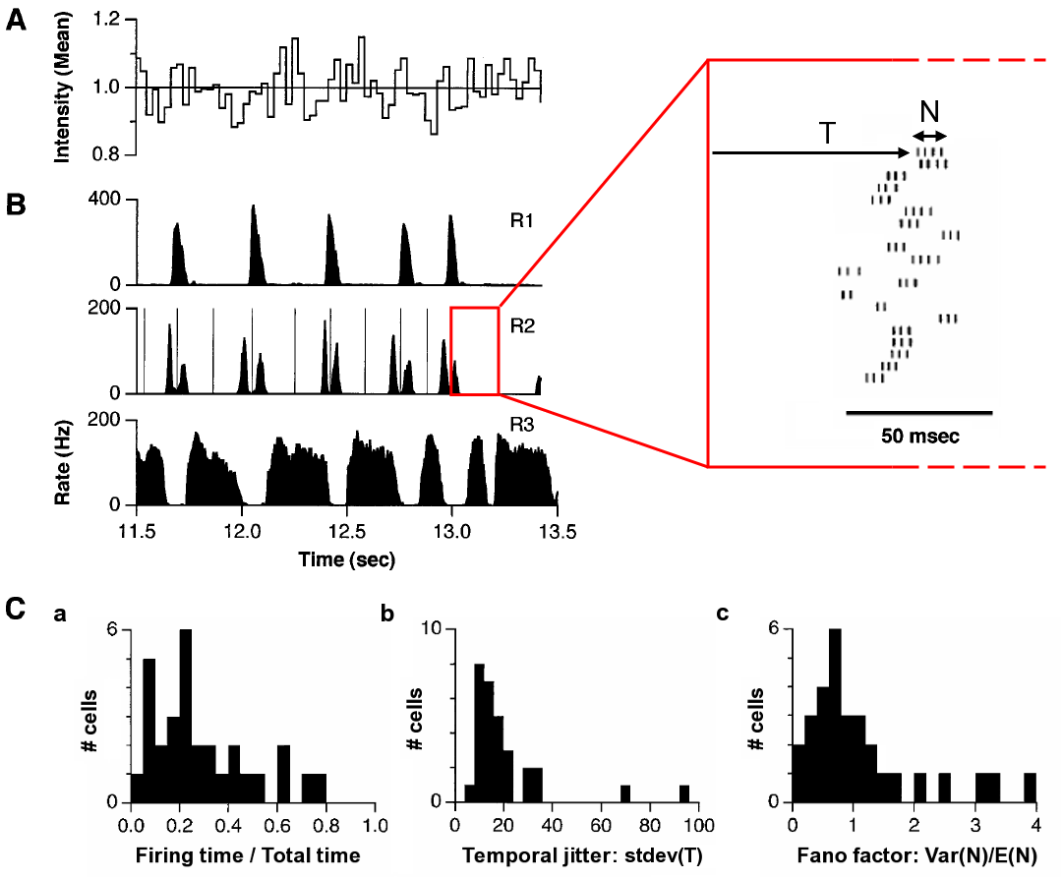

Figure 3.32: *Firing events in the rabbit retina. A:* Input stimulus is a uniform flickering screen following a temporal white noise. *B:* Firing responses of three rabbit cells. The responses naturally define *firing events* separated by long periods of silence. Automatic segmentation can be performed, as shown for cell R2. In each event, two random variables are studied: The time of first spike T and the number of spikes N in the event. *C: Statistical properties of a population of 30 rabbit cells.* Three 'statistical indicators' are derived for each cell, and respectively stored in three population histograms. *a:* Fraction of total time occupied by spiking events. Most cells (like R1 or R2) spend most of the time silent. *b:* Jitter in the time of the first spike in an event. A single indicator is calculated for each cell, as the median of $\sigma(T)$ over all its firing events. As compared to the typical time between successive events, this jitter is strikingly small. *c:* Variation in the number of spikes per events. A single indicator is calculated for each cell, as the average of the Fano factor over all events. The average FF is 0.7 over the whole population, markedly lower than for a Poisson process. Adapted from Berry *et al.* 97 [13].

often used as experimental input- elicit very unnatural responses from retinal cells[18], due to their strong regularity. When white noise stimuli or, better, natural image stimuli are tested on ganglion cells, they generally elicit much *sparser* responses from these cells than a drifting grating.

The responses of rabbit ganglion cells to a white noise stimulus are represented in Figure 3.32: Most cells, such as the depicted R1 and R2, fire strongly only at precise moments of the stimulation, which are rather sparse, and stable over trials. (By opposition, cell R3 has a strong ongoing spiking activity, suggesting that it might be one of the 'suppressed-by-contrast' cells discussed in Section 3.2.7.). In front of natural image stimuli, retina and LGN cells also display the same sort of peaked activity, although the peaks are not always as sparse as in Figure 3.32 (see for example Carandini *et al.* 05 [23]).

Berry *et al.* 97 [13] proposed the term *firing event* to describe these specific bursts of activity for the cells, and suggested that these events, rather than their individual constitutive spikes, could be the fundamental 'brick' of retinal coding. To justify this claim, they designed an automatic segmentation of the average firing rate into a discrete set of events (bumps of strong activity separated by zones of silence, illustrated for cell R2 in Figure 3.32), and measured for each event the statistics of T, time of the first spike, and N, number of spikes in the event (see Figure 3.32). Over a population of 30 rabbit cells, they found that:

1. Most cells spend a lot of time silent, with a small or null spontaneous firing rate, and sparse firing events (Figure 3.32 *C,a*). These observations are at odds with typical responses to drifting gratings, as in Figure 3.12, where some cells have a high spontaneous firing activity.

2. The precision of the first spike time, measured by the variance of T over all trials and events (Figure 3.32 *C,b*), is very small (10 or 20 ms for most cells) as compared to the typical time interval between two successive events (generally, several hundreds of ms). As a result, a lot of information is likely to be carried by the timing T of successive events: The authors estimated roughly this information to be $I_T = 7.3$ bits per spiking event, for a particular cell [13].

3. The number N of spikes per event has a relatively large variation across trials, but still less than a Poisson process (Fano factor of 0.7 on average over cells and events, against 1 for Poisson). A rough information measure yielded $I_N = 1.7$ bits per spiking event, on the same cell as in point 2.

Both information measures were based on the same estimation: Given their typical average and variance, how many different configurations of stimulus is the cell able to discriminate on the single basis of T (I_T, point 2) or N (I_N, point 3). Although very rough calculations, these results suggest that the strongest information carried by the cell in response to this sort of white noise stimulus, is in the successive timings of the events rather than in the total number of spikes in each event.

Remark: Could it be possible that a mathematical formalism should focus on firing events rather than individual spikes? Likely, taking such a wide step in modelization requires more experimental knowledge than is available at present time, and our retina simulator will of course retain spikes at the elemental bricks of signal

[18] And more generally, from the whole visual system.

transmission. However, it should be remarked that there is nothing more 'complicated', or 'integrated', in the notion of firing event than there is in the notion of individual spike: In the end, both criteria rely strongly on our visual segmentation and interpretation capabilities, when we look at the underlying continuous signal. ■

4.2.4 Noisy leaky integrate-and-fire (nLIF) models and derivates

When it comes to modeling the specific statistical structure of single cell firing patterns as presented in Section 4.2.3, the leaky integrate-and-fire model (LIF, see e.g. Rieke *et al* 97 [123]) has generally been presented as the good alternative to Poisson or SMRP models. Indeed, both interval map measures (Figure 3.30) and firing event measures (Figure 3.32) relied in the end on the same fundamental remark: When the cell has been silent for a while and that it undergoes a sudden augmentation of activity (rising phase of a sinusoidal cycle, or sudden strong response to white noise), the first following spike is more deterministic than predicted by SMRP models.

A LIF model precisely allows this first spike to be quite deterministic. The most basic [19] LIF neuron receives its input continuous signal as an excitatory current $I(t)$, from which it generates spike trains with the following procedure:

$$\begin{cases} \dfrac{dV}{dt} = I(t) - g^L V(t) & (3.12) \\ \text{Spike when threshold } \theta \text{ is reached: } V(t_{\text{spk}}^-) = \theta \\ \text{Reset: } V(t_{\text{spk}}^+) = V_R, \\ \text{and } (3.12) \text{ again.} \end{cases}$$

Interestingly, the LIF model can be made a *stochastic* firing process if noise sources are added in its generation. We will term the resulting models nLIF procedures. They are generally much more deterministic than a Poisson model concerning the 'first spike in a firing event'. Indeed, when $I(t)$ undergoes a sudden raise of its values, marking the beginning of a firing event for the cell, the next spike t_{spk} always follows quickly, following (3.12), rather independently of the added noise.

A typical nLIF has been proposed by Reich *et al.* 98 [121], that can reproduce the non-stationary bumps in real cells' rescaled interval maps (Figure 3.30, right column). The noise source they used was an input Poisson shot noise (Diracs fired following a Poisson process) added to the input current $I(t)$.

Similarly, Keat *et al.* 01 [77] have proposed a model very strongly inspired by a LIF, to reproduce the typical statistics of *firing events* in response to a white noise temporal signal, as presented in the preceding section (Figure 3.32). A summary of their model is presented in Figure 3.33. Importantly, their model uses two sources of noise:

- A correlated Gaussian noise $a(t)$ added to their generator potential (equivalent of $V(t)$ in the LIF model (3.12)), that can account for variations in the time of the first spike T in each spiking event.

[19] The LIF model can then undergo several improvements: It can include a refractory period, absolute ($V(t)$ held at V_R for a fixed amount of time after each spike) or relative (a kernel is added after each spike to the threshold $\theta(t)$, which becomes dynamic). It can also be based on conductances rather than currents (see e.g. Tao *et al.* 04 [147]), etc.

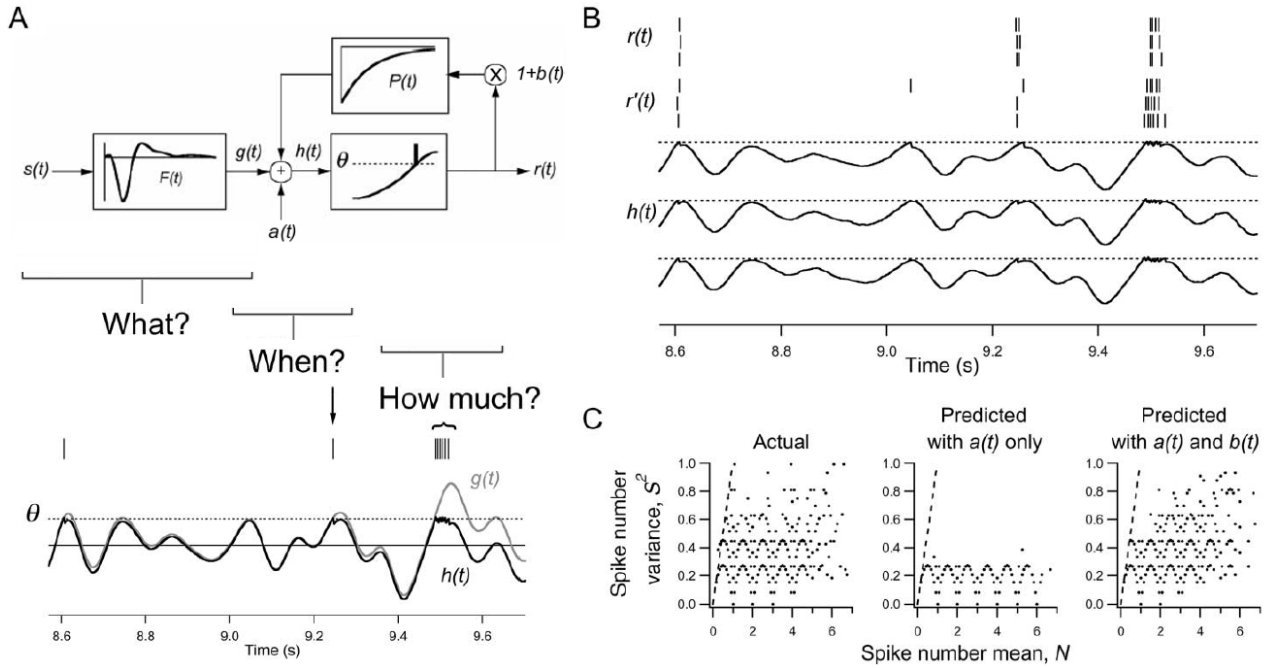

Figure 3.33: *A noisy LIF-inspired model of spike generation.* The model of Keat *et al.* 01 [77] is purely temporal, and reproduces the statistics of firing events for ganglion cells stimulated with white-noise modulated uniform screens. *A: Architecture of the model.* A response $g(t)$ is derived from the input $s(t)$ thanks to the optimal linear kernel $F(t)$. The generator signal $h(t) = g(t) + a(t) - \sum_i (1 + b(t_j))P(t - t_j)$ generates a spike t_i every time it crosses threshold θ. A refractory kernel $-(1+b(t_i))P(t-t_i)$ is added after each spike. The model includes a Gaussian auto-correlated noise $a(t)$, and a noise $b(t_i)$ on the strength of each refractory period. *B:* Compared spikes of a real cell ($r(t)$) and of the model ($h(t)$ producing $r'(t)$) for three trials. *C:* Spike count statistics $\big(\mathbb{E}(N), \mathrm{Var}(N)\big)$ over firing events for a real cell, the model with noise source $a(t)$, and the model with both noise sources $a(t)$ and $b(t)$. When only noise $a(t)$ is present, the jitter $\sigma(T)$ in the time of first spike is well reproduced ('When' criterion of Panel *A*), but the spike count N in each event is too deterministic. The addition of $b(t)$ allows to produce better statistics for N, by adding more noise in the intervals between the successive spikes in an event ('How much' criterion of Panel *A*). From Keat *et al.* 01 [77].

- A noisy refractory after-potential $P(t)$ following each spike, that can account for variations in the number N of spikes in each firing event.

Their model strongly relates to a nLIF model, their variable $g(t)$ (see Figure 3.32 and caption) corresponding to the integrated current $I(t) \overset{t}{*} \exp(-g^L t)$ in (3.12). Although we have preferred to stick to a pure nLIF formalism, the model we have implemented (Wohrer 08 [163], Chapter 4) also has two sources of noise, inspired by the Keat *et al.* model.

This concludes our presentation of single-cell models for spike generation. In a schizophrenic tentative to explain retinal spike coding, we have assumed in this section that all ganglion cells could be modeled as independent spiking encoders, whereas in the following section, we explain how neighboring ganglion cells' spike trains *are not* independent. The theoretical link between these two sections is not evident, since spikes from neighboring cells may possibly influence the spiking statistics at the level of a single cell. We will not enter such considerations, and only present experimental evidence for correlations in neighboring cells' spike trains.

4.3 Spike correlations between neighboring cells

The spike trains emitted by neighboring ganglion cells are generally not statistically independent. Two neighboring cells may have a tendency to fire synchronously, more often than by chance: Then, there is a positive correlation between their spiking outputs. Conversely, some cells (typically, an ON and an OFF cell) may have a tendency to never fire synchronously, implying a negative correlation between their spiking outputs.

Although some pioneering works had already been pursued long before (e.g., Laufer and Verzeano 67 [86], Mastronarde 83 [94]), the subject of correlations between ganglion cells has strongly arisen only in the last decade. This recent trend has different explanations[20]:

- Technical progress: Multi-electrode arrays now allow to record simultaneously from many tens of ganglion cells, rather than from pairs only, as was the case before.
- The introduction into neuroscience of new theoretical tools, such as information theory, allowing a deeper interpretation of experimental data.
- Increasing suspicion that correlations may carry a strong functional role in retinal transmission, as some recent experiments have suggested (see Figure 3.35). However, the functional importance of correlations is not well assessed either, which probably contributes to making this subject so attracting.

Because the subject is quite fresh, a state-of-the-art presentation appears difficult. However, we also feel the possible importance of these correlation mechanisms between ganglion cells, and thus try to provide an overview of current issues in the subject, by presenting some recent and relevant pieces of work.

[20] Others than its being a trend!

4.3.1 Spike correlations and their anatomical origin

Correlograms

Correlations between spiking cells are well represented by using correlograms. A correlogram between two cells A and B is the histogram of all differences $\{t_A^{(i)} - t_B^{(j)}\}_{i,j}$ between the spikes emitted by the two cells. It will be termed an *auto-* correlogram if $A = B$, and a *cross-* correlogram otherwise. If enough samples are available, the correlogram eventually represents $f(\tau) = dP(t_A^{spk} = t_B^{spk} + \tau | t_B^{spk})$, density of probability to have a spike from A at time τ before/after a spike from B.

As a result, two independent cells necessarily have a flat correlogram. By opposition, two *correlated* cells can be either:

- Positively correlated, with a peak in their cross-correlogram near $\tau = 0$.
- Negatively (anti-) correlated, with a dip in their cross-correlogram near $\tau = 0$.

Examples of cross-correlograms with positive correlation are depicted in Figure 3.34, Panel A. Note how different 'zooms' (e.g., insets on the right column) allow to reveal the properties of the correlation on different time scales.

Cross-correlograms are not necessarily symmetric. For example, if a spike from B always elicits a spike from A with a time delay τ_0, the correlogram will have a peak around $\tau = \tau_0$. Conversely, if a spike from A always elicits a spike from B with delay τ_1, there will be a peak around $\tau = -\tau_1$, etc.

Correlations of ON and OFF pathways during spontaneous activity

Correlations can be recorded in the absence of visual stimulation ('spontaneous activity'). This is an interesting experimental protocol, since it reveals the intrinsic biological structures giving rise to correlations, without the additional structure arising from the spatial coherence of an input stimulus.

A first strong observation during spontaneous activity is that neighboring cells of opposite polarity (e.g., On and Off BT cells in the rabbit) are generally *anti-correlated*, with a dip in their cross-correlogram near $\tau = 0$. (Mastronarde 83 [94], not shown). This reveals subtle interactions between the two pathways, generally renown as being segregated. We have not read much about such anti-correlations, but they can clearly lead to interesting synchronization effects: See e.g. the results of Sakai and Naka reproduced in Figure 3.36.

By opposition, neighboring cells from the same pathway are very often *positively* correlated, meaning that they have a tendency to fire in close synchronies. In the next paragraph, we detail the plausible anatomical origins of these positive correlations.

Origins of correlations amongst cells of the same polarity

Correlations between the spike trains of ganglion cells are mediated by different anatomical structures. In salamander retina, Brivanlou *et al.* 98 [17] found that pairs of correlated cells fell in three distinct clusters, according to the typical time scale for the peak in their cross-correlogram, and

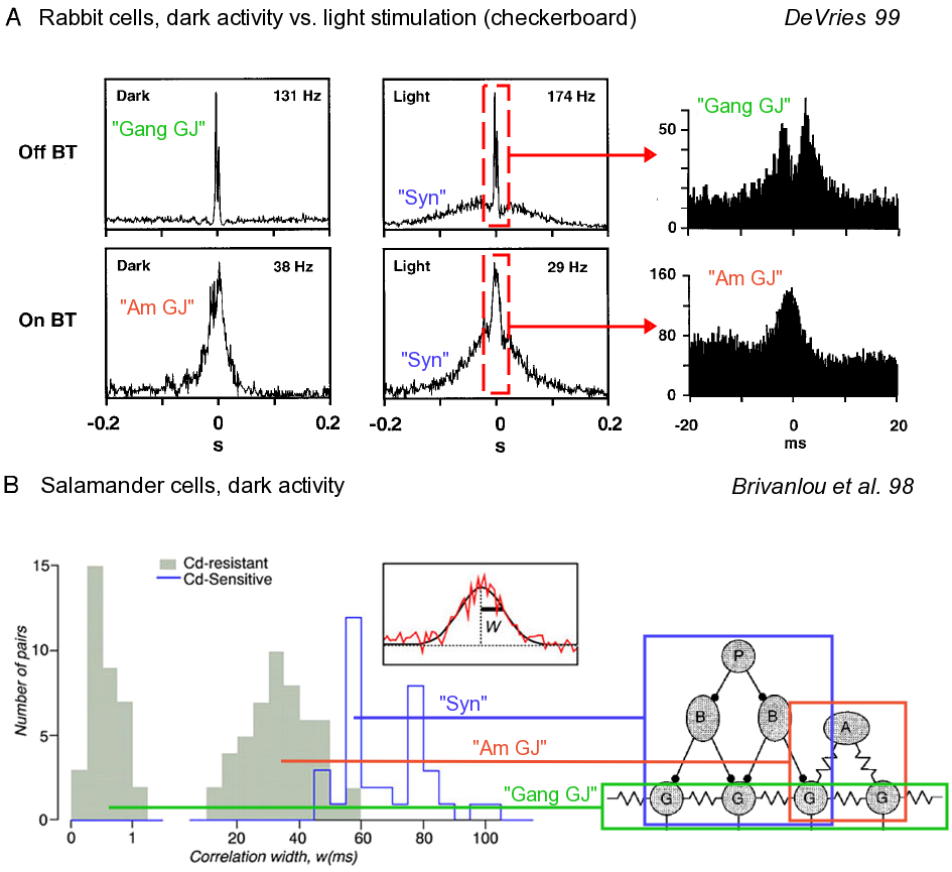

Figure 3.34: *Different temporal scales, and origins, of spike correlations. A: Rabbit On and Off brisk-transient (Y) cells exhibit different types of spontaneous and input-driven correlations.* Short time-scale correlations in Off BT cells reveal direct coupling through gap junctions, as indicated by the double peak (bidirectional transmission, delay of 1-2 ms). Short and medium time-scale correlations in On BT cells reveal a common input from pre-synaptic neurons, likely amacrine, through gap junctions and/or chemical transmission. In the presence of a visual stimulus (checkerboard), broad correlations appear superimposed. Numbers in Hz give a measure for the width of the central peak. Magnified insets are from different cells. Notations "Syn", "Am GJ" and "Gang GJ" refer to Panel *B*; They are schematic interpretations, hypothesized by us, not by the original authors. From DeVries 99 [43]. *B*: *Different scales of correlations, and presumed biological origins, in salamander retina.* When their correlograms are fitted by a Gaussian of deviation w ms, salamander cell pairs fit into three distinct clusters, according to the biological connections that dominate their correlations. Short and Medium time scale clusters are still observed in the presence of cadmium, a blocker of virtually all synaptic transmissions, so they likely arise from gap junctions. Conversely, the Broad time-scale cluster appears mediated by chemical synapses. *Right:* Hypothesized biological origins of the three types of correlations. We also marked their plausible correlates in rabbit retina, in Panel *A*. From Brivanlou *et al.* 98 [17].

the resistance of the peak to synaptic blockade (Figure 3.34, Panel B). Here are the three types of correlations they reviewed:

- 'Short' correlations occur on the time scale of a few milliseconds, and are characterized by a *double peak* in their correlogram (like the one observed in rabbit On BT cells, Figure 3.34 *A*, top right). They likely arise from **gap junctions between neighboring ganglion cells**. Indeed, these correlations persist in the presence of Cadmium which blocks all synaptic transmission. Furthermore, the symmetric peak indicates a fast, bidirectional connection between the two cells. Such correlations were found by [17] in about 10 % of the cells studied.
- 'Medium' correlations occur on the time scale of 20-50 ms and are marked by a single, symmetric peak in the correlogram (like the one observed in rabbit Off BT cells, Figure 3.34 *A*, bottom right). They likely arise from **gap junctions with amacrine cells**. Indeed, the larger time scale of the correlation indicates an indirect effect from non-spiking cells, and the persistence of these correlations in the presence of Cadmium suggests that gap junctions are involved. This effect formed a *majority of the correlations* studied by [17], accounting for $\sim$ 50 % of all emitted spikes during spontaneous activity!
- 'Broad' correlations occur on the time scale of 50-100 ms and are also marked by a single, symmetric peak in the correlogram (like the one observed in rabbit Off BT cells, Figure 3.34 *A*, bottom right). They likely arise from **synaptic connections** from amacrine cells and/or bipolar cells. Indeed, unlike the preceding two types of correlations, these are blocked by Cadmium.

In the overall scheme depicted by the study of Brivanlou *et al.*, amacrine cells are suspected to play a fundamental role in the apparition of correlations, through gap junctions and/or synaptic interactions with neighboring cells. And indeed, studies and models concerning *stimulus-driven* correlations (Section 4.3.2) suggest that an important synchronization is provided by specific populations of amacrine cells.

In the rabbit retina, De Vries 99 [43] has led a similar study with comparable results, depicted in Figure 3.34 *A*. Interestingly, On BT cells (top line) rather displayed the sharp (frequency $\sim$ 150 Hz) double peaked correlogram typical of direct gap junctions, while Off BT (bottom line) displayed the broader (frequency $\sim$ 30 Hz) simple peaked correlogram typical of correlation through intermediate cells. This adds supplementary evidence to the possible different functions of On and Off types of 'Y'-like cells (Section 3.2.2).

In addition, a much broader peak appeared in the presence of a visual stimulus, denoting the synaptic origin of broad correlations, and the increased complexity of the correlation structure in the presence of a visual stimulus, as we now present.

4.3.2 Stimulus-driven oscillations

Although studies of correlations during spontaneous activity are best designed to reveal an underlying biological architecture, the real impact of correlations on retinal coding must be measured in the presence of visual stimulus.

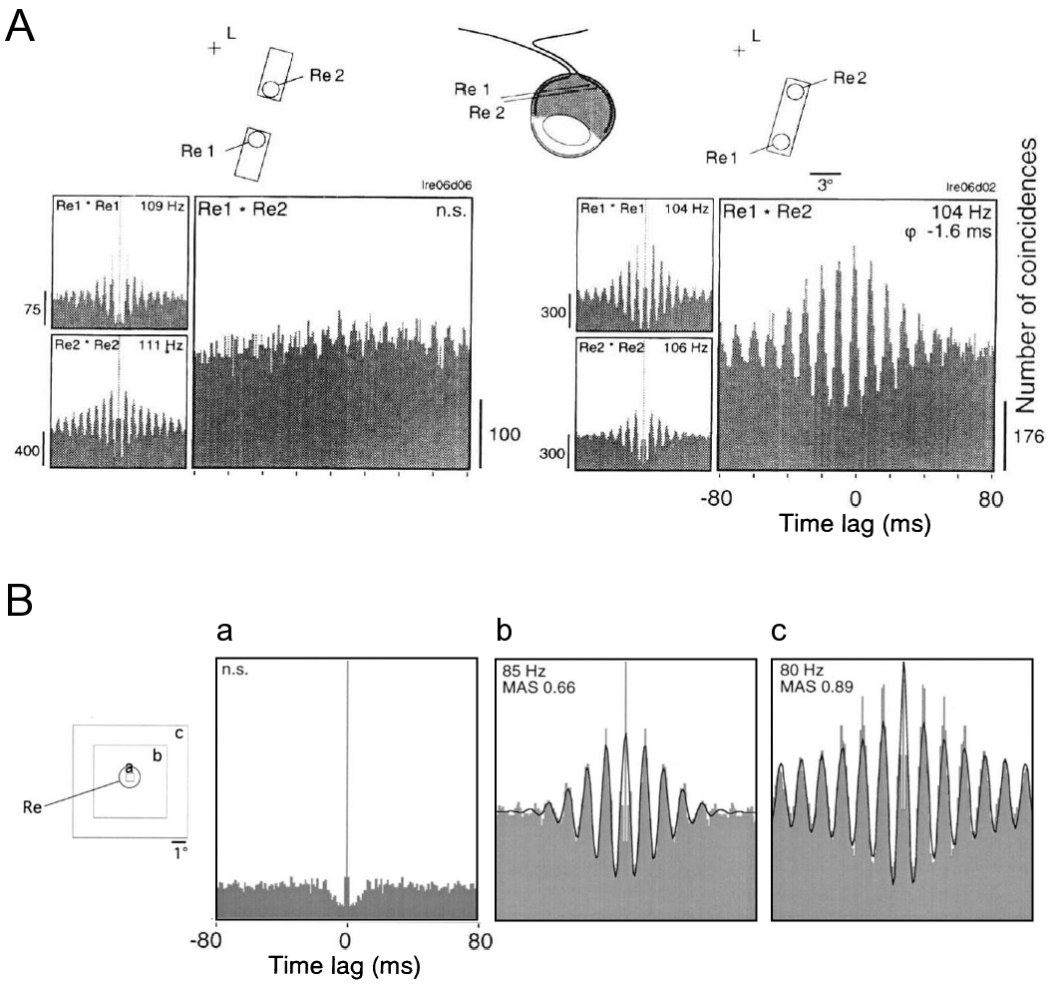

Figure 3.35: *Stimulus-dependent oscillations in the primate retina. A:* Two populations of cells, separated by 3 degrees, have uncorrelated spike trains (flat correlogram) when their receptive fields are lit by two discontinuous bars (left). By opposition, their spike trains are phase locked (oscillations in the correlogram) if they are lit by a single continuous bar (right). From Neuenschwander and Singer 96 [106]. *B:* Autocorrelogram of a single population of cells, for different sizes of a square stimulus. Oscillations, and thus phase locking amongst cells in the measured population, augments with stimulus size. From Neuenschwander *et al.* 99 [105].

Phase locking

The strong characteristic of spike correlations under visual stimulation is the possible apparition of a *phase locking* between the spike trains of two cells, or two populations of cells (Neuenschwander and Singer 96 [106], Neuenschwander *et al.* 99 [105]). In the cross-correlogram, this phase locking translates in fast oscillations, as depicted in Figure 3.35. The properties of the phase locking are the following:

1. It can occur even between distant cells (separated by several degrees), depending on the spatial structure of the underlying visual stimulus. Phase locking will be present between two cells only if their two receptive fields are located on a single spatial structure of homogeneous luminance (Figure 3.35 *A*). Also, the bigger the homogeneous structure around the cell, the stronger the phase locking (Figure 3.35 *B*).

2. It is not locked to the onset of the visual stimulus (not shown). At onset of a stimulus, the first spikes are locked to the onset time: For each cell, the averaged firing rate right after stimulus onset displays peaks because the first spikes are quite deterministic. But soon after stimulus onset, the 'internal' phase locking of the retina takes over: The average firing rate for each cell becomes flat (spikes fall anywhere over the trials), but the cross-correlograms of neighboring cells remain strongly peaked (all spikes are still synchronized).

3. It involves ensembles of cells rather than individual cells. Most of the cross-correlograms of Neuenschwander *et al.* were made directly on populations of cells. When cells are studied at the level of a population, oscillations are even revealed during spontaneous activity [105] (unlike the single-cell correlograms presented in Figure 3.34).

This phase locking is a very intriguing phenomenon. Since it depends on the spatial structure of the stimulus, it could provide a strong and early preprocessing for subsequent *object segmentation* procedures in the brain.

Including some simple model for this phase locking is one of our goals concerning future evolutions of software *Virtual Retina*.

Oscillations and amacrine cells

Because direct gap junctions between ganglion cells appear to make up only for a minority of correlations in the retina (Section 4.3.1, Paragraph "Origins of correlations…"), amacrine cells are the most likely candidate to account for the synchronies.

Speaking in favor of this fact, the results of Sakai and Naka 90 [131, 132] in the carp retina suggest that strong oscillations are induced by interactions with amacrine cells. More precisely, they studied the complex connections between two types of ganglion cells (On-type GA and Off-type GB) and two types of amacrine cells (On-type NA and Off-type NB), by injecting current pulses in one cell and simultaneously recording the voltage response in another cell. Let us comment their main findings with the help of Figure 3.36:

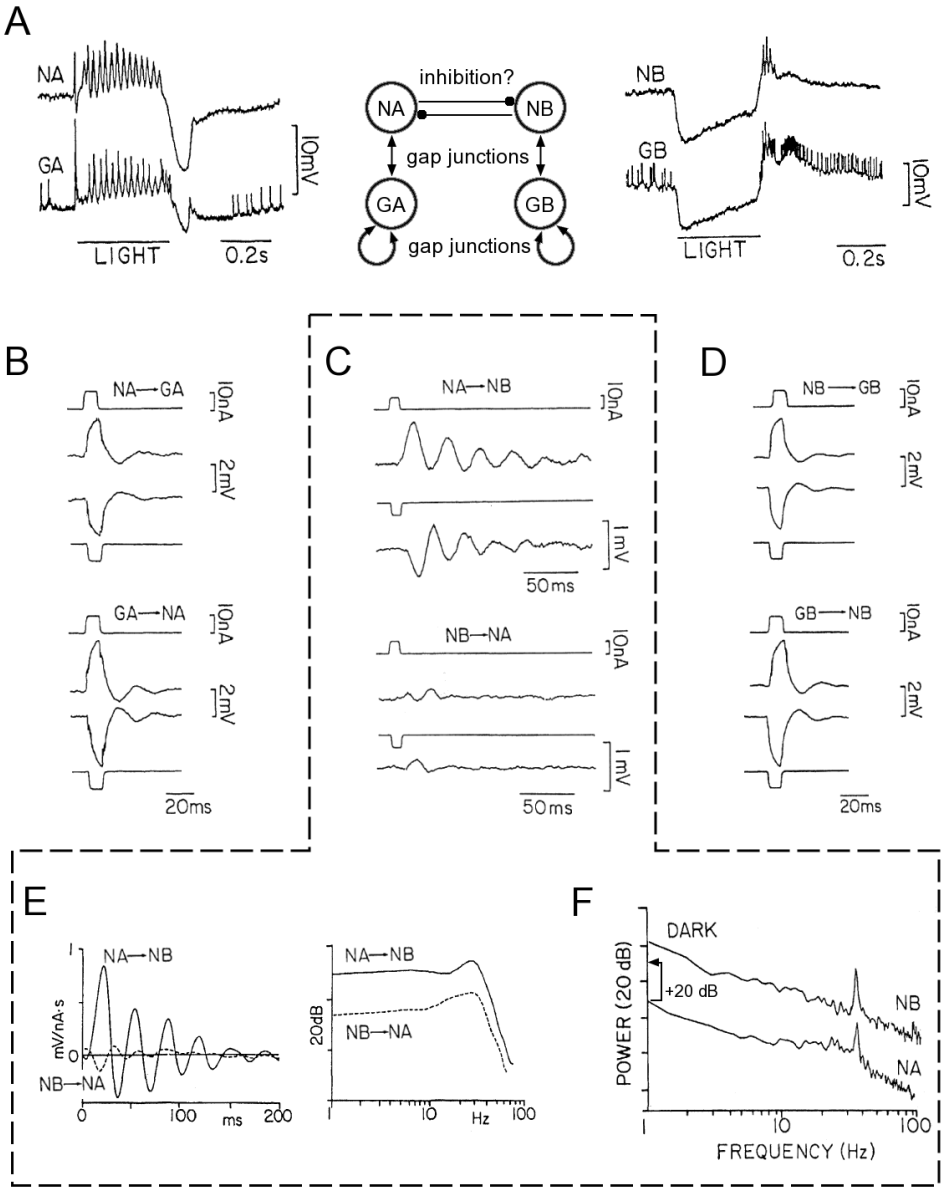

Figure 3.36: *Oscillations between On and Off pathways in the carp retina.* The On pathway (GA ganglion and NA amacrine cells) and the Off pathway (GB ganglion and NB amacrine) are anti-correlated, with the apparition of intrinsic oscillations at around 30 Hz in the responses of the cells. In Panel *F*, the NA curve is shifted of 20 dB downwards for visibility. See text for more details. From Sakai and Naka 90 [131, 132].

1. On-type ganglion and amacrine cells (GA and NA) are linked by strong gap junctions (see the effects of reciprocal current injections, in Panel B), resulting in very similar responses to light (Panel A, left column). The same coupling is observed between the Off-type ganglion and amacrine cells (GB and NB), as assessed from current injections (Panel D) and similar responses to light (Panel A, right column).

2. By opposition, strong anti-correlations (not shown) exist between NA and NB amacrine cells, with the apparition of specific oscillations around 30 Hz. More precisely, a current pulse injected in an NA cell induces strong oscillations in an NB cell, lasting for several hundreds of milliseconds (Panel C). Oscillations around 30 Hz are revealed, both in the linear kernel derived from reverse correlation between NA and NB (Panel E) and from the spectrum of the cells' spontaneous activities (Panel F). Interestingly, the effect is non-symmetric, as current injected in NB elicits much less response in NA (Panels C and E).

In the middle of Panel A, we propose the type of architecture suggested by these interesting results. The oscillations, which appear somehow intrinsic to the NB amacrine cells (Panel C), may serve as a vector for large-scale synchronizations. Unfortunately, by many ways these results are only partial, and difficult to interpret without supplementary research in the same direction.

Modeling stimulus-driven synchronizations

As far as modeling is concerned, the work of Kenyon *et al.* 03 [79, 80, 78] is to our knowledge the most advanced reproduction of the synchronization results of Neuenschwander *et al.* (Figure 3.35). Logically, their model relies on amacrine cell populations, and involves a complex interplay between ganglion cells, short-range inhibitory amacrine cells, and long-range amacrine cells which provide synchronization to ganglion cells through gap junctions.

An interesting question to address is whether stimulus-related synchronizations could arise *without* explicit modeling of amacrine cells, by allowing short-range excitatory / long-range inhibitory connections between model spiking units. Such a simplifying leap from the true structure of a retina (short-range excitation from ganglion cells and possible long-range inhibition from amacrine) could help to better understand the underlying functionality of spiking correlations.

The following results (Section 4.3.3), based on information theoretical measures, provide (amongst other things) informations concerning the feasibility of a model where all interactions would occur directly between the output spiking units. Interestingly, these results suggest that the whole structure of ganglion cell correlations, including negative correlations mediated by amacrine cells, can be accounted for by pairwise interactions between ganglion cells, possibly with negative weights (anti-correlation). However, the exact structure of the weights appears to depend on the type of stimulus used for the experiment, so that the correlation structure may not be directly usable in a generic model.

4.3.3 Applications of information theory

The increasing popularity of information theory in neuroscience has recently allowed to consider spike correlations with a more functional approach, questioning their impact on the statistical structure of the population spike trains. We here review two particular applications.

Pairwise correlations account for the whole correlation structure

For technical reasons, most recordings of spike correlations have only been pursued between pairs of cells. Yet, there is no *a priori* reason why retinal correlations should be understood simply by considering pairwise interactions. Recent studies (Schneidman *et al.* 06 [135], Shlens *et al.* 06 [142]) have questioned whether pairwise correlations are sufficient to account for the statistical structure of the retina.

Maximum entropy distribution. Their approach was based on the *maximum entropy* method, allowing to find the 'most random' probability distribution for a system, given a set of constraints on the observed output of the system:

1. At order 1, this method takes as only constraints the average firing rate measured for each cell. The resulting maximum entropy distribution is that of independent uniform encoders (tending to *Poisson* encoders when the discretization time step tends to zero), where the probability of firing of each cell i is based on a single constant number h_i.

2. At order 2, pairwise correlations are also taken into account. In this case, the maximum entropy distribution is a variation on Ising models: The probability of firing for each cell is coupled to the spikes simultaneously emitted by all other cells, being determined by $h_i + \sum_j J_{ij}\sigma_j$, where σ_j = +1 if cell j also fires a spike, and -1 otherwise. J_{ij} measures the coupling from cell j to i, so that a high J_{ij} tends to imply positive correlation between i and j (although the overall correlation between i and j depends on the whole structure $h, \mathbf{J}$).

Pairwise correlations explain the statistical structure. Both Schneidman *et al.* 06 [135] and Shlens *et al.* 06 [142] found that the statistical structure of the population spike trains is very well accounted for by an Ising model, depending only on pairwise correlations. This finding is especially interesting, because it gives hope to implement easily spike-based correlations. Indeed, the Ising model is closely related to simple Hopfield neural networks [142].

What cells, what stimulus? However, it should be noted that important differences appear in the conclusions of both studies, due to the different experimental procedures.

- In Shlens *et al.* 06 [142], the authors used artificial stimuli with no strong correlations (uniform light, and occasionally white noise), tested on a *single population of cells* (e.g., salamander OFF transient). In their resulting maximum entropy distribution, all the J_{ij} were found positive[21], meaning that each cell only influences the others positively. Also, they could take only

[21] Remark in their Section "Materials and methods", paragraph "*Maximum entropy*"

nearest neighbor correlations into account (imposing $J_{ij} = 0$ otherwise) and still reproduce well the whole statistical structure.

So, the statistical structure for the spikes of a single ganglion pathway under simple stimulation, is totally explained by reciprocal excitations between close neighbors. This finding is consistent with the nature of correlations during spontaneous activity (Section 4.3.1).

- In Schneidman *et al.* 06 [135], by opposition, natural stimuli were used (forest scenes, etc.) and the different cell types in the population were not distinguished. This time, a meaningful percentage of the resulting J_{ij} were negative[22], indicating anti-correlations in the population.

  So, inhibitory spiking interactions *do* exist at the scale of a whole retinal population under visual stimulation. This finding is consistent with the presumed roles of wide-field amacrine cells in creating stimulus-driven synchronizations (Section 4.3.2).

Redundancy and the role of correlations

Another application of information theory is to measure the overall *redundancy* in the retinal code. This has been done recently by Puchalla *et al.* 05 [116]. Based on measures of mutual information between a neuron and the input stimulus, they could derive a global *overrepresentation* factor for the retina, giving an estimate for the number of times the information carried by one neuron is also represented in the spikes of its neighbors. They found this factor to be around 10, suggesting that the retina is a highly redundant transmitter of information.

And indeed, it should be remembered that from an information-theoretic point of view, any deviation from independent spike encoding necessarily leads to a global diminution of the information transmitted by the retina. One can then wonder how spike correlations may still serve a functional role. However, several works attest the efficiency of correlation-based coding (e.g., Kenyon *et al.* 04 [78] in the retina, or Singer 99 [143] for general references).

Very likely, the resolution of this paradox lies in the dual fact that

- Not all 'information' has the same value for the retina. Cues for object segmentation, movement detection, etc., are clearly more valuable than telling the exact shade of gray in the sky, whereas 'information' is a much more abstract concept, especially in the absence of good generative models for natural scenes.

- Constraints in biological architecture probably make the most 'efficient' coding schemes impossible for implementation.

A better formalization of these issues, possibly in an information-theoretic framework, would help to better quantify the *functional* importance of correlations in the retina.

[22] Their Figure 3, Panel *b*

5 NONLINEAR ADAPTATIONS IN THE RETINA

The retina, as most biological organs, is not a static structure. Several mechanisms constantly adapt and regulate the successive stages of signal transmission, through complicated molecular control loops. In this last section, we mention some of the most important expressions of this adaptation.

Amongst various mechanisms of adaptation, a particular distinction can be made between 'fast' and 'slow' ones. The 'fast' adaptations are almost instantaneous mechanisms which allow to control the gains of signal transmission and thus avoid saturation of the system. Two major phenomena enter this category: Rapid adaptations to light and rapid contrast gain control. The term of 'adaptation' may be ill-suited for these mechanisms, because it evokes a somewhat secondary effect to improve performance, whereas these fast gain controls are simply necessary for the system to avoid total saturation and uselessness.

By opposition, 'slow' adaptations are mechanisms which occur in the range of seconds or even minutes. These are truly secondary effects which allow to optimize image processing in terms of acuity and economy of energy. Both types of phenomena will be evoked here.

In Section 5.1 we mention the most fundamental type of adaptation: Adaptation to luminance, which allows our eyes to see from dark night to bright sunlight. However, the huge complexity and numerous mechanisms underlying this functionality are only rapidly evoked, by lack of time and because adaptation to luminance is not in the scope of our simulator for the moment. In Section 5.2, we spend more time describing the phenomenon of *contrast gain control* (or 'contrast adaptation') which is of direct concern to our simulator.

Both adaptations to luminance and contrast possess at the same time fast and slow components. In Section 5.3 we present supplementary examples of slow adaptations, and how they can be interpreted in the theoretical framework of 'predictive coding'.

5.1 Adaptations to luminance

Adaptation to luminance has been a large subject of research in physiology and psychophysics for more than fifty years. The most important site of adaptation is obviously the photoreceptors, but horizontal cells are supposed to also play a role in the process, as well as some specific modulatory amacrine cells. It is not our goal here to review all these mechanisms which we have not investigated in detail.

We simply mention the fundamental effect of adaptation as observed in photoreceptors. The effects of background illumination on the transfer properties of ganglion cells are also evoked in Section 5.3, along with Atick's decorrelation hypothesis. Readers interested in the classical psychophysics of light adaptation are referred to the review of Shapley and Enroth-Cugell 84 [136].

Phototransduction and light adaptation. The main effect of light adaptation is to shift the whole response curve of the photoreceptors, in such a way that response to the background light is always close to the receptor's point of optimal sensitivity (maximum slope in the response function). This

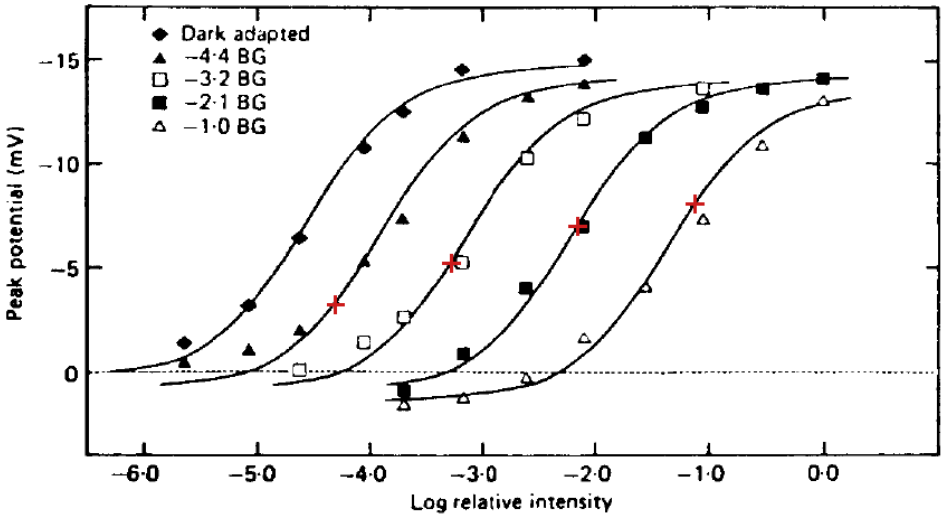

Figure 3.37: *Adaptation to background illumination in turtle cone receptors.* Each point plots the peak of response of a turtle cone receptor to a step of light of 0.5 s (in ordinates), versus the luminous intensity of the step (abscissa, log units). The retina was adapted to different levels of background illumination before the responses were measured, providing different 'response curves'. Through light adaptation mechanisms, the receptor's response curve is shifted so that response to the adapting illumination (red crosses) be always in the 'middle' of the curve. From Normann and Perlman 79 [108].

effect is illustrated in Figure 3.37. This process of 'response shift' remains efficient on a large range of background luminosities (especially in cones), and is sufficient to account for our ability to see at all levels of illumination, regardless of subtler adaptation effects.

From a molecular standpoint, the calcium modulatory feedback of phototransduction (Section 1.1) plays a fundamental role in the 'response shift'. It accounts for most of the receptors' adaptation until very high luminosities, where pigment depletion (massive deactivation of a majority of rhodopsin molecules) is required as an additional mechanism (Valeton and Van Norren 83 [153]).

The calcium modulatory feedback seems to be a rather 'fast' adaptation effect: To provide a good fit to data, Van Hateren and Lamb 06 [156] (Figure 3.3) must use values τ_{Ca} =3-12 ms for their calcium feedback. Experimentally, Schnapf *et al.* 90 [133] report 'fast' adaptation to fully develop within one second after a sudden change of illumination[23]. By opposition, pigment depletion clearly enters the 'slow' category, with depletions and recoveries occurring in the order of one minute [133, 153].

Remark: Weber and Fechner laws
A classical experiment in psychophysics consists in finding, for a given background intensity I, the threshold difference of intensity ΔI which can be detected by an observer. In fact, a relation of proportionality holds over a large range of background illuminations:

$$\frac{\Delta I}{I} = cst, \tag{3.13}$$

a relation known as *Weber's Law*. The physiological correlate of Weber's law can be seen in the receptor responses of Figure 3.37: The slope of the receptors' response curve, in a logarithmic scale, is relatively independent of the adapting background luminance I, meaning that the threshold ΔI inducing a fixed amount of response remains proportional to I.

Relation (3.13) is often integrated to derive a formula where the receptor's instantaneous response is

$$R \sim \log(I),$$

I being the instantaneous incident luminance. This relation, known as *Fechner's Law*, is true only if one supposes that adaptation to light is an *instantaneous* phenomenon. In the log representation of Figure 3.37, Fechner's law would predict a single, linear response curve. As can be seen in Figure 3.37, the real instantaneous response to an incident luminance I_2 is also determined by the 'recent' value I to which the receptor has been adapted. The receptor can possibly saturate if I_2 is very different from I, at odds with Fechner's law. ■

5.2 Contrast gain control

In this section we present the phenomenon of *contrast gain control*, or *contrast adaptation*, a particular nonlinearity in the responses of retinal cells to stimuli of different contrasts. A scheme of contrast adaptation has been implemented in our model and simulator (Wohrer 08 [163], Chapter 4), so we spend some time presenting the effect, quite universal in vertebrate retinas.

[23] This duration of one second seems somewhat at odds with the faster adaptation constant τ_{Ca} required by Van Hateren and Lamb 06 [156]. Again, this raises questions concerning the respective extracellular concentrations of calcium between the two experiments (see Section 1.1.2).

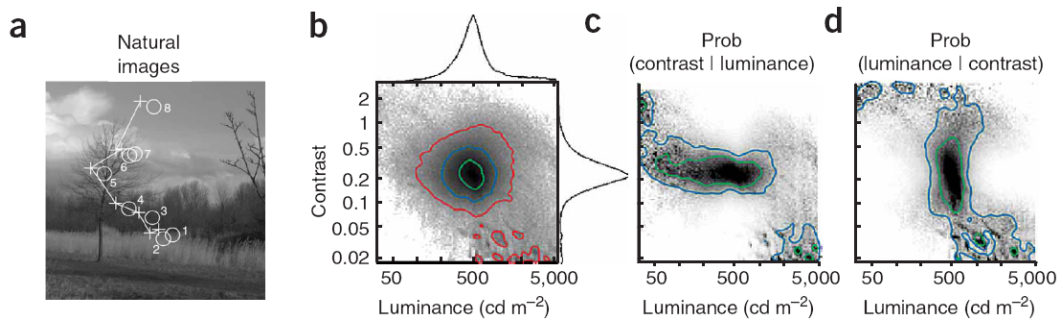

Figure 3.38: *Luminance and contrast have independent statistics in natural images.* The statistical distribution of luminance and contrast across small image patches from natural scenes (*a*) reveals a factorial distribution (*b*) and thus, statistical independence. This is confirmed by a representation of the conditional distributions $P(\text{cont}|\text{lum})$ (*c*, data from *b* normalized by its projection along vertical slices) and $P(\text{lum}|\text{cont})$ (*d*, data from *b* normalized by its projection along horizontal slices). From Mante *et al.* 05 [89].

5.2.1 Contrast, and the statistics of natural images

Contrast. The precise definition for the 'contrast' of a stimulus is variable. The underlying idea, though, is always the same: The 'contrast' seen by a cell located at (x_0, y_0) on the retina is derived from the values of

$$c(x, y, t) = \frac{|I(x, y, t) - \widehat{I}|}{\widehat{I}}, \tag{3.14}$$

where (x, y) belongs to some neighborhood of (x_0, y_0) (typically, the cell's receptive field), $I(x, y, t)$ is the instantaneous luminance at point (x, y) and time t, and $\widehat{I}$ is some 'average' value for luminance in the sequence, generally defined as a spatial and/or temporal linear average. Generally also, the 'contrast' seen by the cell is defined as an average, spatial and/or temporal, for $c(x, y, t)$ over the simulation. We refer to Shapley and Enroth-Cugell 84 [136] for more rigorous definitions (Rayleigh contrast, Michelson contrast).

Contrast, luminance, and retinal responses. The level of contrast is an easy measure to define in artificial images such as drifting grating (amplitude of the sinus divided by the mean luminance), moving bars (difference of intensity between bar and background, divided by background intensity), etc.

In natural images and sequences, by opposition, contrast is not a global feature anymore, but rather a local value depending on which part of the image/sequence is considered. Mante *et al.* 05 [89] have recently led a study on the statistics of luminance and contrast in randomly chosen patches of natural images (Figure 3.38). They found that the distributions of contrast and luminance are generally *independent*, whatever the nature of the observed natural scene (clouds, forest, etc.).

In parallel, Mante *et al.* 05 [89] have recorded the responses of ganglion cells to these various patches of images. Interestingly, they found that retinal responses are well explained by a model with two *independent* stages of gain control: The first providing only independence to luminance, and the second only to contrast. So, retinal processing apparently 'sticks' to the independence of luminance and contrast in natural scenes. These results suggest that invariances to luminance and contrast are provided by distinct stages of retinal processing, as it has long been suspected from physiological observations: Adaptation to luminance is supposed to occur mostly in receptors and horizontal cells, while adaptation to contrast occurs in bipolar cells and on (see the next sections).

In the scope of our model, the results of Mante *et al.* –regardless of necessary experimental limitations on their reach– confirm that even in a simulator bound to function on normalized digital sequences (thus greatly removing issues of luminance adaptation), a nonlinear stage of contrast adaptation is still mandatory to produce correct magnitudes for the responses of the modeled cells.

In the rest of this section, we further characterize the expression of contrast gain control and its possible perceptual consequences, through the presentation of fundamental experimental results.

5.2.2 Multi-sinus experiments

We start by presenting the Shapley and Victor 78 [137] multi-sinus experiments, which gave the first quantitative measures of contrast gain control in the retina. These experiments were pursued on an ON-center cat X cell. Input stimulus $L(x, y, t)$ was a static grating of fixed mean luminance $\bar{L} = 20$ cd/m^2, temporally modulated by a sum of sinusoids with adjustable contrasts:

$$L(x, y, t) = \bar{L} \left(1 + \ \mathrm{Gr}(x, y) \sum_{i=1}^{8} c_i \sin(\xi_i t) \right), \tag{3.15}$$

where $\mathrm{Gr}(x, y)$ is a sinusoidal grating function with normalized amplitude (between -1 and 1). The ξ_i are a set of eight temporal frequencies that logarithmically span the frequency range from about 0.2 Hz to 32 Hz, respectively associated to contrast strengths c_i.

Recordings were made for different distributions of the c_i. For each recording, the cell's output firing rate was Fourier-analyzed at each of the input frequencies ξ_i, thus yielding a set of eight amplitudes and eight phases. This set provided a measure for the linear kernel (first-order Wiener kernel) that best fits the cell's response, *in the given contrast conditions*.

Influence of the mean level of contrast

This first experiment measures how the mean level of contrast changes the best-fitting first-order Wiener kernel for the cell. The c_i are all fixed at the same value $c_i = c$, global level of contrast for the stimulus. The experiment is repeated for four values of contrast, c being doubled each time.

Remark: When $\forall i,\ c_i = c$, the temporal part of signal (3.15) is related to a *pink noise* stimulus (with similar power in each frequency octave, so that for a 1D signal the power spectrum is $\sim |\xi|^{-1}$). Indeed, the power spectrum of (3.15) is uniformly distributed in logarithmic scale, just like pink noise. However, the spectrum of

(3.15) is concentrated on eight discrete values, unlike a real pink noise. The 'pink' spectrum plays a privileged role in natural stimuli (for example, *spatially*, natural images have similar power in each octave (Field 87 [53]). ■

The resulting amplitude and phase diagrams for the cell's output, represented in Figure 3.39-*A* and *B*, reveal deviations from linearity: If the ganglion cell responded linearly to its input, the modulations in its response would simply be proportional to c. Successive amplitude curves in Figure 3.39-*A* would be parallel, spaced by $\log(2)$ as contrast is doubled, and all phase curves in Figure 3.39-*B* would superimpose, since the phase portrait depends only on the nature of the linear filter.

Instead, the cell responds under-linearly to contrast at low temporal frequencies, where successive amplitude curves are spaced by less than $\log(2)$. In the phase portrait, strong contrasts induce a phase-advance of the response (phase curve shifted upwards), meaning that the cell responds *faster* at high contrasts. As resulting from these experiments, contrast gain control is thus characterized by the double behavior:

- Amplitude compression at low frequencies,
- Phase advance with increasing contrasts.

The authors found the two phenomena to be highly correlated in their experiments, probably resulting from a common mechanism. In our model (Wohrer 08 [163], Chapter 4), wetake both phenomena into account in the simplest of ways, through a variable resistance in an 'RC' circuit.

The basic role of contrast gain control is obviously to limit the response of the system at high input contrasts, thus avoiding saturation at high contrasts, and providing a relative enhancement of small contrast stimuli. However, behind this simplified formulation, it is not so clear how the physiological measurements of contrast gain control are reflected in functional and perceptual effects. The issue is presented in more details in Section 5.2.5.

Frequencies that induce contrast gain control

For the moment, we present a second experiment that was crafted by the authors [137] to further investigate the origin of the gain control mechanism. It reveals that the contrast gain control mechanism is preferentially triggered by stimuli with fast temporal variations, in the range of $3 - 10$ Hz. It thus constrains models that can be used to reproduce the effect.

Each input frequency ξ_{i_0} is successively chosen as a 'carrier' frequency with $c_{i_0} = 0.2$, while the other frequencies are added as perturbation terms: $c_i = 0.0125$ for $i \neq i_0$ (see equation (3.15)). Results are compared to a 'low contrast' test condition where $c_i = 0.0125$ for all i.

For each carrier frequency ξ_{i_0} three phase advance indicators $\phi_5(\xi_{i_0})$, $\phi_6(\xi_{i_0})$ and $\phi_7(\xi_{i_0})$ are measured, respectively associated to *assay frequencies* $\xi_5 = 3.9$ Hz, $\xi_6 = 7.8$ Hz and $\xi_7 = 15.6$ Hz. $\phi_5(\xi_{i_0})$ is obtained by measuring output phase at the assay frequency ξ_5 when ξ_{i_0} is the carrier frequency, and subtracting the output phase at ξ_5 in the low-contrast test condition; similarly for $\phi_6(\xi_{i_0})$ and $\phi_7(\xi_{i_0})$.

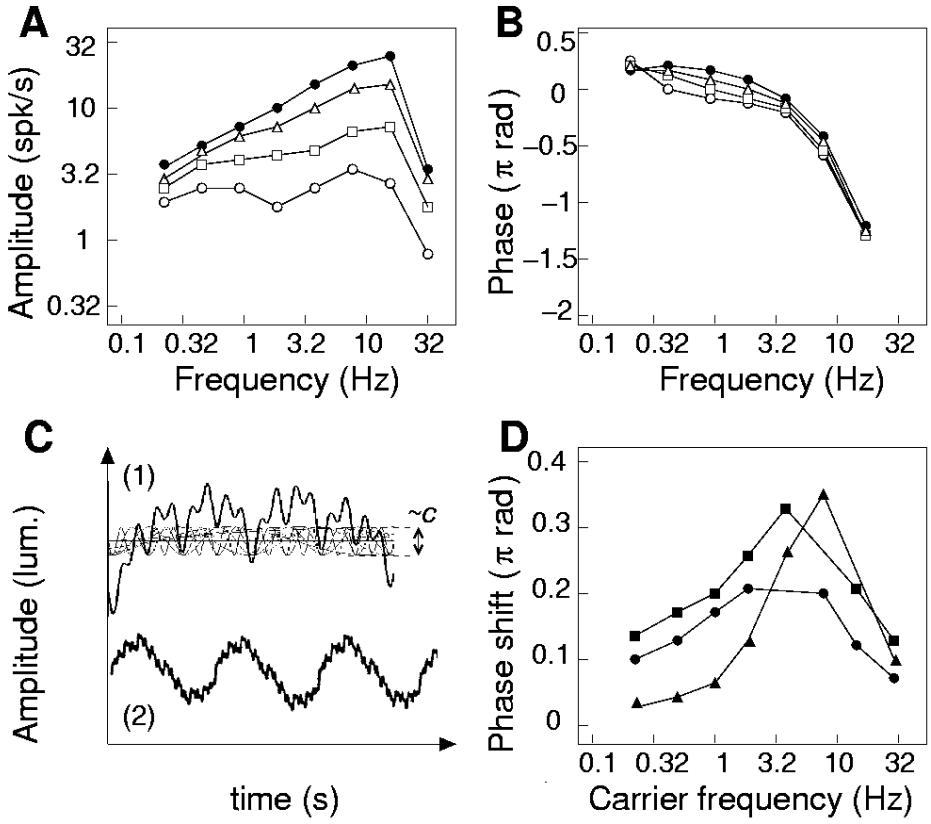

Figure 3.39: *Contrast gain control in a cat ON-center X ganglion cell. A and B*: Response to multi-sinus stimuli of different contrasts c (sample input signal depicted in panel *C*-1). Amplitude curves (*A*) reveal under-linearity at low temporal frequencies. Phase curves (*B*) reveal time advance for high contrasts (see text). Successively, c was 0.0125 (white circles), 0.025 (□), 0.05 (△) and 0.1 (filled circles). *D*: Strength of the gain control effect depends on the dominant frequency ξ_{i_0} present in the input (stimuli with a carrier frequency ξ_{i_0}, as depicted in Panel *C*-2). The three curves represent indicators $\phi_5(\xi_{i_0})$ (filled circles), $\phi_6(\xi_{i_0})$ (■) and $\phi_7(\xi_{i_0})$ (▲) which measure the strength of the gain control (see text). Frequencies that elicit the most gain control are ξ_{i_0} =3–10 Hz. From Shapley and Victor 78 [137].

Since contrast gain control can be measured by a phase advance (previous paragraph), $\phi_5(\xi_{i_0})$, $\phi_6(\xi_{i_0})$ and $\phi_7(\xi_{i_0})$ provide three indicators, hopefully highly correlated, of the strength of the gain control induced by ξ_{i_0}.

Figure 3.39-*D* represents experimental measures for $\phi_5(\xi_{i_0})$, $\phi_6(\xi_{i_0})$ and $\phi_7(\xi_{i_0})$. As predicted, the three indicators are highly correlated, consistently with the global time advance induced by contrast gain control. Phase advance is strongest when the carrier ξ_{i_0} is around $3-10$ Hz. This reveals that the underlying mechanism for the contrast gain control measured here has a 'band-pass' sensitivity, being preferentially triggered by temporal variations around $3-10$ Hz.

Contrast gain control in different types of cells

Retinal cells in most species are subject to contrast gain control. Shapley and Victor 78 [137] measured the effect in both X and Y cat cells (but stronger in Y cells), and measurements in salamander cells (next section) also reveal contrast gain control in different subtypes of cells, although with certain asymmetries, e.g., between ON and OFF cells (Chichilnisky and Kalmar 03 [26], and next section).

However, a notable exception seems to be the case of primate midget cells, which have been reported to display little contrast adaptation (Bernadete *et al.* 92 [11]).

5.2.3 Contrast gain control and LN analysis

Let us now present more recent experiments, which have provided new insights on the nature of contrast gain control. A good number of these experiments (plus the Mante *et al.* 05 [89] experiment presented in Section 5.2.1) are based the application of LN analysis to a cell at different levels of contrast, to measure contrast-related changes in the LN structure.

'Fast' and 'slow' contrast adaptations

Two independent experiments (Kim and Rieke 01 [81], Baccus and Meister 02 [4]) have recently revealed that different (at least two) mechanisms contribute to contrast adaptation in ganglion cells. More precisely, a distinction can be made between 'fast' and 'slow' adaptations to contrast.

The experiment reproduced here (Figure 3.40) is that of Baccus and Meister 02 [4]. They exposed salamander ganglion cells to alternative epochs of high and low contrast white noise stimulus (one 'adaptation epoch' is represented in Figure 3.40-*A* – note the beginning of a new epoch at the far right), and performed LN analysis on a few seconds' periods of firing for the cell, at different instants during the adaptation epoch (Figure 3.40-*A*, bottom). First, LN analysis could be performed on the cell whether during high (H) or low (L) contrast stimulation. Second, the period used for analysis could either be at the *beginning* of a new contrast epoch (periods noted $H_{\rm early}$ and $L_{\rm early}$), or at the *end* ($H_{\rm late}$ and $L_{\rm late}$).

The resulting analysis was performed for different cells throughout the whole retinal pathway. Here, we only show results of LN analysis obtained from ganglion cells' firing rates (Figure 3.40-*B*) and intracellular potentials (Figure 3.40-*C*). They reveal two distinct components of adaptation.

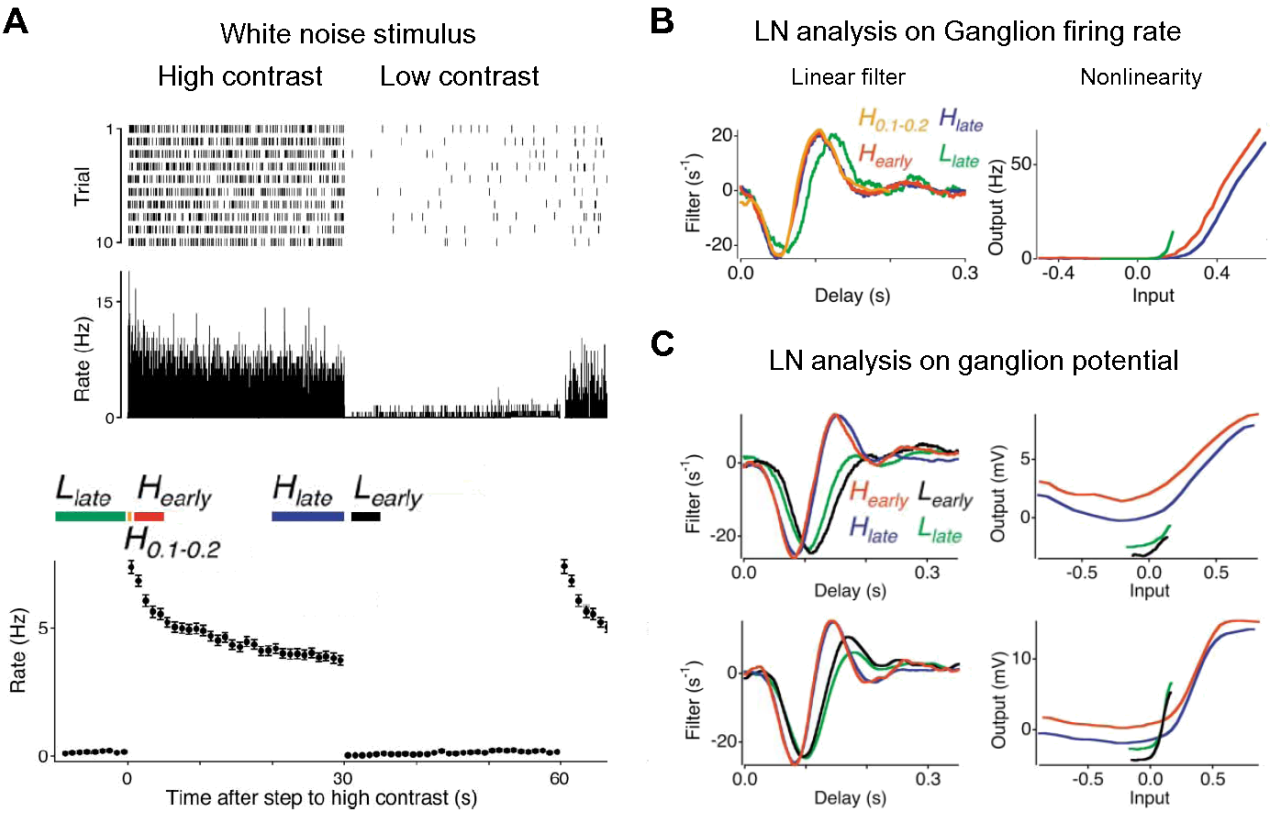

Figure 3.40: *'Fast' and 'slow' contrast adaptation in the salamander retina.* When a cell undergoes an alternation of high and low contrast epochs, its filtering properties continuously change, as measured from LN analysis performed at different instants of the cycle (Panel *A*, see text). The LN results (Panels *B* and *C*) reveal two speeds of adaptation. 'Fast' adaptation lowers the amplification gain of the cell (smaller slope in the 'Nonlinearity' panels) and speeds up filtering (time advance in the 'Linear filter' panels), in a few hundreds of milliseconds. 'Slow' adaptation progressively shifts the cells' baseline potential downwards, over several tens of seconds, as reflected in the 'Nonlinearity' panels.

'Fast' component. The strong difference in LN characteristics for the cell between periods right before and after a change of contrast ($L_{\rm late}$ to $H_{\rm early}$, and $H_{\rm late}$ to $L_{\rm early}$) reveals a 'fast' component of contrast adaptation. It is characterized by a double impact on the LN characteristics for the cell:

1. A reduction of the filtering gain at high contrasts, as measured by the lowered slope of the LN static nonlinearity in the 'H' modalities as compared to the 'L' modalities (Figure 3.40-*B*, 'Nonlinearity' panel).

2. A reduction of the time scale of filtering at high contrasts, as measured by the time advance of the best-fitting LN linear filter between the 'H' and 'L' modalities (Figure 3.40-*B*, 'Linear filter' panel).

These two effects precisely correspond to the dual mark of contrast gain control, as measured by Shapley and Victor 78 in their original experiments (Section 5.2.2).

Further evidence for the speed of apparition of the fast gain control is provided by the response of the cells during the 100-200 ms period right after onset of the high contrast (period noted $H_{0.1-0.2}$ in Figure 3.40): The best-fitting linear filter is already characteristic of 'high' rather than 'low' contrast behavior (Figure 3.40-*B*, 'Linear filter' panel).

'Slow' component. By opposition, a more subtle change occurs between the beginning and end of an epoch of same contrast ($H_{\rm early}$ to $H_{\rm late}$, and $L_{\rm early}$ to $L_{\rm late}$), revealing a 'slow' component of contrast adaptation. The main expression of the slow adaptation is a progressive downwards shift of the LN static nonlinearity between beginning and end of the epoch, which can be observed both at the level of firing rates (Figure 3.40-*B*, 'Nonlinearity' panel) and of intracellular potentials (Figure 3.40-*C*, 'Nonlinearity' panel). The downwards shift suggests an effect intrinsic to the spiking ganglion cell, such as the opening of specific conductances that would shift the cell's baseline potential downwards.

Biological origins of fast and slow gain controls

Another study in salamander cells was pursued in parallel by Kim and Rieke 01 [81, 122], which has led to similar conclusions as the study of Baccus and Meister 02 (preceding paragraph). Furthermore, thanks to comparative study of the effect in ganglion cells (Kim and Rieke 01 [81]) and bipolar cells (Rieke 01 [122]), their study provided supplementary insights on the biological origins of gain controls.

We here review their results, and those from previous work, which have started to clarify the underlying mechanisms of contrast adaptation in bipolar and ganglion cells.

Fast adaptation in bipolar cells. Interestingly, fast contrast adaptation is already observed to a large extent in bipolar cells (Mao *et al.* 98 [90], Shiells and Falk 99 [141], Nawy 00 [102], Rieke 01 [122]), whereas it is absent from the previous layers of cells (receptors and horizontal, Rieke 01 [122], Baccus and Meister 02 [4]).

However, the origin of the gain control in bipolar cells is still controversial. Here are the main possible hypothesis, and how they have been infirmed / confirmed by recent experiment:

- *Feedback inhibition from amacrine cells* has been the 'historical' claim. However, this hypothesis has been infirmed by recent studies (Rieke 01 [122], and also Beaudoin *et al.* 07 [8] in mammalian retina), as contrast gain control is still observed under blockade of all amacrine synapses.

- *Voltage-gated conductances* can easily account for the time advance and gain reduction typical of contrast gain control. Mao *et al.* 98 [90] found that current injected into salamander bipolar cells could elicit contrast gain control depending on the strength of the average input current, and that adaptation was eliminated after blockade of a potassium current, suggesting that the adaptation might be elicited by voltage-gated potassium (inhibitory) currents. On the other hand, Rieke *et al.* 01 [122] found no effects of voltage nor current clamps on the adaptation properties of the cells, in contradiction with a voltage-dependent origin for the adaptation. In the end, the role of voltage-gated conductances remains controversial.

- *Calcium adaptation in bipolar dendrites* has been observed as another plausible candidate. In ON salamander bipolar cells, Nawy 00 [102] found that contrast adaptation in bipolar cells is associated to a rise in intracellular $[Ca^{2+}]$, and that the adaptation was largely suppressed when Calcium was buffered from the intracellular medium[24] (see also Shiells and Falk 99 [141]). Oddly, still in the salamander, Rieke 01 [122] also found that calcium buffering affected adaptation in bipolar cells, but rather in OFF type than ON type. Anyway, it seems likely that calcium plays a crucial role in contrast adaptation.

- *Feedforward control from horizontal cells* has sometimes been hypothesized. However, Rieke 01 [122] demonstrated that contrast gain control persists in bipolar under blockade of horizontal cells.

- The fast *desensitization/recovery* of bipolar cell AMPA receptors at the cone synapses (De Vries 00, Section 2.4) is also an intrinsically nonlinear phenomenon. Its modalities should be studied in more detail to investigate its possible role in contrast gain control.

Slow adaptation in ganglion cells. By opposition, the 'slow' adaptation effect seems rather weak in bipolar cells (Rieke 01 [122]), although some slow changes have also been reported (Baccus and Meister 02 [4]).

Rather, slow adaptation seems to be particularly strong at the level of the ganglion cells themselves. Kim and Rieke 01 [81] have suggested that spike-frequency adaptation (inhibitory conductance which slowly builds up with repeated spikes) may be largely responsible for the process. In their proposed scheme, bipolar cells would account for most of the fast adaptation, and ganglion cells for most of the slow adaptation.

[24] This observation may recall calcium adaptation in photoreceptors. In fact, the whole scheme of activation of ON bipolar cells through the metabotropic receptor mGluR6 and a messenger G protein – as imposed to produce a hyperpolarization in response to the excitatory transmitter glutamate (Section 2.1) – is strikingly similar to that occurring in phototransduction (1.1).

Undoubtedly, the arousal of contrast adaptation is not a closed subject yet, especially in bipolar cells, for which experimental data is still relatively rare.

5.2.4 Modeling contrast gain control

Many models of temporal contrast gain control rely on the original ideas introduced by Shapley and Victor 81 [138] (general form for linear temporal filtering in ganglion cells) and Victor 87 [159] ('neural measure of contrast' applied as feedback). We present their model in a 'general' form, and some of its subsequent applications / simplifications in other model.

The Shapley and Victor 81 model

In Shapley and Victor 81 [138], the authors proposed a general form for temporal linear filtering in ganglion cells, from input signal $X(t)$ to output signal $Y(t)$. This filter involves a cascade of low-pass filters followed by a single high-pass stage. In our terminology for linear filters introduced in Chapter 2, Section 3, the general form writes:

$$Y(t) = A\, T_{w_H,\tau_H} * E_{n_L,\tau_L} * X\ (t). \tag{3.16}$$

Shapley and Victor 81 [138] fitted the parameters of this formula to reproduce the response curves of ganglion cells at different contrasts (as in Figure 3.39 *A-B*). However, they did not provide equations to link the various parameters to the levels of contrast, so that (3.16) was used only in a descriptive, not predictive, fashion.

The Victor 87 model

In Victor 87 [159], the author proposed an enhancement of (3.16) allowing to reproduce the curves at different contrasts from a single set of parameters (Figure 3.41-*A*). Naturally, some dynamic non-linearity must be introduced in the system to reproduce the nonlinear responses of Figure 3.39 *A-B*. The 'minimal' solution proposed by Victor, in order to reproduce the responses of X cell *center* signals, is to make the high-pass time constant τ_H in (3.16) a dynamic value of the cell's own recent level of response:

$$X_L(t) = E_{n_L,\tau_L} * X\ (t), \tag{3.17}$$

$$\tau_H(t)\frac{dY}{dt} = \tau_H(t)\frac{dX_L}{dt} + (1 - w_H)X_L(t) - Y(t), \tag{3.18}$$

where $\tau_H(t)$ is now an instantaneous time constant, whose value is determined by the recent values of contrast, as measured from the cell's own recent activity $Y(t)$:

$$c(t) = E_{\tau_C} * |Y|\ (t), \tag{3.19}$$

$$\tau_H(t) = \tau_H^0 \frac{c_{1/2}}{c_{1/2} + c(t)}. \tag{3.20}$$

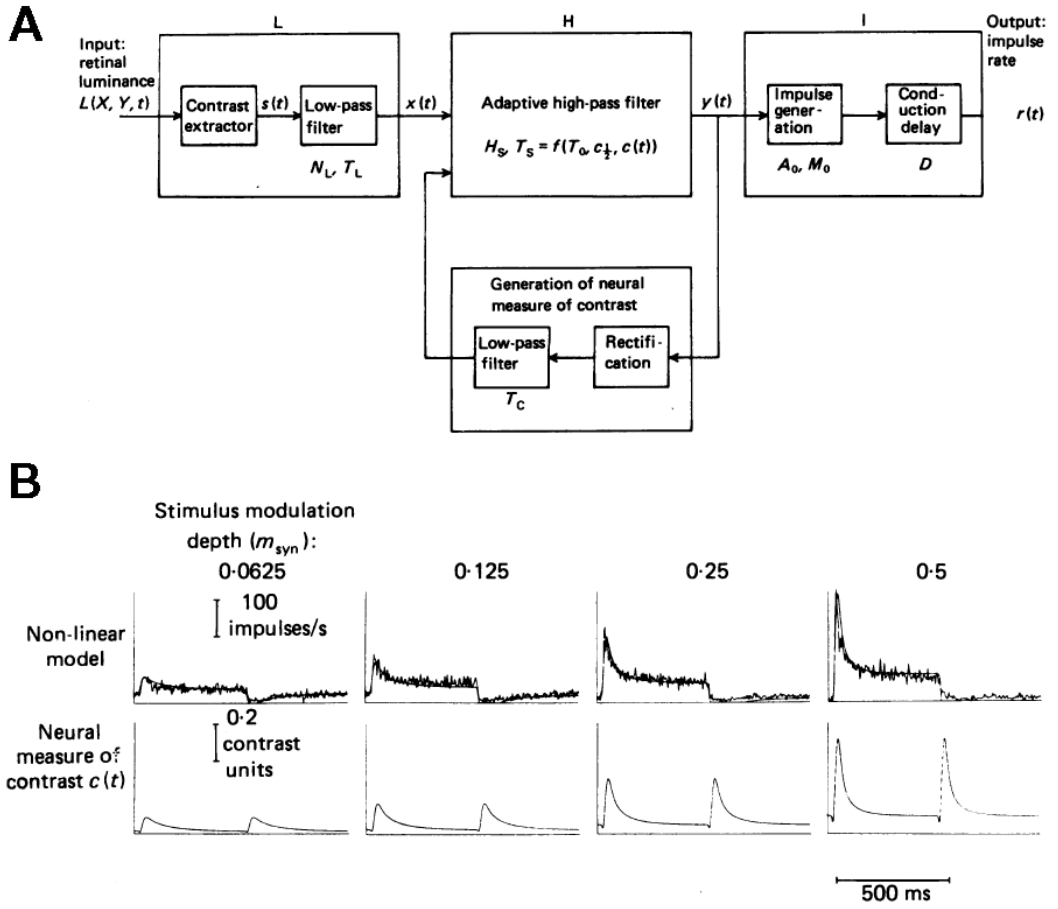

Figure 3.41: *The Victor 87 model for temporal gain control. A:* Schematic representation of the model. After a traditional stage of low-pass linear filtering (box L), a high-pass stage is added (box H), whose instantaneous time constant $\tau_H(t)$ depends on the recent values of contrast, as measured by feedback from the cell's own recent levels of response. *B:* The model successfully reproduces the progressive shortening of real cells' response time, in response to grating reversals of increasing contrasts. The 'neural measure of contrast' $c(t)$ is derived from the cell's own recent levels of activity, positive or negative (typically, with time constant τ_C=15 ms). From Victor 87 [159].

Note that (3.18) is directly linked to filter T_{w_H,τ_H} in the linear system (3.16). If τ_H was constant, (3.18) would simply be the linear ODE implementing convolution by T_{w_H,τ_H} (see Chapter 2, Section 3). Here, the ODE formulation allows extension to the nonlinear case where $\tau_H(t)$ depends on the current estimation of contrast $c(t)$ (3.20), as measured by an average (3.19) of $|Y(t)|$ over recent time, with time constant τ_C (typically small, around 15 ms).

Finally, the cells' response (firing rate) is derived from $Y(t)$ through amplification, rectification, etc. (Figure 3.41-*A*).

The Victor model performs well on reproducing responses of an X cell to grating reversals at different contrasts, including the progressive speeding-up of the transient as contrasts get higher (Figure 3.41-*B*).

Derived and alternative models

Feedback measure of contrast. A strong idea of the Victor 87 model was to introduce contrast gain control thanks to a feedback derived from the cell's own recent levels of activity. Several models of gain control have been built on the same principle: See e.g. the Y cell model of Enroth-Cugell and Freeman 87 [47], or the Van Hateren *et al.* 02 model for primate Parasol cells [154].

Explicit dependence of filtering gain. In the original model of Victor 87, the contrast gain control mechanism only acts on the temporal scale τ_H of the high-pass stage: Contrast does not explicitly modify the *gain* of filtering, as defined by A in (3.16). In fact, such a dependence of A is not mandatory for the Victor model to reproduce frequency kernels as in Figure 3.39 *A*-*B*, because the cut-off frequency τ_H^{-1} of the high-pass stage augments with input contrast, strongly 'cutting off' low temporal frequencies only in the case of high input contrasts.

However, an explicit dependence of A on input contrast is more intuitive, and often convenient for modelers. Some models explicitly add a control on A, based on recent values for the cells' activity (Van Hateren *et al.* 02 [154]). Finally, some modelers totally forget the dependence of the time scale τ_H on contrast (possibly even, forget the totality of the high-pass stage), and simply implement a feedback control on A. This is for example the case of the gain control model in Figure 3.42.

Varying resistance in an RC model. In an old model for light adaptation in horseshoe crab photoreceptors, Fuortes and Hodgkin 64 [57] proposed that both time advance and gain reduction (which are linearly anti-correlated during light adaptation) could arise from a simple extension of a first-order RC equation, but with an adaptable resistance. This gives, in reduced units:

$$\frac{dY}{dt} = X(t) - Y(t)/\tau_L(t), \tag{3.21}$$

where $\tau_L(t)$ (obtained as $\tau_L(t) = R(t)C$) is a function of recent illumination levels (model reviewed in Enroth-Cugell and Shapley 84 [136]).

If τ_L remained constant, (3.21) would be the ODE expression of convolution by $\tau_L^{-1} E_{\tau_L}$ (Chapter 2, Section 3). It is thus the direct extension of a low-pass filter. Such a scheme is likely the simplest implementation allowing to reproduce the dual mark of contrast gain control: Gain reduction (because of the multiplication by τ_L^{-1}) and phase advance for high contrasts.

In our model (Wohrer 08 [163], Chapter 4, Section 4), this is the implementation retained to account for contrast gain control. Its simplicity allows to rigorously track some of its mathematical properties (Wohrer 08 [163], Chapter 5). However, such a scheme cannot by itself account for the high-pass behavior observed in Figure 3.39-*A*. It must thus be included in a broader model of retinal processing (see Wohrer 08 [163]).

5.2.5 Perceptual impact of contrast adaptation

To conclude this presentation of contrast gain control, we question its possible functional, and even perceptual, roles. The first obvious answer is that it avoids saturation of bipolar and ganglion cells in response to high contrast stimuli. Or, put in another way, that it allows to enhance the response to low contrasts, relatively to the response to high contrasts.

However, characterizing with more precision the perceptual effects of the mechanism is not evident, because the strength of contrast gain control apparently depends strongly not only on 'contrast' (a rather vague definition, see Section 5.2.1), but more precisely on the temporal (and possibly, spatial) composition of the input stimulus. As a single example, we refer to the various strengths of contrast gain control observed according to the dominant temporal frequency in the input (Figure 3.39-*D*).

Global repartition of contrast levels in the retinal image. In our model (Wohrer 08 [163], Chapter 4, Section 7.2.2), we study the possible impacts of the gain control mechanism on the global repartition of contrasts in the output retinal image, especially when the local measure of contrast (function $c(t)$, eq. (3.19), in Victor's model) is allowed to operate with a spatial extent.

These results suggest that contrast gain control may help to locally equalize the levels of contrast in the retinal output 'image', an effect which reminds some classical techniques in image processing.

Enhancement of moving object's leading edges. However, the strongest presumed perceptual role for contrast gain control, supported by recent experimental data, is to allow enhancement of the leading edges of moving objects. This work of Berry *et al.* 99 [12] in the salamander retina is illustrated in Figure 3.42. For a moving bar of high contrasts, the lateral profile of activation for the cells is typically displaced towards the bar's leading edge, at odds with the simple output of a linear filter (whose normalized profile is represented a single time, in gray).

This effect can be explained by a simple model of temporal contrast gain control, implemented by a varying gain G on the response of the cells. In this simple model, when cells at the leading edge are first reached by the advancing bar, they are adapted to the background's low contrast, and thus respond with a high gain. As the bar advances over the cell, contrast gain control sets in, contributing to lower the response of cells once the leading edge has passed.

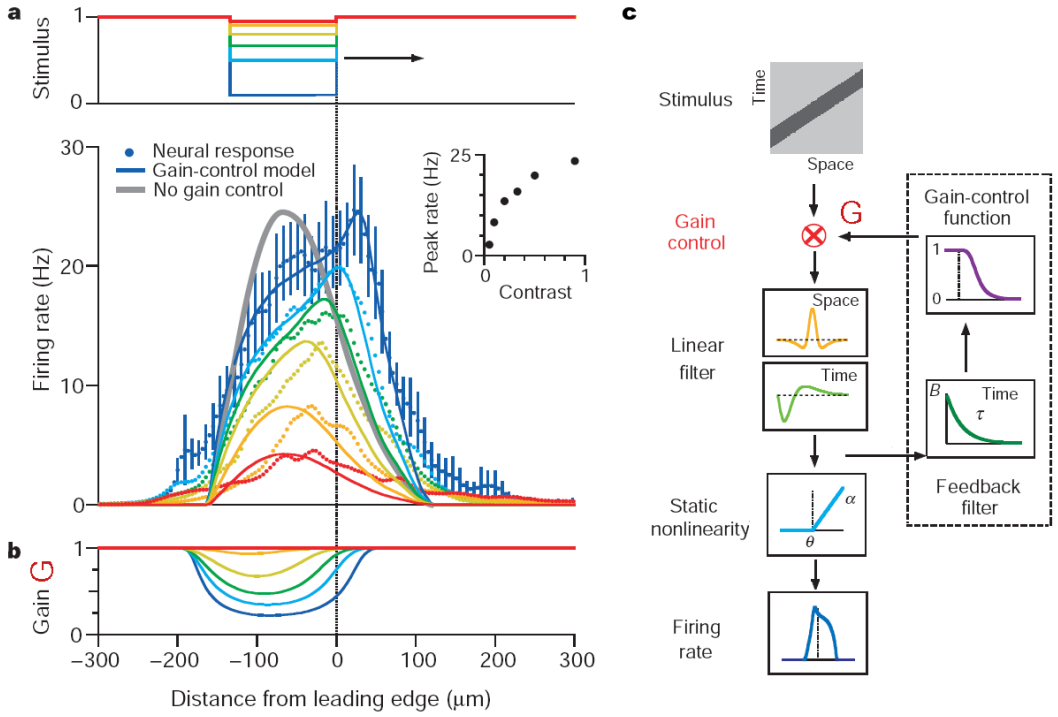

Figure 3.42: *The leading edges of a moving bar are enhanced at high contrast. a:* In response to a drifting bar (width 133 μm, speed $0,44$ mm s^{-1}) at different contrasts, salamander ganglion cells progressively shift from a 'linear' response profile at low contrasts, with the peak lagging behind the bar's leading edge, to an 'enhanced' profile at high contrasts, with the peak lying ahead of the bar's leading edge. *b* and *c*: A simple model of contrast gain control, where the cell's gain $G(t)$ is driven by a dynamic feedback (Panel *c*), is sufficient to account for the effect (Panel *a*, plain curves). The corresponding profile for $G(t)$ in given in Panel *b*. From Berry *et al.* 99 [12].

This effect might be an important perceptual role of contrast adaptation. Indeed, mammalian 'Y-like' cells, the presumed movement detectors, are the cells which are most subject to contrast gain control (Section 5.2.2, Paragraph "Contrast gain control in different types of cells").

5.3 Slow adaptation and predictive coding

We have seen in the preceding sections that both adaptations to luminance and contrast presented at the same time fast and slow components. We argued that fast adaptations likely have a fundamental role in avoiding system saturation. The slow adaptations, conversely, seem to be precision mechanisms allowing to *optimize* the retinal response to its current type of stimulus, following different possible criteria.

Possibly, the optimizations provided by slow adaptation mechanisms serve an *economical* purpose, such as limiting the amount of fired spikes in response to strong stimulations, static stimuli, etc.

More precisely, it has been suggested that slow adaptation may help to optimize the *information transfer* in the retina, an idea obviously linked to the economical optimization mentioned above, since each fired spike provides additional information to the brain, but costs some energy to the cell.

The sort of coding schemes allowing the retina to optimize its information transfer are often referred to as examples of *predictive coding*. This denomination, somewhat frightening, comes from the fact that generally speaking, each cell should 'remove' from its response the part which can be *predicted* from the responses of its neighbors, in order to optimize independence of the various sources and thus, the output information rates.

We finish this presentation of nonlinear adaptations by two accounts of slow adaptation phenomena, which can be interpreted in terms of predictive coding.

5.3.1 Adaptation of spatial receptive fields to background luminance

Modulatory changes in the spatial structure of the retina. A particularly interesting slow modulatory effect is the dynamic change in the spatial structures of receptive fields for different levels of background illumination. Figure 3.43-*A* depicts the sensitivity of ganglion cells (inverse of the threshold contrast detectable by the cell) at different background intensities. At low illuminations, the sensitivity to contrast of the retina is globally diminished. Furthermore, the spatial cut-off frequency is lower for low illuminations, and there is no band-pass behavior anymore. All these observations can be resumed by saying that filtering in the retina becomes *more low pass spatially* under low illumination.

In fact, correlates to these physiological effects have been found anatomically, and appear particularly linked to the effects of dopamine. Dopamine is a neuromodulator of crucial importance in the brain. In the retina, it is believed to be released by specific *dopaminergic* amacrine cells, possibly directly in the extracellular medium, without the need for synapses[25]. Importantly, dopamine is released in the presence of light. It has several modulatory effects at different stages of retinal processing. In particular, it is known to *uncouple* cells linked by gap junctions: Horizontal cells

[25]For references, we refer to the Webvision page http://webvision.med.utah.edu/amacrines3.html#A18

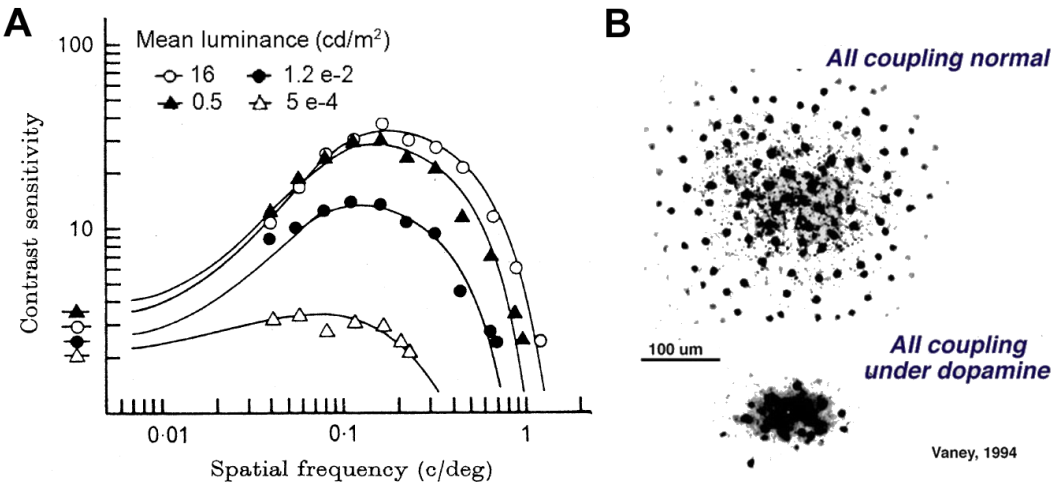

Figure 3.43: *Adaptation of retinal spatial filtering to background illumination. A:* The response (sensitivity) curves of ganglion cells become relatively more low-pass spatially at low illuminations, implying that spatial couplings likely become stronger at low illuminations (see text). From Enroth-Cugell and Robson 66 [48]. *B:* The modulatory effects of dopamine have been found to reduce the amount of gap junction spatial coupling, in various retinal cells, at high illuminations. From Vaney 94.

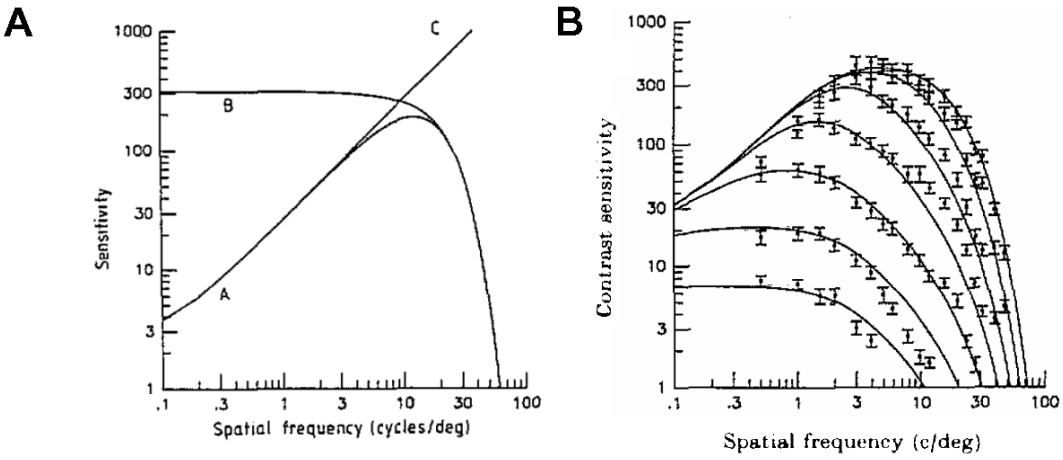

Figure 3.44: *Adaptation to background illumination and the decorrelation hypothesis. A:* Modeling by Atick 92 [3] of the trade-off between optimal decorrelation of ganglion cells' signals (high-pass filter 'C') and noise removal based on pooling from neighboring receptors (low-pass filter 'B'). The optimal filter 'A' is influenced by both behaviors. *B:* The formalism of Atick 92 [3] allows to find back the change of shape of real cells' sensitivity curves. Original data are psychophysical measures from Van Nes *et al.* 67 [157]. Background intensities range from 9.10^{-4} to 900 photopic td, each time multiplied by 10.

and various amacrine cells (such as the rod system's AII amacrine cell, Figure 3.43-*B*). As a result, dopamine contributes to make receptive fields smaller at high illuminations, with the likely physiological correlates of Figure 3.43-*A*.

Predictive coding. Interestingly, theoretical considerations (Srinivasan *et al.* 82 [144], Atick 92 [3]) allow to interpret illumination-related changes in spatial receptive fields. Both pieces of work have somewhat different formalisms, but the same underlying idea: To optimize information transmission in the presence of noise, ganglion cell receptive fields implement a trade-off between noise removal and statistical decorrelation of neighboring cells' outputs. More precisely:

1. To optimize *statistical independence* with their neighbors (and thus optimize information transmission, Atick 92 [3]), ganglion cells tend to perform a spatial opposition between their 'direct' signal and some neighborhood signal. Because of the typical amplitude spectrum of natural images ($\sim 1/|f|$, Field 87 [53]), the optimal decorrelating filter has a Fourier transform proportional to $|f|$ (line 'C' in Figure 3.44-*A*)(Atick 92 [3]). This sort of filter requires to use an 'infinitely small' neighborhood to perform the spatial opposition.

2. By opposition, to optimize *noise reduction*, the cells must proceed to spatial pooling over a *finite* neighborhood, whose extent depends on the typical length of spatial correlations in the

noiseless input image, and on the signal-to-noise (SNR) ratio in the real, noisy image. The resulting pooled signal can be viewed as the best prediction by the cell of its own value, based on the values of its neighbors (Srinivasan *et al.* 82 [144]). In Atick's formalism, this 'optimal noise reduction pooling' is modeled as a low-pass filter (line 'B' in Figure 3.44-*A*), whose cut-off frequency depends on the SNR in the input image.

In the Fourier domain, the optimal retinal filter must then achieve a trade-off between decorrelation and noise removal. In Figure 3.44-*A*, Atick's optimal filter (line A) is thus constructed from the two preceding filters B and C.

Interestingly, the mean illumination I_0 of a scene has a profound influence on the SNR ratio. Indeed, the input of retinal processing, the photocurrent, is subject to an intrinsic 'phototransduction noise', with an incompressible background level (the 'dark noise') that does not scale with I_0. So, the SNR in the photocurrent becomes significantly lower (more noise) at low illuminations. According to the preceding argumentation (point 2), this implies that spatial poolings must get larger at low illuminations.

Conversely, the value of I_0 does not change the nature of spatial correlations in an image (simply, the whole autocorrelation function is multiplied by I_0^2).

Figure 3.44 presents the formalization of these issues by Atick 92 [3], and an application to the reproduction of retinal sensitivity curves from the psychophysical literature. Because SNR changes, the pooling for optimal noise removal becomes more low-pass, following the same trend as real retinal processing (Figure 3.44 -*B*).

This is a very interesting result linking retinal physiology to advanced functional interpretations.

5.3.2 Predictive coding of spatio-temporal correlations in the stimulus

Recent work by Hosoya *et al.* 05 [70] has suggested that cells in the retina are even capable of adapting their receptive fields in response to much more complex spatio-temporal correlations in their input. An example of their results is presented in Figure 3.45. When presented with a 'complex' spatial structure (here a checkerboard, but see the whole article) for several seconds, a cell slowly adapts its receptive field to counteract the persistent correlations in the input. The resulting effect in terms of information transmission would be, here also, to increase independence of the responses of neighboring ganglion cells. The authors suggest that short-term synaptic plasticity in the IPL may be involved in this phenomenon.

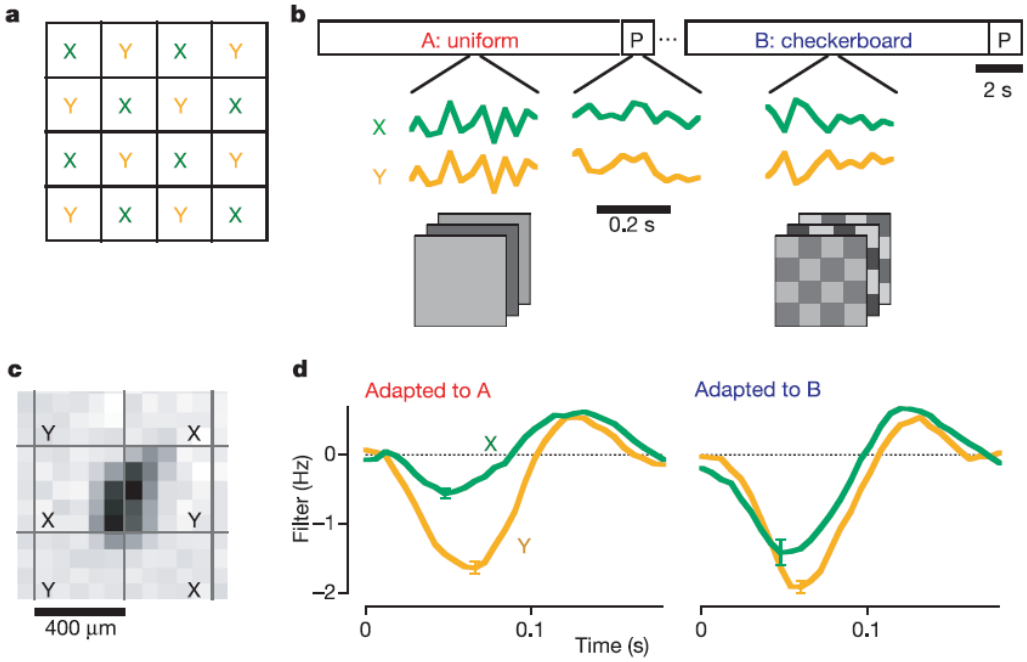

Figure 3.45: *Dynamic adaptation in the salamander retina. a:* Simple stimuli are based on a partition into two regions X and Y of homogeneous luminance, following a checkerboard pattern. *b:* The cell is alternatively adapted to two environments A and B based on white noise. In A, the stimuli for regions X and Y are totally correlated (flickering uniform screen) while in B, regions X and Y are totally anti-correlated (flickering checkerboard). The cell's adapted response to both environments is measured by reverse correlation with an independent probe P, providing a kernel with only two spatial components: Response to X and response to Y. *d:* Adapted to environment A, the cell reveals a kernel with asymmetric weights between zones X and Y. When applied to environment B, this kernel would produce a response strongly biased towards the signal of zone Y. However, slow adaptation to environment B counteracts this bias, by enhancing the gain over zone X. As a result, the cell's response to environment B after adaptation is more centered around zero mean. From Hosoya *et al.* 05 [70]

CONCLUSION

The retina is a complex neural structure, which does not only detect an incoming light signal, but also proceeds to many complex signal transformations. The characteristics of retinal processing have been reviewed extensively in this work: It is a very ordered structure, which proceeds to band-pass spatio-temporal enhancements of the incoming light, along different parallel output pathways with distinct spatio-temporal properties. The spike trains emitted by the retina have a complex statistical structure, such that precise spike timings may play a role in the code conveyed by each ganglion cell, and even more in the code conveyed by a cell population, due to stimulus-driven spike synchronizations. Finally, several mechanisms of gain control, with different time scales, provide a constant adaptation of the retina to the input levels of luminosity and contrast, and even to more complex spatio-temporal correlations in the input.

We believe that several of these features are fundamental for further cortical interpretation, and should be included in the retina models used as input to models of cortical processing. Based on the review herein, we have developped a retina simulator (*Virtual Retina* [164, 163]) which will be useful to cortical modelers, and also to study retinal coding theoretically.

APPENDIX: CONVOLUTION OF EXPONENTIAL FILTERS

In the retina, the transmission of visual signal through multiple layers of cell membranes and through chemical synapses induces a series of low-pass convolutions of the signal with decaying exponential filters. If linear, the related delays can be accounted for through a single filter, resulting from the convolution of many exponential filters, possibly with different characteristic times. This annex proposes a generic approximation for the resulting filter, depending on two time parameters $\tau_{\max}$ and τ_{dec}.

In this annex, we deal with normalized decaying exponential filters:

$$E_\tau(t) = \frac{1}{\tau} \exp\left(-\frac{t}{\tau}\right), \tag{22}$$

as that of Figure 46 (A), and try to calculate or approximate the filter resulting from a cascade of such exponential decays, whose convolution kernel is:

$$F_{\tau_1,\tau_2,\ldots,\tau_N}(t) = E_{\tau_1} * E_{\tau_2} * \cdots * E_{\tau_N} \quad (t), \tag{23}$$

with some of the $\{\tau_n\}$ possibly being equal one to another.

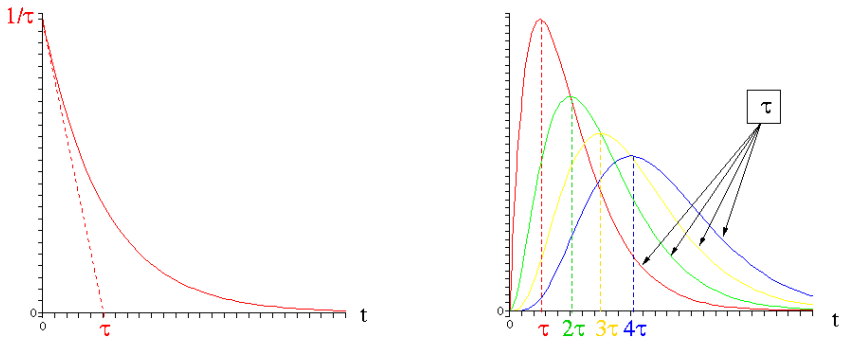

(A) Exponential kernel (B) Self-convolutions of an exponential kernel

Figure 46: An exponential kernel and its four first self-convolutions. All filters decay with the same characteristic time τ. Note that when n self-convolutions occur, the resulting filter peaks at time $n\tau$.

1. Exact calculations

Self-convolution of a filter. From a few algebra, it appears that when one exponential filter is convolved with itself k times, the resulting filter is:

$$F_{\underbrace{\tau,\tau,\ldots,\tau}_{k+1}}(t) = E_{k,\tau}(t) = \frac{t^k}{\tau^{k+1}k!}\exp\left(-\frac{t}{\tau}\right). \tag{24}$$

This function is a positive 'blob' that reaches its maximum value at time $k\tau$ and then decays exponentially with a time constant τ (Figure 46 (B)). Note that (24) for $k = 0$ gives the filter in (22), meaning

$$E_{0,\tau} = E_\tau.$$

Remark: Different notations. As opposed to the body of the thesis, notation $E_{k,\tau}$ here defines the k-fold convolution of filter $E_\tau(t)$, peaking at time $k\tau$. In the body of the thesis, we had defined it as the k-fold convolution of filter $E_{\tau/k}(t)$, peaking at time τ. ■

Convolution of different filters. Another derivable case is when exponential filters with different scales are convolved one to another. If N exponential filters E_{τ_n} are convolved, *with each τ_n being different from all the others*, the resulting filter writes:

$$\begin{aligned} F_{\tau_1,\tau_2,\ldots,\tau_N}(t) \;&=\; \sum_{n=1}^{N} \gamma_n\, E_{\tau_n}(t), \;\; \text{with:} \\ \gamma_n &= \prod_{p\neq n} \frac{\tau_n}{\tau_n - \tau_p}. \end{aligned} \tag{25}$$

This function is also a positive 'blob' (Figure 47), but its peak time is not calculable anymore. Neither is its 'apparent' decay time, as defined by the strength of the decrease after the peak of the filter.

General case. Merging (24) and (25) should lead to a formula for the general case when N different exponential filters E_{τ_n} are convolved, with each filter n being cascaded K_n times. This most general case can be seen as a degenerated limit of (25) when different times get very close one to another. As a result, it also possesses the typical 'blobby' shape (Figure 47). It corresponds to a pondered sum of E_{k,τ_n} filters, with $k \in \{0, K_n\}$, but the corresponding coefficients $\gamma_{n,k}$ do not bear any simple expression anymore.

Calculating the transfer function. An alternative approach is to obtain the transfer function in the Fourier domain. This is straightforward, since convolution in the time domain corresponds to

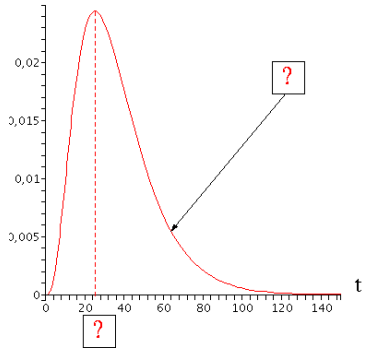

Figure 47: Convolution of exponential kernels with different decay times. Four filters were convolved here, with characteristic times of 5, 6, 10 and 15 ms, which are characteristic times for retinal low-pass filters (see report). Visually, the resulting filter still has typical rising time and decay time, but their exact calculation is impossible in general.

the multiplication in the Fourier domain. As a result, in the Fourier domain, any convolution of exponential filters has the following transfer function:

$$\widetilde{F}_{\tau_1,\tau_2,\ldots,\tau_N}(\xi) = \prod_{n=1}^{N} \frac{1}{1-\mathbf{j}\tau_n\xi}, \tag{26}$$

where some of the $\{\tau_n\}$ can possibly be equal one to another (general case).

Equation (26) is a more convenient way to work on the filter, since its properties are now described by a simple equation. Note also that coefficients γ_n in (25) can be obtained by reducing the total fraction of (26) in its simple elements. Similarly, one can derive the coefficients $\gamma_{n,k}$ for the general case, but the degenerated times τ_n lead to a term $1/(1-\mathbf{j}\tau_n\xi)^{K_n}$ in (26) that yields harder calculations for the simple elements' coefficients.

2. An approximate two-parameter filter

How can such an exponential cascade be described by few parameters? We believe that in the case of biological systems where all equations are approximate, a two-parameter model defined by a rising time $\tau_{\max}$ and a decay time τ_{dec} is a sufficient fit for any low-pass cascade.

The parametric function we use is defined by:

$$E_{\alpha,\tau}(t) = \frac{t^\alpha}{\tau^{\alpha+1}\Gamma(\alpha+1)} \exp\left(-\frac{t}{\tau}\right), \tag{27}$$

where α and τ are any real positive numbers. Γ is the mathematical Gamma function; it only serves as a normalization factor. Its most classical definition is precisely as being the integral of function $t^{\alpha-1}e^{-t}$ over $\mathbb{R}^+$, when $\alpha > 0$. Here again, notations are coherent. Indeed, function $x \to \Gamma(x+1)$ is an interpolation of the integer 'factorial' function. This means that (27) defines the same function as (24), when $\alpha \in \mathbb{N}$.

$E_{\alpha,\tau}$ is a function that reaches its maximum at time $\alpha\tau$, before decaying with time constant τ (Figure 48). Thus α and τ govern the two parameters we have chosen to describe our exponential 'blobs', with:

$$\begin{cases} \tau_{\max} = \alpha\tau, \\ \tau_{\text{dec}} = \tau. \end{cases} \tag{28}$$

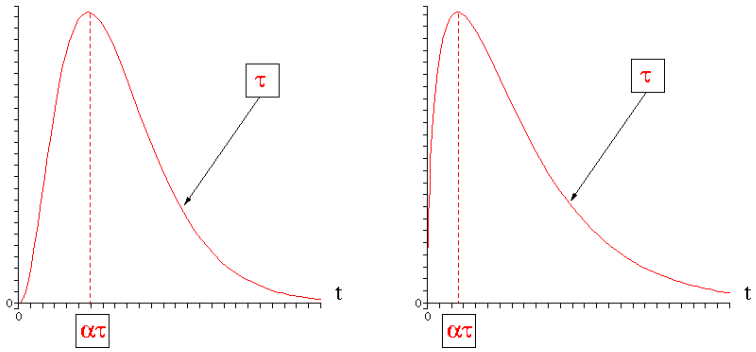

(A) $\alpha = 2.3$ (B) $\alpha = 0.5$

Figure 48: Two examples of kernel $E_{\alpha,\tau}$. Note that when $\alpha < 1$ (case (B)), the derivative of the kernel in $t = 0$ is always infinite. This is the main limitation for visual fitting of kernel $F_{\tau_1,\tau_2,\ldots,\tau_n}$ with a function $E_{\alpha,\tau}$ in some cases (see Figure 49).

Empirically one finds that any convolution of exponential filters is always well approached by some function $E_{\alpha,\tau}(t)$, except in its initial rising phase when the best fitting α is smaller than 1 (Figure 49). For this reason, we describe all retinal low-pass filters by appropriate functions $E_{\alpha,\tau}(t)$. However, one last question should be addressed. What links are there between the values for (α, τ) found empirically, and the times $(\tau_1, \tau_2, \ldots, \tau_n)$ of the original exponential filters that generated the blob?

Deriving parameters α and τ. We generated exponential cascades, numerically calculated the corresponding kernel, and looked for the visually best-fitting pair (α, τ). Empirically, we find out that for our best-fitting (α, τ), the sum of time-to-peak $\tau_{\max} = \alpha\tau$ and of decay time $\tau_{\text{dec}} = \tau$ is

always close to the sum of all generating times. That is:

$$(1+\alpha)\tau \simeq \sum_{n=1}^{N} \tau_n. \tag{29}$$

Empirically still, the visually best-fitting decay time τ for the whole cascade is a pondering of all individual exponential decay times, but with a pass filtersative contribution of big (slow) exponential filters. That big time constants have a bigger impact on the decay time of the cascade is intuitive: a fast filter i in the cascade, with characteristic time $\tau_i \simeq 0$, does not modify the signal at all, so it cannot influence the visually best-fitting decay time. The simplest way to do this is to have each term in the sum pondered by its own value. And indeed, we find

$$\tau = \frac{\sum_{n=1}^{N} \tau_n^2}{\sum_{n=1}^{N} \tau_n} \tag{30}$$

to be a suitable choice for the decay time in most cases. Then, according to observation (29), we chose:

$$\alpha = \frac{\sum_{n=1}^{N} \tau_n}{\tau} - 1 \tag{31}$$

as our value for α. Using these approximations always provides a relatively correct fit of the real cascaded filter, as shown in Figure 49.

These empirical choices for (α, τ) can actually be justified in the Fourier domain. Indeed, one can check easily that the general Fourier transform of function $E_{\alpha,\tau}$ is given by:

$$\widetilde{T}_{\alpha,\tau}(\xi) = \frac{1}{(1-\mathbf{j}\tau\xi)^{\alpha+1}}. \tag{32}$$

Then, developping the actual transfer function $\widetilde{F}_{\tau_1,\tau_2,\ldots,\tau_N}(\xi)$ of (26) and its approximation $\widetilde{T}_{\alpha,\tau}(\xi)$, both at the second order in ξ, provides:

$$\begin{cases} \widetilde{F}_{\tau_1,\tau_2,\ldots,\tau_N}(\xi) = 1 + \mathbf{j}\left(\sum_{n=1}^{N}\tau_n\right)\xi - \frac{1}{2}\left((\sum_{n=1}^{N}\tau_n)^2 + \sum_{n=1}^{N}\tau_n^2\right)\xi^2 + o(\xi^2), \\ \text{and:} \\ \widetilde{T}_{\alpha,\tau}(\xi) = 1 + \mathbf{j}\left((\alpha+1)\tau\right)\xi - \frac{1}{2}\left(\tau^2(\alpha+1)(\alpha+2)\right)\xi^2 + o(\xi^2). \end{cases} \tag{33}$$

As a result, imposing that $\widetilde{T}_{\alpha,\tau}(\xi)$ be equal to $\widetilde{F}_{\tau_1,\tau_2,\ldots,\tau_N}(\xi)$ as far at the second order in ξ yields the approximation for α and τ that was empirically proposed in (30,31).

Best approximation with an integer α. Kernels $E_{\alpha,\tau}$ for which $\alpha \in \mathbb{N}$ have the computational advantage to be implementable through recursive filtering. Hence we also tested visual differences between the best-fitting $E_{\alpha,\tau}$ as described through (30,31) and its "integer alpha" approximation as defined by:

$$\begin{cases} \alpha_{\mathbb{N}} = \mathrm{round}(\alpha) \\ \tau_{\mathbb{N}} = \tau \dfrac{1+\alpha}{1+\alpha_{\mathbb{N}}}. \end{cases} \tag{34}$$

Function $round$ returns the closest integer to α. $\tau_{\mathbb{N}}$ is still any real number, but it is calculated so as for $(\alpha_{\mathbb{N}}, \tau_{\mathbb{N}})$ to verify observation (29), or equivalently, to fit the first-order developments of Fourier transforms in (33) . This procedure still yields visually satisfying kernels, as illustrated in Figure 49.

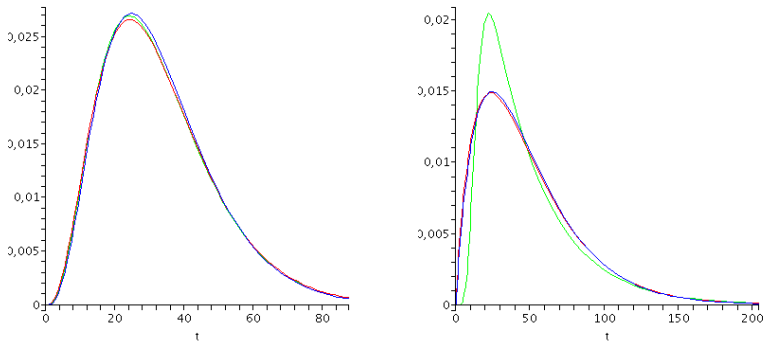

(A) $(8, 10^2, 15) \to (2.8, 11.5)$ (B) $(2^7, 35) \to (0.9, 25.5)$

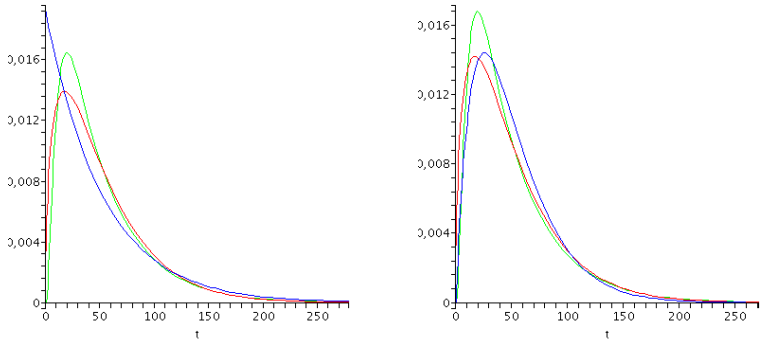

(C) $(5^2, 42) \to (0.49, 34.84)$ (D) $(5^2, 41) \to (0.50, 33.90)$

Figure 49: Four approximations of exponential cascades by $E_{\alpha,\tau}$ kernels. Notation is $(\tau_1, \tau_2, \ldots, \tau_N) \to (\alpha, \tau)$ using formulas (30,31). *Green Curve*: original cascade kernel. *Red Curve*: best approximation as described through (30,31). *Blue Curve*: Best approximation with integer α, as in (34). Figures comment: (A) very good fitting case. (B) problematic fitting case. The 7-fold repetition of exponential kernel $\tau = 2$ provides the real kernel with null derivatives in $t = 0$ at the 5 first orders, whereas the derivative of the approximate kernel is infinite, since $\alpha < 1$. (C) and (D) worst-case scenario for the fitting of best kernel $E_{\alpha,\tau}$ with an "integer α" kernel, through equation (34). A slight change of one of the original exponential times makes the best-fitting α cross value 0.5, yielding two different approximations for the Blue curve.

Bibliography

[1] D. Alleysson, S. Susstrunk, and J. Herault. Linear demosaicing inspired by the human visual system. *Image Processing, IEEE Transactions on*, 14(4):439–449, 2005.

[2] F.R. Amthor, E.S. Takahashi, and C.W. Oyster. Morphologies of rabbit retinal ganglion cells with complex receptive fields. *Journal of comparative neurology*, 280(1):97–121, 1989.

[3] J.J. Atick. Could information theory provide an ecological theory of sensory processing? *Network: Computation in Neural Systems*, 3(2):213–251, 1992.

[4] S. Baccus and M. Meister. Fast and slow contrast adaptation in retinal circuitry. *Neuron*, 36(5):909–919, 2002.

[5] H.B. Barlow, R.M. Hill, and W.R. Levick. Retinal ganglion cells responding selectively to direction and speed of image motion in the rabbit. *The Journal of Physiology*, 173(3):377, 1964.

[6] H.B. Barlow and W. R. Levick. The mechanism of directionally selective units in rabbit's retina. *J Physiol*, 178:477–504, 1965.

[7] D.A. Baylor, B.J. Nunn, and J.L. Schnapf. The photocurrent, noise and spectral sensitivity of rods of the monkey macaca fascicularis. *The Journal of Physiology*, 357(1):575–607, 1984.

[8] D.L. Beaudoin, B.G. Borghuis, and J.B. Demb. Cellular basis for contrast gain control over the receptive field center of mammalian retinal ganglion cells. *Journal of Neuroscience*, 27:2636–2645, 2007.

[9] WHA Beaudot. *The neural information processing in the vertebrate retina: A melting pot of ideas for artificial vision*. PhD thesis, PhD Thesis in Computer Science, INPG (France), dec 1994.

[10] E. A. Bernadete and E. Kaplan. Dynamics of primate P retinal ganglion cells: responses to chromatic and achromatic stimuli. *Journal of Physiology*, 519(3):775–790, 1999.

[11] E.A. Bernadete, E. Kaplan, and B.W. Knight. Contrast gain control in the primate retina: P cells are not X-like, some M cells are. *Visual Neuroscience*, 8(5):483–486, 1992.

[12] M.J. Berry, I.H. Brivanlou, T.A. Jordan, and M. Meister. Anticipation of moving stimuli by the retina. *Nature*, 398(6725):334–8, 1999.

[13] M.J. Berry, D.K. Warland, and M. Meister. The structure and precision of retinal spike trains. *Proc Natl Acad Sci USA*, 94:5411–5416, 1997.

[14] G.G. Blasdel. Orientation selectivity, preference, and continuity in monkey striate cortex. *Journal of Neuroscience*, 12(8):3139–3161, 1992.

[15] B.B. Boycott and H. Wassle. The morphological types of ganglion cells of the domestic cat's retina. *The Journal of Physiology*, 240(2):397–419, 1974.

[16] B.B. Boycott and H. Wassle. Morphological classification of bipolar cells of the primate retina. *Eur J Neurosci*, 3(11):1069–1088, 1991.

[17] I. H. Brivanlou, D. K. Warland, and M. Meister. Mechanisms of concerted firing among retinal ganglion cells. *Neuron*, 20:527–529, March 1998.

[18] ME Burns and TD Lamb. *Visual transduction by rod and cone photoreceptors*, chapter 16, pages 215–233. In Chalupa and Werner [24], 2004.

[19] J.J. Bussgang. Crosscorrelation functions of amplitude-distorted gaussian signals. *Research Laboratory of Electronics, Massachusetts Institute of Technology, Tech Report*, (216), 1952.

[20] D. Cai, G. C. Deangelis, and D. Freeman. Spatiotemporal receptive field organization in the lateral geniculate nucleus of cats and kittens. *Journal of Neurophysiology*, 78(2):1045–1061, August 1997.

[21] J.H. Caldwell and N.W. Daw. New properties of rabbit retinal ganglion cells. *The Journal of Physiology*, 276(1):257–276, 1978.

[22] J.H. Caldwell, N.W. Daw, and H.J. Wyatt. Effects of picrotoxin and strychnine on rabbit retinal ganglion cells: lateral interactions for cells with more complex receptive fields. *The Journal of Physiology*, 276:277, 1978.

[23] M. Carandini, J. B. Demb, V. Mante, D. J. Tollhurst, Y. Dan, B. A. Olshausen, J. L. Gallant, and N. C. Rust. Do we know what the early visual system does? *Journal of Neuroscience*, 25(46):10577–10597, November 2005.

[24] L. M. Chalupa and J.S. Werner, editors. *The visual neurosciences*. MIT Press, 2004.

[25] E. J. Chichilnisky. A simple white noise analysis of neuronal light responses. *Network: Comput. Neural Syst.*, 12:199–213, 2001.

[26] E. J. Chichilnisky and R. S. Kalmar. Temporal resolution of ensemble visual motion signals in primate retina. *The Journal of Neuroscience*, 17:6681–6689, 2003.

[27] B.G. Cleland and W.R. Levick. Brisk and sluggish concentrically organized ganglion cells in the cat's retina. *The Journal of Physiology*, 240(2):421–456, 1974.

[28] B.G. Cleland and W.R. Levick. Properties of rarely encountered types of ganglion cells in the cat's retina and an overall classification. *The Journal of Physiology*, 240(2):457–492, 1974.

[29] D. Colella. Web : http://www.mitre.org/news/the_edge/september_99/fifth.html, 1999.

[30] L. J. Croner and E. Kaplan. Receptive fields of P and M ganglion cells across the primate retina. *Vision Research*, 35(1):7–24, jan 1995.

[31] D. Dacey, O. S. Packer, L. Diller, D. Brainard, B. Peterson, and B. Lee. Center surround receptive field structure of cone bipolar cells in primate retina. *Vision Research*, 40:1801–1811, 2000.

[32] D. Dacey and M. Petersen. Dendritic field size and morphology of midget and parasol ganglion cells of the human retina. *Proc Natl Acad Sci*, 89:9666–70, 1992.

[33] D.M. Dacey. Primate retina: cell types, circuits and color opponency. *Progress in Retinal and Eye Research*, 18(6):737–763, 1999.

[34] D.M. Dacey and B.B. Lee. The'blue-on' opponent pathway in primate retina originates from a distinct bistratified ganglion cell type. *Nature*, 367(6465):731–735, 1994.

[35] D.M. Dacey, B.B. Peterson, F.R. Robinson, and P.D. Gamlin. Fireworks in the primate retina in vitro photodynamics reveals diverse LGN-projecting ganglion cell types. *Neuron*, 37(1):15–27, 2003.

[36] R.F. Dacheux and E. Raviola. Horizontal cells in the retina of the rabbit. *Journal of Neuroscience*, 2(10):1486, 1982.

[37] R.F. Dacheux and E. Raviola. The rod pathway in the rabbit retina: a depolarizing bipolar and amacrine cell. *Journal of Neuroscience*, 6(2):331, 1986.

[38] P. Dayan and L. F. Abbott. *Theoretical Neuroscience : Computational and Mathematical Modeling of Neural Systems*. MIT Press, 2001.

[39] F.M. De Monasterio and P. Gouras. Functional properties of ganglion cells of the rhesus monkey retina. *The Journal of Physiology*, 251(1):167–195, 1975.

[40] J. B. Demb, K. Zaghloul, L. Haarsma, and P. Sterling. Bipolar cells contribute to nonlinear spatial summation in the brisk-transient (Y) ganglion cell in mammalian retina. *Journal of Neuroscience*, 21(19):7447–7454, October 2001.

[41] J.B. Demb and E.N. Pugh. Connexin36 forms synapses essential for night vision. *Neuron*, 36(4):551–553, 2002.

[42] J.B. Demb, K. Zaghloul, and P. Sterling. Cellular basis for the response to second-order motion cues in Y retinal ganglion cells. *Neuron*, 32(4):711–721, 2001.

[43] S.H. DeVries. Correlated firing in rabbit retinal ganglion cells. *Journal of Neurophysiology*, 81(2):908–920, 1999.

[44] S.H. DeVries. Bipolar cells use kainate and AMPA receptors to filter visual information into separate channels. *Neuron*, 28(3):847–856, 2000.

[45] S.H. Devries and D.A. Baylor. Mosaic arrangement of ganglion cell receptive fields in rabbit retina. *Journal of Neurophysiology*, 78(4):2048–2060, 1997.

[46] S.H. DeVries and E.A. Schwartz. Kainate receptors mediate synaptic transmission between cones and 'off' bipolar cells in a mammalian retina. *Nature*, 397(6715):157–60, 1999.

[47] C. Enroth-Cugell and A. W. Freeman. The receptive-field spatial structure of cat retinal Y cells. *Journal of Physiology*, 384(1):49–79, 1987.

[48] C. Enroth-Cugell and J. G. Robson. The contrast sensitivity of retinal ganglion cells of the cat. *J Physiol*, 187:517–552, 1966.

[49] C. Enroth-Cugell, J. G. Robson, D. E. Schweitzer-Tong, and A. B. Watson. Spatio-temporal interactions in cat retinal ganglion cells showing linear spatial summation. *J Physiol*, 341:279–307, 1983.

[50] H. Erwin. Web : http://scat-he-g4.sunderland.ac.uk/ harry-erw/phpwiki/index.php/tonicphasic, 2004.

[51] T. Euler, P.B. Detwiler, and W. Denk. Directionally selective calcium signals in dendrites of starburst amacrine cells. *Nature*, 418:845–852, 2002.

[52] T. Euler and R. H. Masland. Light-evoked responses of bipolar cells in a mammalian retina. *J. Neurpohysiology*, 83(4):1817–1829, April 2000.

[53] D.J. Field. Relations between the statistics of natural images and the response properties of cortical cells. *J. Opt. Soc. Am. A*, 4(12):2379–2394, 1987.

[54] N. Flores-Herr, D. A. Protti, and H. Wässle. Synaptic currents generating the inhibitory surround of ganglion cells in the mammalian retina. *Journal of Neuroscience*, 21(13):4852–4863, jul 2001.

[55] S.I. Fried, T.A. Muench, and F.S. Werblin. Mechanisms and circuitry underlying directional selectivity in the retina. *Nature*, 420(6914):411–414, 2002.

[56] K. Funke and U. Eysel. Inverse correlation of firing patterns of single topographically matched perigeniculate neurons and cat dorsal lateral geniculate relay cells. *Visual Neuroscience*, 15(04):711–729, 1998.

[57] M.G.F. Fuortes and A.L. Hodgkin. Changes in time scale and sensitivity in the ommatidia of limulus. *The Journal of Physiology*, 172(2):239, 1964.

[58] N. Gazeres, L. Borg-Graham, and Y. Fregnac. A model of non-lagged X responses to flashed stimuli in the cat lateral geniculate nucleus. *Visual Neuroscience*, 1998.

[59] K.R. Gegenfurtner. Cortical mechanisms of colour vision. *Nature Reviews Neuroscience*, 4(7):563–572, 2003.

[60] T. Gollisch and M. Meister. Rapid neural coding in the retina with relative spike latencies. *Science*, 319:1108–1111, 2008. DOI: 10.1126/science.1149639.

[61] W. Hare and W. Owen. Spatial organization of the bipolar cell's receptive field in the retina of the tiger salamander. *J Physiol*, 421:223–245, 1990.

[62] W.A. Hare and W.G. Owen. Receptive field of the retinal bipolar cell: a pharmacological study in the tiger salamander. *Journal of Neurophysiology*, 76(3):2005–2019, 1996.

[63] S.H.C. Hendry and R.C. Reid. The koniocellular pathway in primate vision. *Annual Review of Neuroscience*, 23(1):127–153, 2000.

[64] M. H. Hennig, K. Funke, and F. Wörgötter. The influence of different retinal subcircuits on the nonlinearity of ganglion cell behavior. *Journal of Neuroscience*, 22(19):8726–8738, oct 2002.

[65] J. Herault. A model of colour processing in the retina of vertebrates: from photoreceptors to colour opposition and colour constancy phenomena. *Neurocomputing*, 12:113–129, 1996.

[66] J. Hérault. *De la rétine biologique aux circuits neuromorphiques*, chapter 3. Hermès science publications, 2001.

[67] J. Herault, editor. *Vision: Signals, Images and Neural Networks*. World Scientific Publications, 2008.

[68] J. Hérault and B. Durette. Modeling visual perception for image processing. In F. Sandoval, A. Prieto, J. Cabestany, and M. Gra na, editors, *Computational and Ambient Intelligence : 9th International Work-Conference on Artificial Neural Networks, IWANN 2007*, 2007.

[69] S. Hochstein and R. M. Shapley. Linear and nonlinear spatial subunits in Y cat retinal ganglion cells. *J Physiol*, 262:265–284, 1976.

[70] T. Hosoya, S. A. Baccus, and M. Meister. Dynamic predictive coding by the retina. *Nature*, 436:71–77, 2005.

[71] D. H. Hubel and T. N. Wiesel. Receptive fields of optic nerve fibres in the spider monkey. *J. Physiol.*, 154:572–80, December 1960.

[72] M. Hubener, D. Shoham, A. Grinvald, and T. Bonhoeffer. Spatial relationships among three columnar systems in cat area 17. *Journal of Neuroscience*, 17(23):9270–9284, 1997.

[73] A. L. Jacobs and F. S. Werblin. Spatiotemporal patterns at the retinal output. *Journal of Neurophysiology*, 80(1):447–451, jul 1998.

[74] M. Kamermans, I. Fahrenfort, K. Schultz, U. Janssen-Bienhold, T. Sjoerdsma, and R. Weiler. Hemichannel-mediated inhibition in the outer retina. *Science*, 292(5519):1178–1180, 2001.

[75] E.R. Kandel, J.H. Schwartz, and T.M. Jessel. *Principles of Neural Science*. McGraw-Hill, 4th edition, 2000.

[76] P. Kara, P. Reinagel, and R. C. Reid. Low response variability in simultaneously recorded retinal, thalamic, and cortical neurons. *Neuron*, 27(3):635–646, 2000. Poisson, retina, spike variability.

[77] J. Keat, P. Reinagel, R. C. Reid, and M. Meister. Predicting every spike: a model for the responses of visual neurons. *Neuron*, 30:803–817, 2001.

[78] G. T. Kenyon, J. Theiler, J. S. George, B. J. Travis, and D. W. Marshak. Correlated firing improves stimulus discrimination in a retinal model. *Neural Computation*, 16:2261–2291, 2004.

[79] G.T. Kenyon, B. Moore, J. Jeffs, K.S. Denning, G.J. Stephens, B.J. Travis, J.S. George, J. Theiler, and D.W. Marshak. A model of high-frequency oscillatory potentials in retinal ganglion cells. *Visual Neuroscience*, 20(05):465–480, 2003.

[80] G.T. Kenyon, B.J. Travis, J. Theiler, J.S. George, G.J. Stephens, and D.W. Marshak. Stimulus-specific oscillations in a retinal model. *Neural Networks, IEEE Transactions on*, 15(5):1083–1091, 2004.

[81] K. J. Kim and F. Rieke. Temporal contrast adaptation in the input and output signals of salamander retinal ganglion cells. *Journal of Neuroscience*, 21(1):287–299, jan 2001.

[82] H. Kolb. The inner plexiform layer in the retina of the cat: electron microscope observation. *Journal of Neurocytology*, 8:295–329, 1979.

[83] H. Kolb, E. Fernandez, and R. Nelson. Webvision : the Organization of the Retina and Visual System. Web : http://webvision.med.utah.edu/, 2001.

[84] S. W. Kuffler. Discharge patterns and functional organization of mammalian retina. *Journal of Neurophysiology*, 16:37–68, 1953.

[85] T. D. Lamb. Spatial properties of horizontal cell responses in the turtle retina. *J Physiol*, 263(2):239–55, 1976.

[86] M. Laufer and M. Verzeano. Periodic activity in the visual system of the cat. *Vision Res*, 7(3):215–29, 1967.

[87] W.R. Levick. Receptive fields and trigger features of ganglion cells in the visual streak of the rabbits retina. *The Journal of Physiology*, 188(3):285–307, 1967.

[88] M. A. Mahowald and C. Mead. The silicon retina. *Sci. Am.*, 264(5):76–82, 1991.

[89] V. Mante, R. A. Frazor, V. Bonin, W. S. Geisler, and M. Carandini. Independence of luminance and contrast in natural scenes and in the early visual system. *Nature Neuroscience*, 2005.

[90] B.U.Q. Mao, P.R. Macleish, and J.D. Victor. The intrinsic dynamics of retinal bipolar cells isolated from tiger salamander. *Visual Neuroscience*, 15(03):425–438, 1998.

[91] P.R. Martin. Colour processing in the primate retina: recent progress. *The Journal of Physiology*, 513(3):631–638, 1998.

[92] R. Masland. The fundamental plan of the retina. *Nature neuroscience*, 4(9), September 2001.

[93] R.H. Masland. Neuronal diversity in the retina. *Current Opinion in Neurobiology*, 11(4):431–436, 2001.

[94] D.N. Mastronarde. Correlated firing of cat retinal ganglion cells. I. Spontaneously active inputs to X-and Y-cells. *Journal of Neurophysiology*, 49(2):303–324, 1983.

[95] B.A. McGuire, J.K. Stevens, and P. Sterling. Microcircuitry of bipolar cells in cat retina. *Journal of Neuroscience*, 4(12):2920, 1984.

[96] M. J. McMahon, O. S. Packer, and D. M. Dacey. The classical receptive field surround of primate Parasol ganglion cells is mediated primarily by a non-GABAergic pathway. *Journal of Neuroscience*, 24(15):3736–3745, apr 2004.

[97] SL Mills and SC Massey. Distribution and coverage of A-and B-type horizontal cells stained with neurobiotin in the rabbit retina. *Vis Neurosci*, 11(3):549–60, 1994.

[98] D. Weedman Molavi, J. Price, H. Burton, and D. Van Essen. The W.U.S.M Neuroscience Tutorial. Web : http://thalamus.wustl.edu/course/, 1997.

[99] K.T. Mullen. The contrast sensitivity of human colour vision to red-green and blue-yellow chromatic gratings. *J Physiol*, 359:381–400, 1985.

[100] K.T. Mullen and F.A.A. Kingdom. Differential distributions of red–green and blue–yellow cone opponency across the visual field. *Visual Neuroscience*, 19(01):109–118, 2002.

[101] K. I. Naka and W. A. Rushton. The generation and spread of s-potentials in fish (cyprinidae). *J Physiol*, 192(2):437–61, September 1967.

[102] S. Nawy. Regulation of the On bipolar cell mGluR6 pathway by Ca2+. *Journal of Neuroscience*, 20(12):4471, 2000.

[103] R. Nelson, E.V. Famiglietti, and H. Kolb. Intracellular staining reveals different levels of stratification for on-and off-center ganglion cells in cat retina. *Journal of Neurophysiology*, 41(2):472–483, 1978.

[104] R. Nelson and H. Kolb. Synaptic patterns and response properties of bipolar and ganglion cells in the cat retina. *Vision Res*, 23(10):1183–95, 1983.

[105] S. Neuenschwander, M. Castelo-Branco, and W. Singer. Synchronous oscillations in the cat retina. *Vision Research*, 39(15):2485–2497, 1999.

[106] S. Neuenschwander and W. Singer. Long-range synchronization of oscillatory light responses in the cat retina and lateral geniculate nucleus. *Nature*, 379(6567):728–732, February 1996.

[107] S. Nirenberg and M. Meister. The light response of retinal ganglion cells is truncated by a displaced amacrine circuit. *Neuron*, 18:637–650, 1997.

[108] R.A. Normann and I. Perlman. The effects of background illumination on the photoresponses of red and green cones. *The Journal of Physiology*, 286(1):491–507, 1979.

[109] B.J. O'Brien, T. Isayama, R. Richardson, and D.M. Berson. Intrinsic physiological properties of cat retinal ganglion cells. *The Journal of Physiology*, 538(3):787–802, 2002.

[110] B.P. Ölveczky, S.A. Baccus, and M. Meister. Segregation of object and background motion in the retina. *Nature*, 423:401–408, 2003.

[111] G. Osterberg. Topography of the layer of rods and cones in the human retina. *Acta Ophthal.*, suppl. 6:1–103, 1935.

[112] C.W. Oyster, E. Takahashi, and H. Collewijn. Direction-selective retinal ganglion cells and control of optokinetic nystagmus in the rabbit. *Vision Res*, 12(2):183–93, 1972.

[113] I. Perlman and J. Ammermuller. Receptive-field size of L1 horizontal cells in the turtle retina: effects of dopamine and background light. *Journal of Neurophysiology*, 72(6):2786–2795, 1994.

[114] A. Polans, W. Baehr, and K. Palczewski. Turned on by Ca^{2+}! The physiology and pathology of Ca^{2+}-binding proteins in the retina. *Trends in Neurosciences*, 19(12):547–554, December 1996.

[115] M. Pu, D.M. Berson, and T. Pan. Structure and function of retinal ganglion cells innervating the cat's geniculate wing: an in vitro study. *Journal of Neuroscience*, 14(7):4338, 1994.

[116] J.L. Puchalla, E. Schneidman, R.A. Harris, and M.J. Berry. Redundancy in the population code of the retina. *Neuron*, 46(3):493–504, 2005.

[117] EN Pugh and TD Lamb. Amplification and kinetics of the activation steps in phototransduction. *Biochim Biophys Acta*, 1141(2-3):111–49, 1993.

[118] E.N. Pugh, S. Nikonov, and T.D. Lamb. Molecular mechanisms of vertebrate photoreceptor light adaptation. *Current Opinion in Neurobiology*, 9(4):410–418, 1999.

[119] D. Purves, G.J. Augustine, D. Fitzpatrick, W.C. Hall, LaMantia A-S., McNamara J.O., and Williams S.M. *Neuroscience*. Sinauer Associates, Inc, 3rd edition, 2004.

[120] E. Raviola and N. B. Gilula. Gap junctions between photoreceptor cells in the vertebrate retina. *Proceedings of the National Academy of Sciences*, 70(6):1677–1681, jun 1973.

[121] D.S. Reich, J.D. Victor, and B.W. Knight. The power ratio and the interval map: Spiking models and extracellular recordings. *Journal of Neuroscience*, 18(23):10090, 1998.

[122] F. Rieke. Temporal contrast adaptation in salamander bipolar cells. *Journal of Neuroscience*, 21(23):9445–9454, dec 2001.

[123] F. Rieke, D. Warland, R. de Ruyter van Steveninck, and W. Bialek. *Spikes: Exploring the Neural Code*. Bradford Books, 1997.

[124] D. Ringach and R. Shapley. Reverse correlation in neurophysiology. *Cognitive Science*, 28(2):147–16620, 2004.

[125] R.L. Rockhill, F.J. Daly, M.A. MacNeil, S.P. Brown, and R.H. Masland. The diversity of ganglion cells in a mammalian retina. *Journal of Neuroscience*, 22(9):3831, 2002.

[126] R.W. Rodieck. Quantitative analysis of cat retinal ganglion cell response to visual stimuli. *Vision Research*, 5:583–601, 1965.

[127] R.W. Rodieck and M. Watanabe. Survey of the morphology of macaque retinal ganglion cells that project to the pretectum, superior colliculus, and parvicellular laminae of the lateral geniculate nucleus. *The Journal of Comparative Neurology*, 338(2):289–303, 1993.

[128] B. Roska, A. Molnar, and F.S. Werblin. Parallel processing in retinal ganglion cells: How integration of space-time patterns of excitation and inhibition form the spiking output. *Journal of Neurophysiology*, 95(6):3810–3822, 2006.

[129] B. Roska and F. Werblin. Vertical interactions across ten parallel, stacked representations in the mammalian retina. *Nature*, 410:583–7, mar 2001.

[130] M.H. Rowe and J. Stone. Properties of ganglion cells in the visual streak of the cat's retina. *J Comp Neurol*, 169(1):99–125, 1976.

[131] H.M. Sakai and K.I. Naka. Dissection of the neuron network in the catfish inner retina. IV. Bidirectional interactions between amacrine and ganglion cells. *Journal of Neurophysiology*, 63(1):105–119, 1990.

[132] H.M. Sakai and K.I. Naka. Dissection of the neuron network in the catfish inner retina. V. Interactions between NA and NB amacrine cells. *Journal of Neurophysiology*, 63(1):120–130, 1990.

[133] J. L. Schnapf, B. J. Nunn, M. Meister, and D. A. Baylor. Visual transduction in cones of the monkey macaca fascicularis. *J Physiol*, 427(1):681–713, 1990.

[134] D.M. Schneeweis and J.L. Schnapf. Photovoltage of rods and cones in the macaque retina. *Science*, 268(5213):1053–1056, 1995.

[135] E. Schneidman, M.J. Berry, R. Segev, and W. Bialek. Weak pairwise correlations imply strongly correlated network states in a neural population. *Nature*, 440(7087):1007–1012, 2006.

[136] R. Shapley and C. Enroth-Cugell. Visual adaptation and retinal gain controls. *Progress in retinal research*, 3:263–346, 1984.

[137] R. M. Shapley and J. D. Victor. The effect of contrast on the transfer properties of cat retinal ganglion cells. *The Journal of Physiology*, 285(1):275–298, 1978.

[138] R. M. Shapley and J. D. Victor. How the contrast gain control modifies the frequency responses of cat retinal ganglion cells. *The Journal of Physiology*, 318(1):161–179, 1981.

[139] L.T. Sharpe and A. Stockman. Rod pathways: the importance of seeing nothing. *Trends in Neurosciences*, 22(11):497–504, 1999.

[140] S.M. Sherman and R.W. Guillery. *The Visual Relays in the Thalamus*, chapter 35, pages 565–591. In Chalupa and Werner [24], 2004.

[141] R.A. Shiells and G. Falk. A rise in intracellular Ca2+ underlies light adaptation in dogfish retinal 'on' bipolar cells. *The Journal of Physiology*, 514(2):343–350, 1999.

[142] J. Shlens, G.D. Field, J.L. Gauthier, M.I. Grivich, D. Petrusca, A. Sher, A.M. Litke, and E.J. Chichilnisky. The structure of multi-neuron firing patterns in primate retina. *Journal of Neuroscience*, 26(32):8254, 2006.

[143] W. Singer. Neuronal synchrony: a versatile code for the definition of relations? *Neuron*, 24(1):49–65, 1999.

[144] M.V. Srinivasan, S.B. Laughlin, and A. Dubs. Predictive coding: A fresh view of inhibition in the retina. *Proceedings of the Royal Society of London. Series B, Biological Sciences*, 216(1205):427–459, 1982.

[145] J. Stone and Y. Fukuda. Properties of cat retinal ganglion cells: a comparison of W-cells with X-and Y-cells. *Journal of Neurophysiology*, 37(4):722–748, 1974.

[146] G. Svaetichin. The cone action potential. *Acta Physiol. Scand*, 29(suppl 106):565–599, 1953.

[147] L. Tao, M. Shelley, D. McLaughlin, and R. Shapley. An egalitarian network model for the emergence of simple and complex cells in visual cortex. *Proc Natl Acad Sci*, 101(1):366–371, January 2004.

[148] W.R. Taylor and D.I. Vaney. New directions in retinal research. *Trends in Neurosciences*, 26(7):379–385, 2003.

[149] R. Tootell, E. Switkes, M. Silverman, and S. Hamilton. Functional anatomy of the macaque striate cortex. ii. retinotopic organization. *Journal of neuroscience*, 8(5):1531–1568, 1988.

[150] V. Torre, HR Matthews, and TD Lamb. Role of Calcium in regulating the cyclic GMP cascade of phototransduction in retinal rods. *PNAS*, 83(18):7109–7113, 1986.

[151] J.B. Troy, G. Einstein, J.G. Schuurmans, R.P .and Robson, and C. Enroth-Cugell. Responses to sinusoidal gratings of two types of very nonlinear retinal ganglion cells of cat. *Vis Neurosci*, 3(3):213–23, 1989.

[152] J.B. Troy and T. Shou. The receptive fields of cat retinal ganglion cells in physiological and pathological states: where we are after half a century of research. *Progress in Retinal and Eye Research*, 21(3):263–302, 2002.

[153] J.M. Valeton and D. Van Norren. Light adaptation of primate cones : An analysis based on extracellular data. *Vision Research*, 23(12):1539–1547, 1983.

[154] J. H. van Hateren, L. Rüttiger, H. Sun, and B. B. Lee. Processing of natural temporal stimuli by macaque retinal ganglion cells. *J. Neuroscience*, 22(22):9945–9960, 2002.

[155] J.H. van Hateren. A cellular and molecular model of response kinetics and adaptation in primate cones and horizontal cells. *Journal of Vision*, 5(4):5, 2005.

[156] J.H. van Hateren and T.D. Lamb. The photocurrent response of human cones is fast and monophasic. *BMC Neuroscience*, 7(1):34, 2006.

[157] F.L. Van Nes, J.J. Koenderink, H. Nas, and M.A. Bouman. Spatiotemporal modulation transfer in the human eye. *J Opt Soc Am*, 57(9):1082–8, 1967.

[158] M. van Wyk, W.R. Taylor, and D.I. Vaney. Local edge detectors: A substrate for fine spatial vision at low temporal frequencies in rabbit retina. *Journal of Neuroscience*, 26(51):13250, 2006.

[159] J. D. Victor. The dynamics of the cat retinal X cell centre. *The Journal of Physiology*, 386(1):219–246, 1987.

[160] J.D. Victor. Spike train metrics. *Current Opinion in Neurobiology*, 15(5):585–592, 2005.

[161] H. Wassle. Parallel processing in the mammalian retina. *Nat Rev Neurosci*, 5(10):747–57, 2004.

[162] F. S. Werblin and J. E. Dowling. Organization of the retina of the mudpuppy. *Journal of Neurophysiology*, 32(3):339–355, 1969.

[163] Adrien Wohrer. *Model and large-scale simulator of a biological retina with contrast gain control*. PhD thesis, University of Nice Sophia-Antipolis, 2008.

[164] Adrien Wohrer, Pierre Kornprobst, and Thierry Viéville. Virtual retina: a biological retina model and simulator, with contrast gain control. Research Report 6243, INRIA, jul 2007.

[165] Y. Xu, N.K. Dhingra, R.G. Smith, and P. Sterling. Sluggish and brisk ganglion cells detect contrast with similar sensitivity. *Journal of Neurophysiology*, 93(5):2388–2395, 2005.

[166] G.M. Zeck, Q. Xiao, and R.H. Masland. The spatial filtering properties of local edge detectors and brisk-sustained retinal ganglion cells. *Eur J Neurosci*, 22(8):2016–26, 2005.

Unité de recherche INRIA Sophia Antipolis
2004, route des Lucioles - BP 93 - 06902 Sophia Antipolis Cedex (France)

Unité de recherche INRIA Futurs : Parc Club Orsay Université - ZAC des Vignes
4, rue Jacques Monod - 91893 ORSAY Cedex (France)
Unité de recherche INRIA Lorraine : LORIA, Technopôle de Nancy-Brabois - Campus scientifique
615, rue du Jardin Botanique - BP 101 - 54602 Villers-lès-Nancy Cedex (France)
Unité de recherche INRIA Rennes : IRISA, Campus universitaire de Beaulieu - 35042 Rennes Cedex (France)
Unité de recherche INRIA Rhône-Alpes : 655, avenue de l'Europe - 38334 Montbonnot Saint-Ismier (France)
Unité de recherche INRIA Rocquencourt : Domaine de Voluceau - Rocquencourt - BP 105 - 78153 Le Chesnay Cedex (France)

Éditeur
INRIA - Domaine de Voluceau - Rocquencourt, BP 105 - 78153 Le Chesnay Cedex (France)
http://www.inria.fr
ISSN 0249-6399